

N 7 2 - 2 8 8 8 6

NASA CR-112049

REPORT NO. GDCA-DDG71-009

INVESTIGATION OF SAFE - LIFE / FAIL - SAFE  
CRITERIA FOR THE SPACE SHUTTLE

18 May 1972

**CASE FILE  
COPY**

Prepared Under Contract NAS 1-6024 by  
CONVAIR AEROSPACE DIVISION OF GENERAL DYNAMICS  
San Diego, California

for  
National Aeronautics and Space Administration  
LANGLEY RESEARCH CENTER  
Hampton, Virginia



## FOREWORD

This investigation was conducted for the NASA Langley Research Center by the Convair Aerospace Division of the General Dynamics Corporation, acting as subcontractor to McDonnell Douglas Corporation under Contract NAS1-6024.

The NASA Task Manager was Mr. J. R. Hall; Mr. C. C. Poe, Jr. was the NASA Technical Manager; and the McDonnell Douglas Program Manager was Mr. R. H. Christensen. Mr. J. E. Jensen was the Principal Investigator for General Dynamics/Convair Aerospace, assisted by Mr. D. E. Diller and Mr. N. R. Strandlund of the Space Structural Analysis Group, Mr. T. C. Johnson of the Economic Analysis Group, Mr. C. B. Wells of Logistics and Maintenance, and Mr. W. D. Honeycutt of Mass Properties.





## TABLE OF CONTENTS, Contd

Section	Page
3 ANALYSIS OF BASELINE BOOSTERS	85
3.1 STRUCTURAL SIZING FOR STATIC LOADS	85
3.1.1 LO <sub>2</sub> Tank	85
3.1.2 LH <sub>2</sub> Tank	93
3.1.3 Vertical Tail Box	107
3.1.4 Thrust Structure	109
3.1.5 Aft Orbiter Support Frame	125
3.1.6 B-9U Delta Wing Box	128
3.1.7 B-16B Swept Wing Box	134
3.2 FATIGUE ANALYSIS	148
3.3 SAFE-LIFE ANALYSIS	169
3.3.1 Cyclic and Sustained Flaw Growth Rate Curves	169
3.3.2 LO <sub>2</sub> Tank Safe-Life Analysis	169
3.3.3 LH <sub>2</sub> Tank Safe-Life Analysis	181
3.3.4 Wing Spar Caps Safe-Life Analysis	188
3.3.5 Vertical Tail Safe-Life Analysis	195
3.3.6 Thrust Beam Cap Safe-Life Analysis	199
3.3.7 Aft Orbiter Support Frame Safe-Life Analysis	204
3.4 FAIL-SAFE ANALYSIS	206
3.4.1 Fail-Safe Analysis — LO <sub>2</sub> Tank Skin Under Internal Pressure	206
3.4.2 Fail-Safe Analysis — LH <sub>2</sub> Tank Skin Under Internal Pressure	210
3.4.3 Fail-Safe Analysis — LH <sub>2</sub> Tank Skin Under Longitudinal Loads	211
3.4.4 B-9U Delta Wing Fail-Safe Analysis	214
3.4.5 B-16B Five-Spar Swept Wing Fail-Safe Analysis	221
3.4.6 B-16B Three-Spar Swept Wing Fail-Safe Analysis	221
3.4.7 Vertical Tail Fail-Safe Analysis	223
3.4.8 Thrust Structure Fail-Safe Analysis	225
3.5 FATIGUE AND SAFE-LIFE USING ALTERNATIVE MATERIALS	232
3.5.1 Analysis of B-9U Delta Wing Box Using 2219-T87 Aluminum Alloy	232
3.5.2 Analysis of Thrust Structure Using 2219-T87 Aluminum Alloy	235

## TABLE OF CONTENTS

Section		Page
1	INTRODUCTION	1
1.1	SPACE SHUTTLE REQUIREMENTS AND CRITERIA DEVELOPMENT	1
1.2	SAFE-LIFE AND FAIL-SAFE DESIGN PHILOSOPHY	2
1.3	OBJECTIVE OF STUDY	3
1.4	STUDY APPROACH	3
2	BASELINE BOOSTER DEFINITION	7
2.1	BOOSTER MISSION	7
2.1.1	Ascent	7
2.1.2	Entry	7
2.1.3	Atmospheric Flight	11
2.2	BOOSTER CONFIGURATIONS	11
2.2.1	B-9U Delta Wing Booster	11
2.2.2	B-16B Swept Wing Booster	25
2.3	BOOSTER STRUCTURAL MATERIALS	26
2.4	BOOSTER WEIGHT SUMMARY	34
2.5	DESIGN CRITERIA	37
2.6	DESIGN CONDITIONS	41
2.7	SERVICE LOAD SPECTRA	53
2.7.1	Wing Load Spectra	53
2.7.2	Vertical Tail Load Spectra	53
2.7.3	Fuselage Load Spectra	53
2.7.4	Orbiter-To-Booster Attachment Load Spectra	53
2.7.5	Thrust Load Spectra	53
2.7.6	Propellant Tank Pressure Spectra	59
2.8	STRUCTURAL TEST PLANS	61
2.8.1	Test Requirements	61
2.8.2	Test Criteria	61
2.8.3	Structural Development Tests	63
2.8.4	Structural Qualification Tests	66
2.8.5	Wing Qualification Tests	69
2.8.6	Vertical Tail Qualification Tests	71
2.8.7	Structural Proof Tests	72
2.9	QUALITY CONTROL AND MAINTENANCE PLANS	72
2.9.1	Quality Control and Non-Destructive Evaluation	72
2.9.2	Maintenance Plan	73
2.10	COSTS	83

## TABLE OF CONTENTS, Contd

Section		Page
4	DEVELOPMENT OF SAFE-LIFE BOOSTER	239
4.1	DESCRIPTION OF STRUCTURAL AND OPERATIONAL CHANGES	242
4.2	EFFECTS OF SAFE-LIFE APPROACH ON DEVELOPMENT PLANS	242
4.2.1	Structural Test Plans	242
4.2.2	Quality Control and Maintenance Plans	243
4.2.3	Costs	248
5	DEVELOPMENT OF FAIL-SAFE BOOSTER	253
5.1	DESCRIPTION OF STRUCTURAL CHANGES	253
5.2	EFFECTS OF FAIL-SAFE APPROACH ON DEVELOPMENT PLANS	258
5.2.1	Structural Test Plans	258
5.2.2	Quality Control and Maintenance Plans	258
5.2.3	Costs	261
6	CONCLUSIONS AND RECOMMENDATIONS	265
6.1	SUMMARY OF STUDY RESULTS	265
6.1.1	Capability of Baseline Boosters	265
6.1.2	Adequacy of Baseline Development Plans	267
6.1.3	Impact of Safe-Life/Fail-Safe Design Approaches	268
6.1.4	Effects of Alternate Materials	268
6.2	CONCLUSIONS	270
6.3	RECOMMENDED SPACE SHUTTLE BOOSTER STRUCTURAL DESIGN APPROACH	272
6.4	RECOMMENDED CHANGES TO DESIGN CRITERIA	272
7	REFERENCES	281

## LIST OF FIGURES

Figure		Page
1-1	Safe-Life/Fail-Safe Criteria Identification Logic for Space Shuttle Booster	5
2-1	Elements of Space Shuttle Operations	8
2-2	Booster Flight Profile	9
2-3	Ascent Trajectory Parameters	10
2-4	Booster Entry Trajectory Key Events	10
2-5	B-9U Delta Wing Booster Vehicle Configuration	12
2-6	B-9U Delta Wing Booster Three View	13
2-7	B-9U Booster Inboard Profile	15
2-8	B-9U Booster Body Structure	17
2-9	B-9U Intertank Section	18
2-10	B-9U Thrust Structure	19
2-11	B-9U Forward Skirt Structure	20
2-12	B-9U Wing General Arrangement	22
2-13	B-9U Nacelle Location, Retracted and Deployed Positions	23
2-14	B-9U Canard Structure	23
2-15	B-9U Vertical Tail Structure	24
2-16	B-16B Booster Basic Configuration	27
2-17	B-16B Booster Safe-Life Wing Concept	31
2-18	B-16B Booster Fail-Safe Wing Concept	32
2-19	Mission Center of Gravity Travel Check	38
2-20	B-9U Booster Peak Limit Load Intensities	44
2-21	LH <sub>2</sub> Tank Gage Pressures vs Tank Station	47
2-22	LO <sub>2</sub> Tank Gage Pressures vs Tank Station	47
2-23	Wing Loads (Limit)	48
2-24	Canard Loads (Limit)	49
2-25	Vertical Tail Loads (Limit)	49
2-26	Design Temperatures	50
2-27	Temperature and Materials Distribution	50
2-28	Acoustics on Launch Pad	51
2-29	Contours of Equal Overall Sound Pressure Levels, Wing	51
2-30	Contours of Equal Overall Sound Pressure Levels, Vertical Tail	52
2-31	B-9U Wing Load Spectra	54
2-32	B-9U Vertical Tail Load Spectra	55
2-33	B-9U Fuselage Station 2600 Load Spectra	56
2-34	B-9U Orbiter Forward Attachment Load Spectra	57
2-35	B-9U Orbiter Aft Attachment Load Spectra	58
2-36	Total Mean Booster Main Engine Thrust	59

# LIST OF FIGURES, Contd

Figure		Page
2-37	Thrust Spectrum (One Flight)	59
2-38	Booster Main LH <sub>2</sub> Tank Pressure Schedule	60
2-39	Booster Main LO <sub>2</sub> Tank Pressure Schedule	60
2-40	Typical Fatigue Test Spectrum for Body Structure	69
2-41	Typical Fatigue Test Spectrum for Aerodynamic Surfaces	71
2-42	Structural Element Non-Destructive Testing Plan	73
3-1	LO <sub>2</sub> Tank Plate-Stringer Sizing	91
3-2	LH <sub>2</sub> Tank Plate-Stringer Effective Thickness Versus Frame Spacing	99
3-3	Integral Tee Plate-Stringer, Optimization of Stringer Spacing and Height — 0.122 Inch Skin Thickness	100
3-4	Integral Tee Plate-Stringer, Optimization of Stringer Spacing and Height — 0.162 Inch Skin Thickness	101
3-5	Vertical Tail Configuration	108
3-6	Thrust Structure Finite Element Model	110
3-7	Aft Thrust Bulkhead Model, Station 3913	111
3-8	Forward Thrust Bulkhead Model, Station 3831	112
3-9	Backup Frame Model, Station 3756	113
3-10	Y-Ring Tank Frames Model	114
3-11	Thrust Beam Models	115
3-12	Thrust Structure Model Elements	116
3-13	Critical Applied Loads (Ultimate), Aft Orbiter Attachment Frame	125
3-14	Aft Orbiter Attachment Frame Element Identification	126
3-15	B-9U Wing Structural Simulation Model	128
3-16	Idealized Integrally Stiffened Skin Elements (Three-Spar, Swept-Wing B-16B Booster)	134
3-17	Estimated Fatigue Curves for 2219-T87 Aluminum Alloy at Room Temperature with $K_t = 3.0$	148
3-18	Fatigue Curves for Annealed Ti-6Al-4V at Room Temperature with $K_t = 3.0$	149
3-19	Fatigue Curves for Annealed Ti-6Al-4V at 650°F with $K_t = 3.0$	149
3-20	Cyclic Flaw Growth Rate for 2219-T87 Aluminum Alloy at Room Temperature	170
3-21	Sustained Flaw Growth Rate for 2219-T87 Aluminum Alloy at Room Temperature	171
3-22	Cyclic Flaw Growth Rate for 2219-T87 Aluminum Alloy at -320°F	172
3-23	Sustained Flaw Growth Rate for 2219-T87 Aluminum Alloy at -320°F	173
3-24	Cyclic Flaw Growth Rate for Ti-6Al-4V (ELI) Annealed Titanium Alloy at Room Temperature	174

# LIST OF FIGURES, Contd

Figure		Page
3-25	Sustained Flaw Growth Rate for Ti-6Al-4V(ELI) Annealed Titanium Alloy at Room Temperature	175
3-26	Crack Growth in LO <sub>2</sub> Tank for Pressure Load Spectrum (Surface Flaw, $a/2c = 0.1$ )	181
3-27	Crack Growth in LO <sub>2</sub> Tank for Pressure Load Spectrum (Surface Flaw, $a/2c = 0.4$ and Equivalent Through Crack)	182
3-28	Crack Growth in LH <sub>2</sub> Tank for Pressure Load Spectrum (Surface Flaw, $a/2c = 0.1$ )	187
3-29	Crack Growth in LH <sub>2</sub> Tank for Pressure Load Spectrum (Surface Flaw, $a/2c = 0.4$ and Equivalent Through Crack)	187
3-30	Crack Growth in Titanium Wing Spar Caps	190
3-31	Stress Intensity Factor ( $\Delta K_I$ ) Multiple for a Crack Initiating at a Fastener Hole	194
3-32	Critical Flaw Size Versus Stress Level for the Titanium Wing Spar Caps	196
3-33	Allowable Maximum Operating Stress Level versus the Number of Flights to Failure (Safe-Life) for the Titanium Wing Spar Caps	197
3-34	Crack Growth in the Vertical Tail Skin	201
3-35	Crack Growth in the Titanium Thrust Beam Caps (Flow Configuration — Corner Crack)	202
3-36	Crack Growth in the Titanium Thrust Beam Caps (Flow Configuration — Crack Emanating from a Hole)	203
3-37	LO <sub>2</sub> Tank Crack Arrest Effectiveness of Graphite/Epoxy Tear Straps, 36-inch Strap Spacing	208
3-38	LO <sub>2</sub> Tank Crack Arrest Effectiveness of Graphite/Epoxy Tear Straps	209
3-39	LH <sub>2</sub> Tank, Crack Arrest Effectiveness of Graphite/Epoxy Test Straps	212
3-40	LH <sub>2</sub> Crack Arrestment by Integral Stringers for Longitudinal Loading	213
3-41	Relationship Between Stress Intensity Factor and Crack Length for Panels with Integral Stringers	222
3-42	B-16B Three-Spar Wing Lower Surface Stress Intensity Factor Versus Crack Length	224
3-43	Vertical Tail Box, Stress Intensity Factor Versus Crack Length	226
3-44	Comparison of Crack Growth in Aluminum and Titanium Wing Span Caps	235
3-45	Comparison of Crack Growth in Titanium and Aluminum Thrust Beam Caps (Flaw Configuration — Corner Crack)	237
3-46	Comparison of Cyclic Crack Growth Rate in Titanium and Aluminum Material at Room Temperature	238
5-1	Aft Orbiter Support Frame Design Concepts	257

## LIST OF TABLES

Table	Page
2-1 Data Comparison of Models B-9U and B-16B	29
2-2 Booster Materials	33
2-3 Weight Summary	35
2-4 B-16B Wing Weight Summary	36
2-5 Sequence Mass Properties Statement, B-9U Delta Wing Booster	39
2-6 Design Criteria	40
2-7 Summary of Booster Design Conditions and Loads	42
2-8 Summary of Design Conditions	43
2-9 Booster/Orbiter Interconnection Loads	46
2-10 External Noise Levels on Booster Structure	52
2-11 Typical Shuttle System Maintenance/Support Actions by Level	76
2-12 Maintenance Manhours/Turnaround Study of Baseline Booster Components	78
2-13 Baseline B-9U Program — WBS Level 4 Summary Costs (\$ million)	83
2-14 Baseline B-9U Structural Group Cost Calculation (\$ million)	84
3-1 LH <sub>2</sub> Tank Critical Design Loads (Ultimate)	102
3-2 LH <sub>2</sub> Tank Plate Stringer Sizing	105
3-3 Thrust Structure Model Coordinates	117
3-4 Thrust Structure Ultimate Design Loads	119
3-5 Thrust Structure Model Element Loads, Areas, Thicknesses, Stresses, and Weights	120
3-6 Aft Orbiter Attachment Frame, Cap Axial Loads and Cross-Sectional Areas	127
3-7 Aft Orbiter Attachment Frame, Web Shear Flows and Thicknesses	127
3-8 Spar Cap Loads, B-9U Wing	129
3-9 Sizing Data — Spar No. 1 (WS 515), B-9U Wing	130
3-10 Sizing Data — Spar No. 2 (WS 633), B-9U Wing	131
3-11 Sizing Data — Spar No. 3 (WS 751), B-9U Wing	131
3-12 Sizing Data — Spar No. 4 (WS 941), B-9U Wing	132
3-13 Sizing Data — Spar No. 5 (WS 1042), B-9U Wing	133
3-14 Input, Wing Box Multiple Station Sizing Program, B-16B Three-Spar Wing	138
3-15 Output, Final Sizing Run, B-16B Three-Spar Wing	139
3-16 LO <sub>2</sub> Tank Pressure Spectrum and Damage Analysis at Upper Dome Equator	150
3-17 LH <sub>2</sub> Tank Pressure Spectrum and Damage Analysis at Upper Dome Equator	151

# LIST OF TABLES, Contd

Table		Page
3-18	Fuselage Load Spectrum — Station 2600 Bottom Centerline	152
3-19	Fuselage Damage Analysis — Station 2600 Bottom Centerline	155
3-20	B-9U Wing Load Spectrum	157
3-21	B-9U Wing Spar Caps Fatigue Damage Analysis	160
3-22	B-9U Vertical Tail Load Spectrum	163
3-23	B-9U Vertical Tail Fatigue Damage Analysis	165
3-24	Thrust Beam Cap Fatigue Damage Analysis	166
3-25	Aft Orbiter Support Frame Load Spectrum and Damage Analysis	167
3-26	Wing Spar Cap Loading Spectrum	189
3-27	Vertical Tail Loading Spectrum	198
3-28	Aft Orbiter Support Frame Loading Spectrum	204
3-29	Internal Loads — Ultimate Versus Fail Safe — B-9U Wing	215
3-30	Margins of Safety for Baseline Structure, and Area Increases for Fail-Safe Design, B-9U Delta Wing	220
3-31	Percent Stiffening and Gross Tension Stresses in B-16B Wing Lower Surface	222
3-32	Thrust Structure Fail-Safe Analysis	227
3-33	B-9U Wing Box Fatigue Analysis — 2219 Aluminum Alloy	233
3-34	Thrust Beam Cap Damage Analysis, 2219 Aluminum Alloy	236
4-1	Development of Safe-Life Booster Design — B-9U Configuration	240
4-2	Development of Safe-Life Booster Design — B-16B Configuration	241
4-3	Costs for Safe-Life Tests	244
4-4	Maintenance Manhours/Turnaround Safe-Life Concept	248
4-5	Booster Program Cost Penalties, Safe-Life Design	252
5-1	Development of Fail-Safe Booster Design — B-9U Configuration	254
5-2	Development of Fail-Safe Booster Design — B-16B Configuration	255
5-3	Aft Orbiter Support Frame Modifications for Fail-Safe Capability	256
5-4	Costs for Fail-Safe Tests	259
5-5	Maintenance Manhours/Turnaround, Fail-Safe Design	261
5-6	Booster Program Cost Penalties, Fail-Safe Design	263
6-1	Summary of Analytical Results for Baseline Booster Vehicles	266
6-2	Weight Impact of Safe-Life/Fail-Safe Design Approaches (Pounds of Structure Added)	269
6-3	Performance Impact of Safe-Life/Fail-Safe Design Approaches (Pounds of Payload Lost)	270
6-4	Cost Impact of Safe-Life/Fail-Safe Design Approaches ( $\Delta$ \$ on Total Program)	270
6-5	Summary of Fatigue Life and Safe-Life of Titanium and Aluminum Components	271



## **SUMMARY**

An investigation was made to determine the effects of (1) a safe-life design approach and (2) a fail-safe design approach on the space shuttle booster vehicle structure, and to recommend any changes to the structural design criteria document, NASA SP-8057, that might appear advisable as a result of this study. Two configurations of the booster vehicle were considered, one incorporating a delta wing (B-9U configuration) and the other a swept wing (B-16B configuration). Advantage was taken of Phase B studies already made by Convair Aerospace on the space shuttle booster. These studies provided extensive data on structural arrangements, member sizing, weight, cost, and other aspects of design, construction, and operation of the space shuttle booster.

Several major structural components of the booster were studied in depth, each being examined to determine the fatigue life, safe-life, and fail-safe capabilities of the baseline design. Each component was further investigated to determine the practicability of applying a safe-life or fail-safe design philosophy, the changes such design approaches might require, and the impact of these changes on weight, cost, development plans, and performance.

It was found that:

- a. Conventional fatigue is not a critical design condition for the booster structure because of its short design service life.
- b. Most components investigated showed safe-lives in excess of the 100 mission design level. The wing box, however, showed a short safe-life of three missions in both the B-9U delta and the B-16B swept configurations with an initial flaw of the maximum size permitted by NDE methods. The short life is ascribed to the severity of the loading spectrum and the criticality of the assumed flaw configuration.
- c. The baseline propellant tanks are not fail-safe. Moreover, attempts to provide fracture arrest capability by means of crack stoppers showed prohibitive weight increase.
- d. The B-9U delta wing and the thrust structure are shown to require some increase in section to attain full fail-safe capability, while a change in basic configuration appeared advisable in the case of the aft orbiter support frame if fail-safe design is required. The other components investigated were shown to have a high degree of fail-safe capability in their baseline configuration.

- e. The weight impact of the safe-life or fail-safe design approaches for the components investigated was small, being 0.5 to 1.0 percent of their baseline weight.
- f. The choice of a safe-life or fail-safe design approach did not exert a strong influence on booster cost or performance.

Finally, a number of modifications to NASA SP-8057, "Structural Design Criteria Applicable to a Space Shuttle," are proposed, based primarily on the study results.

## SECTION 1

### INTRODUCTION

#### 1.1 SPACE SHUTTLE REQUIREMENTS AND CRITERIA DEVELOPMENT

The space shuttle system represents a major advance in structural technology. It embodies the characteristics of aircraft, spacecraft, and launch vehicles and their associated severe environments and loads, long mission life, high-reliability requirement, and considerations for low cost and weight.

New requirements (Reference 1) for "fracture control" to prevent catastrophic service failures of pressure vessels, pressurized structures, and other primary structural components necessitate that the structure be assumed to contain initial flaws prone to brittle fracture. For space shuttle vehicles it is imperative that the need for damage tolerance be recognized and provided for in the initial design. Prediction of residual strength and residual life assuming damaged structural elements must supplement conventional static strength and fatigue analysis. Materials and structural arrangement selected must provide sufficient residual strength and life to allow the vehicle to remain flightworthy to the next major structural inspection after initiation of an unanticipated fatigue crack. In addition, the critical fatigue crack size must be large enough to be reliably detected by conventional inspection methods.

Preliminary structural design criteria (Reference 2) have been developed for the space shuttle system. These criteria were prepared by a committee formed from representatives of major aerospace companies with an interest in the space shuttle, and reviewed by NASA personnel experienced in structures technology. They are the required criteria to develop a successful space shuttle system as determined by the committee. A number of important structural criteria problems were identified by this activity, and the present study was directed toward providing greater insight into one of these problem areas: safe-life and fail-safe criteria.

Since the preliminary criteria developed in Reference 2 were based on past experience with either very short life aerospace systems (e.g., one-mission expendable spacecraft or launch vehicles) or very long life aircraft systems, it appeared prudent to re-examine the preliminary safe-life and fail-safe criteria and their weight, cost, and performance impact in the light of the anticipated space shuttle mission requirements. Such examination is the primary purpose of this study.

The emerging role of fracture mechanics as an engineering tool may have significant effects on the choice of safe-life or fail-safe criteria and design approaches on the

space shuttle. Similarly, non-destructive testing (NDT) capability can also introduce constraints. These disciplines are used in this study to determine these effects and to illustrate their potential usage.

## 1.2 SAFE-LIFE AND FAIL-SAFE DESIGN PHILOSOPHY

All vehicles are designed for fatigue life in excess of the expected service life; however, the approach to providing residual strength or residual life in structures in the event of induced or inherent damage can be provided by designing for fail-safe or safe-life. For example, in commercial transport aircraft where safety is of utmost concern, fail-safe capability is provided to the greatest possible extent. For military aircraft where performance is of primary concern, fail-safe capability is not provided where it would cost weight to do so, reliance being placed on the fatigue analysis and tests to screen out potential structural damage, and safe-life analysis of assumed defects is used to establish safe inspection intervals. For single mission launch vehicles and spacecraft, reliance is placed on safe-life analysis of assumed defects and proof tests of each article to provide safe-life in excess of the short service life.

Fail-safe design requires that the failure of any single structural component will not degrade the strength or stiffness of the remainder of the structure to the extent that the vehicle cannot complete the mission at a specified percentage of limit loads. Fail-safe design is normally achieved by providing structural redundancy and the means for arresting unstable crack growth. On the other hand safe-life design requires sufficiently low design stresses that catastrophic failures of critical structural components will not occur during a specified service life due to initiation and growth of fatigue cracks, or due to the growth of flaws and defects that already exist in the structure. The safe-life of a structure is usually taken as an arbitrary multiple or increment of the specified service life depending on whether the concern is for the initiation of fatigue cracks or the growth of existing defects. For fatigue the arbitrary multiple is usually taken as four service lives and for the growth of flaws or defects the increment is usually taken as the interval between major scheduled inspections.

Some confusion exists in Reference 2, the aerospace industry, and NASA regarding a precise definition of safe-life. Some engineers, particularly aircraft designers concerned with long life structures, define safe-life as the life of a component to the initiation of fatigue cracks. Other engineers, particularly those with fracture mechanics training, define safe-life as the component life for initial defects in the component to grow to critical size and failure. A third group, including the authors, feel that safe-life encompasses both of the above failure modes. For purposes of this report and to be consistent with the definitions of Reference 2, the following definitions are adopted:

- a. Fatigue life is the life of an unflawed structural component to the initiation of visible fatigue cracks.

- b. Safe life is the life for initial defects in a component to grow to a critical size for catastrophic failure.

### 1.3 OBJECTIVE OF STUDY

The present study was undertaken with the following objectives:

- a. To determine the extent to which application of the present space shuttle booster structural design criteria, as contained in Reference 2, results in safe-life (safe flaw growth) and fail-safe capabilities, as well as adequate fatigue life, in the space shuttle booster structure.
- b. To determine the effects of the safe-life or fail-safe design approaches, or combinations of these, on weight and cost of the space shuttle booster, including the sensitivities of quality control, operational, and maintenance plans to such approaches.
- c. To identify the optimum criteria for safe-life or fail-safe design, based on the impact of the criteria on weight, cost, and service life, giving consideration to vehicle performance and inspection intervals.
- d. To formulate specific revisions to Reference 2 as required to impose the optimum design criteria requirements identified in the study.
- e. To propose modification to the space shuttle operations plan, if the criteria revisions recommended are incompatible with the existing plan.

### 1.4 STUDY APPROACH

The study approach consisted of selecting two baseline heat-shield-protected space shuttle booster vehicles, performing safe-life and fail-safe analyses on them, and determining the impact of alternatively emphasizing safe-life or fail-safe design approaches on booster weights, performances, costs, and service lives. From these investigations the fatigue, safe-life, and fail-safe capability of the booster structural elements which resulted from following the preliminary structural design criteria of Reference 2 were determined. Also evaluated were the structural weight increases required to meet selected safe-life and fail-safe requirements and the adequacy of preliminary test and maintenance plans developed for the baseline boosters. With this background, recommended safe-life/fail-safe criteria and design approaches were developed.

Two booster configurations were studied because it was anticipated that the study results would be sensitive to configuration. For example, a delta wing configuration

would be less sensitive than a swept wing configuration to alternatively applied safe-life and fail-safe design approaches, because of the inherent fail-safe capability of the multispar delta wing. The two booster configurations selected are presented in Section 2; they are essentially the same booster with alternative delta and swept wing planforms.

The study did not include the orbiter because of lack of detail knowledge and data on the orbiter (i.e., Convair Aerospace's Phase B studies have been limited to the space shuttle booster) and the low funded effort. It is believed by the authors that the study results are generally applicable to the orbiter; however, caution should be exercised and orbiter studies accomplished before this conclusion can be fully satisfied.

The scope of the program also did not permit study of the entire booster structural system; however, the major structural components were studied. These included the main LO<sub>2</sub> and LH<sub>2</sub> propellant tanks, thrust structure, vertical tail box, aft orbiter support frame, and wing boxes, which represent approximately 45 percent of the booster primary structural weight, 25 percent of the booster dry weight, and 60 percent of the total booster structural system cost. Not included in the study were the thermal protection system, canards, crew cabin, intertank adapter and other miscellaneous sub-components.

The choice of safe-life or fail-safe design criteria and approaches have significant impact on development plans such as structural test and maintenance plans; these plans are examined in some detail in Sections 4 and 5. Other development plans such as operational plans, quality control plans, and engineering are not examined in detail because the effects of design criteria and approaches on these factors are not considered significant, or the impact is measured indirectly through the maintenance and test plans discussed above.

Cost effects are presented as increments to the preliminary cost estimates for the development, acquisition, and operation of the baseline booster systems. Total costs are also presented. Cost increments are calculated for any changes identified in the booster structure and weight, and for test hardware and manhours to accomplish additional tasks.

In Figure 1-1, the procedural path followed in accomplishing the study is diagrammed.

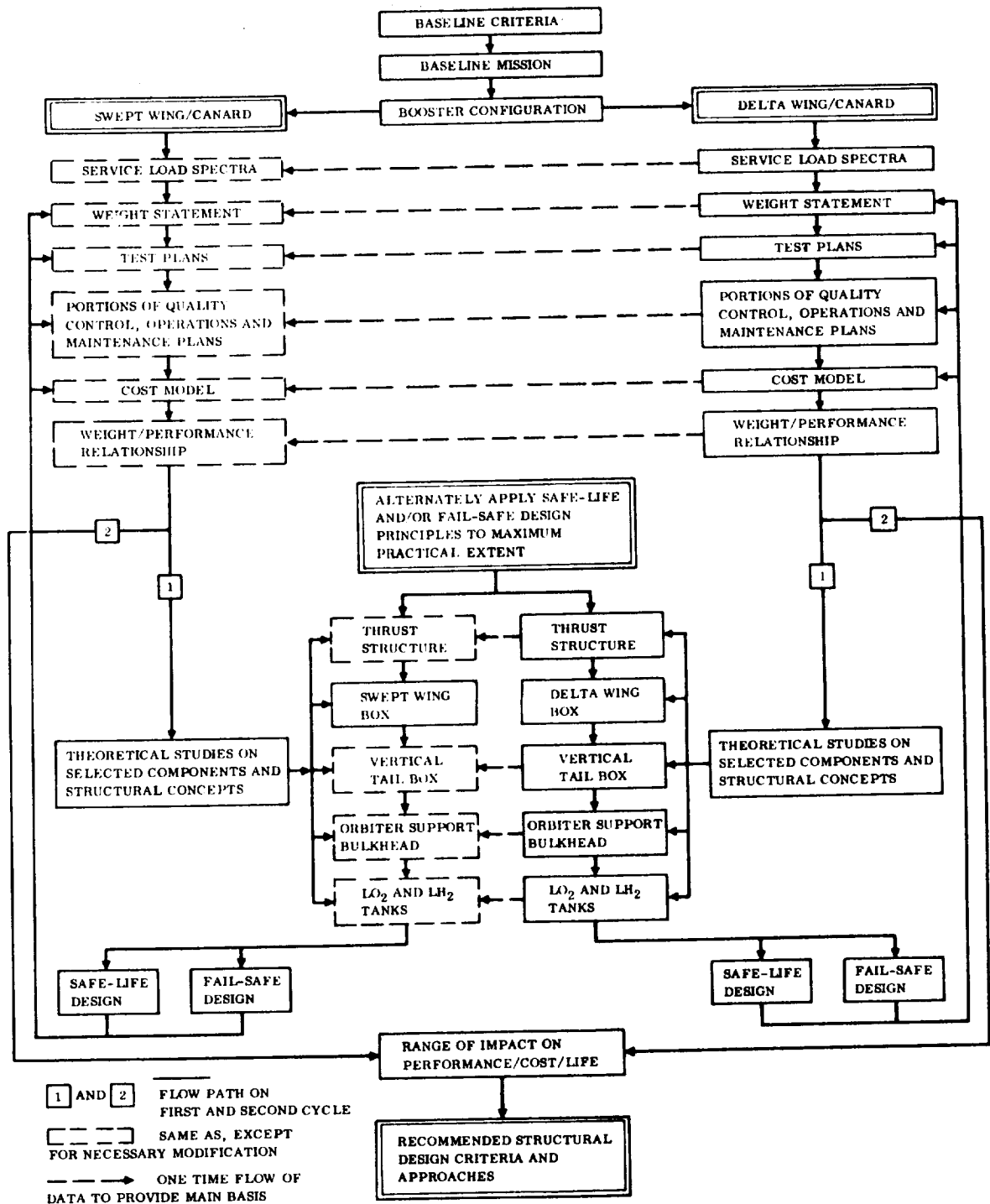


Figure 1-1. Safe-Life/Fail-Safe Criteria Identification Logic for Space Shuttle Booster





## SECTION 2

### BASELINE BOOSTER DEFINITION

#### 2.1 BOOSTER MISSION

The Space Shuttle Program is designed to provide a space transportation system capable of placing and/or retrieving payloads in earth orbit. The specific mission considered in this study consists of launching an orbiter vehicle into a 100 n.mi. south polar orbit from WTR with a 40,000-pound payload. These objectives are achieved using a two-stage (booster and orbiter) vehicle capable of boost and earth entry with cruise-back to a designated landing site. This cycle is accomplished with reasonable acceleration levels and shirt-sleeve cabin environment. The significant elements of this mission are ground operations, mating of booster and orbiter, launch followed by staging of the two vehicles, with the booster returning to the launch area and the orbiter continuing on to its prescribed orbit. A complete mission cycle is shown in Figure 2-1.

A typical mission flight profile for the booster is shown in Figure 2-2.

**2.1.1 ASCENT.** The ascent phase is defined as beginning with engine ignition and ending with the initiation of separation. In the ignition/lift-off sequence, the thrust rises to 50 percent of full thrust and holds at that level until main-stage in all engines can be verified and holddown release is verified. Upon verification, the thrust is increased at a controlled rate to 100 percent. The vehicle lift-off occurs when the thrust-to-weight ratio (T/W) is greater than 1.

After the vehicle has cleared the service towers, the vehicle is oriented to the correct azimuth and pitch to provide the proper trajectory such that the vehicle assumes a wing-level, pilot-side-up attitude and correct azimuth. As propellant is depleted, along with increased thrust at altitude, the vehicle acceleration increases to 3 g. At this point, the main engines are throttled to maintain 3 g for crew comfort and vehicle design loads. Ascent phase is terminated by initiation of separation based on attainment of desired velocity or by indication of fuel depletion. Figure 2-3 gives a variety of ascent trajectory parameters. The booster weight decreases from 4,188,000 pounds at launch to about 808,000 pounds at separation, while achieving a velocity of 10,824 fps at an altitude of 244,784 feet. After separation the orbiter continues on its mission and the booster positions itself for entry.

**2.1.2 ENTRY.** The entry mode for the booster is a supersonic gradual transition. High-lights of the entry are shown in Figure 2-4. During the first 40 seconds after staging the booster pitches to 60 degrees angle of attack and banks to 48 degrees. That

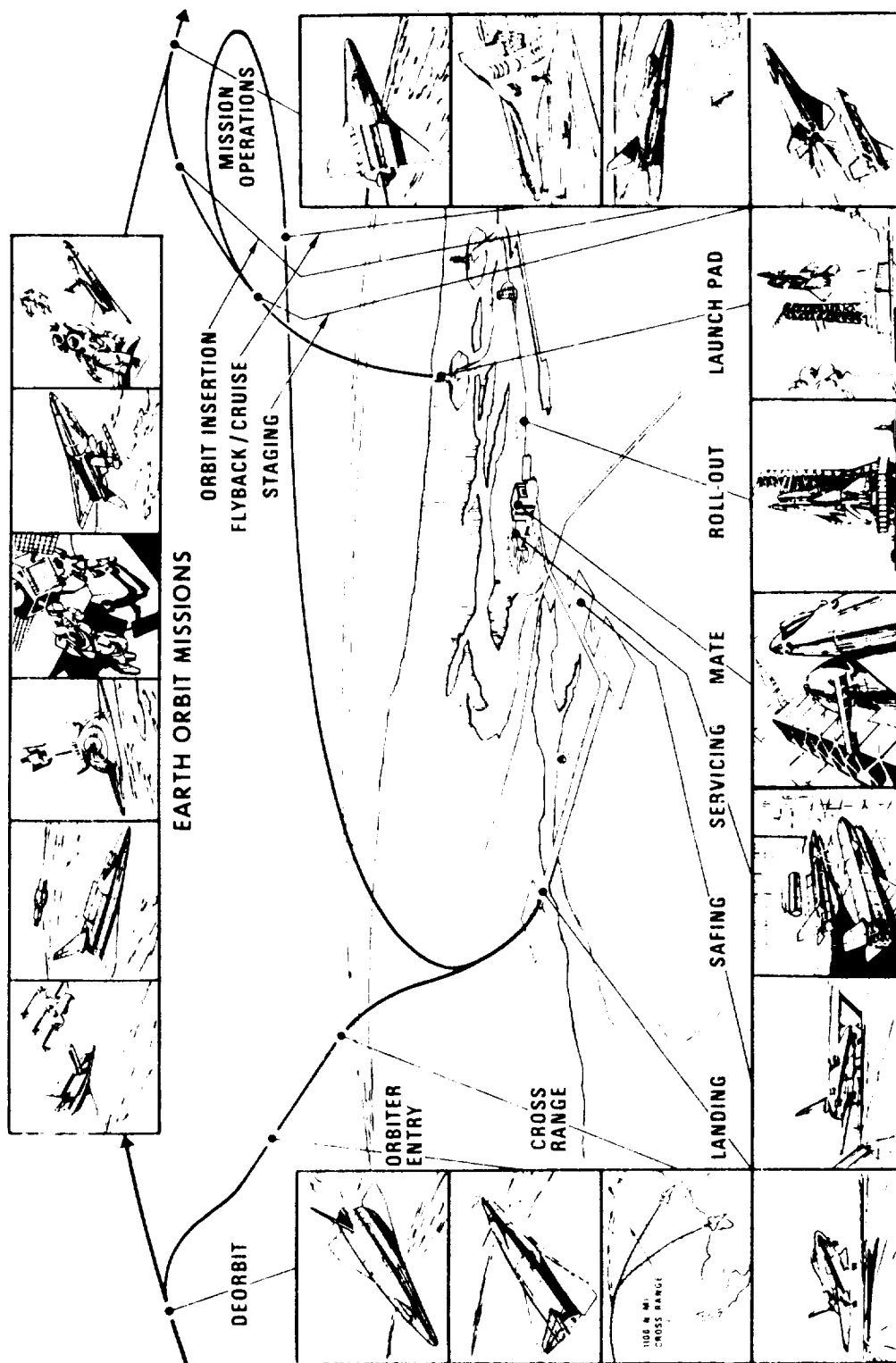


Figure 2-1. Elements of Space Shuttle Operations

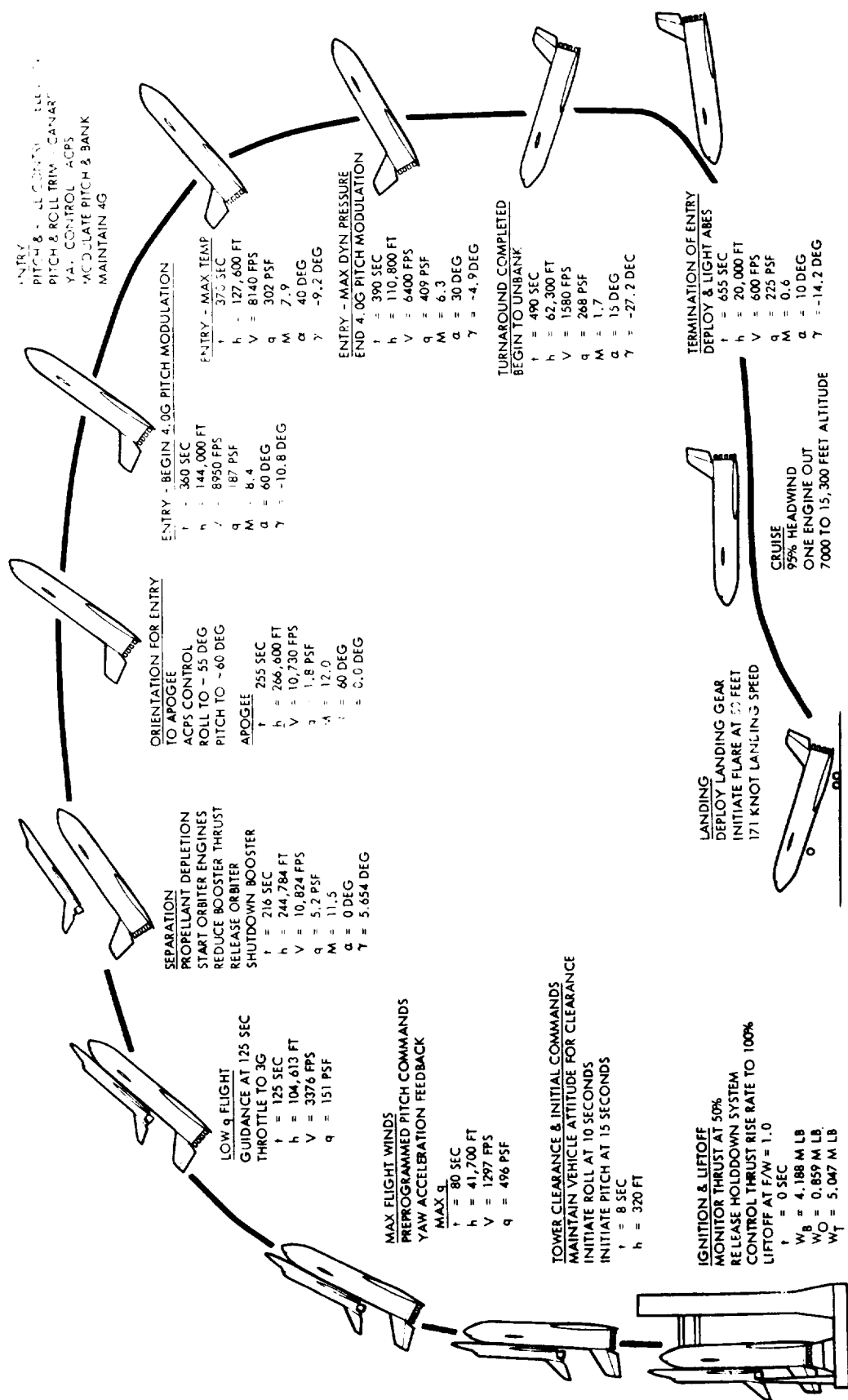


Figure 2-2. Booster Flight Profile

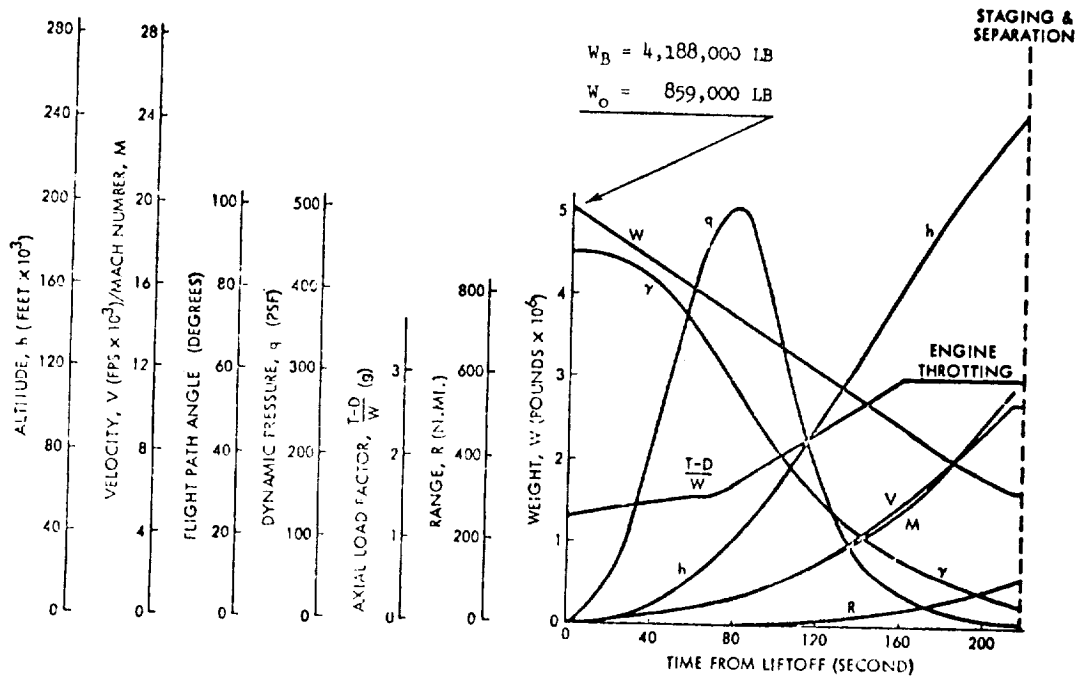


Figure 2-3. Ascent Trajectory Parameters

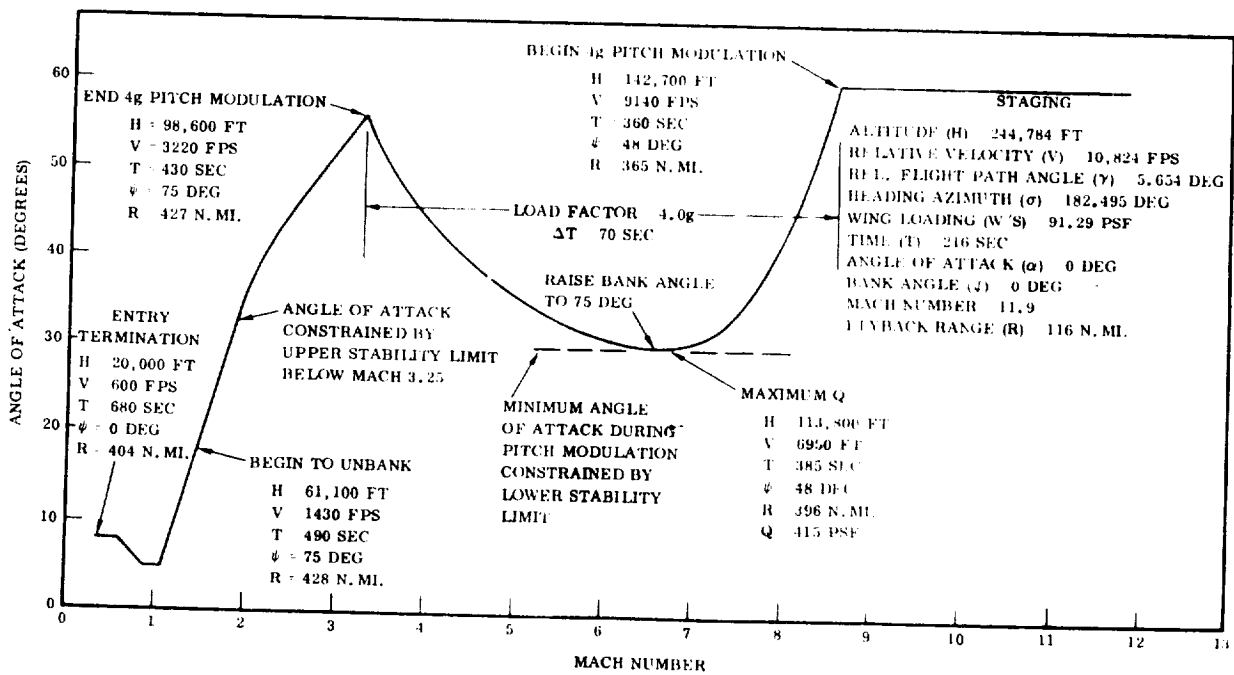


Figure 2-4. Booster Entry Trajectory Key Events

attitude is maintained until the resultant load factor reaches 4.0 g, occurring at Mach 8.4 and 144,000 feet altitude. Pitch modulation starts at this time to keep from exceeding 4.0 g. The lower stability limit constrains the angle of attack from going below 30 degrees during this maneuver. Upon reaching 30 degrees, the bank angle is raised to 75 degrees, which is held until the vehicle has completed its turn. A maximum  $q$  of 409 psf is reached at Mach 6.3 and 110,800 feet altitude. By Mach 3.25, the angle of attack has returned to 56 degrees. Beginning there, the angle of attack is constrained by the upper stability limit, reducing to 5 degrees at Mach = 1.1. When the booster reaches 20,000 feet, the flyback range is 404 n.mi. At the completion of the entry phase the gross weight of the booster has decreased slightly to about 787,000 pounds.

**2.1.3 ATMOSPHERIC FLIGHT.** At approximately 20,000 feet, the air-breathing engines are deployed and the return cruise is initiated.

The vehicle descends to approximately 13,000 feet and is flown at the altitude that is for best cruise specific range (maximum n.mi. per pound of fuel) for the required flyback range of 404 n.mi. Landing is based on a touchdown speed at the trimmed power-off  $C_L$  for an angle of attack of 14 degrees. The landing distance varies with the vehicle gross weight, but with a touch down weight of 628,000 pounds, about 5625 feet are required for landing over a 50-foot obstacle. This distance is for a standard day condition at sea level using braking on a dry concrete runway.

## 2.2 BOOSTER CONFIGURATIONS

As discussed in Section 1.4, two booster configurations are studied to determine the effect of configuration on safe-life/fail-safe design criteria and related weight, performance, and cost impact.

**2.2.1 B-9U DELTA WING BOOSTER.** The B-9U booster is a low, delta wing vehicle with a single vertical tail and a small canard surface mounted forward above the body centerline. The body is basically a cylinder with fairings added to streamline the intersections with the aerodynamic surfaces. Figure 2-5 shows a general view of the delta wing booster.

The baseline booster configuration consists of cylindrical tanks to contain the launch propellants and to serve as the structural backbone. Surrounding the basic body structure is an outer heat shield assembly that provides the protective layer against aerodynamic heating and an aerodynamic surface for the body. This aerodynamic surface varies from a round body section at the nose to a flat-bottomed section at the delta wing, which is attached to the underside of the body structure. The delta wing, with its elevons, canards, and the vertical tail, provides the aerodynamic surfaces required for stability and control for both supersonic and subsonic flight.

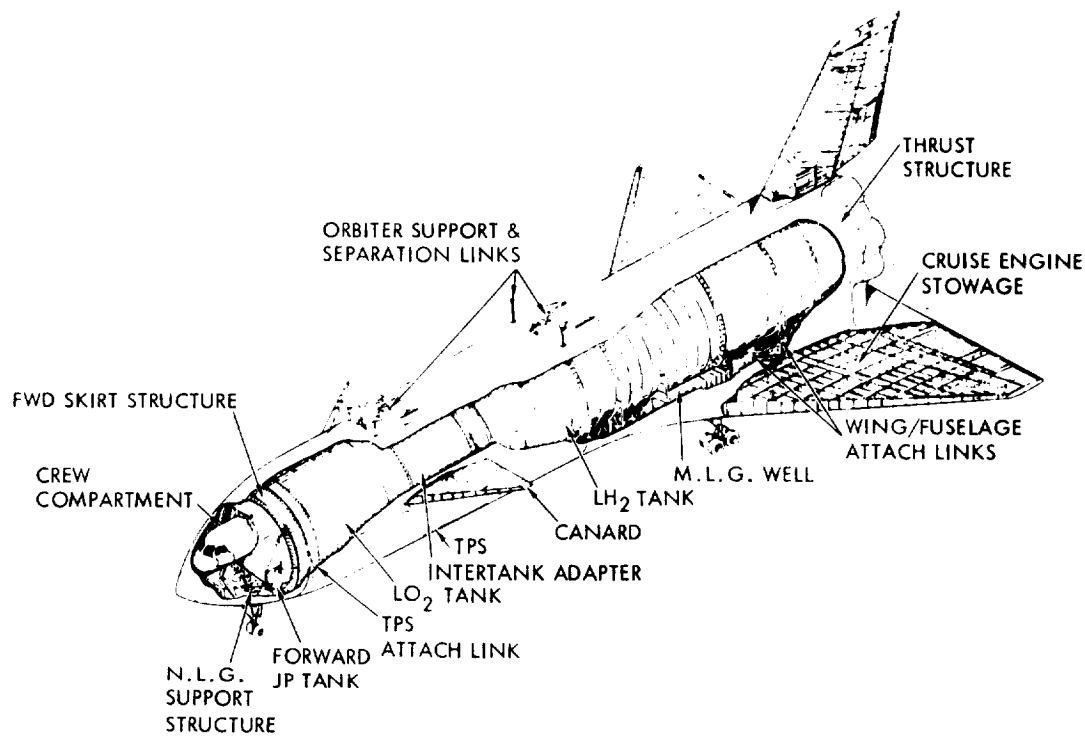


Figure 2-5. B-9U Delta Wing Booster Vehicle Configuration

For the vertical launch, mated with the orbiter, the booster thrust is provided by 12 main propulsion engines, with a nominal thrust of 550,000 pounds per engine, that burn liquid hydrogen and oxygen and are arranged in the aft end of the vehicle.

Control of the vehicle during powered ascent is provided by gimballing the main engines for thrust vector control and by using elevons for additional roll control. Subsonic cruise thrust for flyback after a space mission or for ferry flight is provided by 12 air-breathing engines mounted in nacelles. These engines are normally stowed within the wing and body structure envelope during the vertical flight and entry.

Attitude control outside the earth's atmosphere is provided by the attitude control propulsion system (ACPS) engines installed on the fuselage and wings. The ACPS engines use  $\text{LO}_2/\text{LH}_2$  propellants and provide 2100 pounds thrust each.

Landing is accomplished using a conventional tricycle landing gear, including two 4-wheel-bogie main landing gear assemblies and a dual-wheel steerable nose gear assembly.

The booster incorporates a mating and separation system on its top surface to support the orbiter during vertical flight and to perform the separation of the two vehicles. Figure 2-6 shows a three-view drawing of the booster basic configuration.

Internally the booster is arranged with the  $\text{LO}_2$  tank forward and the  $\text{LH}_2$  tank aft. The selection of cylindrical tanks with separate, state-of-the-art bulkheads, and of cylindrical intertank section and thrust barrel all combined into a primary load-carrying structure, was made to maintain simplicity of the design and manufacture, to increase confidence, and to reduce development risk.

The tanks have ellipsoidal bulkheads with radius-to-height ratios equal to  $\sqrt{2}$  to minimize hoop compression effects. The tanks are of aluminum alloy, with longitudinal integral T-stringers. They provide the primary load-carrying structure of the booster as well as functioning as pressure vessels. The tank diameters are 33 feet. All structural frames are external to the main tanks. The  $\text{LO}_2$  tank is 667 inches long, as shown in Figure 2-7. The  $\text{LO}_2$  tank is not insulated.

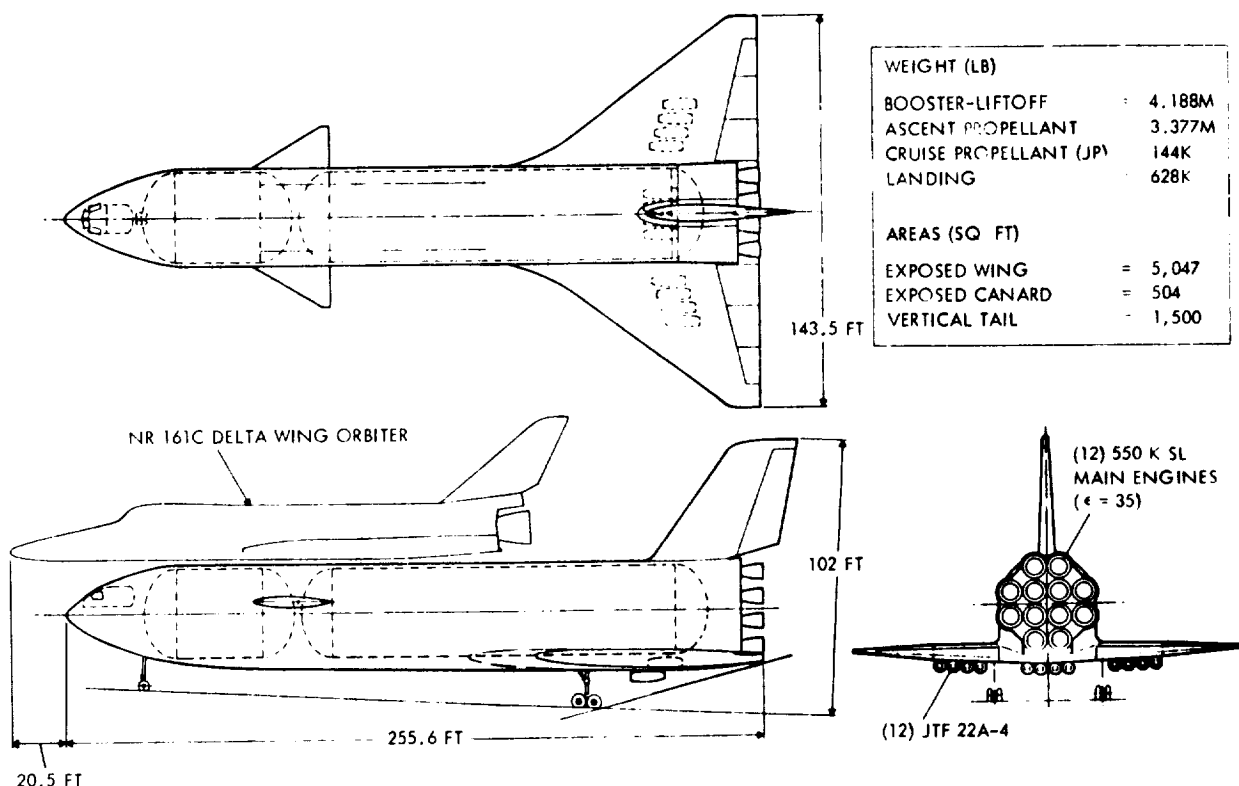


Figure 2-6. B-9U Delta Wing Booster Three View

Four main  $\text{LO}_2$  lines are routed through the lower body main structure/heat shield interspace, past the main landing gear and aft to the vehicle base.

The  $\text{LH}_2$  tank is similar in geometry to the  $\text{LO}_2$  tank, except for the length of 1779 inches, as shown in Figure 2-7. Figure 2-8 shows the body structure.

For the mixture ratio of 6:1, with added volume of 7.1 percent (for ullage, potential tanking at minimum specific impulse, and for internal insulation) a total  $\text{LH}_2$  tank volume of 120,160 cubic feet results; for the  $\text{LO}_2$  tank, which does not have any insulation, a factor of 4.5 percent is added to cover ullage and minimum specific impulse, for a tank volume of 40,900 cubic feet. The  $\text{LH}_2$  tank construction is similar to the  $\text{LO}_2$  tanks except that there are no anti-slosh baffles in the  $\text{LH}_2$  tank because the low density fuel does not require them. Internal insulation is used to reduce thermal shock at tanking and to reduce heat leaks and cryopumping potentials associated with external insulation. The basic structural external frames are increased in section modulus at the aft attach points to the orbiter and in the main landing gear and wing box attach link pickup points.

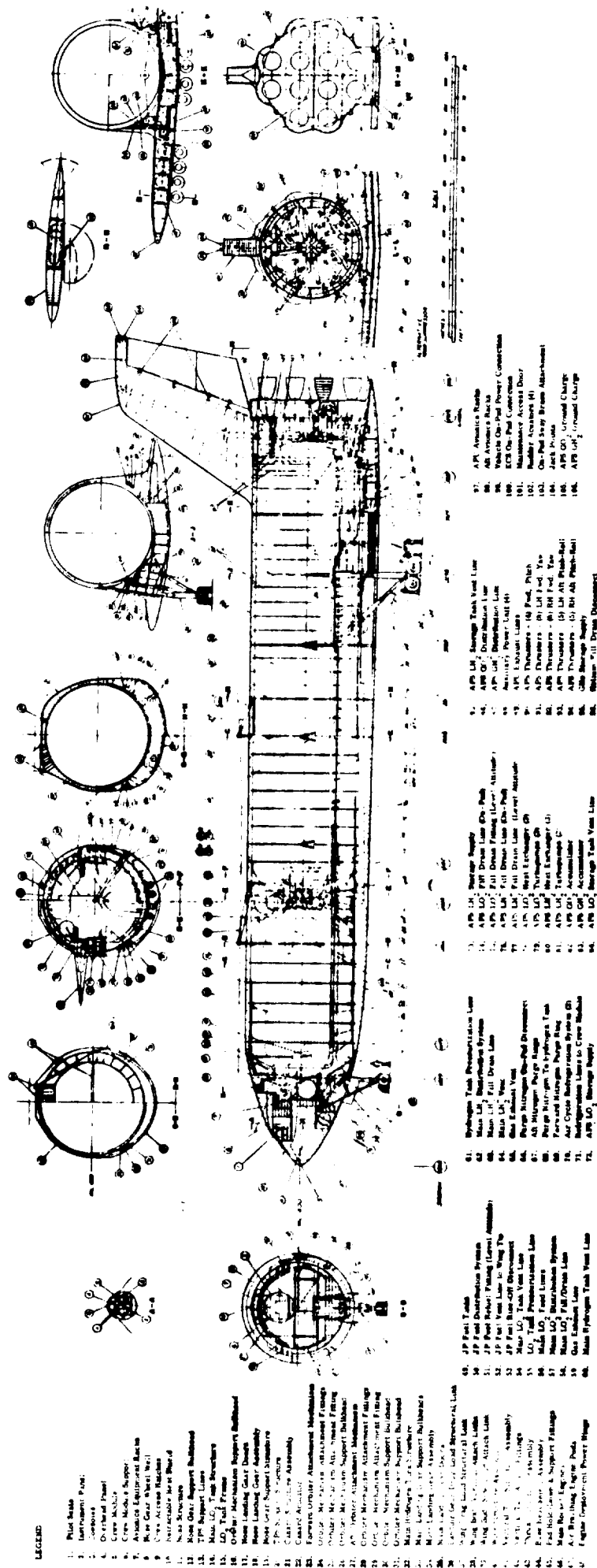
The tanks are joined by a cylindrical intertank section that supports the canard pivot and the forward attach links to the orbiter. The intertank section is shown in Figure 2-9.

The intertank section is a conventional skin-stringer-frame assembly with built-up frames to support the orbiter attach links and the canard pivot points. The  $\text{LO}_2$  lines run aft and occupy the lower intertank space. The canard pivot actuators are shown, four per side below the pivot point 50 inches above the body centerline. The intertank section contains the  $\text{LH}_2$  and  $\text{LO}_2$  tanks for the ACPS and auxiliary power unit (APU) supply. A single  $\text{LH}_2$  tank for both systems is provided. The orbiter forward attach points are at the aft  $\text{LO}_2$  dome/intertank joint and take the axial loads as well as pitch and side loads, while the aft attach points, which take pitch and sideloads only, are at Station 2666 in the  $\text{LH}_2$  tank region (Section G-G of Figure 2-7.)

The top of the booster is flat in the stage interface region to fair out the attach frames of the booster and to accommodate the booster linkage after separation. The booster/orbiter separation system is a linkage type using booster thrust and orbiter inertia to produce positive separation. It is selected as the only system with the present configuration that will operate feasibly in the case of high dynamic pressure separation, as is required by abort criteria. The orbiter is arranged piggyback on the booster. This mating was initially done to allow rollout of the mated configuration to the launch pad on the booster main gear.

The aft end of the  $\text{LH}_2$  tank picks up the cylindrical thrust skirt, which is also 33 feet in diameter and includes truss-type thrust beams that intersect to form the main







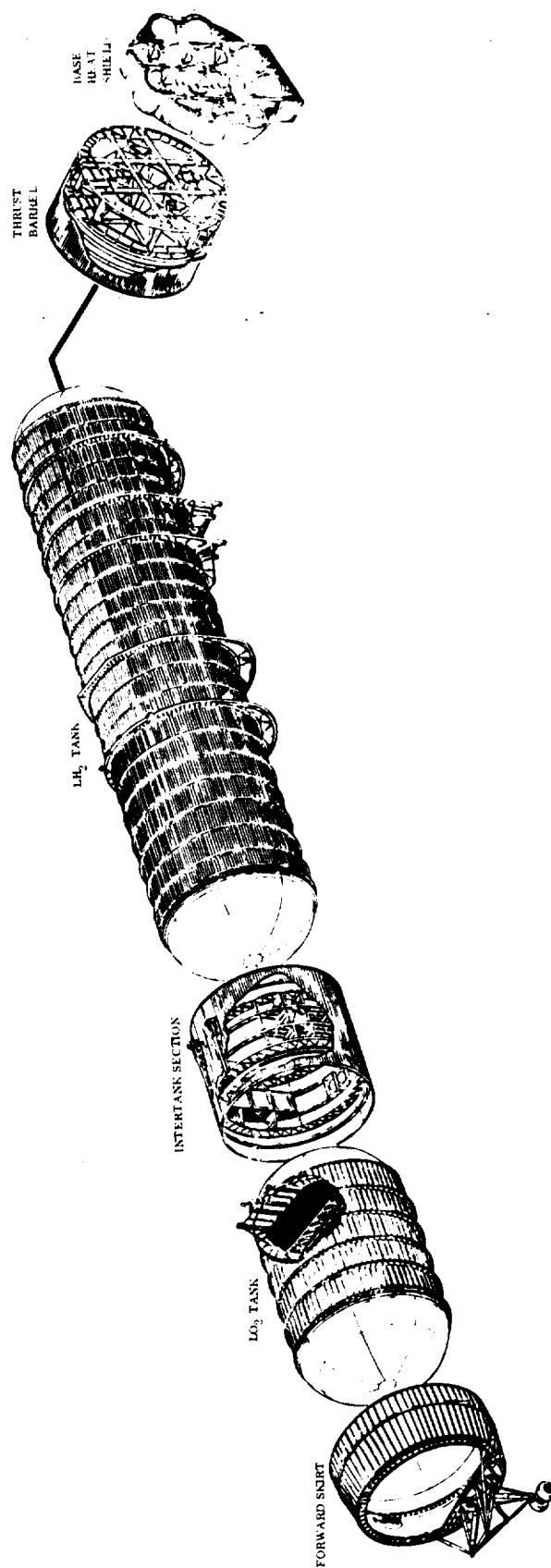


Figure 2-8. B-9U Booster Body Structure

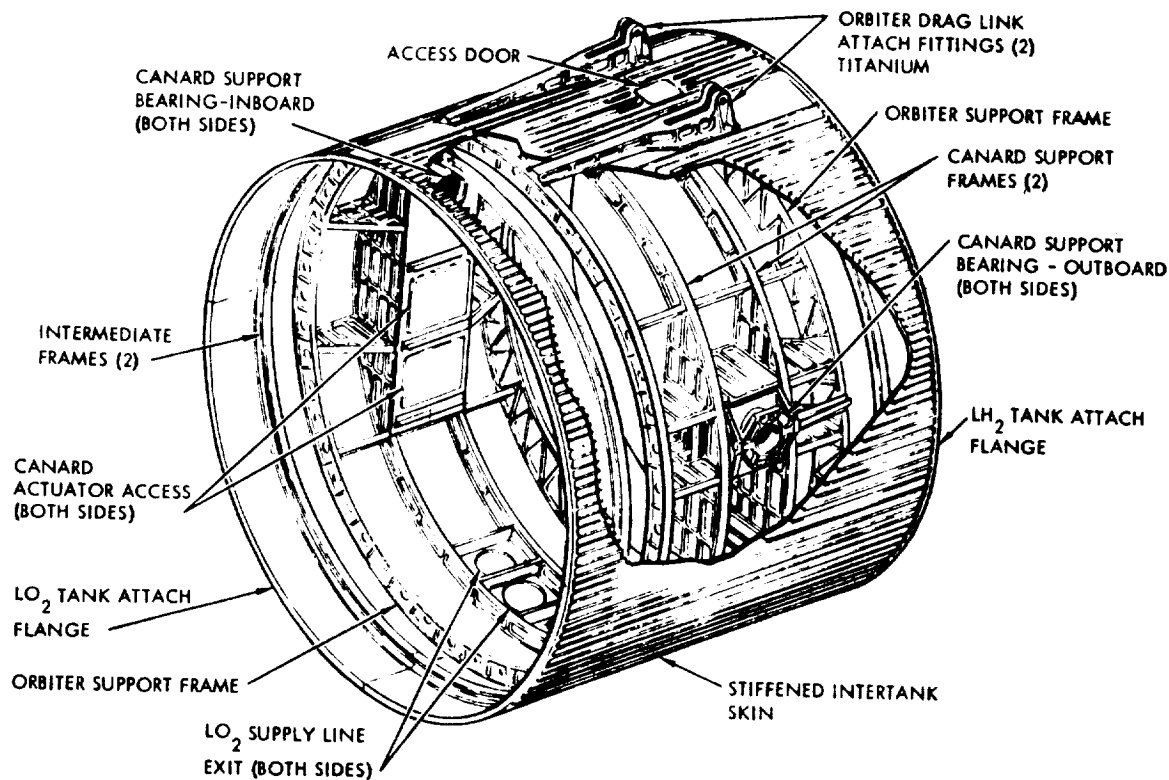


Figure 2-9. B-9U Intertank Section

engine thrust pad/gimbal support points. The thrust structure is a structurally connected titanium truss beam assembly with intersecting parallel vertical and horizontal beams, as shown in Figure 2-10. The beam intersections support the gimbal pad points. The beams are constrained by peripheral frames that transfer the loads into the cylindrical thrust skirt. The LH<sub>2</sub> tank exits via a vortex baffle into a sump that branches into 12 fuel ducts to each engine. The engines have a fixed, low-pressure pump attached to the booster structure and a high-pressure pump on the engine. This arrangement allows the feed lines traversing the gimbal point to be of reduced diameter, eliminating the need for heavy pressure volume compensating ducts, and facilitating gimbaling to the required  $\pm 10$  degrees. The four LO<sub>2</sub> lines branch at the aft end of the booster into three lines each to serve the 12 engines. The engine propellant inlets and thrust structure are arranged for acceptable clearance in the selected pattern. The LO<sub>2</sub> lines are designed to have equal lengths from tank exit to pump inlet to minimize residuals. Each individual propellant feed line has a pre valve for a total of 12 for LO<sub>2</sub> and 12 for LH<sub>2</sub>.

The aft skirt that flares out for the rocket pump packages is an extension of the thermal protection system (TPS). The fairing is pocketed to accommodate the four support and

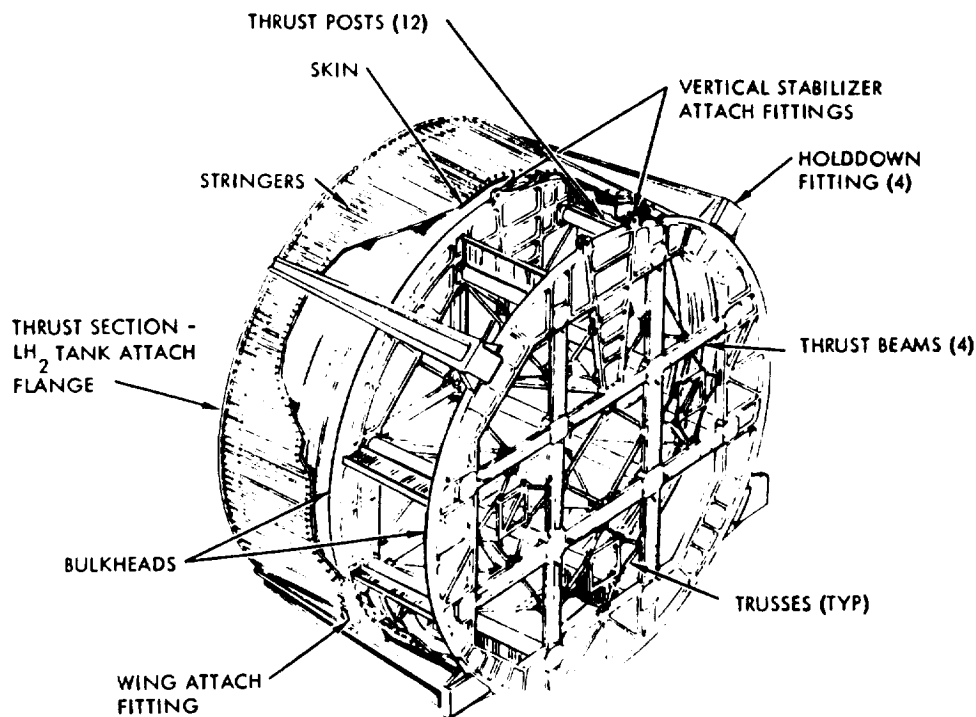


Figure 2-10. B-9U Thrust Structure

hold-down longerons that transmit their axial load directly into the thrust barrel. The external skirt that protects the thrust structure and engine pump packages from thermal and aerodynamic loads is shaped to minimize booster base area as is seen in view M-M of Figure 2-7. The base heat shield consists of corrugated sheet with internal insulation. The heat shield is located in a plane through the nozzle throats of the main engines. Each engine has a spherical radius collar at the throat that wipes a matching hole in the heat shield to allow gimbal motion while maintaining a seal. The base heat shield is penetrated by fill-and-drain lines and pressurization-and-purge lines. Electrical and other service disconnects are located as shown. The JP tank will be pressure fueled via a single point in the upper surface of the wing root.

The forward end of the  $\text{LO}_2$  tank supports a tapered skirt that terminates in a bulkhead that supports the nose landing gear. See Figure 2-11. The main landing gear is supported from trunnion points on external frames attached to the  $\text{LH}_2$  tank. As shown in Figure 2-7, the main gear retracts forward into the wing root fillet region. The main gear bogies incorporate 60 x 20 inch 40 PR tires. The nose gear has dual 47 x 18 inch tires.

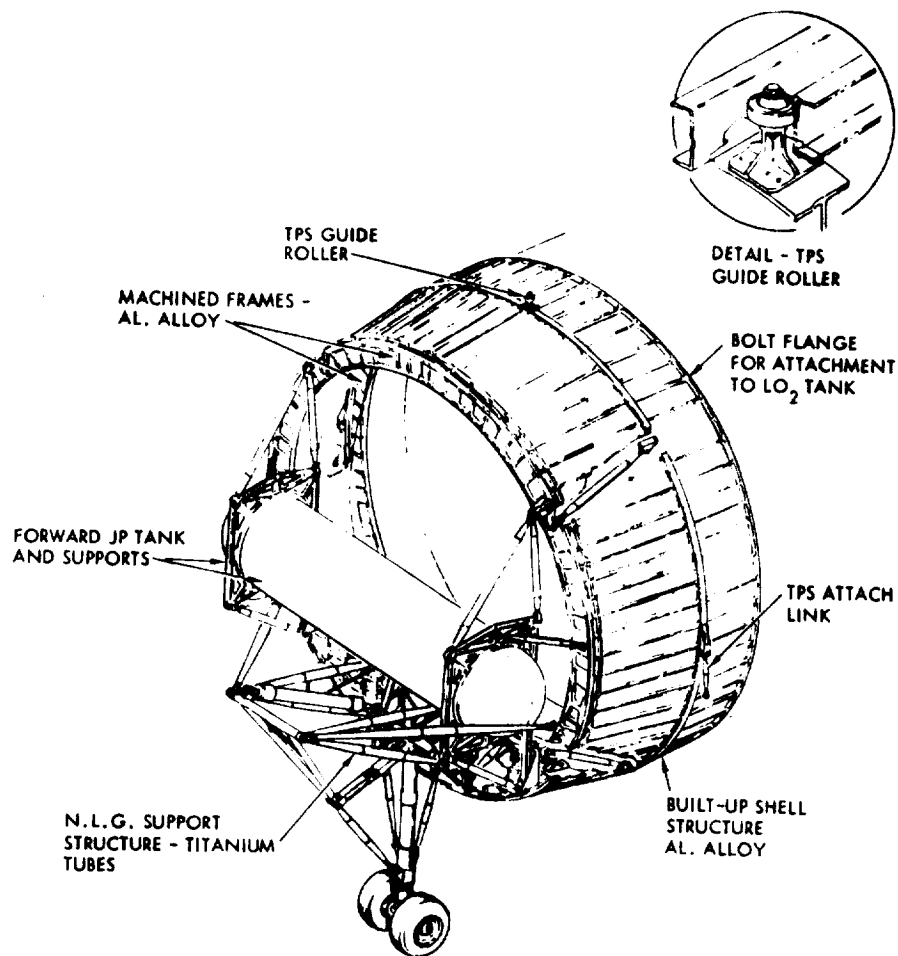


Figure 2-11. B-9U Forward Skirt Structure

The outer heat shield provides an aerodynamic surface for the body which varies from a circular cross-section at the nose gear station to a gradually flattening lower surface transitioning into the wing fillet. The heat shield is primarily of shallow corrugated frame stiffened panels utilizing Rene '41 alloy principally, and titanium alloy in the regions of lower aerodynamic heating. The heat shield is supported via links from the primary structure to allow for expansion. The forebody ahead of Station 1479 is supported as an extension of the heat shield itself and moves with it, except for the nose gear that, as previously explained, is supported from an extension skirt on the primary load-carrying LO<sub>2</sub> tank. The body heat shield frames are on 20-inch centers below the body maximum breadth and on 40-inch centers above it.

The delta wing is mounted below the LH<sub>2</sub> tank. The wing carrythrough spars are tapered in the center section to allow the wing to overlap the tank in the side view and thus minimize base area. The wing attaches to the hydrogen tank frames and to the thrust structure via a series of links designed to take out relative expansion differentials between the wing and the body. See Figure 2-7. A low wing is selected principally to reduce the entry reradiation wing/body intersection temperature increase

effects in a high wing arrangement. The low wing/fillet arrangement also provides main landing gear stowage space.

The wing is located aft for balance purposes. Because of the large weight of boost engines it is necessary to move the aerodynamic center aft to accommodate the aft cg in a balanced configuration. A low aspect ratio delta wing of 53-degree sweep is selected to provide minimum flyback system weight, within the constraints of satisfactory stability characteristics and landing speed. The delta wing also allows sufficient thickness to stow the flyback engines internally, which is particularly desirable since the shock impingement of lower surface nacelles creates excessively high temperatures. The high-sweep delta wing tends to minimize both heating and boosting drag (also reduced with retracted flyback engines) and promises better transonic characteristics.

Figure 2-12 shows the general arrangement of the delta wing. The wing is spliced at span Station 507.5 to allow disassembly for shipping. Five ACPS engines are located next to the rear spar.

The delta wing has a theoretical area of 8451 square feet and an exposed area of 5047 square feet installed at +2-degree angle of incidence to the body centerline to facilitate cruise and to reduce landing angle within the constraints of the boost loads on the wing. The leading edge sweep is 53 degrees. The installation of the JTF22A-4 air-breathing engines in the wing requires a maximum thickness chord ratio of 10.3 percent at wing Station 507.5 just outboard of the outboard engine. Installation of these engines below the body in the center section requires a 7.1-percent theoretical root thickness at the vehicle centerline. The airfoils are NASA four digit series with modifications to the leading edge radii and with conical camber at the tips to improve L/D. The trailing edge of the wing is perpendicular to the body centerline with elevons segmented into three spanwise parts for varying degrees of control. The wing structure is primarily titanium alloy with two main structural boxes. The forward box accommodates the air-breathing engines. The lower surface of the wing is thermally protected by a system of dynaflex insulation with metallic radiation cover panels.

Flyback engines are selected from among off-the-shelf candidates. The JTF22A-4 is the lowest bypass ratio candidate and presents the smallest package for installation. This condition permits low wing thickness-to-chord ratio ( $t/c$ ) thus minimizing potential control problems during transonic passage at the end of entry. Overall system weight differences between the JTF22A-4 and the F101 (higher bypass ratio engine) are small, the savings in fuel being offset by the increase in engine and installation weight and increased cruise drag effects. The air-breathing engines are installed in podded configurations, pivoted at the aft support point. Each engine assembly has its own deployment rotary actuators. Longitudinal doors in the lower surface open to allow deployment of the air-breathing engines to the subsonic cruise position. The

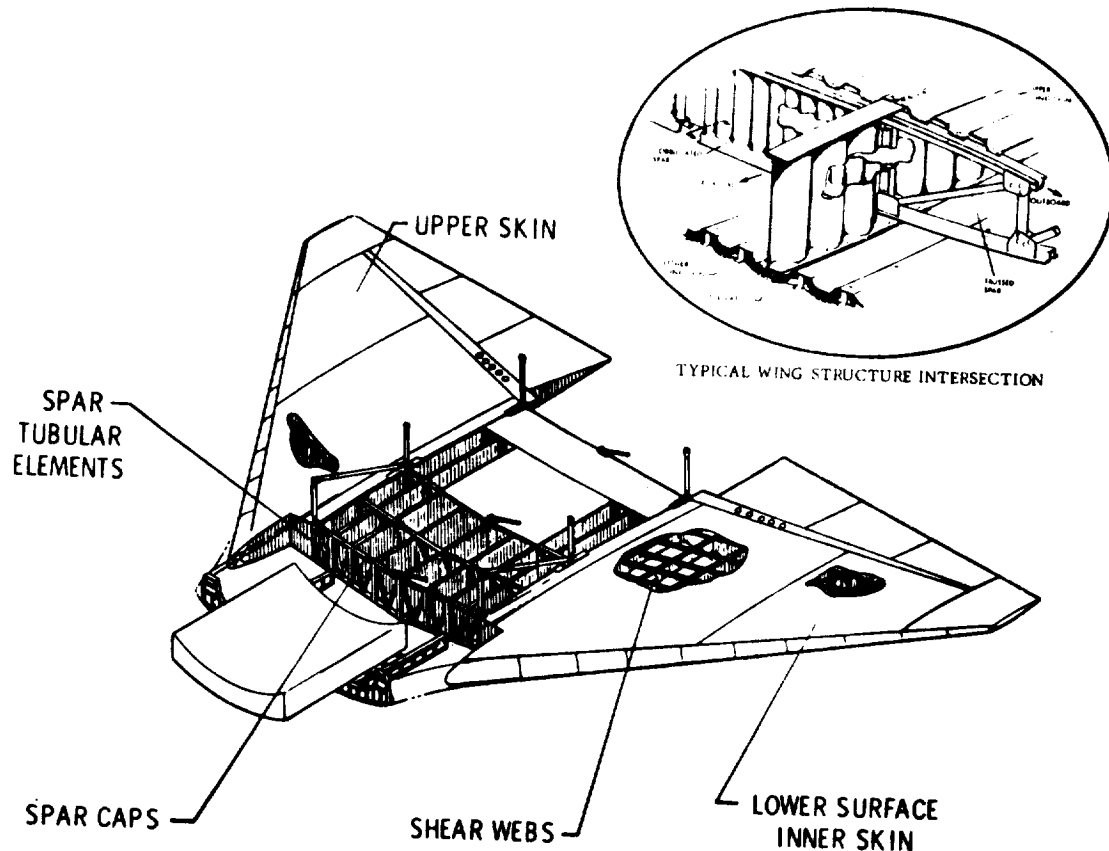


Figure 2-12. B-9U Wing General Arrangement

engines rotate through 180 degrees to the locked-extended position. Upon engine deployment the engine bay doors close to present a clean surface for cruise and landing. See Figure 2-13.

The JP flyback fuel is currently stowed in a single tank on the booster centerline, near the center of gravity. While no fuel transfer is currently anticipated in the B-9U configuration for balance purposes, JP fuel presents an advantage in this respect for configurations having a closely coupled hypersonic/subsonic relationship requiring fuel transfer for cg control. The fuel is fed to the four engines under the body at Station 3560 and to the four engines in each wing.

The fully pivoting canard is selected as a trim and control device and as an adjunct to rotation for takeoff on ferry flights. The canard is located as far forward of the wing as feasible to increase control effectiveness. Use of the canard allows reduction in wing area and elevon size and permits the use of wing high-lift devices at landing and for cruise improvements in the typical high drag booster configuration. A general view of the canard is shown in Figure 2-14. The canard provides a total exposed area



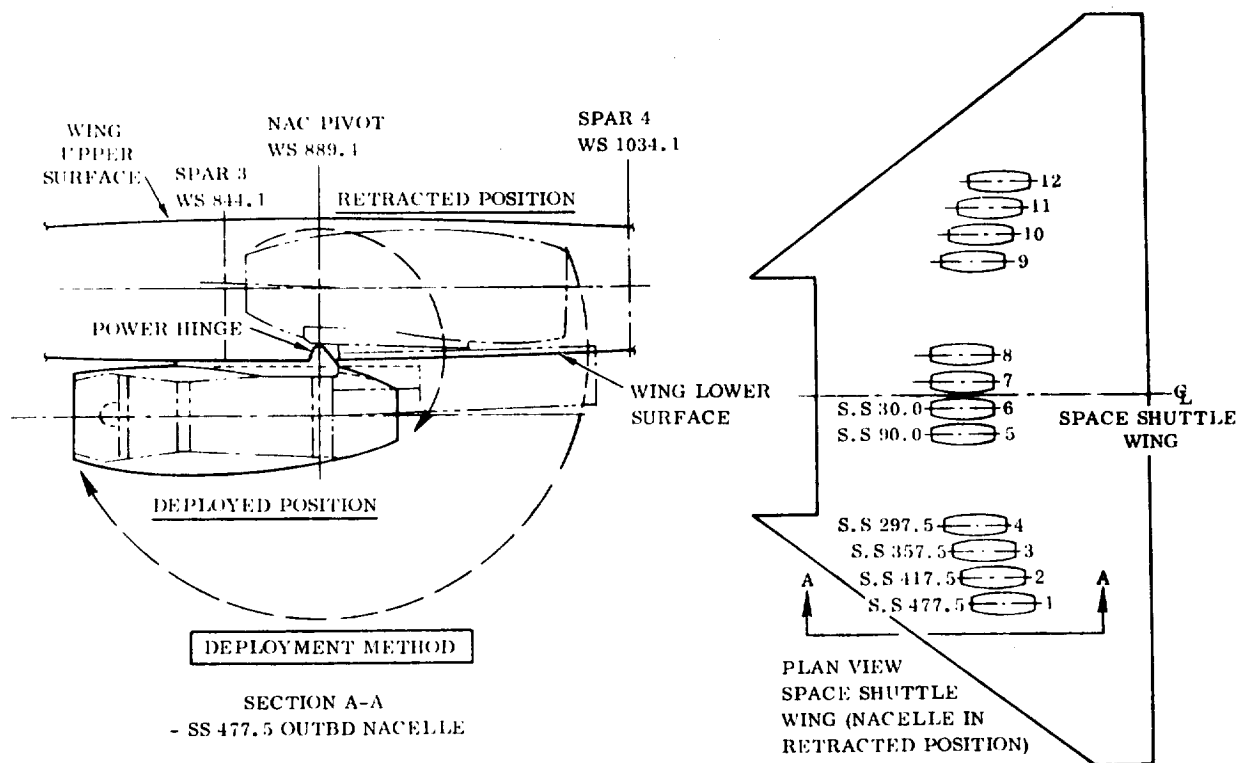


Figure 2-13. B-9U Nacelle Location, Retracted and Deployed Positions

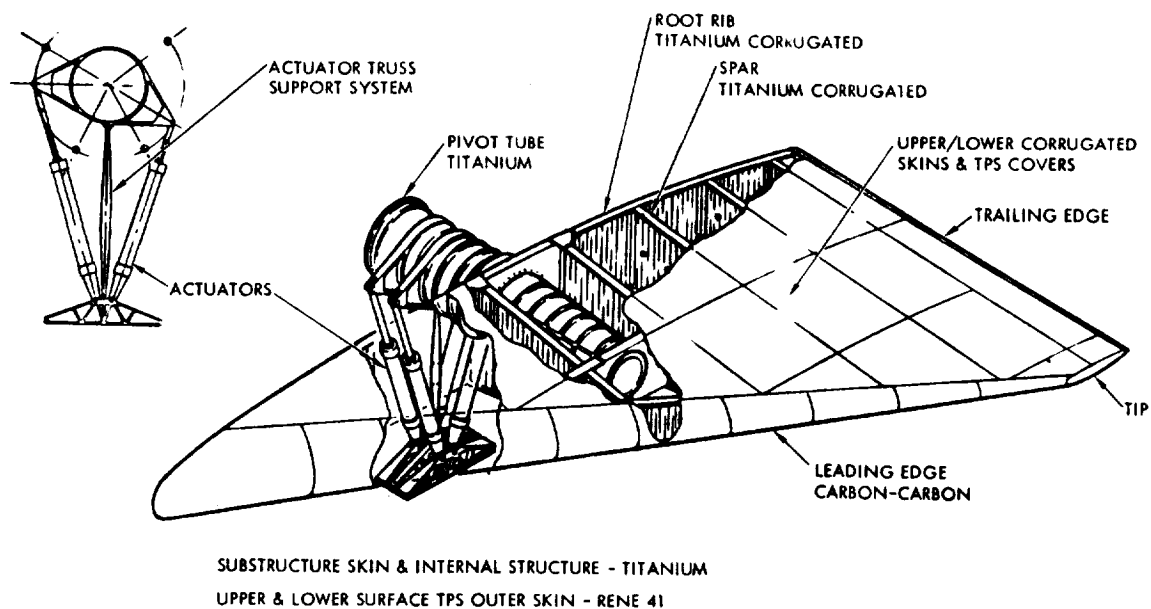


Figure 2-14. B-9U Canard Structure

of 540 square feet. The leading edge sweep is 60 degrees and the thickness is 14 percent. The entire surface is pivoted at 56 percent of the root chord and moves 65 degrees nose down to decouple the effect of the surface during hypersonic entry. The surface wipes a body fairing to maintain a seal at all points along the down travel. This seal is to minimize entry heating. Upward travel of the leading edge of the canard is 30 degrees.

The vertical tail is on the centerline of the body to minimize weight relative to tip fins that weigh more in themselves and impose an added weight to the outboard wing sections due to maximum boost  $\beta q$  loads and the attach complexity. Directional stability is maintained in the booster during reentry in the high-angle-of-attack mode by using the ACPS yaw engines. Even after the heat sink leading edge and the extra ACPS weights were incorporated, a centerline vertical still showed the least overall system weight. The general configuration of the vertical tail structure is shown in Figure 2-15.

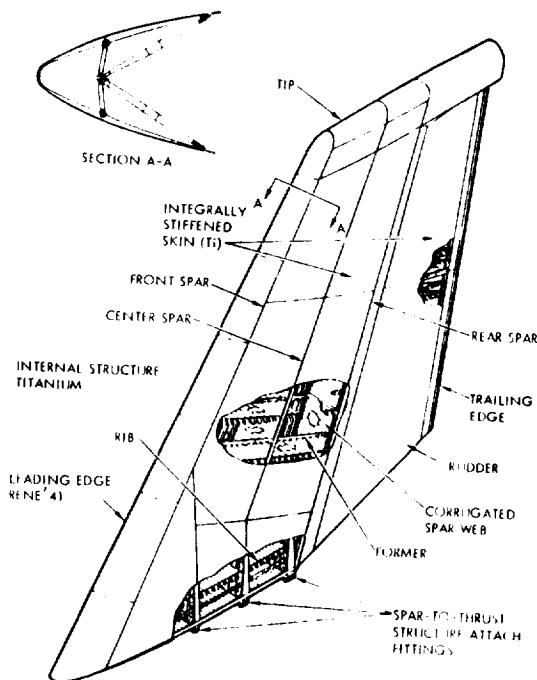


Figure 2-15. B-9U Vertical Tail Structure

The vertical stabilizer has an area of 1500 square feet with a leading edge sweep of 35 degrees to provide orbiter separation clearance consistent with weight and aerodynamic considerations. The tail thickness varies from 13 percent at the root to 11 percent at the tip. A 35-percent chord rudder is provided with  $\pm 25$  degrees of travel. The base of the rudder is cut off at 15 degrees to provide plume clearance for the upper rocket engines. Vent and exhaust lines are terminated at the fin tip trailing edge. The leading edge of the vertical tail has increased material thickness to act as a heat sink during the brief period of plume impingement during orbiter separation.

The crew compartment is conventionally located in the nose structure (see Figure 2-5). Swivel seats adjustable for the vertical flight, entry, and cruise flight are provided in conventional locations for captain and co-pilot. The crew compartment is pressurized for shirtsleeve en-

vironment. Heat shields are provided over the windshields, which are sized for adequate landing visibility at the maximum 15-degree touchdown angle. Access with the

booster in the vertical position is via a door to the left of the pilot seat. Access with the booster in the horizontal position is via a door in the compartment floor reached through the nose-gear wheel well. Immediately behind the crew is space for an additional jump seat available for horizontal flight test or checkout purposes. Aft of the crew compartment are the booster avionics systems installed in a controlled environment but separate from the crew compartment. Below the crew and avionics compartments is the nose-gear wheel well.

**2.2.2 B-16B SWEPT WING BOOSTER.** The original plans were to generate a straight-wing/horizontal-tail booster which would be directly comparable to the Model B-9U delta-wing/canard booster, and its mission profile. However, no straight-wing/horizontal-tail configuration with high-cross-range capability had been investigated at Convair Aerospace. It was decided to adapt a swept-wing/canard configuration to the B-9U body, canard and vertical tail. This configuration meets the intent of the study by providing a wing structure that can be designed using safe-life and fail-safe design principles.

Previous Convair Aerospace studies had generated a low-cross-range booster using swept wings and canards (Model B-16A), that offered a desirable wing structure. A combination of the B-9U body, canards, and vertical tail with a scaled-up version of the B-16A wing was determined to be aerodynamically feasible. This configuration was designated as Model B-16B booster. The Model B-16B booster, similar to the B-9U booster, is a low, swept wing vehicle with a single vertical tail and two canard surfaces mounted forward above the body centerline. Figure 2-16 shows a three-view drawing of the basic B-16B booster configuration. Table 2-1 lists comparative data for the B-9U delta-wing/canard and B-16B swept-wing/canard baseline boosters.

The uninterrupted wing box is attached to the booster body with a system of statically determinate links, as in the B-9U delta wing vehicle. The  $\text{LH}_2$  tank wing support frames require relocation, but the tank structural design philosophy remains unchanged.

Details of the structural arrangement of the two swept wing concepts are shown in Figures 2-17 and 2-18. Figure 2-17 shows a three-spar box (i.e., safe-life concept), with bending reacted by heavy integrally stiffened skins, and Figure 2-18 shows a five-spar box (i.e., fail-safe concept) with bending reacted by the heavy spar caps.

The temperatures of the non-corrugated upper and lower structural skins shown in Figure 2-17 are assumed to remain at a relatively low uniform temperature due to the skin mass and the thermal protection for the lower structural skin. The relatively thin upper and lower skins in Figure 2-18 are corrugated to allow for differential thermal expansion. The lower skin is insulated to prevent temperatures exceeding about 650°F.

The wing spars for both designs are located at constant percent chord lines outboard of the main landing gear (MLG) support bulkhead. The center spar is located midway between the front and rear spars, and the auxiliary spars are located at the quarter points. A conventional aileron is provided outboard of wing station 585, and an up-only aileron and spoiler is provided over the air-breathing engines. The air-breathing engine system (ABES) is a problem on the relatively thin (10 percent) short chord wing. For comparability with the delta-wing booster, it was desirable to retract the engines when not in use. However, it is not practical to cut out such a large portion of the swept wing box.

The selected approach, shown in Figure 2-16, clusters the engines on the lower aft wing surface, six to a side, in a common pod. They are located below the basic wing structure. The engine inlets are protected by a retractable ramp during the high temperature portion of flight.

The wing structural materials, noted on Figures 2-17 and 2-18, are identical to the delta wing. Annealed titanium (6Al-4V), is used throughout the structural box, except for the lower surface thermal skin of either HS188 or coated columbium. The spar and rib webs are composed of corrugated annealed titanium, and the method of fabrication and attachment is similar to the delta wing. A more detailed discussion of structural materials is given in Section 2.3.

### 2.3 BOOSTER STRUCTURAL MATERIALS

Materials for the space shuttle booster structure fall into several categories: (1) aluminum alloys, (2) beryllium alloys, (3) titanium alloys, (4) nickel base alloys, (5) cobalt base alloys, (6) columbium alloys, and (7) composite materials. Primary candidate materials have been selected on existing properties data or data generated under space shuttle studies. To provide an efficient final design, the properties of some of these materials must be investigated to determine their allowable properties after exposure to the expected environments. Table 2-2 lists the primary structural materials for both the B-9U delta wing and B-16B swept wing booster systems under detailed study.

The wing box is primarily fabricated from titanium with a thermal limit of 800°F. Titanium was selected due to its high specific modulus and strength and low thermal stress index at 650°F. Titanium has well defined mechanical and physical properties and the fabrication, machining, and welding techniques are well known.

The basic structural concept of the wing is based on the use of a metallic standoff heat shield combined with insulation between the shield and the wing lower surface structure to provide thermal protection for the whole wing structure except for the





Table 2-1. Data Comparison of Models B-9U and B-16B

Item	Configuration	
	B-9U	B-16B
Booster		
Launch weight, M lb	4.188	4.188
Empty weight, M lb	0.627	0.627
Cruise weight, M lb	0.787	0.787
Landing weight, M lb	0.639	0.639
Orbiter weight, M lb	0.859	0.859
Landing c.g. station, in.	3,166	3,166
Flyback range, n.mi.	404	404
Staging velocity (relative), fps	10,824	10,824
Staging altitude, ft	245,000	245,000
Body		
Planform area, ft <sup>2</sup>	8,728	8,728
Volume, ft <sup>3</sup>	274,650	274,650
Tank diameters, in.	396	396
Length, in.	3,067	3,067
LH <sub>2</sub> tank volume, ft <sup>3</sup>	120,161	120,161
LO <sub>2</sub> tank volume, ft <sup>3</sup>	40,901	40,901
Wing (Theoretical)		
Area, ft <sup>2</sup>	8,451	6,834
Span, in.	1,722	1,983.8
Aspect ratio	2.436	4.0
MAC ( $\bar{c}$ ), in.	860.6	558.8
Wing station, in.	314.3	393.2
1/4 $\bar{c}$ , in.	215.2	139.7
1/4 $\bar{c}$ station, in.	3,421	3,387
Wing (Exposed)		
Area, ft <sup>2</sup>	5,047	4,613
Span (semi), in.	645	775.9
Aspect ratio	2.289	3.625
MAC ( $\bar{c}$ ), in.	671.8	473.2
Wing station, in.	456	531.2
1/4 $\bar{c}$ , in.	167.9	118.3
1/4 $\bar{c}$ station, in.	3,563	3,482
Load landing, lb/ft <sup>2</sup>	126.6	138.6
Max cruise, lb/ft <sup>2</sup>	155.9	170.6
Location, c.g. to 1/4 $\bar{c}$ , in.	397	316
Canard pivot to 1/4 $\bar{c}$ , in.	1,539	1,458
Wing 1/4 $\bar{c}$ to tail 1/4 $\bar{c}$ , in.	285	386

Table 2-1. Data Comparison of Models B-9U and B-16B, Contd

Item	Configuration	
	B-9U	B-16B
Wing (Exposed), Continued		
Thickness ratio t/c	0.101	0.100
Taper ratio	—	0.28
Miscellaneous		
Canard area (exposed), ft <sup>2</sup>	504	504
Canard pivot to c.g., in.	1,142	1,142
Canard span, in.	800.4	800.4
Vertical tail area (exposed), ft <sup>2</sup>	1,500	1,500
Tail 1/4 c̄ to c.g., in.	682	682
Tail span (exposed), in.	533.8	533.8
Gear axis to c.g., in.	129.0	118.0

hot leading edge. This allows efficient use of titanium for all of the primary and secondary structure above the TPS while the TPS shield itself can be made of HS188 and coated columbium. The Haynes 188 material is thermally limited to about 1900°F and the coated columbium to 2500°F. Both these materials were selected for their thermal strength properties.

The vertical stabilizer structural arrangement is a three-spar, multi-rib configuration with integrally stiffened skin/stringer panels. Spar and rib webs are of corrugated or trussed construction to allow for differential thermal expansion. The rudder is of similar construction. The entire structure is titanium except for the leading edge which is Inconel 718. The segment of leading edge that is subjected to the orbiter engine exhaust impingement is "heat sink" designed to withstand the increased temperature. Again titanium is selected due to its strength at temperatures that preclude aluminum, and its adaptability to a variety of proven fabrication techniques.

The main LO<sub>2</sub> and LH<sub>2</sub> fuel tanks are fabricated almost entirely of 2219 aluminum. Both 2219 and 2014 aluminum alloys were considered for the main tanks and other body structures. Both alloys possess excellent strength-toughness properties in the base metal at all temperatures down to -423°F, with the 2014 alloy being somewhat stronger than 2219. However, welded joints in the 2014 alloy exhibit a tendency towards brittle fracture and greater sensitivity to minor weld flaws at liquid oxygen to liquid hydrogen temperatures. The significantly greater resistance to stress corrosion possessed by the 2219 alloy has been thoroughly demonstrated, as has its superior weldability and weld repairability. The combination of better fracture toughness in welded joints at reduced temperatures and superior resistance to stress



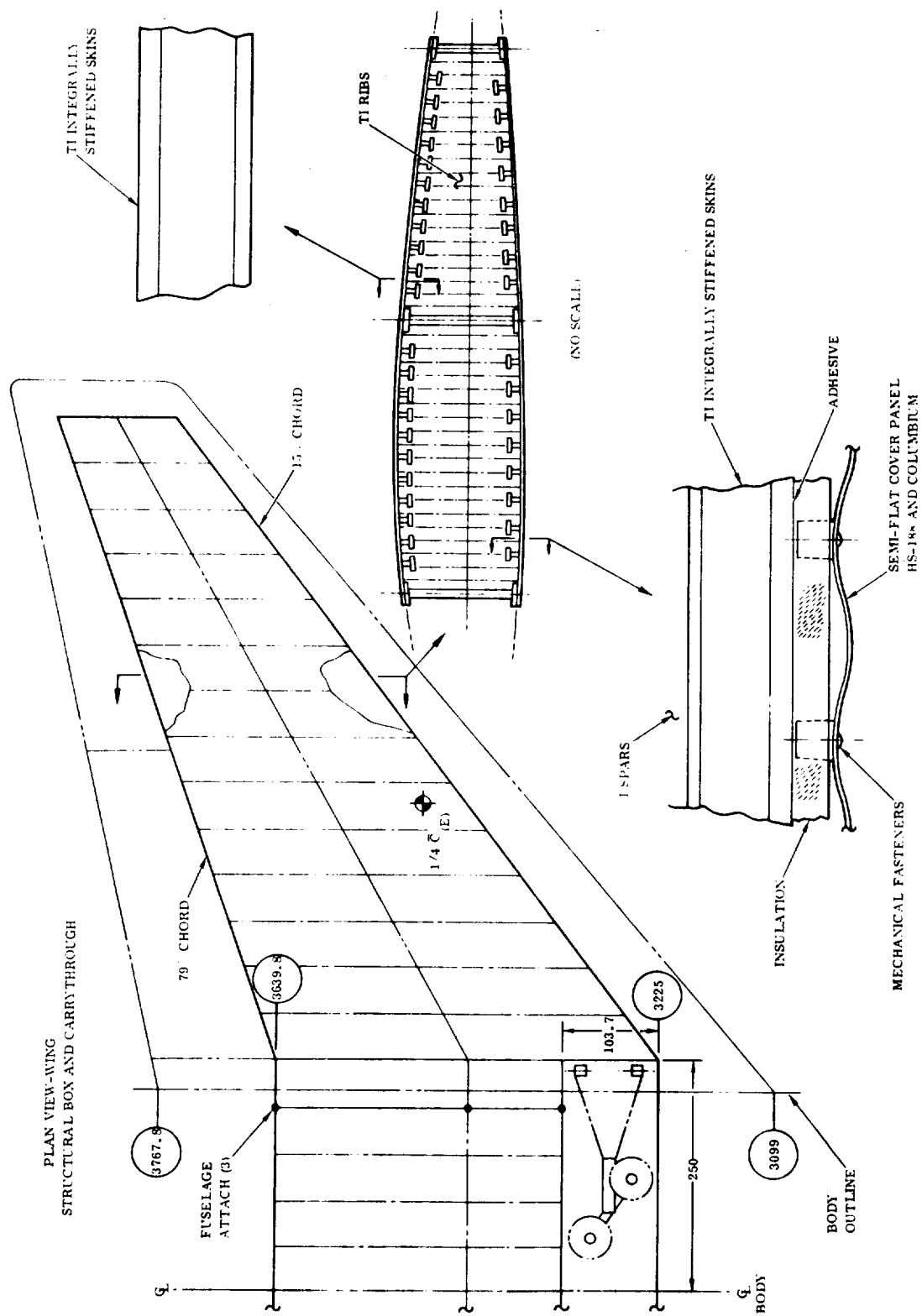


Figure 2-17. B-16B Booster Safe-Iife Wirz Concept

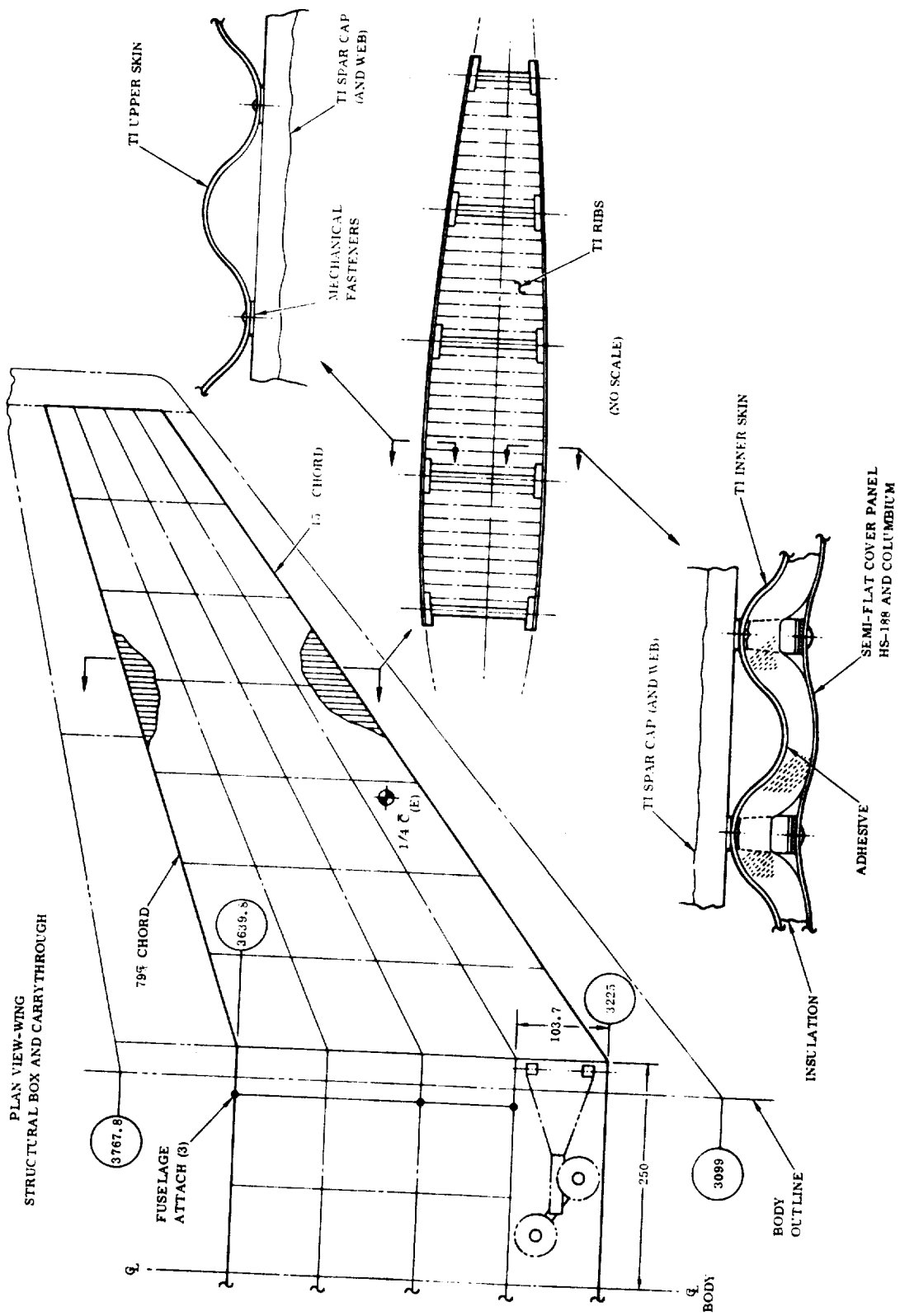


Figure 2-18. B-16B Booster Fail-Safe Wing Concept

Table 2-2. Booster Materials

Booster Components	Sub-Components	Materials
Wing Box	Spar Caps	Annealed Titanium (6Al-4V)
	Spar Webs	Annealed Titanium (6Al-4V)
	Rib Caps	Annealed Titanium (6Al-4V)
	Rib Webs	Annealed Titanium (6Al-4V)
	Intercostals	Annealed Titanium (6Al-4V)
	Lower Surface Thermal Skins	Haynes HS-188/Coated Columbium
	Upper & Lower Structural Skins	Annealed Titanium
	Trusses	Annealed Titanium
	Fasteners	Conventional Except for Lower Thermal Skin
Vertical Tail Box	Spar Caps	Annealed Titanium (6Al-4V)
	Spar Webs	Annealed Titanium (6Al-4V)
	Ribs and Bulkhead Caps	Annealed Titanium (6Al-4V)
	Ribs and Bulkhead Webs	Annealed Titanium (6Al-4V)
	Integrally Stiffened Skins	Annealed Titanium (6Al-4V)
	Stiffeners	Annealed Titanium (6Al-4V)
	Fasteners	Conventional
LO <sub>2</sub> Tank	Integrally Stiffened Skins	Aluminum Alloy 2219-T87
	Frame Caps	Aluminum Alloy 2219-T87
	Frame Webs	Aluminum Alloy 2219-T87
	Bulkheads (Dome)	Aluminum Alloy 2219-T87
	Fasteners	Conventional
LH <sub>2</sub> Tank	Note LO <sub>2</sub> Tank	Same as LO <sub>2</sub> Tank Except for Polyphenylene Oxide Insulation
Orbiter Support Bulkhead	Beam Caps	Aluminum Alloy 2219-T81/T851
	Beam Web	Aluminum Alloy 2219-T81/T851
	Bulkhead Caps	Aluminum Alloy 2219-T81/T851
	Bulkhead Webs	Aluminum Alloy 2219-T81/T851
	Fasteners	Conventional
Thrust Structure	Skins	Annealed Titanium (6Al-4V)
	Thrust Beams	Annealed Titanium (6Al-4V)
	Thrust Posts	Annealed Titanium (6Al-4V)
	Bulkheads	Annealed Titanium (6Al-4V)
	Vertical Stabilizer Attach	Annealed Titanium (6Al-4V)
	Fittings	

Table 2-2. Booster Materials, Contd

Booster Components	Sub-Components	Materials
	Intermediate Frames	Annealed Titanium (6Al-4V)
	Attachment Flange	Annealed Titanium (Al1-4V)
	Fasteners	Conventional
	Base Heat Shield	Rene ' 41 & coated Columbium

corrosion result in a significantly higher reliability for the 2219 alloy as compared to 2014.

Both 2219 and 2014 exhibit a decrease in strength properties as the plate thickness increases. Both the ultimate and the yield tensile strengths of 2014 decrease with increasing thickness at a greater rate than does the yield strength of 2219. Consequently, if the tank walls must be machined from 3 to 4 inch plate in order to accommodate integral stiffeners or weld lands, the strength advantage of 2014 is minimized.

Although 2014 shows an advantage in strength of the base metal, Convair Aerospace's choice of the 2219 aluminum alloy for the space shuttle propellant tankage is based upon its superior weldability, much better resistance to stress corrosion cracking, better overall toughness, and better reliability for the reusable manned space launch vehicle.

#### 2.4 BOOSTER WEIGHT SUMMARY

Table 2-3 is a summary weight statement for the B-9U delta wing booster and the B-16B swept wing boosters in the launch condition. This launch condition is for the mission described in Section 2.1, and assumes that the orbiter launch weight will be about 859,000 pounds. In Table 2-3, weights are broken down to show individual major system weights.

Table 2-4 shows the wing group weight breakdown. Weights are detailed to show both exposed wing and carry-through structure. The wing structural weights are separated into major components such as spars, ribs, and skins.

The B-9U weights were taken from Reference 13. The B-16B five-spar wing weights were derived from preliminary stress analysis and unit weights for the B-9U. The B-16B three-spar wing weights were derived as follows: the skin weight was obtained by using the theoretical weights from a finite element analysis and the non-optimum factor for T-stringer integral skin panels; the rib weights were obtained from

Table 2-3. Weight Summary

Description	B-16B		
	B-9U (lb)	Five Spar (lb)	Three Spar (lb)
Wing	59,063	56,221	65,491
Tail	17,908	17,908	17,908
Body	174,052	174,052	174,052
Induced environment, protection	86,024	97,024	97,024
Landing, recovery, dock	28,457	28,457	28,457
Propulsion-ascent	124,786	124,786	124,787
Propulsion-cruise	49,513	44,747	44,747
Propulsion-auxiliary	12,126	12,126	12,126
Prime power	1,930	1,930	1,930
Electrical	1,682	1,682	1,682
Hydraulics	2,201	2,201	2,201
Surface controls	9,620	9,620	9,620
Avionics	5,582	5,582	5,582
Environmental control	1,648	1,648	1,648
Personnel provisions	1,636	1,636	1,636
Contingency	50,705	47,313	38,042
Dry weight	626,933	626,933	626,933
Personnel	476	476	476
Residual fluids	11,503	11,503	11,503
Inert weight	638,912	638,912	638,912
Inflight losses	21,718	21,718	21,718
Propellant-ascent	3,382,307	3,382,307	3,382,307
Propellant-cruise	143,786	143,786	143,786
Propellant-ACS	1,500	1,500	1,500
Gross weight	4,188,223	4,188,223	4,188,223

preliminary stress analysis using rib data from the five-spar wing analysis and the B-9U unit weights. Although the B-16B wing carry-through structure is smaller in area than the B-9U carry-through structure, it was assumed to be the same weight because of the initial assumption of similar wing loads. Reduction in carry-through weight because of smaller size is compensated for, in part at least, by increase in body weight. The induced environment protection on the B-16B wing was assumed to be the same as on the B-9U. Based on past analysis of similar configurations, 11,000 pounds was added for the temperature effects on engine pods being below the wing.

Table 2-4. B-16B Wing Weight Summary

Description		Three Spar (lb)	Five Spar (lb)
Wing		(65,491)	(56,221)
Box			(39,399)
Spar caps		(1,440)	(11,816)
Upper spar	1	260	1,240
	2	0	1,246
	3	238	1,164
	4	0	1,030
	5	222	818
Lower spar	1	260	1,418
	2	0	1,406
	3	238	1,332
	4	0	1,178
	5	222	984
Spar webs		(4,248)	(4,998)
Web spar	1	1,580	1,086
	2	0	1,120
	3	1,551	1,066
	4	0	958
	5	1,117	768
Ribs		(2,824)	(1,504)
No.	1	350	350
	2	330	0
	3	304	304
	4	280	0
	5	256	256
	6	236	0
	7	216	216
	8	190	0
	9	164	164
	10	140	0
	11	120	120
	12	96	0
	13	70	70
	14	48	0
	15	24	24
Upper skin panels		(15,190)	(2,598)
Skin		15,161	2,281
Standoffs		0	288
Fasteners		29	29

Table 2-4. B-16B Wing Weight Summary, Contd

Description	Three Spar (lb)	Five Spar (lb)
Lower skin panels	(8,771)	(2,287)
Splices	(1,449)	(1,449)
Carry-through	(14,747)	(14,747)
Leading edge	(5,776)	(5,776)
Trailing edge	(598)	(598)
Tip	(348)	(348)
Engine penalty	(2,000)	(2,000)
Elevon	(7,500)	(7,500)
Links wing attach	(600)	(600)

The dry weight was held constant for all three vehicles.

Figure 2-19 shows the change in cg during the mission. Both the combined vehicle (booster and orbiter) and separate booster cg changes are shown. Vehicle weight is shown for various points in the mission.

Table 2-5 gives the booster mass properties sequence during the mission detailed in Section 2.1. Changes in weight, center of gravity, moment of inertia, and product of inertia are given.

## 2.5 DESIGN CRITERIA

The booster vehicle is designed to provide adequate structural strength for a safe life of 100 missions, or for a ten year life, without the need for major repairs. This design is capable of withstanding the service life of flight and pressure loads combined with the thermal and acoustic environment. Booster structure is designed for minimum weight commensurate with overall costs and the vehicle is designed to minimize post-flight inspection requirements for rapid turnaround. Design technology will represent that prevalent in 1972.

For purposes of this study, design loads on the selected components are assumed to be identical for both the B-9U and B-16B booster configurations. Structural components are designed to provide the yield and ultimate factors of safety, proof, and other factors used in the booster design, as shown in Table 2-6. Static and fatigue factors are both summarized in Table 2-6.

The LO<sub>2</sub> tank is designed to be proof-tested in segments because of weight savings, using a three-phase proof test. The entire LH<sub>2</sub> tank is designed to be pneumatically proof-tested at room temperature. The thermal protection system (TPS) structure

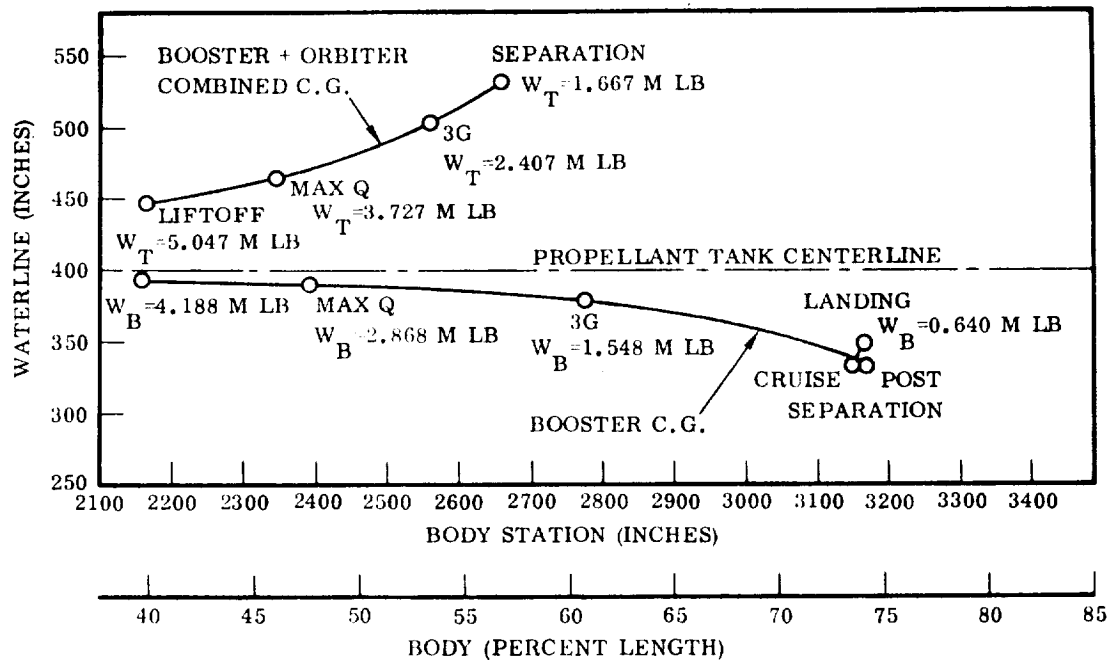


Figure 2-19. Mission Center of Gravity Travel Check

is also designed for the load factors in Table 2-6, as applicable. In addition, an allowable creep strain of 0.2 percent per 10 hours exposure at maximum temperature will be used, and for corrugated panels in the transverse direction, 1.0 percent creep strain per 10 hours exposure at maximum temperature. A minimum clearance of 1.0 inch between the inner tank structure and the outer TPS structure will be maintained at limit load.

The booster is designed to withstand the repeated loads incurred in 400 flights without failure, including a scatter factor of four. Consideration will be given to the effects of acoustic fatigue loads. The booster will withstand the mission thermal environments with a minimum of post-flight inspection and subsequent structural refurbishment and/or replacement.

The primary structural components will be designed fail-safe insofar as practical, considering weight, cost, and manufacturing. When primary structure fail-safe design



Table 2-5. Sequence Mass Properties Statement, B-9U Delta Wing Booster

Mission Event	Weight (lb)	Center of Gravity (inches)			Moment of Inertia (slug-ft <sup>2</sup> × 10 <sup>6</sup> )				Product of Inertia (slug-ft <sup>2</sup> × 10 <sup>6</sup> )		
		X	Y	Z	I <sub>x-x</sub>	I <sub>y-y</sub>	I <sub>z-z</sub>	I <sub>xy</sub>	I <sub>xz</sub>	I <sub>yz</sub>	
Liftoff	4,188,223	2,163	0	392	13.160	549.200	549.300	0	-10.200	0	
Prop to max q	-1,320,000										
Max q	2,868,223	2,389	0	388	12.370	404.700	404.800	0	- 8.490	0	
Prop to 3-g	-1,320,000										
3-g	1,548,223	2,771	0	378	11.200	232.400	232.500	0	- 5.650	0	
Prop to burnout	- 736,547										
Thrust decay prop	-3,340										
Burnout (entry)	808,336	3,167	0	333	8.782	102.000	102.700	0	- 1.380	0	
Inflight losses	-18,332										
ACPS props	-3,450										
Start cruise	786,554	3,151	0	332	8.715	100.200	101.000	0	- 1.530	0	
APU propellants	-4,218										
Flyback fuel (JP)	-143,786										
Landing (gear down)	638,550	3,166	0	353	8.386	99.710	100.400	0	- 2.000	0	

Table 2-6. Design Criteria

Component	Yield	Ultimate	Proof	Applied On
Main Propellant Tanks	1.10	1.40	*	Maximum relief valve pressure only
	1.10	1.40	—	Loads (+ limit pressure)
	1.00	—	—	Proof pressures
Personnel Compartments, Windows, Doors, Hatches	1.10	1.50	—	Loads (+ limit pressure)
	1.50	2.00	1.50	Maximum operating pressure only
	1.00	—	—	Proof pressure
Airframe Structure	1.10	1.40	—	Boost + entry loads
	1.10	1.50	—	Aircraft mode loads
Pressure Vessels	—	2.00	1.50	Maximum operating pressure
Pressurized Lines Fittings	—	2.50	1.50	Maximum operating pressure
Fatigue	4.00	—	—	Design Service Life
Flow Growth to Leak or Failure	1.50	—	—	Design Service Life
Thermal Stresses	1.00	—	—	Temperature gradients
*Based on Fracture Mechanics Analysis				Assumed service life = 100 missions

is not practical, a safe-life design concept will be applied. The primary structure includes the wing box, tanks, fin box, thrust structure, major bulkheads, intertank adapter, and similar major load-carrying structural components or elements such as spar caps and wing/body attach links.

Safe-life designs will be compatible with latest NDI (nondestructive inspection) techniques and limitations and residual strength and crack propagation analyses will be used to ensure that adequate safe-life has been provided.

Conventional strength, fail-safe, and fatigue analyses will be supplemented by fracture mechanics analysis to determine critical flaw sizes and residual life assuming pre-existing flaws.

## 2.6 DESIGN CONDITIONS

Booster design conditions were generated from ground handling procedures and from mission flight characteristics. The flight conditions investigated include: launch, ascent, entry, subsonic cruise, and horizontal takeoff and landing. Effects of Mach number, angle of attack, and control surface deflections on longitudinal and lateral directional characteristics were also included. The ground conditions investigated were taxi, towing, mating, and launch preparation and erection.

In most instances, the aerodynamic data was based on available experimental data adjusted for differences between tested and current configuration.

Table 2-7 summarizes limit flight loads and design load factors for a number of the critical mission conditions. Maximum loads on the body, wing, and canard occur during maximum  $g$  recovery (i.e., entry), while maximum  $\beta q$  during ascent yields the greatest load on the vertical stabilizer. Critical design conditions and considerations for aerodynamic surfaces are summarized in Table 2-8.

Internal loads consisting of axial and shear loads and bending and torsion moments were determined at 48 stations along the body length for 25 load conditions. The conditions investigated are:

1. One-hour ground head winds, fueled, unpressurized
2. One-hour ground tail winds, fueled, unpressurized
3. One-hour ground side winds, fueled, unpressurized
4. Liftoff + 1-hour ground head winds
5. Liftoff + 1-hour ground tail winds
6. Liftoff + 1-hour ground side winds
7. Maximum  $\alpha$   $q$  head winds
8. Maximum  $\alpha$   $q$  tail winds
9. Maximum  $\beta$   $q$
10. Three- $g$  maximum thrust
11. Booster burn-out
12. Maximum  $g$  entry
13. Subsonic gust
14. Two-point landing
15. Three-point landing

Table 2-7. Summary of Booster Design Conditions and Loads

Condition	Component (or Mass Item)	$n_x$	$n_y$	$n_z$	Limit Air Load (lb/panel)	Remarks
Two week standby		1.0				
One day hold		1.0				
One hour to launch		1.0				
Lift-off	(LO <sub>2</sub> mass)	1.31 ± 0.15				
	(LH <sub>2</sub> mass)	1.31 ± 0.25				
	(Orbiter & other)	1.31 ± 0.21				
Max. dynamic pressure						
Max $\alpha q$						
Headwind	Body	1.61	0	0.51	537,000	
	Wing	1.61	0	0.51	666,800	
	Canard	1.61	0	0.51	45,430	
Tailwind	Body	1.67	0	-0.19	-220,000	
	Wing	1.67	0	-0.19	-98,600	
	Canard	1.67	0	-0.19	-45,360	Provides, with booster burnout condition, critical loads for orbiter-booster attachment.
Max $\beta q$	Body	1.60	± 0.213	0.016	130,000	
	Wing	1.60	± 0.213	0.016	485,000	
	Canard	1.60	± 0.213	0.016	19,520	
	Vertical tail	1.60	± 0.213	0.016	187,100	
Max. thrust	Body	3.3	0	0.242		
	Wing	3.3	0	0.242		
	Canard	3.3	0	0.242		
Booster burnout	Body	3.3	0	0.343		
	Wing	3.3	0	0.343		
	Canard	3.3	0	0.343		Provides critical inertia loads for wing-to-body drag links, and together with max. $\alpha q$ condition, critical loads for orbiter-booster attachment.
Max. g recovery	Body		0	4.0	1,507,000	
	Wing		0	4.0	808,600	
	Canard		0	4.0	0	
2.5g maneuver	Wing	0	0	2.5	617,600	
	Canard	0	0	2.5	71,370	
Rudder kick	Vertical tail				204,000	
Subsonic gust	Body	0	0	2.1	488,000	
	Wing	0	0	2.1	591,500	
	Canard	0	0	2.1	-4,957	
	Vertical tail	0	0.5	1.0	1272,000	
Landing	Body	0	± 0.35	2.35	208,000	
	Wing	0	± 0.35	2.35	376,000	
	Canard	0	± 0.35	2.35	47,000	

Table 2-8. Summary of Design Conditions

Structural Design Summary Chart		
Structural Component	Critical Condition	Design Considerations
<b>Wing:</b> Primary Sub-Structure Upper Skin Panels Lower Skin Panels TPS Heat Shield Elevon Sub-Structure Leading Edge	Max $\alpha q$ ~ Boost Liftoff Sound Pressure Max $g$ ~ Recovery Liftoff Sound Pressure Max $g$ ~ Recovery Max Heating ~ Recovery	Wing Shear & Bending Sonic Fatigue Pressure & Temp Differential Sonic Fatigue Air Pressure Pressure & Temperature
<b>Wing/Body Attachment:</b> Fwd Vertical Attach Center Vertical Attach Aft Vertical Attach Drag Attach Fwd Side Load Attach Aft Side Load Attach Center Side Load Attach	Subsonic Gust ~ Flyback Max $\alpha q$ ~ Boost Max $\alpha q$ ~ Boost Max Thrust ~ Boost Max Thrust ~ Boost Max Thrust ~ Boost Taxi	Safe-Life Safe-Life Safe-Life Fail-Safe Fail-Safe Fail-Safe Fail-Safe
<b>Canard</b> Primary Substructure Torque Tube	Max $g$ ~ Recovery	Canard Structure & Torque Tube Shear, Bending, Torsion
<b>Vert. Tail</b> Primary Structure	Max $\beta q$ ~ Launch	Box Shear, Bending

- |  |                                       |
|--|---------------------------------------|
| 16. Two-g landing                          | 21. Two-week ground tail winds, empty |
| 17. One-day ground head winds, pressurized | 22. Two-week ground side winds, empty |
| 18. One-day ground tail winds, pressurized | 23. 2.5g positive maneuver            |
| 19. One-day ground side winds, pressurized | 24. -1.0g negative                    |
| 20. Two-week ground head winds, empty      | 25. Maximum operating pressure        |

An envelop of the resulting peak load intensities ( $N_x$ ) for the most critical conditions is shown in Figure 2-20, where  $N_x$  is the longitudinal axial load in the tank wall. The major loading conditions on the forward skirt are due to axial loads occurring during boost phase and shear loads during landing and taxiing conditions.

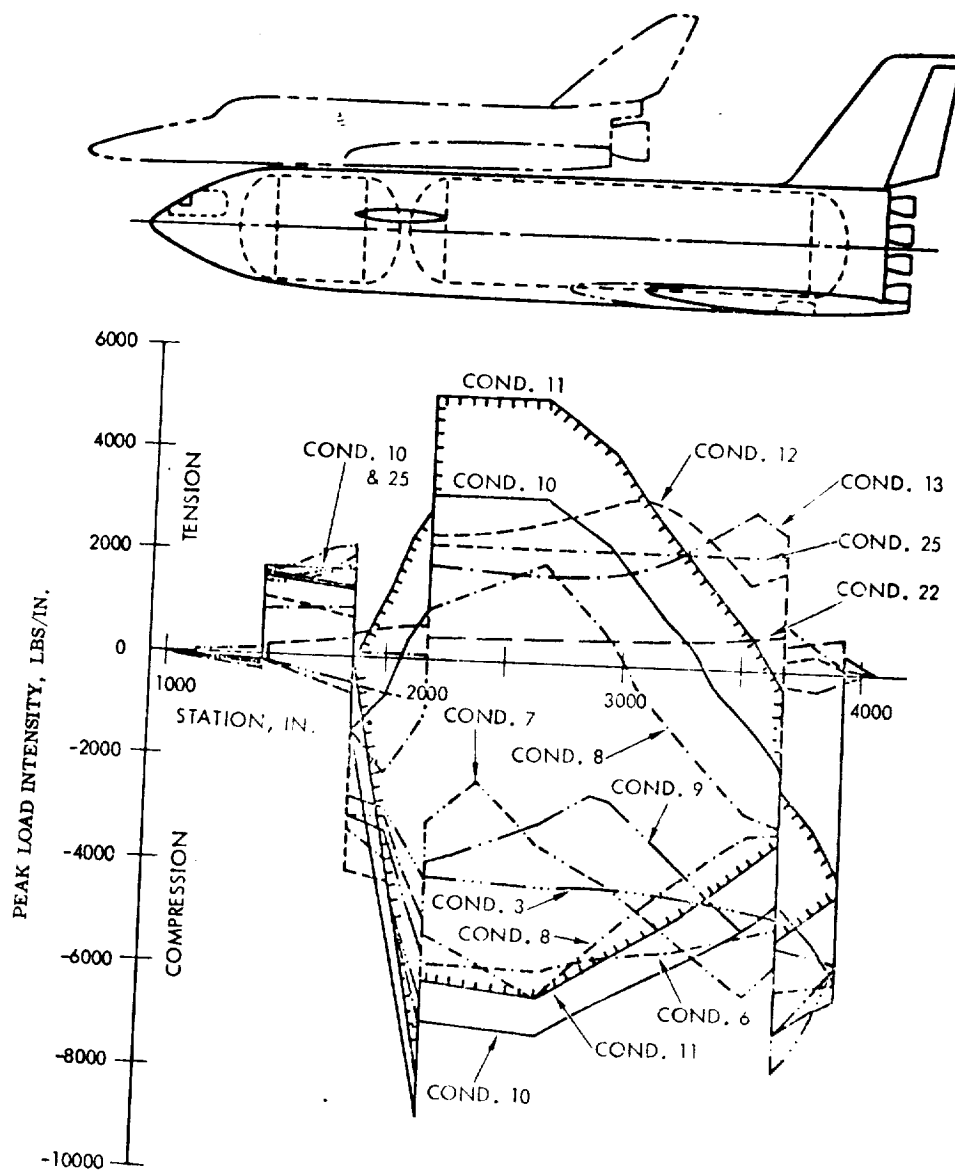


Figure 2-20. B-9U Booster Peak Limit Load Intensities

Proof pressures on the  $\text{LO}_2$  tank determine the skin gages of domes and the cylinder. Stiffening on the cylindrical body is required for flight and ground loads. The aft dome is grid-stiffened close to the equator because of compressive hoop loads occurring in the partially filled condition. External stiffening, consisting of tee stringers and trussed frames, was optimized for the low load intensities typical of the  $\text{LO}_2$  tank, and the results are incorporated in the present design.

$\text{LH}_2$  tank skin gages of domes and cylinders are determined by proof-test requirements. Tank stiffening is in the form of external frames and tee stringers sized from axial and bending loads occurring during ground-wind and boost phase loads. An optimization study was performed on stiffening requirements and the results are incorporated in the present design.

Critical design conditions for the intertank adapter are derived from axial loads due to the  $\text{LO}_2$  weight forward and the bending and axial load introduced at the forward attachment by the eccentric orbiter weight.

A total of 27 loading conditions on the thrust structure were investigated, including ground-wind, launch, and boost phase loads with and without engine-out conditions. Ground-wind conditions are critical for hold-down fittings, back-up longerons, and adjacent skin on the skirt. Thrust beams, posts, frames, and skin away from hold-down longerons are critical for maximum  $\alpha q$  and 3g maximum thrust conditions with one engine out.

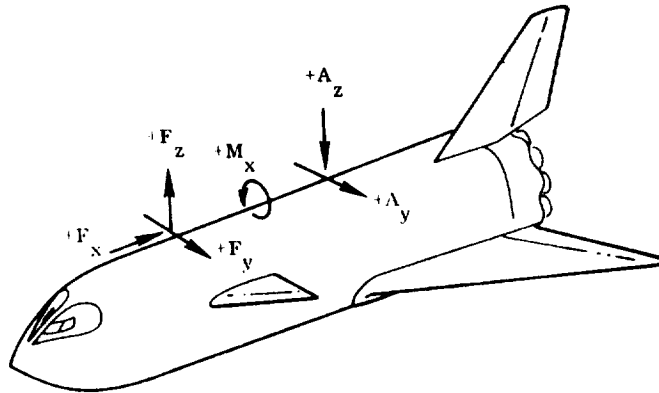
Table 2-9 summarizes the orbiter/booster interconnection loads, including loads for a number of critical conditions.

Total gage pressure (including dynamic head) versus tank station at various times during boost is shown in Figure 2-21 for the  $\text{LH}_2$  tank. These pressures correspond to the upper bound of a 3 psi regulating band. Also shown is the pressure line for a pneumatic proof test, which requires a proof factor equal to 1.13 based on 150 missions.

Total gage pressure for the  $\text{LO}_2$  tank (including dynamic head) versus tank station at various times during boost is shown in Figure 2-22. These pressures pertain to the upper bound of the relief valve tolerance band. Also shown are the pressure lines for a three-phase proof test program using a 1g  $\text{LN}_2$  head on a vertical tank position for the first two phases and a room-temperature pneumatic phase. A proof factor of 1.23 is required based on 150 missions.

The tank proof test factors of 1.13 and 1.23 are based on fracture mechanics analysis, assuming the given service life spectrum, material, and flaw growth characteristics.

Table 2-9. Booster/Orbiter Interconnection Loads



Condition	Wind	$F_x$ ( $\times 10^3$ lb)	$F_y$ ( $\times 10^3$ lb)	$F_z$ ( $\times 10^3$ lb)	$A_y$ ( $\times 10^3$ lb)	$A_z$ ( $\times 10^3$ lb)	$M_x$ ( $10^6$ in-lb)
Two-Week	Head	268		65		-46	
Ground Winds	Tail	268		-151		179	
Unfueled	Side	268	$\pm 121$	31	$\pm 37$	38	$\mp 22.2$
1-Hr Ground	Head	859		84		76	
Winds Fueled	Tail	859		25		137	
Unpressurized	Side	859	$\pm 33$	75	$\pm 10$	99	$\mp 6.10$
Dynamic Liftoff	Head	1296		112		133	
+ 1-Hr Ground	Tail	1296		74		180	
Winds	Side	1296	$\pm 21$	113	$\pm 2$	149	$\mp 4.52$
Max $\alpha$ -q	Head	1628		66		-367	
	Tail	1674		162		846	
Max $\beta$ -q	Side	1659	$\mp 37$	134	$\pm 341$	488	$\mp 50.33$
3g Max Thrust	—	2822		168		376	
Booster Burnout	—	2816		115		410	



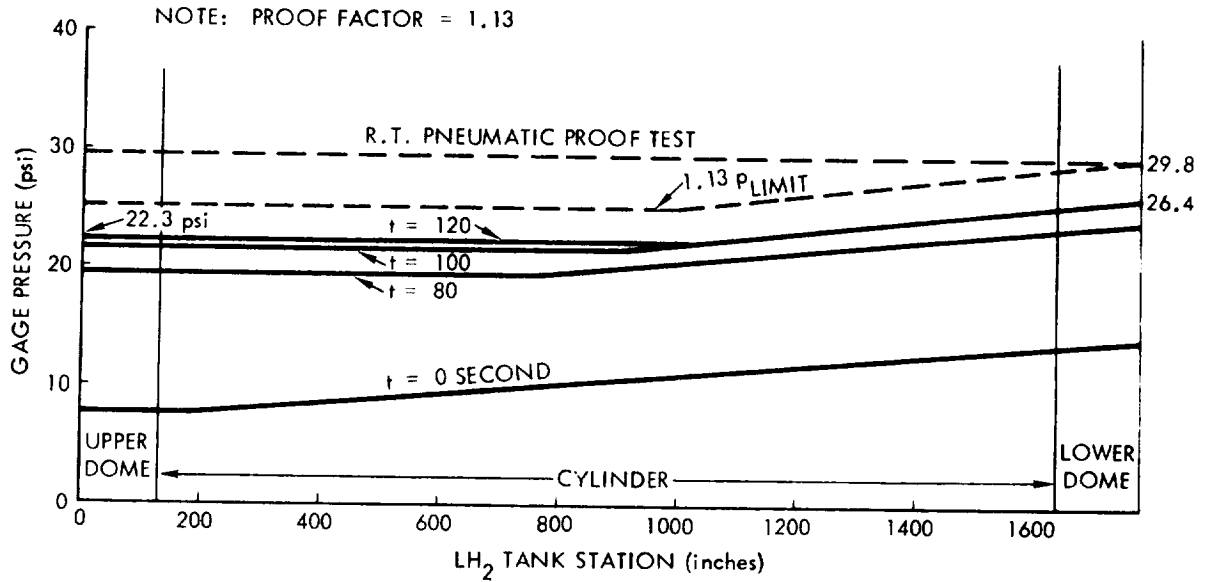


Figure 2-21.  $LH_2$  Tank Gage Pressures vs Tank Station

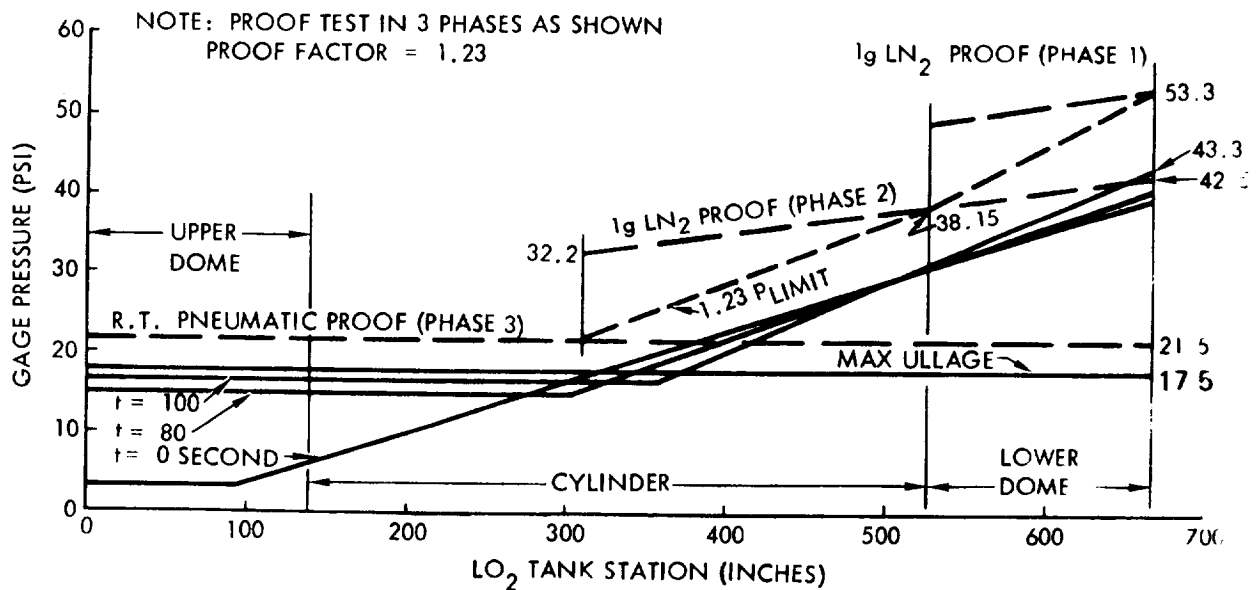


Figure 2-22.  $LO_2$  Tank Gage Pressures vs Tank Station

Critical design conditions for the body, wing, canard, and vertical tail structure are summarized in Table 2-7.

Figures 2-23, 2-24, and 2-25 present critical shear moment and torque values, together with bending moment curves, for the wing, canard, and vertical tail respectively.

The major critical thermal environment for the booster occurs during the entry portion of the mission. Local critical heating of the base heat shield and rudder occurs during ascent, and the top of the body and the vertical tail leading edge receive critical heating during orbiter separation.

Design temperatures used in sizing the booster outer thermal protection system structure are shown in Figures 2-26 and 2-27.

The acoustical environment to which the booster will be exposed during launch is shown in Figure 2-28, and summarized for all conditions in Table 2-10. For rocket noise at launch the exposure is general over the entire vehicle surface. For boundary layer shock wave interaction and for the air-breathing engine noise, the excitation is fairly localized. Figure 2-29 shows the wing acoustical environment for both booster noise at launch and air-breathing engine noise during cruise. The vertical tail acoustical inputs for launch are shown in Figure 2-30.

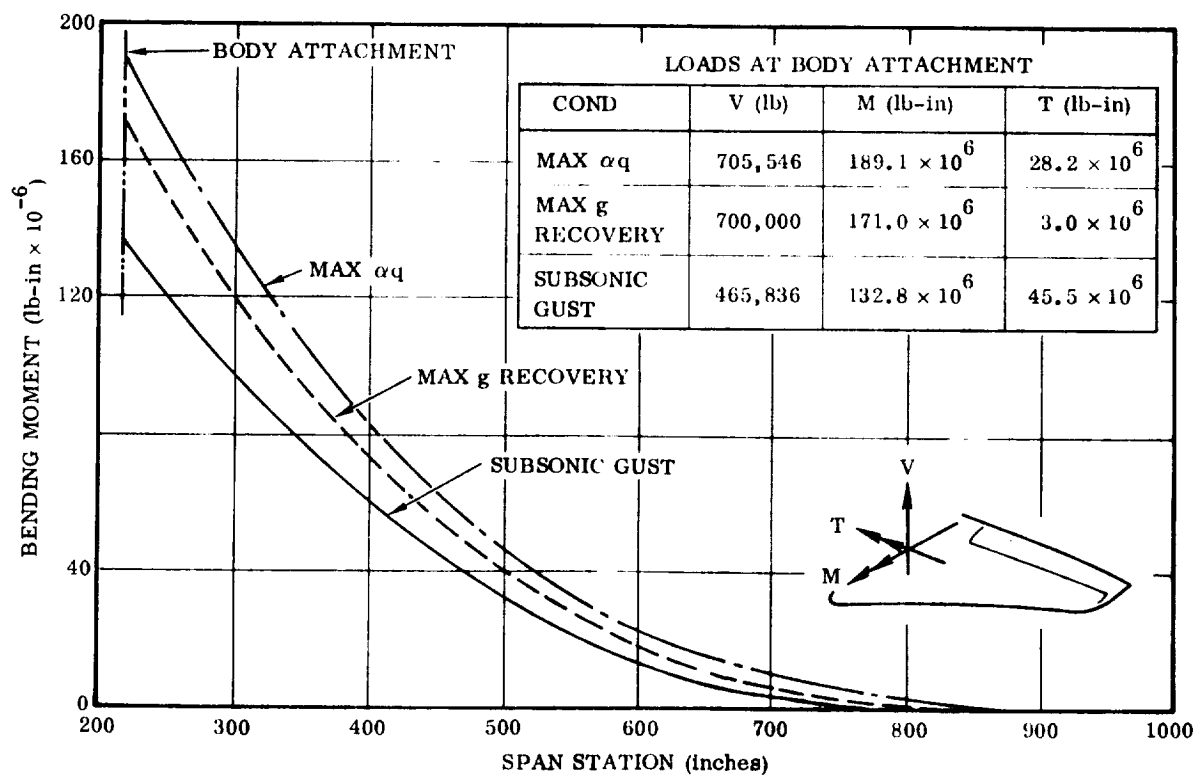


Figure 2-23. Wing Loads (Limit)

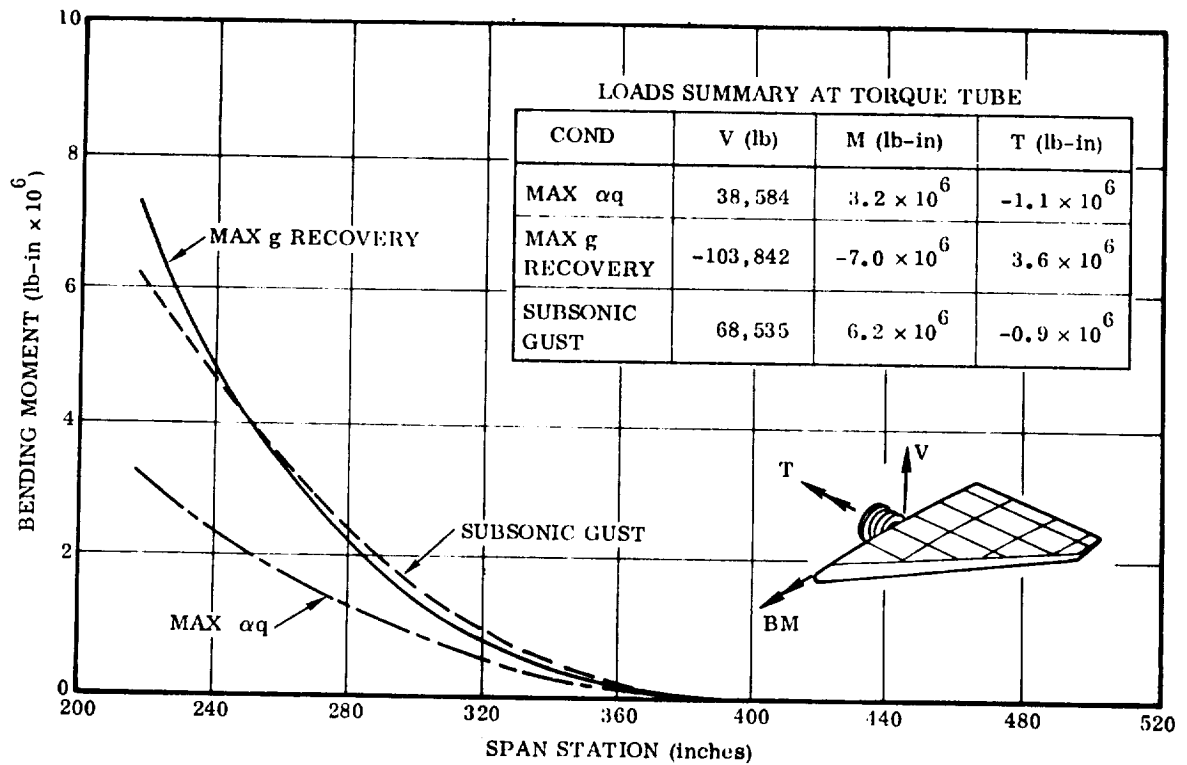


Figure 2-24. Canard Loads (Limit)

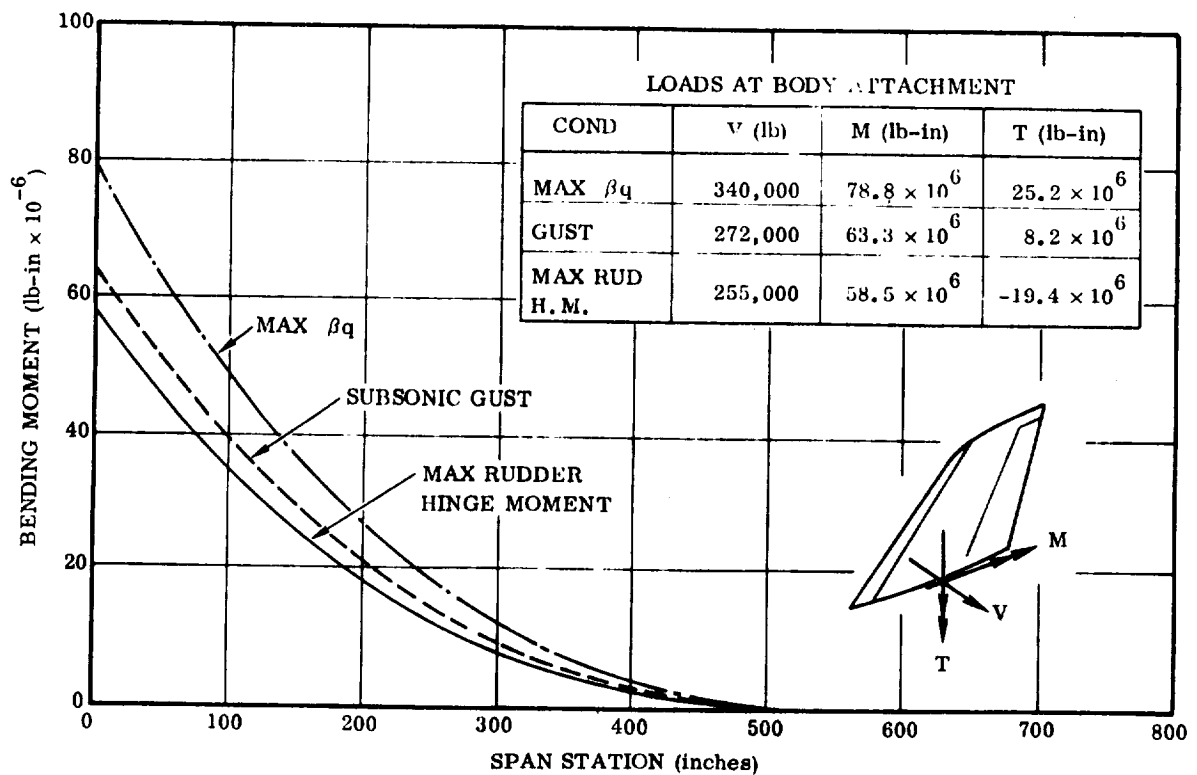


Figure 2-25. Vertical Tail Loads (Limit)

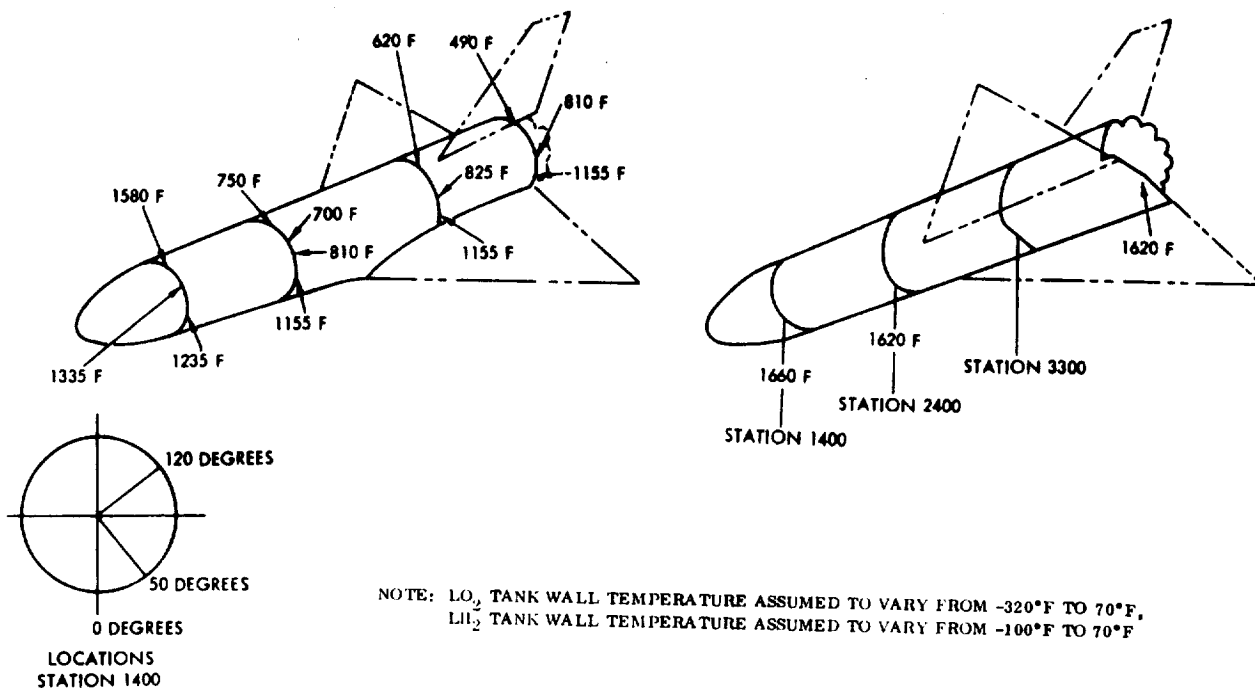


Figure 2-26. Design Temperatures

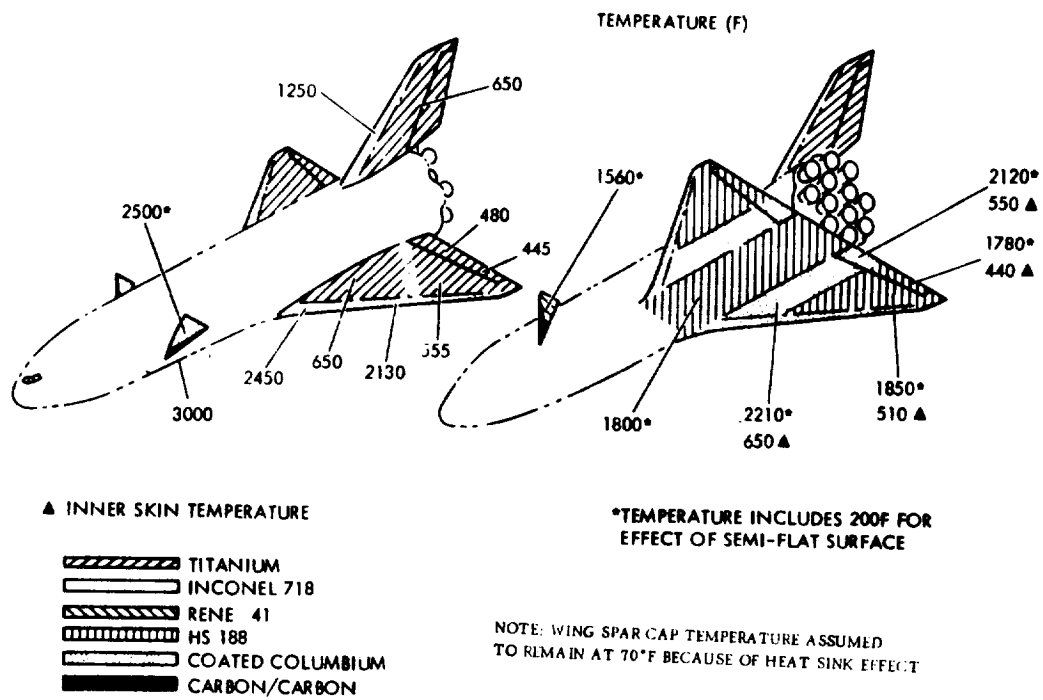


Figure 2-27. Temperature and Materials Distribution

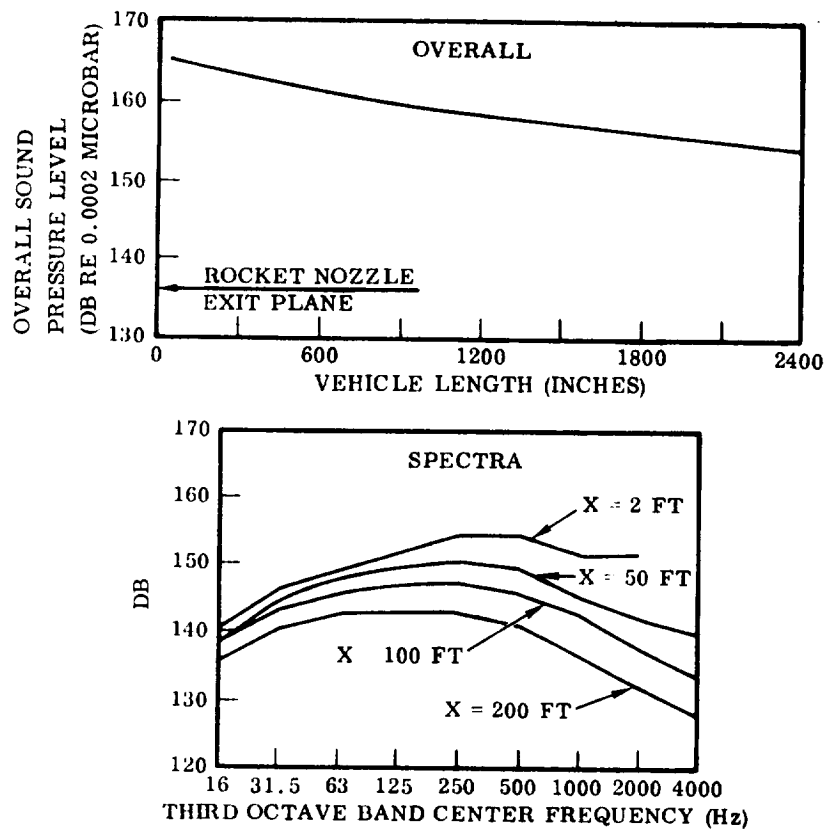


Figure 2-28. Acoustics on Launch Pad

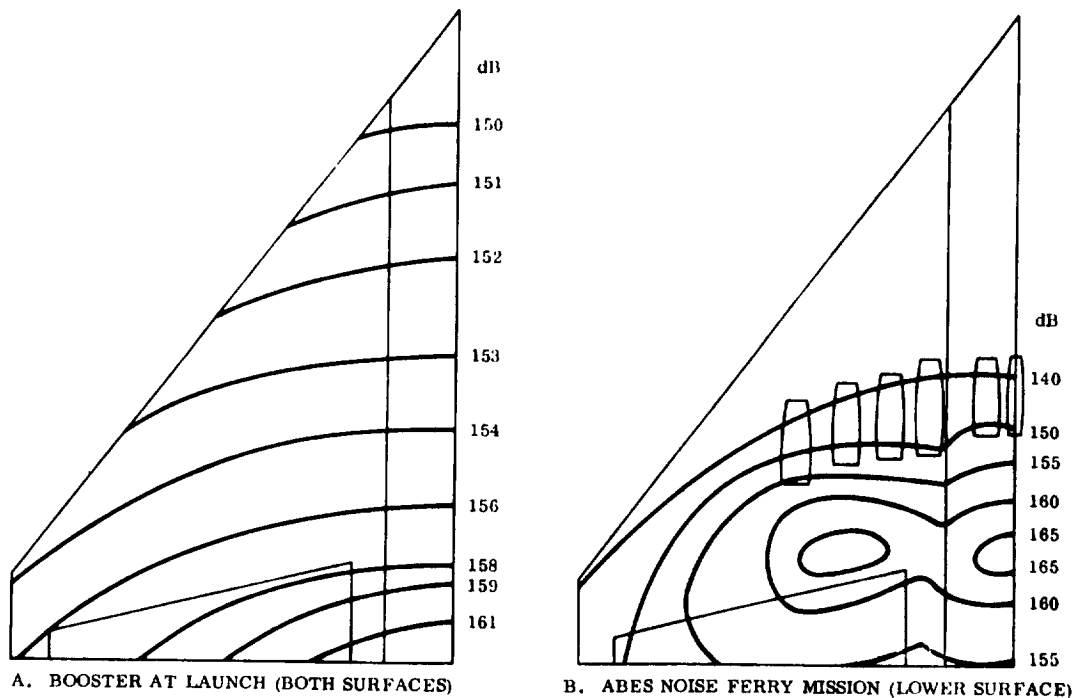


Figure 2-29. Contours of Equal Overall Sound Pressure Levels, Wing

Table 2-10. External Noise Levels on Booster Structure

Flight Condition	Noise Source	OASPL (db)(4)	Max. 1/3 OBSPL (db)(4)	Max. 1/3 OBSPL GMF(Hz) (4)	Incidence	Correlation Distance
Launch	Rockets	165(1) 154.5(2)	153 143	250 63-250	Random Random	Large Large
Ascent	Unperturbed boundary layer (B. L.)	149(2)	140	4000	Grazing	Small
	Shock - B. L. interaction	154.5(2)	146	10	Grazing	Small/medium
Reentry	Unperturbed B. L.	151(2)	141	4000	Grazing	Small
Cruise* (per engine)	ABES @ 10,000-ft alt. and 0.5 Mach	133(3)	123	560	Grazing/random	Small/medium
Ferry takeoff* (per engine)	ABES @ S. L. and zero air-speed	170(3)	160	1000	Grazing/random	Small/medium

Notes: (1) 15 feet above rocket nozzle plane.  
(2) Area of crew compartment.  
(3) About 10 feet aft of engine exhaust nozzle and 5 feet off engine centerline.  
(4) OASPL = overall sound pressure level  
OBSPL = octave band sound pressure level  
GMF = geometrical mean frequency

\*These levels are given per engine because they represent very near field data that are subject to wide variations for small changes in reference coordinates. The levels shown are for a plane through the apex of the jet exhaust core.

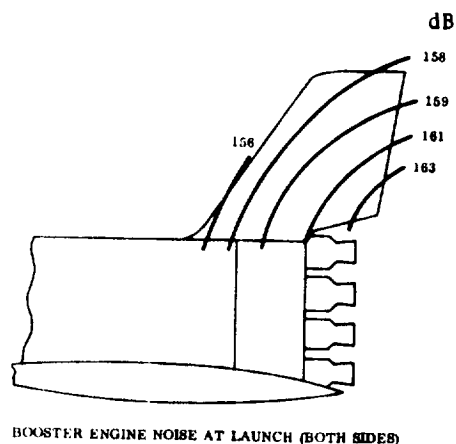


Figure 2-30. Contours of Equal Overall Sound Pressure Levels, Vertical Tail

## 2.7 SERVICE LOAD SPECTRA

This section presents the flight load and pressure load spectra expected during the 100-mission service life of the space shuttle booster. Load spectra for the components selected for detail study (i.e., tanks, wing, vertical tail, thrust structure, and orbiter support) are presented. These spectra are obtained from the work accomplished under MDAC Contract L.S. 2590-A3 (Determination of Load Spectra).

**2.7.1 WING LOAD SPECTRA.** Figure 2-31 presents the wing flight load spectra for a 100-mission vehicle life under ascent, entry, cruise/landing, and taxi conditions. The spectra are expressed in terms of number of exceedences versus alternating and mean bending moment, which are shown in percent of the critical value for the condition considered. These values are converted to number of cycles of mean and alternating stress, with the ascent condition represented by various segments of the total ascent flight to orbiter separation.

**2.7.2 VERTICAL TAIL LOAD SPECTRA.** The vertical tail flight load spectra are presented in Figure 2-32. As with the wing, the numbered lines represent various segments of the ascent flight.

**2.7.3 FUSELAGE LOAD SPECTRA.** The spectra of booster fuselage axial load intensity (i.e., net longitudinal load in the tank shell due to axial and bending loads, in lb/in.) are presented in Figure 2-33 for the top and bottom centerline locations at Fuselage Station 2600. Station 2600 is located at the aft orbiter-to-booster attachment and is the most highly loaded fuselage section. For the top centerline location, the design load intensity and cyclic load are compression. For the bottom centerline location, the design load intensity and cyclic loads are tension.

**2.7.4 ORBITER-TO-BOOSTER ATTACHMENT LOAD SPECTRA.** The forward orbiter-to-booster attachment flight load spectra are presented in Figure 2-34. Only vertical ( $F_Z$ ) and lateral ( $F_Y$ ) loads are shown, as the drag load (i.e.,  $F_X$ ) is taken through the aft attachment.

The aft orbiter-to-booster attachment flight load spectra are given in Figure 2-35.

**2.7.5 THRUST LOAD SPECTRA.** Figure 2-36 is a plot of the total mean thrust versus time for the 12 booster main rocket engines. Superimposed on this is the transient thrust load spectrum presented in Figure 2-37.

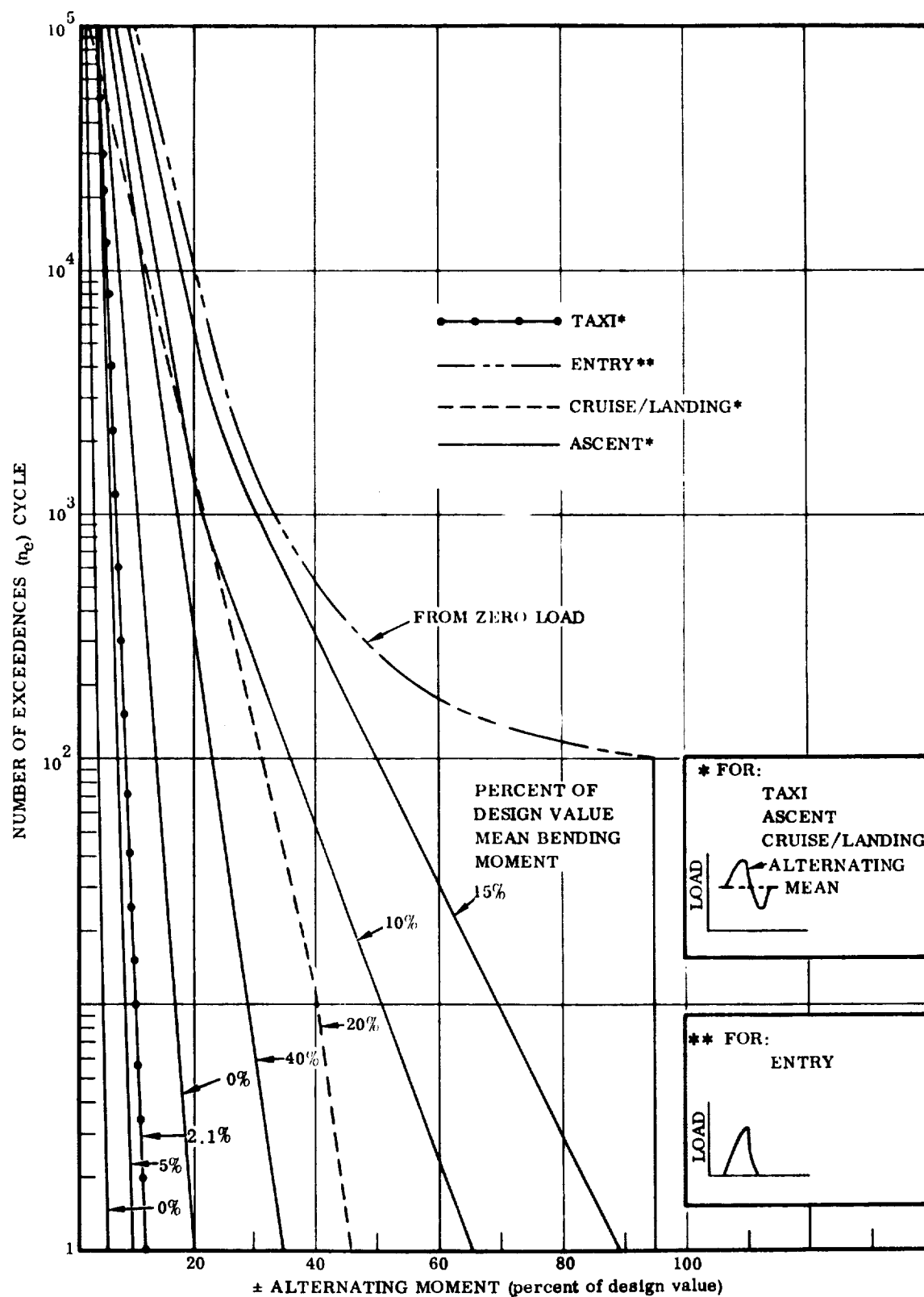


Figure 2-31. B-9U Wing Load Spectra



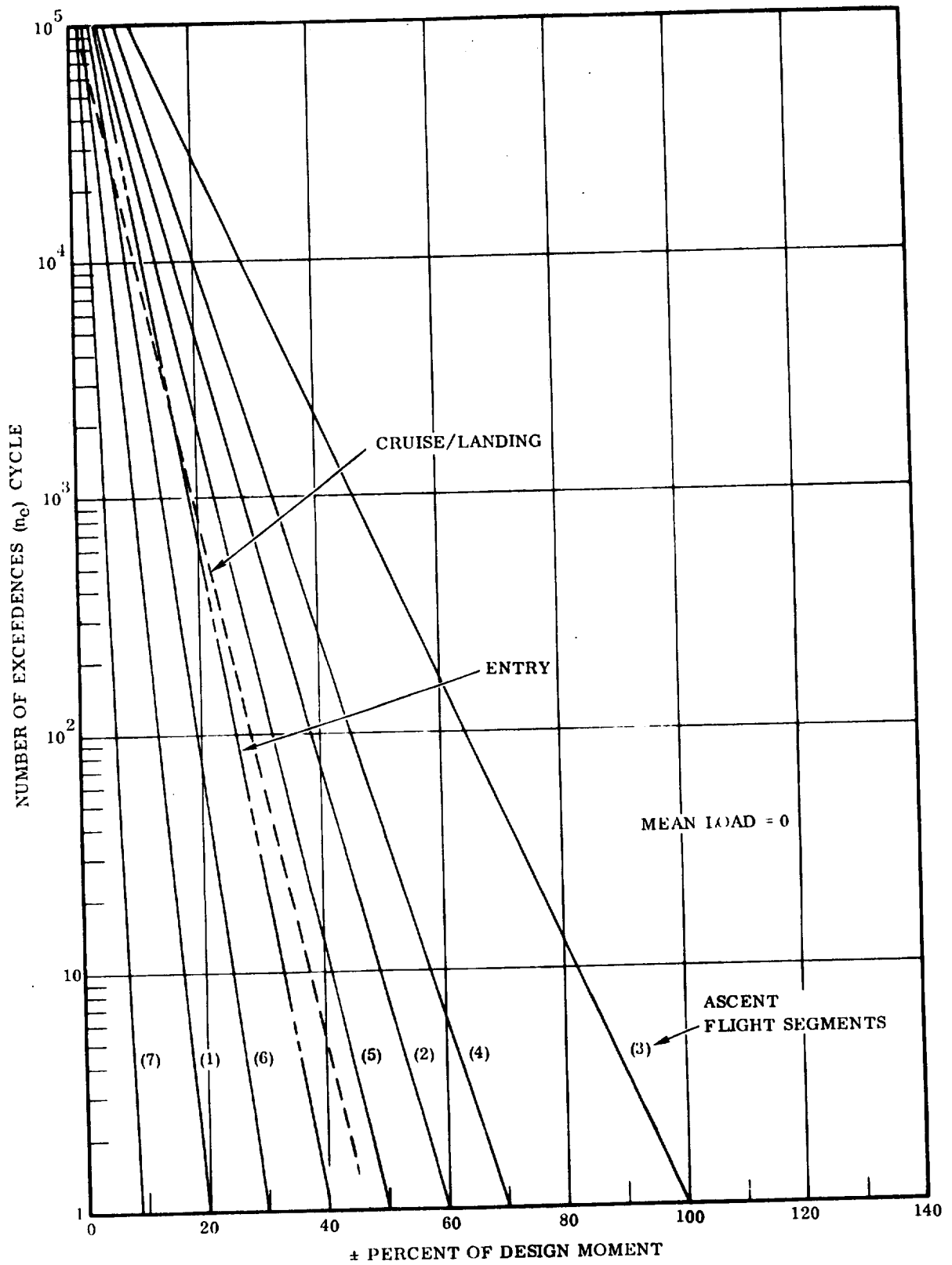


Figure 2-32. B-9U Vertical Tail Load Spectra

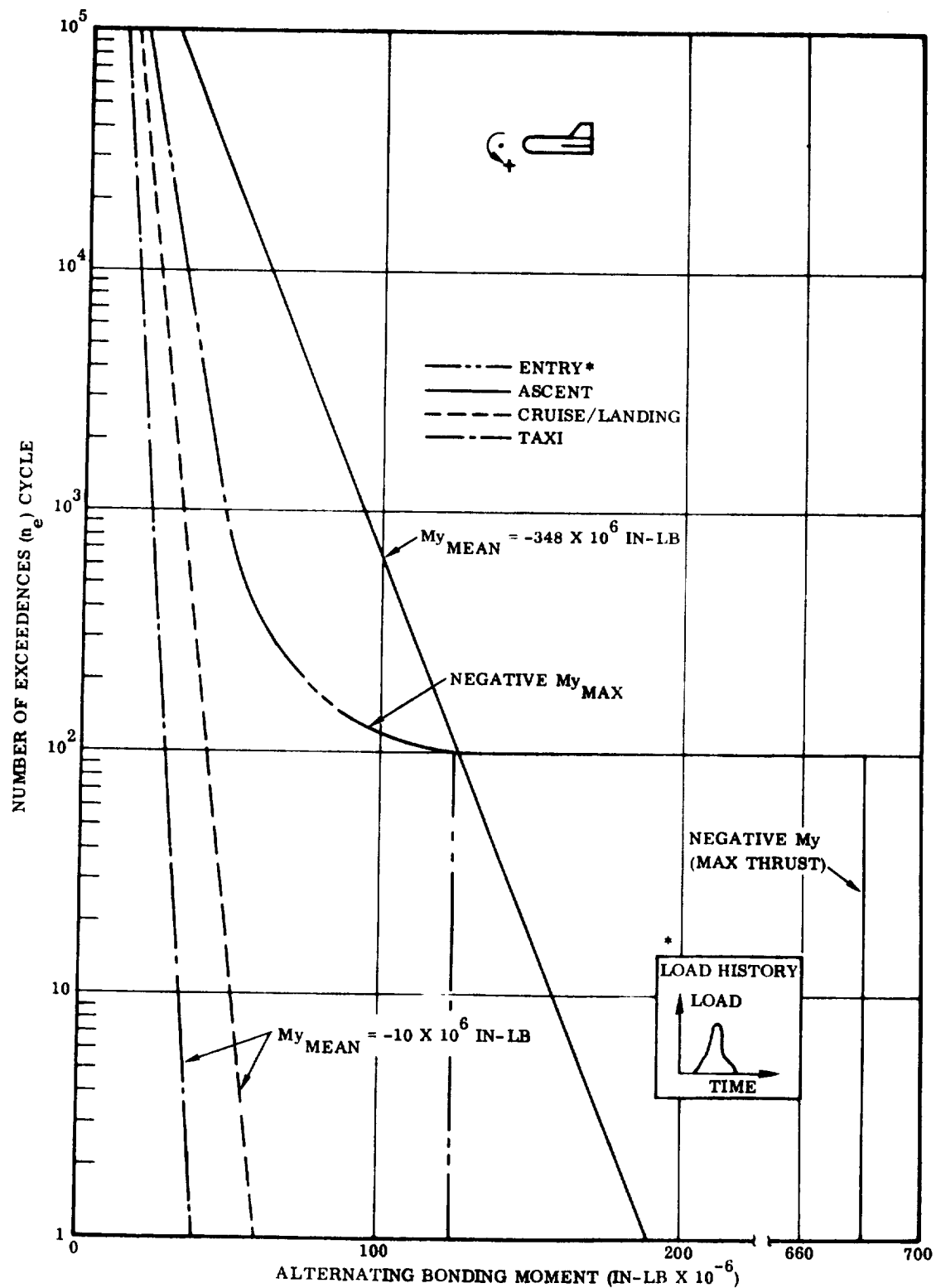


Figure 2-33. B-9U Fuselage Station 2600 Load Spectra

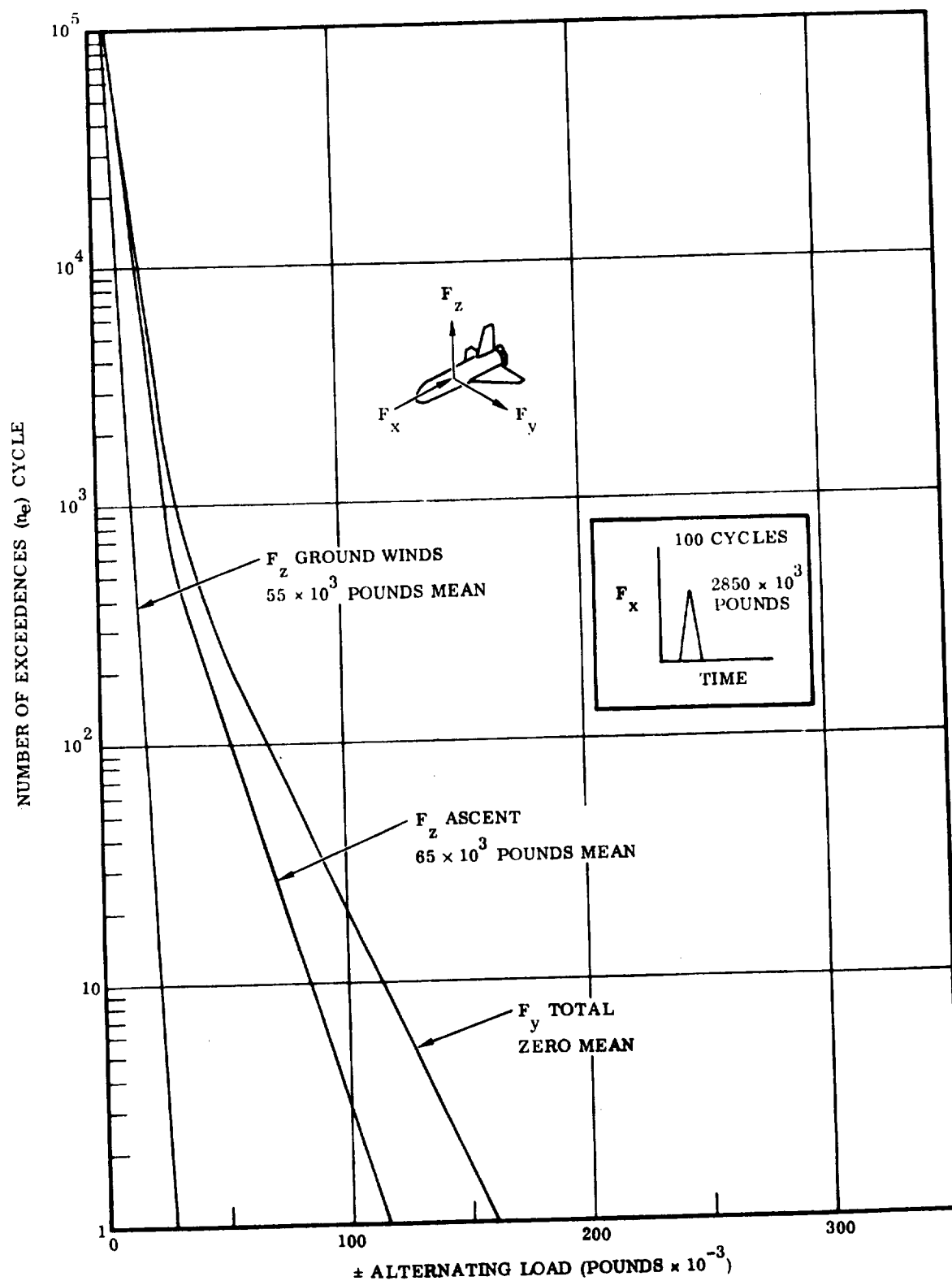


Figure 2-34. B-9U Orbiter Forward Attachment Load Spectra

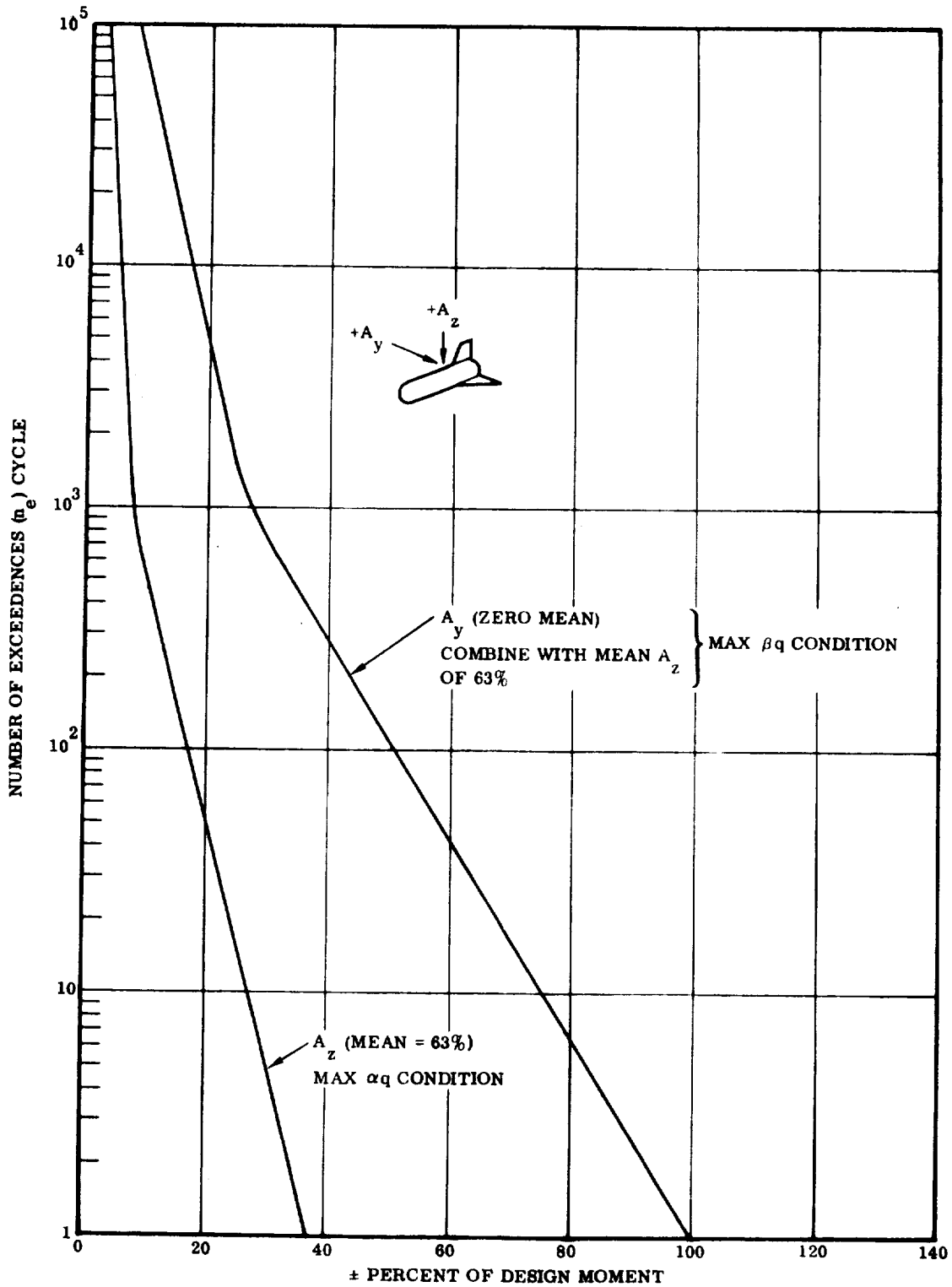


Figure 2-35. B-9U Orbiter Aft Attachment Load Spectra

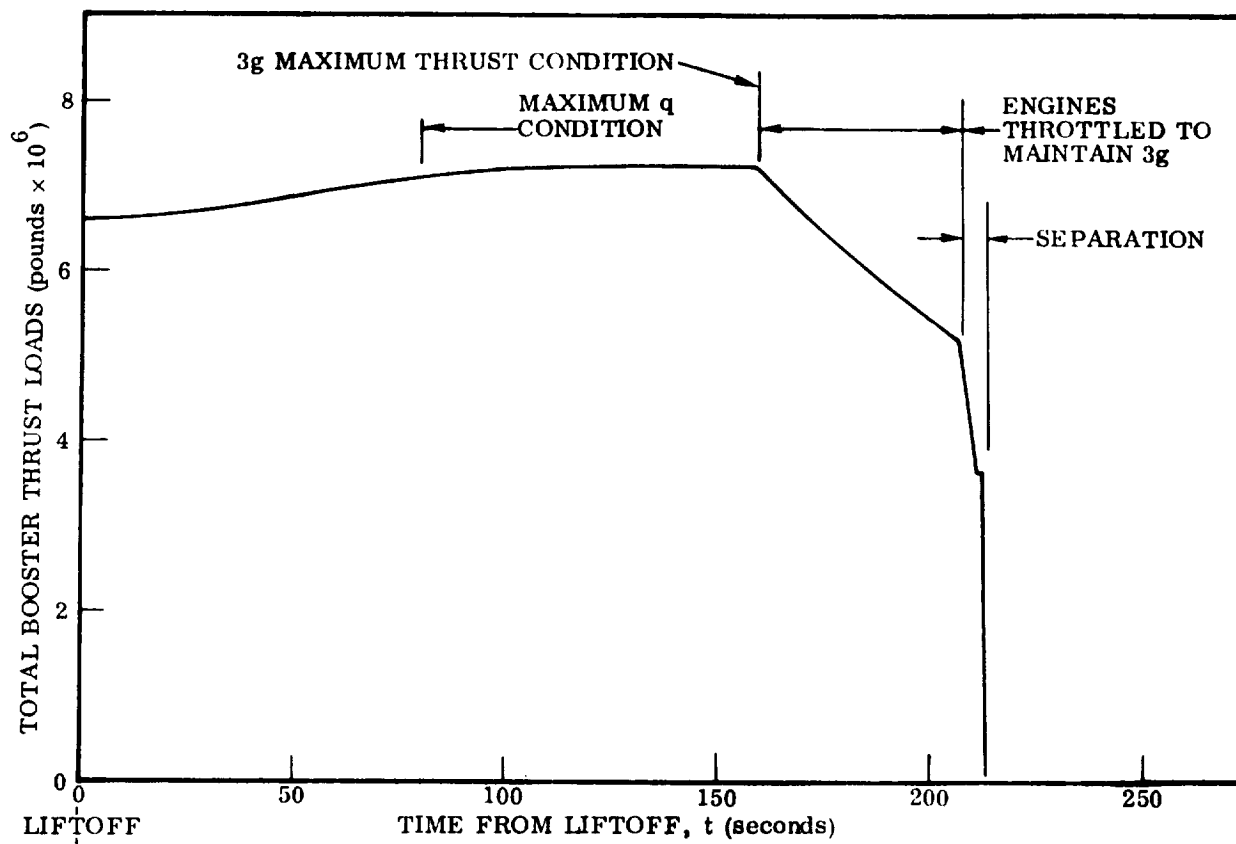


Figure 2-36. Total Mean Booster Main Engine Thrust

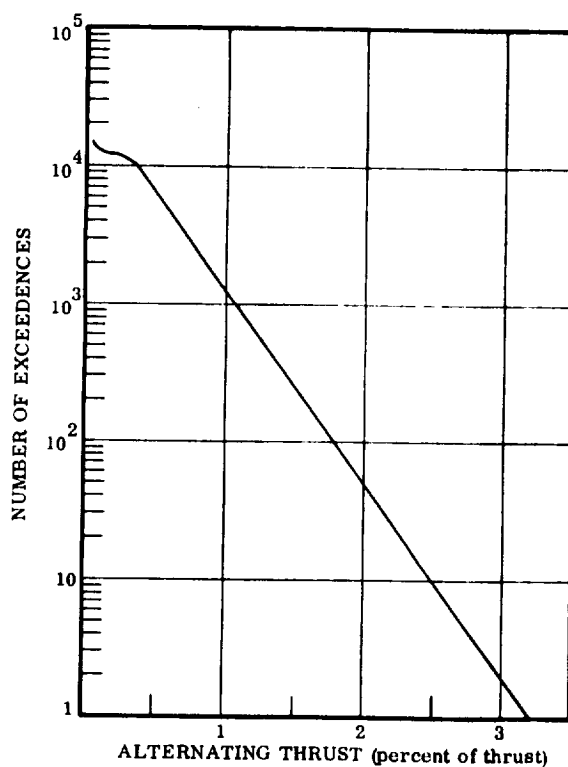


Figure 2-37. Thrust Spectrum (One Flight)

**2.7.6 PROPELLANT TANK PRESSURE SPECTRA.** The main LH<sub>2</sub> and LO<sub>2</sub> propellant tank pressure schedules are presented in Figures 2-38 and 2-39, respectively. Nominal ullage and ullage plus fuel head pressure at the lower tank apex are shown. In addition, the maximum design pressure (i. e., maximum relief valve setting plus fuel head) assuming a pressure regulator malfunction is shown. For fatigue and flaw growth studies, it will be assumed that a pressure regulator malfunction occurs once every 20 flights.

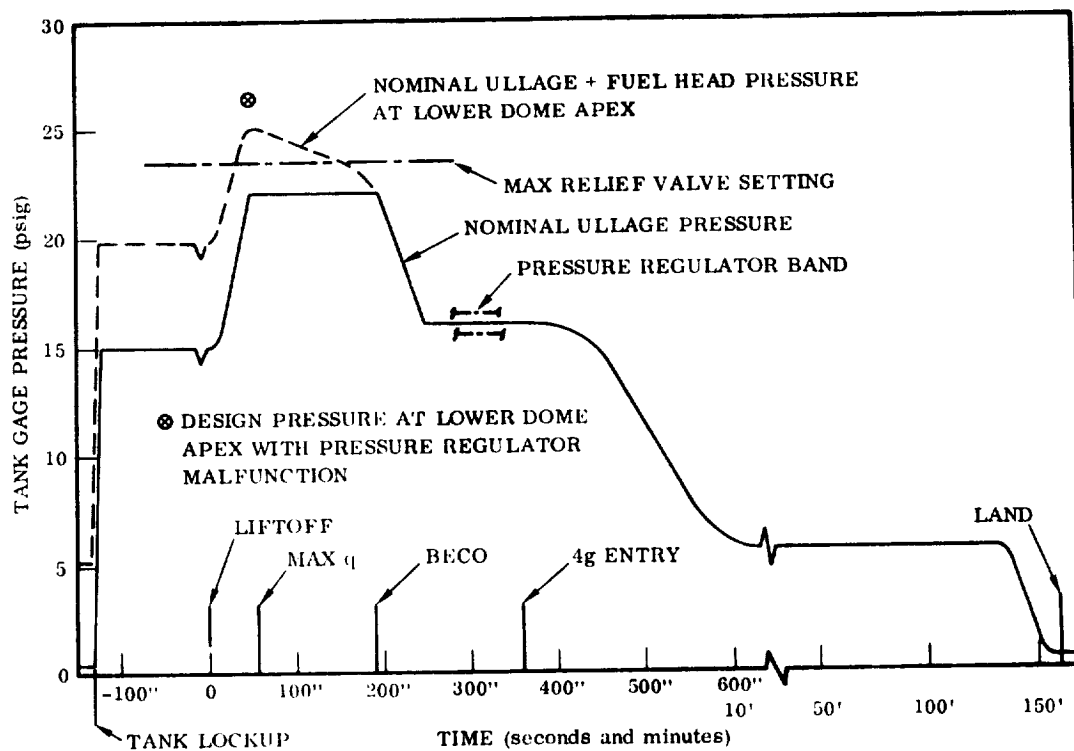


Figure 2-38. Booster Main LH<sub>2</sub> Tank Pressure Schedule

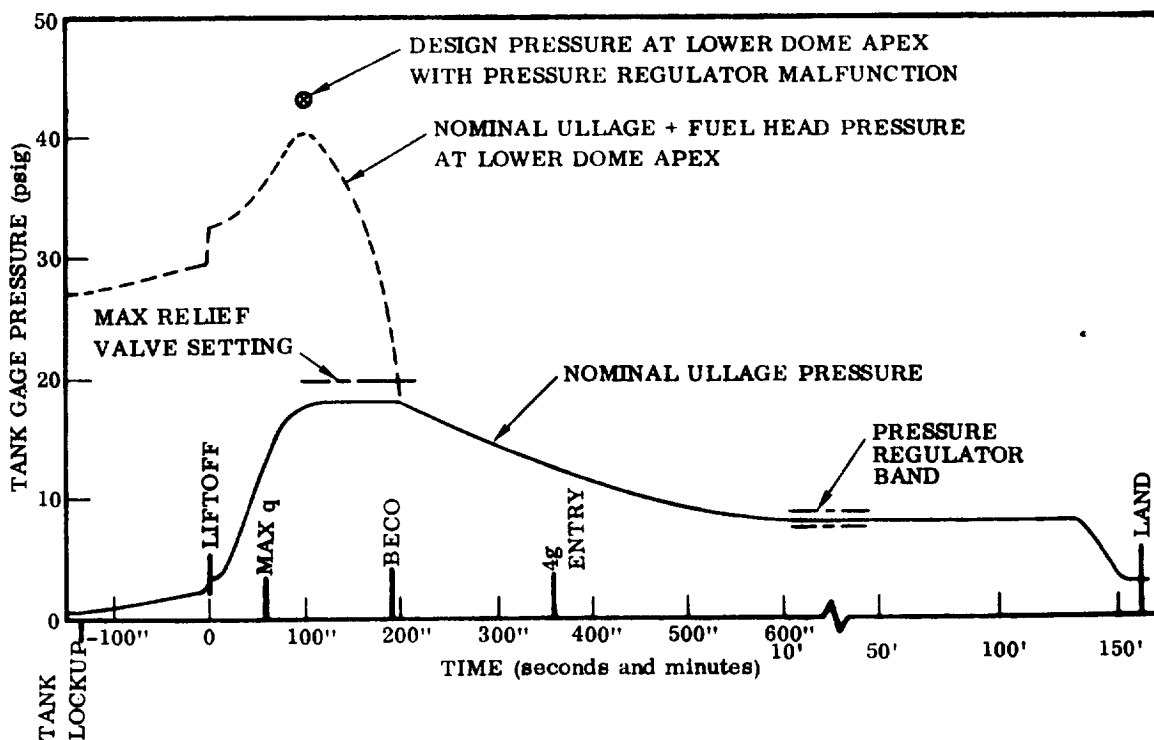


Figure 2-39. Booster Main LO<sub>2</sub> Tank Pressure Schedule

## 2.8 STRUCTURAL TEST PLANS

**2.8.1 TEST REQUIREMENTS.** The booster missions dictate the structural requirements from which a vehicle design is evolved. To certify that the vehicle design will meet the mission requirements, a combination of structural analysis and testing will be conducted. The test program attempts to verify the structural analysis (in regions of uncertainty) and drive out overlooked design deficiencies within the limits of physical practicality and cost.

The booster test program will be broken down into three hardware levels and three test categories:

- a. Hardware levels
  - 1. Subcomponents
  - 2. Components
  - 3. Major combined components or complete vehicles
- b. Test Categories
  - 1. Development tests
  - 2. Qualification tests
  - 3. Proof tests

The tests described in the following section represent a minimum "bare bones" test program, and it is anticipated that when the sensitivities of the structure to safe-life/fail-safe requirements are established, additional development and qualification tests will be added (see Sections 4.3.1 and 5.3.1).

### 2.8.2 TEST CRITERIA

**2.8.2.1 Development Tests.** Structural development tests will be conducted to determine basic design information and assist in designing those structures for which analysis is difficult.

Development tests may serve as qualification tests in those certain cases where confidence is such that this action has a high probability of success and is cost beneficial, providing the following additional criteria and rigors are met:

- a. Predeclaration of intent to use test for qualification.
- b. "No impact" waivers obtained for flight configuration differences.
- c. Facility certified (calibrated).
- d. Contractor inspection on-site, as necessary.
- e. Test requirement/procedure/tolerance approved.
- f. Pre-functional and post-functional successful.

Testing will be structured to provide initial information on maintenance, and projected service life requirements will be established during the operational test phase.

2.8.2.2 Qualification Tests. Qualification tests will be conducted to prove structural adequacy of the design for all anticipated conditions. This will be accomplished for:

- a. Hardware which could potentially result in loss of crew or vehicle shall receive a qualification test to the specified environments. Environments selected shall be those that the hardware is expected to experience in its service life (ground and flight) plus the design margin. The environment levels and durations shall be the worst case condition and shall demonstrate the design margins.
- b. Hardware, the failure of which would result in loss of primary or secondary mission objectives or launch scrub, shall be certified flightworthy by an accumulation of data from its test history during development, acceptance, off-limit, checkout, and flight test in lieu of rigorous qualification testing.
- c. Qualification testing requirements may be waived when equipment is selected that has been previously qualified to the level required for the proposed shuttle application. In these cases, adequate substantiation of configuration, inspection, facility certification, etc., must be submitted with supporting rationale to the contracting agency for approval of the waiver.
- d. Qualification testing of components and/or subsystems will be accomplished on the highest practical level of assembly.
- e. Qualification test levels must include verification of design safety factors.
- f. Components to be subject to qualification tests shall first be subjected to the same proof tests applied to flight components.



**2.8.2.3 Proof Tests.** Proof tests will be conducted as an assist in quality control procedures by screening manufacturing errors or flaws which could grow to critical size in the life of the vehicle. Proof tests are required on each production component based on a safe-life design philosophy and whose criticality requires further testing in addition to that performed during qualification testing.

Proof test factors will be based on the minimum of that required by the structural design criteria (reference Attachment E of first monthly progress report) or from fracture mechanics analysis considering the anticipated service load spectra and environments.

**2.8.3 STRUCTURAL DEVELOPMENT TESTS.** The development test plans that follow emphasize the booster structural components selected for detailed study, namely those listed below and shown in the figures of Section 2.2.

- a. Wing structural box (delta and swept)
- b. Vertical tail structural box
- c. Ascent engine thrust structure
- d. Orbiter support frame
- e. Main propellant tanks

Development testing at the subcomponent level includes:

- a. LO<sub>2</sub> Tank. Tank-to-forward support structure joint specimens for static/fatigue loading.
- b. Intertank Section
  - 1. Integral plate-stringer panels for static shear and compression loading.
  - 2. Y-joint specimens for static loading.
  - 3. Weld joint specimens for static loading.
  - 4. Tank-to-intertank section joint specimens for static/fatigue loading.
  - 5. Stringer-frame intersection specimens for fatigue loading.
  - 6. Tank wall and weld joint flaw growth specimen for fatigue loading.
  - 7. Full-scale quarter-setment frames for static/fatigue loading.
  - 8. Access door cutouts and covers for static/fatigue loading.

9. Fuel and pressurization line cutouts and attachments for static/fatigue loading.
  10. TPS attachments for static/fatigue loading.
  11. Full scale diameter LO<sub>2</sub> feed line sections for static/fatigue loading.
- c. LH<sub>2</sub> Tank
1. Tank-to-thrust structure joint specimens for static/fatigue loading.
  2. A wing support bulkhead, full-scale, half-segment for static/fatigue loading.
  3. A subscale tank specimen for development of the cryogenic insulation under combined heat, simulated body loads as required, internal pressure and vibration. Tests will include tanking and detanking with LH<sub>2</sub>.
  4. Main landing gear support fitting and back-up structure for static/fatigue loading.
  5. Orbiter support bulkhead, full-scale, half-segment for static/fatigue loading.
- d. Thrust Structure
1. Truss columns for static compression loading.
  2. Truss end fittings and beam cap intersections for static/fatigue loading.
  3. Truss beam caps for static loading at elevated temperatures.
  4. Wing and vertical stabilizer support bulkhead shear fittings for static/fatigue loading.
  5. Vertical stabilizer attachment lugs for static/fatigue loading.
  6. Base heat shield panels for static loading and sonic fatigue loading at elevated temperature.
  7. Thrust cylinder panels for static shear and compression loading.
  8. A one-half scale truss beam for static/fatigue loading.
  9. Hold-down, release, engine mount, and gimbal actuator support fittings for static/fatigue loading.
  10. Rise-off disconnect, TPS attachment, and wing attachment support structures for static/fatigue loading.
- e. Wing
1. Corrugated web shear beams for static/fatigue loading at elevated temperature.
  2. Spar cap tension and compression elements for static loading at elevated temperature.
  3. Cover panels and TPS panels for static shear and sonic fatigue at elevated temperature.

4. Cover panel joints and TPS panel joints for static/fatigue loading at elevated temperature.
  5. Wing spar lugs for static/fatigue loading at elevated temperature.
  6. Leading edge skin and rib elements for static/fatigue loading at elevated temperature.
  7. Leading edge hinge and front spar attachment for static/fatigue loading at elevated temperature.
  8. Wing cover access cutout and door for static/fatigue loading at elevated temperature.
  9. Body attachment fitting and backup structure for static/fatigue loading.
  10. Full wing support links for static/fatigue loading.
  11. A full leading edge rib for static/fatigue loading at elevated temperature.
  12. Leading edge slip joint and seals for static/fatigue loading at elevated temperature.
- f. Vertical Stabilizer
1. Cover plate stringer panels for static compression and shear.
  2. Vertical stabilizer attachment lugs for static loading.
  3. Cover panels for sonic fatigue at elevated temperature.
- g. Orbiter Support Frame (included in LH<sub>2</sub> tank tests).

Development tests will not be accomplished at the full component level, but the following tests will be performed on simplified components.

- a. Body Structures. Component level development tests of the body structure will include a simplified intertank adapter, simplified thrust structure, and simplified LH<sub>2</sub> propellant tank. This tank will be full-scale diameter, with full end domes, wing attachment and orbiter attachment frames, TPS attachment, shell discontinuities such as access doors, and fuel and pressure line attachments. This article will aid in developing tooling and fabrication techniques. The major development test articles for the intertank adapter and thrust structure will be installed on this tank specimen for final development tests on all three components.
- b. Wing Structure. Component level tests will include a wing section at least three spars wide, a leading edge section, and an elevon (aileron) section, for static and fatigue tests at elevated temperatures.
- c. Vertical Tail Structure. Component level tests will include a section of the heat sink leading edge and a portion of the three spar box for static/fatigue tests at elevated temperature.

**2.8.4 STRUCTURAL QUALIFICATION TESTS.** The following types of structural testing will be conducted to certify adequacy of the booster design:

- a. Static tests to verify that the structure does not experience detrimental deformation at design limit loads and pressure, and does not rupture or collapse at design ultimate loads and pressures.
- b. Fatigue tests to verify fatigue-life requirements; as follows:
  - 1. The test articles will be load-cycled through a spectrum equivalent to one life times a scatter factor of four (100 missions  $\times$  4 = 400 missions). The test will demonstrate that the structure experiences no detrimental damage throughout this test life; for structures that depend on non-destructive inspection for structural life assurance, it will demonstrate that these techniques are adequate to ensure detection of significant defects.
  - 2. Fatigue loading includes the effects of low-frequency cycling due to tank pressurizations, aerodynamics and inertia loading and high-frequency cycling, where applicable, due to acoustic fatigue.
- c. Thermal cycling, where applicable, concurrent with the static and fatigue testing, to simulate environmental effects significantly contributing to loads (thermal stresses) or altering material properties.

**2.8.4.1 Static Tests.** The following static qualification tests are planned for the body structure components under study. Two major hardware structures are planned.

- a. One static test article and one fatigue test article qualifies the LO<sub>2</sub> tank, forward LO<sub>2</sub> tank support structure including the nose landing gear support structure.
- b. One static test and one fatigue test article qualifies the LH<sub>2</sub> tank, intertank adapter, orbiter support and separation structure and mechanism, and thrust structure.

The above static test articles will be subjected to five overall static qualification conditions at room temperature:

- a. Dynamic lift-off plus tail wind. Maximum axial load. Critical on forward inter-tank adapter, thrust structure.
- b. Maximum  $\alpha$  q plus tail wind. Maximum body bending load. Critical on LH<sub>2</sub> tank and wing.
- c. Three-g maximum thrust plus tail wind. Critical on LH<sub>2</sub> tank and wing.

- d. Booster recovery. Critical on TPS and wing.
- d. Asymmetrical maneuver. Critical on vertical stabilizer.

In addition to these overall load conditions, local areas will be loaded to design ultimate if not covered in the overall conditions as follows:

- a. LO<sub>2</sub> Tank
  - 1. All TPS support link attachments.
  - 2. All TPS support roller attachments.
  - 3. All TPS fixed attachments.
- b. LH<sub>2</sub> Tank
  - 1. Orbiter support and separation structure attachment.
  - 2. Wing support structure.
  - 3. All TPS support link attachments.
  - 4. All TPS support roller attachments.
  - 5. All TPS fixed attachments.
  - 6. Main landing gear support structure.
- c. Thrust Structure
  - 1. Wing support structure.
  - 2. TPS support link attachments.
  - 3. TPS support roller attachments.
  - 4. Hold-down fitting structure.

During the static tests, LO<sub>2</sub> and LH<sub>2</sub> tank internal pressures will be applied, using a gas for pressurization, combined with external body loads. Pressures will be factored to account for the difference in material properties between cryogenic and room temperatures. Since the pressure is beneficial to compressive loading, design limit tank pressures will be combined with design ultimate external forces. However, both tanks will be pressurized to design ultimate without external loads. For the LO<sub>2</sub> tank ultimate pressure test, the tank will be filled with water, in the vertical position, to provide partial pressure head simulation. For each combined test condition, full design limit pressure for that condition will be applied first, followed by application of external forces in increments to design ultimate.

**2.8.4.2 Fatigue Tests.** Separate test articles (noted above), are planned for the body static and fatigue tests. The use of separate major component articles is justified by eliminating the high risk of premature structural failures from fatigue flaws during static ultimate tests on a fatigue test article.

All body qualification fatigue tests will be conducted at room temperature, except for the LO<sub>2</sub> tank, which will be under LN<sub>2</sub> temperatures in a vertical position. This will provide a partial simulation of the pressure gradient due to the head of LO<sub>2</sub> as well as a close simulation of the environmental conditions which significantly affect fatigue and fracture characteristics. The LH<sub>2</sub> tank will be protected by cryogenic insulation, and consequently does not experience such low temperature extremes. It, therefore, will be tested at room temperature, in the horizontal position to facilitate loading.

The fatigue test spectrum will be based on flight-by-flight loading. This will provide the correct interspersal of load distributions and magnitudes. It also will break the test down into small blocks for the multi-life program. This means the test life can be equated closely with service life at any time during the test.

The relatively short time from lift-off to the start of the low-altitude flyback cruise allows fatigue test simulation of this portion of each flight in true time. This is significant for the LO<sub>2</sub> tank tested at cryogenic temperatures, since the true temperature-time program can be used, ensuring the correct interaction between applied load and thermal stresses. It also means that the total time at temperature will be correctly simulated throughout the fatigue test, incorporating the effects of material property variations.

A typical fatigue spectrum per flight for the qualification fatigue tests is presented in Figure 2-40. Three symmetric overall loading conditions (distributions) are planned: a launch condition, a recovery condition covering orbiter separation and entry, and an atmospheric cruise (gust and maneuver) condition. The first two conditions would be applied with true-time simulation of load, tank pressures and temperatures. The third condition, with the most load cycles, would be time-compressed in accordance with aircraft-type fatigue testing practice. Orbiter separation and (booster) landing loads will be introduced locally as applicable. If possible, the atmospheric cruise condition load levels will be interspersed to approach a random-type sequence. The LN<sub>2</sub> cycling of the LO<sub>2</sub> tank will be required to properly cycle the tank structure. One tanking/detanking cycle per flight will be required. Volume-displacement devices will be used to expedite tanking and detanking of LN<sub>2</sub> for the LO<sub>2</sub> tank, and pressurization and depressurization of the LH<sub>2</sub> tank. The total number of load cycles is relatively low compared to a typical aircraft program.

As shown in Reference 4, the method of component or parallel qualification testing is planned. This not only minimizes facility requirements, but permits testing in more

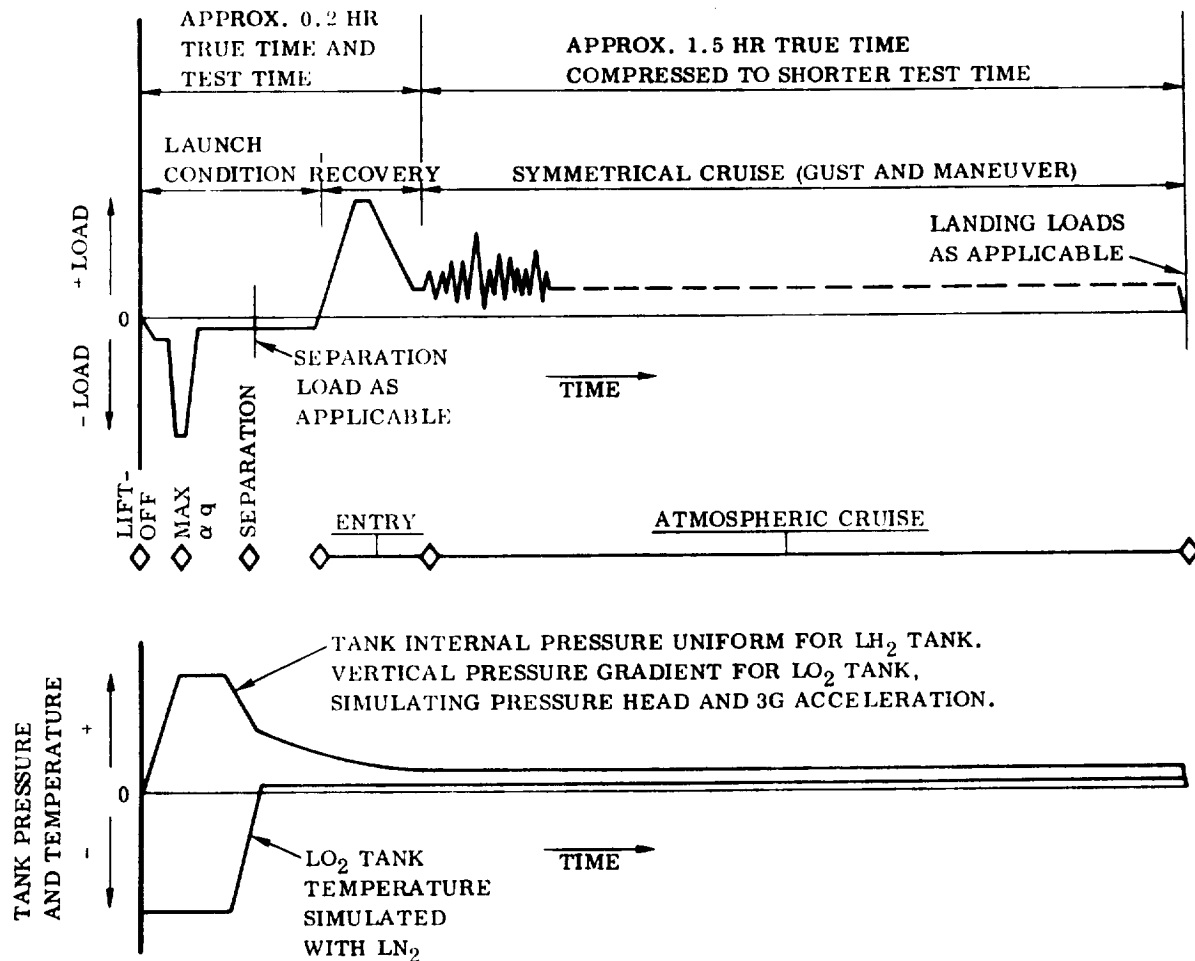


Figure 2-40. Typical Fatigue Test Spectrum for Body Structure

than one facility. It also offers the best approach for accomplishing a valid structural test program in the shortest span time, in that failures in one component do not cause a cessation of testing. Also, the potential for failure of one component to cause unrelated damage to another component will be reduced. The component test articles will contain sufficient overlap of attaching structure to ensure proper load interactions at the structural interface of the individual components.

## 2.8.5 WING QUALIFICATION TESTS

**2.8.5.1 Static Tests.** The following static tests are planned for the basic wing structure. One test article will be used, consisting of a complete left wing structural box and carrythrough structure, all wing attachment links, ABES engine doors, and a stub portion of the right wing. Test procedures will generally follow MIL-A-8867 and NASA SP-8044 as guides.

The wing will be subjected to four overall static conditions, each with appropriate temperatures:

- a. Maximum  $\alpha_q$
- b. Maximum g entry
- c. 3-g thrust/burnout
- d. Subsonic gust

In addition to these overall conditions, the following local areas will be loaded to design ultimate if not covered in the overall condition:

- a. ABES fuel tank support attachments
- b. ABES engine support structure and doors
- c. Elevon hinge and support structures
- d. Elevon actuator support structures
- e. Leading edge attachment structure
- f. Body attachment links

All static qualification tests will be conducted at elevated temperatures as required. The time-temperature profile will be programmed in true time to produce correct thermal stresses and combined thermal/external force induced stresses.

The planned static test sequence for these thermo-structural tests requires an initial application of static load only, to a prescribed level, followed by a thermal cycle while holding the static load. This is repeated in increasing load increments to design ultimate.

**2.8.5.2 Fatigue Tests.** A separate wing test article, described above, will be used for fatigue qualification tests. The separate article costs are again justified by separation of high risk static ultimate tests from the fatigue article.

A typical fatigue spectrum per flight for the qualification fatigue tests is presented in Figure 2-41. Three overall symmetric loading conditions will be applied, with true-time simulation of loads and heating and cooling effects through the first two conditions. This is followed by room temperature load cycling for the third (atmospheric cruise) condition, ending in local landing loads as applicable. This means that the total time at temperature will be correctly simulated throughout the fatigue test, incorporating the effects of creep and mechanical property degradation.



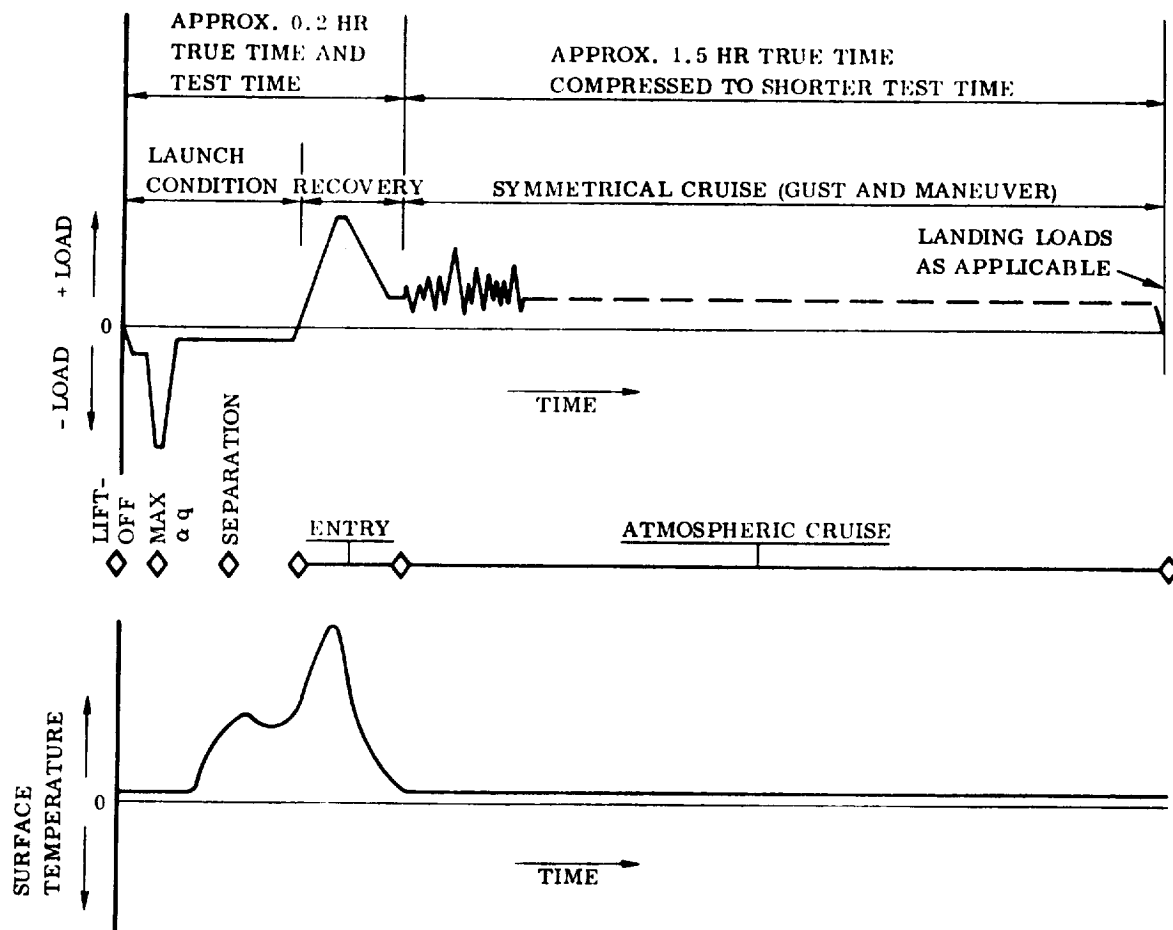


Figure 2-41. Typical Fatigue Test Spectrum for Aerodynamic Surfaces

## 2.8.6 VERTICAL TAIL QUALIFICATION TESTS

2.8.6.1 Static Tests. A complete vertical stabilizer with attachment structure, rudder, and leading edge will be used for conducting static tests. The tail will be subjected to three major overall conditions, each with appropriate temperatures:

- a. Maximum  $\beta q$
- b. Subsonic gust
- c. Rudder kick

The maximum temperature condition, which occurs during entry, is not a critical overall condition.

In addition to the overall condition, the following local areas will be qualified at ultimate loads if not covered in the overall conditions:

- a. Rudder hinges
- b. Rudder actuator support
- c. Leading edge attachment

**2.8.6.2 Fatigue Tests.** It is planned that no overall fatigue tests will be conducted on the vertical tail. The elimination of a fatigue qualification test is considered justified, as the structure is stiffness designed, and the loads produced by  $\beta q$  are rarely encountered. Therefore, the fatigue damage that will accumulate during a life can be shown by analysis to be too low to require testing.

**2.8.7 STRUCTURAL PROOF TESTS.** Each test and flight article will undergo structural proof tests. The LO<sub>2</sub> tank will be proof-pressure tested in three steps: (1) the lower dome will be pressurized by attaching a jig bulkhead to form a tight enclosure, (2) the lower dome will be assembled to the lower half of the cylindrical section, the top sealed with a jig bulkhead, and this pressurized and (3) the complete tank will be pressurized. All of these tests will be conducted in the vertical position. The first two steps will be accomplished with LN<sub>2</sub>. The final step will utilize pneumatic pressurization. This procedure will permit a higher proof pressure on the lower tank than the upper tank area, thus more closely following the design pressure envelope.

The LH<sub>2</sub> tank will be proof-pressure tested in the horizontal position using dry gas and volume displacement devices.

## **2.9 QUALITY CONTROL AND MAINTENANCE PLANS**

Those portions of the quality control and maintenance plans that are relevant to the study are presented and discussed in this section.

**2.9.1 QUALITY CONTROL AND NON-DESTRUCTIVE EVALUATION.** Figure 2-42 presents a schematic of the various elements of a quality control and non-destructive evaluation (NDE) plan for a typical structural component and their sequencing. For components which are not welded or proof tested the related elements of the NDE plan are eliminated.

The important features of the NDE plan which require strong emphasis on the Space Shuttle Program are:

- a. Inspection and non-destructive testing (NDT) at each important phase of fabrication, qualification, and operation for the life of the space shuttle vehicle. These phases include material procurement, detail part fabrication, assembly, proof test, post proof test, and flight operations.

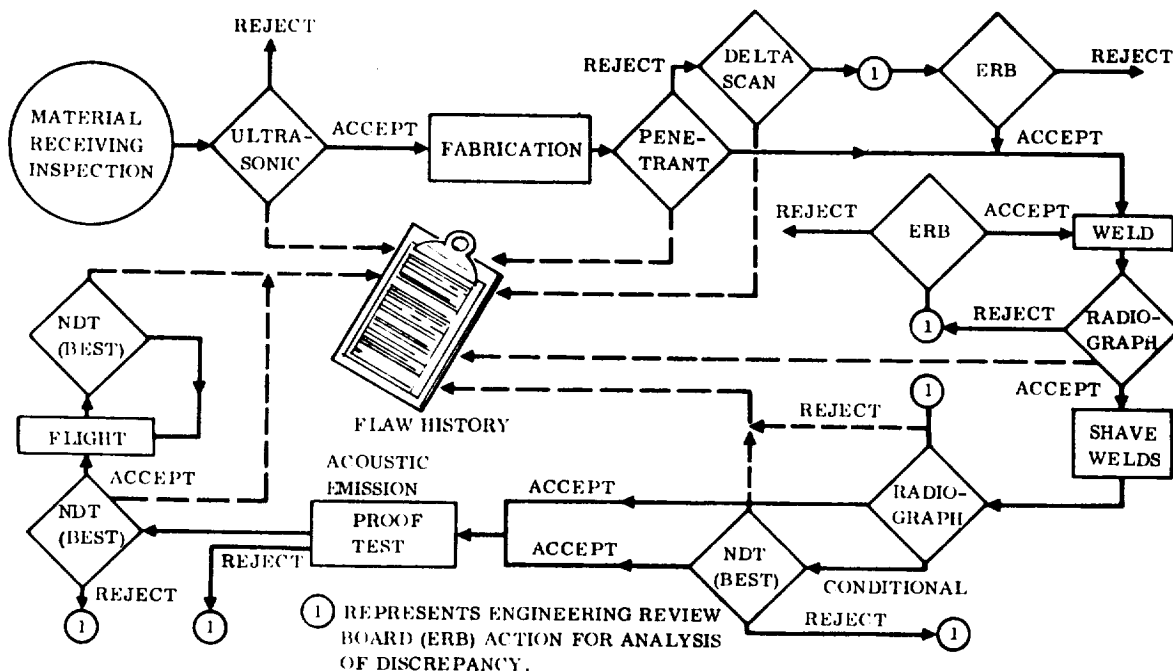


Figure 2-42. Structural Element Non-Destructive Testing Plan

- b. Maintenance of a history of each flaw through the phases mentioned above and/or repair.
- c. Engineering Review Board (ERB) action on the reported flaws. The ERB will consist of qualified engineering personnel representing structural design, stress, materials, and NDT. The ERB will evaluate all flaw indications, accept or reject the item under consideration, or plan the corrective action.

For purposes of this study, it is assumed that the differences in the factory quality control and NDE plans for components designed using safe-life or fail-safe principles are small and beyond definition at this time - frame of the space shuttle development program. It is recognized that it may be necessary to inspect for smaller defects in safe-life structures; however, this mainly applies to the operation phase. In the factory, all defects above certain specification or engineering standards will be removed, repaired, or rejected regardless of the design approach.

## 2.9.2 MAINTENANCE PLAN

2.9.2.1 General Maintenance Concept. The space shuttle maintenance concept is the principal element of the space shuttle integrated logistics support and maintenance

programs. The maintenance concept is the basis for the shuttle system maintainability program and dictates the basic approach required in all related areas of the integrated logistics support program, including training, spares, maintenance plan, technical data, field support, personnel, etc. The baseline maintenance concept as established herein is in consonance with the following Space Shuttle Program requirements.

- a. Reduced operational costs
- b. Airline type operation
- c. A reusable system with a high launch rate capability and short ground turnaround time.

Maintenance for the shuttle system is defined as the function of retaining material in, or restoring it to, a serviceable condition. This includes servicing, repair, modification, overhaul, rebuild, refurbishment, verification, reclamation, inspection, and condition determination. Tasks generated by this definition, as it applies to the space shuttle system, may take a few minutes at or on the vehicle, wherever it may be located, or several days in a primary support facility. Shuttle system maintenance also includes maintenance activity accomplished in supporting shops and contractor facilities.

The shuttle system maintenance concept embraces the general philosophy of "as required" inspection and repair (maintenance). Scheduled maintenance will be minimized with each requirement fully justified. Maintenance will be facilitated by use of an optimized mix of onboard, build-in test, fault isolation, and ground support equipment. Application of non-destructive testing (NDT) processes and techniques will be considered to the fullest extent at all levels of maintenance, particularly in support of Level I (line) maintenance. The requirements for specialized facilities for maintenance and support operations will be minimized.

Specific maintenance concepts upon which detailed shuttle system maintenance and support policies and procedures will be based are set forth in the following paragraphs.

**2.9.2.2 Levels of Maintenance.** Space shuttle system maintenance will be categorized by three maintenance levels:

- a. Level I Maintenance performed in or at the vehicle (system, booster, orbiter or GSE as applicable)
- b. Level II Maintenance performed off the vehicle in supporting shops, normally located at primary operations site.

- c. Level III Maintenance performed off the vehicle or equipment at remote sites such as depots, contractor facilities, etc.

Specific identification of those maintenance actions directly impacting shuttle system (flight and ground) availability is also enhanced. Table 2-11 depicts general types of maintenance that will normally be performed at each maintenance level.

Level I maintenance is performed at or on the shuttle system flight vehicle or associated ground support equipment at any point in the ground turnaround cycle. It includes those actions in support of test, training, ferry, and operational missions.

Level II maintenance is performed in supporting shops normally located immediately adjacent to or at the primary operations site. This maintenance level includes line replaceable unit (LRU) test, checkout, repair, calibration, modification, service, etc., capability consistent with the basic concept of optimizing maintenance support capability by level. Shop facilities provide individual shuttle system, subsystem, assembly, and subassembly processing capability consistent with results of maintenance requirements analysis conducted in accordance with maintenance program requirements contained within this document.

Level III maintenance is conducted off the vehicle at a site remote from the normal operations site. Examples include contractor facilities and vendor facilities. Specific Level III maintenance requirements will be developed by analysis and justified in each case on the basis cost related factors including the need for special facilities, skills, and support equipment. Examples of maintenance requirements that are candidates for Level III designation include overhaul of main rocket engines, gyro overhaul or repair, major modification of selected line replaceable units, etc.

**2.9.2.3 Types of Maintenance.** Shuttle system maintenance is generally defined as scheduled (routine) and unscheduled (non-routine). Each of these general categories contains a number of specific items, some of which are common to both categories (servicing, calibrate, etc.) in that they will normally be performed on both a scheduled basis and/or, as a specific need arises, on an unscheduled basis. Table 2-11 contains a summary breakdown of both of these major types of maintenance. The following paragraphs contain a discussion of the two basic types of shuttle system maintenance from a conceptual viewpoint.

Scheduled maintenance is that maintenance (routine) necessary to ensure or maintain a stated level of system operational readiness. Scheduled maintenance will be initiated on the basis of pre-determined criteria such as elapsed calendar time, accumulated operating hours, and cycles. Scheduled maintenance requirements will be predicated upon specific design requirements, failure and effects analysis, and safety considerations. This type maintenance includes activities such as servicing, inspection,

Table 2-11. Typical Shuttle System Maintenance/Support Actions by Level

Maintenance/Support Actions	Level I Line	Level II Shops	Level III Contractor-Facility
<b>Scheduled Maintenance</b>			
Preflight Inspection	x <sup>(1)</sup>		
Postflight Inspection	x		
Major Periodic Inspection	x <sup>(2)</sup>		
Special Inspection	x		
Replacement Life Assemblies	x	x	x
Overhaul (Refurbishment)		x <sup>(3)</sup>	x
Calibration-Service-Clean-Lube-Etc.	x	x	x
Corrosion Control	x	x	x
<b>Unscheduled Maintenance</b>			
Repair by Replacement Assemblies	x	x	x
Repair in Place	x	x	x
Service	x	x	x
Calibrate-Clean-Adjust-Etc.	x	x	
<b>Servicing</b>			
Post-Maintenance Verification (Checkout)	x	x	x
<b>Miscellaneous</b>			
Modifications	x	x	x
Manufacture/Fabricate		x <sup>(4)</sup>	x <sup>(5)</sup>
Tow	x		
Preservation	x	x	x
Operational Test	x	x	x
GSE Support	x	x	x
Non-Destructive Testing (X-ray-Sonic-Etc.)	x	x	x

Notes: (1) Preflight inspections will be required to support both mission and ferry flights. Requirements will vary.

(2) Incrementally accomplished. Phased inspections.

(3) Limited overhaul capability will exist in supporting shops in immediate area.

(4) Within capability of supporting shops in immediate area.

(5) Fully justified in each case.

periodic removal and replacement, and calibration. Scheduled maintenance will be performed only as required and will be minimized with each requirement fully justified. Scheduled maintenance will normally be accomplished during the turnaround cycle and phased inspections.

Unscheduled maintenance is basically that corrective maintenance generated as a result of discrepancies determined by inflight analysis of shuttle system performance using built-in test and fault isolation capability as well as crew analysis and reporting. Corrective maintenance requirements are also generated during the performance of scheduled maintenance. Unscheduled maintenance will be performed at all three levels of maintenance as indicated in Table 2-11.

On-vehicle (Level I) corrective maintenance will be by replacement of line replaceable units to the maximum extent possible. This concept will be supported through the system design approach, augmented by the maintainability program. Defective assemblies removed from the shuttle system will be transported to a Level II (shop) or Level III (contractor facility) maintenance site for disposition. Normally structural repair will be accomplished at the primary operation site. Emergency repair, necessary to permit ferry, will be performed at alternate landing sites as necessary.

Off-vehicle corrective maintenance involving assemblies and components removed from the space shuttle will be performed at shop and contractor activities as necessary. Determination of where to repair each assembly/component will be made as a level of repair decision process. This decision process will include consideration for design characteristics including predicted failure rates as well as economic considerations involved.

**2.9.2.4 Detail Booster Structure Maintenance Plans.** A two-week turnaround time was established by NASA for the space shuttle booster. It was further established that the work week will be five 16-hour days. This results in a total turnaround time of 160 calendar hours. Eighty calendar hours are allocated to turnaround maintenance, which includes safing the vehicle and the performance of all scheduled and unscheduled maintenance tasks necessary to prepare the booster and make all systems operational for the next mission. The remaining 80 calendar hours are allocated to erection, checkout, and prelaunch tasks. The maintenance manhours required to perform the turnaround maintenance tasks were estimated by making a determination of the number of personnel and the time required to inspect, repair, or replace and check out each subsystem and the scheduling of the effort within the allocated time. It is estimated that 2400 maintenance manhours are required to perform the turnaround maintenance tasks, of which 160 hours are allocated to the structural subsystem. The remaining 2240 hours are allocated to the propulsion, avionics, hydraulic, and similar subsystems.

To the degree possible with the design details available turnaround maintenance actions have been established for the components selected for study in this program. These result in the maintenance manhour allocations presented in Table 2-12. For the baseline boosters, all the structural components studied were considered to be fail-safe except the propellant tanks, which were considered safe-life. In addition, the requirements of the B-9U delta wing booster and B-16B swept wing booster were considered identical. The turnaround maintenance actions are discussed in Section 2.9.2.5.

These detail maintenance plans will be reviewed when the sensitivities of the structure to fatigue, safe-life, and fail-safe requirements are determined (see Sections 4.3.2 and 5.3.2).

Table 2-12. Maintenance Manhours/Turnaround Study of Baseline Booster Components

	Scheduled		Unscheduled	Total
	Routine	Phased		
LO <sub>2</sub> Tank	3	7-1/2	2-1/2	13
LH <sub>2</sub> Tank	3	7-1/2	2-1/2	13
Wing Box	2	4-1/2	3-1/2	10
Vertical Tail	1/2	4-1/2	3	8
Thrust Structure	4	12	9	25
Aft Orbiter Support Frame	1/2	3.0	2	5-1/2
				74-1/2

#### 2.9.2.5 Turnaround Maintenance Actions

##### a. LO<sub>2</sub> Tank

1. Leak check every flight
2. Visual inspection every flight
  - (a) Forward bulkhead area
    - (1) For broken/cracked weldments
    - (2) Security of closure door and fasteners
    - (3) Forward skirt attachment flange damage
    - (4) For evidence of corrosion



- (b) Tank body
  - (1) TPS attachment for condition
  - (2) Frames, skins and stringers for cracks, damage, and evidence of corrosion
  - (3) Separation attachments for condition
- (c) Aft bulkhead
  - (1) For broken/cracked weldments
  - (2) Security of fluid line attachments
  - (3) Evidence of corrosion
  - (4) Condition of inter-tank attachment
- 3. Phased inspections (five flight intervals)
  - (a) First phase
    - (1) NDE of the forward frame
    - (2) NDE of the separation system attach frame
  - (b) Second phase
    - (1) NDE of aft frame
    - (2) NDE of propellant line attachment
- 4. Unscheduled (To be accomplished only if conditions disclosed by other inspections indicate a need.)

Remove upper forward TPS segment for NDE and visual inspection of the upper one-half area of the tank structure

b. Wing

- 1. Visual inspection every flight
  - (a) Exterior
    - (1) Condition of surface for cracks, heat damage, and evidence of corrosion
    - (2) Access panels and doors for condition and security
    - (3) Surface areas for evidence of hydraulic and fuel leakage

- (b) Interior
  - (1) Exposed structure in engine cavities and main landing gear wheel wells for cracks, mechanical damage, and evidence of corrosion
  - (2) Wing to body attach fittings for security and damage
- 2. Phased inspections (five flight intervals)
  - (a) First phase
    - (1) NDE of forward wing to body attach fittings
    - (2) NDE of inboard elevon hinge fittings
  - (b) Second phase
    - (1) NDE of aft wing to body attach fittings
    - (2) NDE of outboard elevon hinge fittings
- 3. Phased inspections (25 flight intervals)
  - (a) Remove selected exterior panels and visually inspect for cracks and deformation.
  - (b) NDE selected lower spar caps
- c. LH<sub>2</sub> tank
  - 1. Leak check every flight
  - 2. Visual inspection every flight
    - (a) Forward bulkhead area
      - (1) For broken/cracked weldments
      - (2) Security of closure door and fasteners
      - (3) Inter-tank attach frame for damage
      - (4) For evidence of corrosion
    - (b) Tank body
      - (1) TPS attachment for condition
      - (2) Frames, skins and stringers for cracks, heat damage and evidence of corrosion
      - (3) Separation attachments for condition
      - (4) Main landing gear attachments for condition
      - (5) Wing attachments for condition

- (c) Aft bulkhead
  - (1) For broken and cracked weldments
  - (2) Security of fluid line attachments
  - (3) Evidence of corrosion
  - (4) Condition of thrust section attachment.
- 3. Phased inspections (five flight intervals)
  - (a) First phase
    - (1) NDE of the forward tank frame
    - (2) NDE of forward separation system attach frame
    - (3) NDE of forward, wing/main landing gear attach frames.
  - (b) Second phase
    - (1) NDE of aft tank frame
    - (2) NDE of the aft separation system attach frame
    - (3) NDE of aft wing attach frame
- 4. Unscheduled (To be accomplished only if conditions disclosed by other inspections indicate a need).
  - (a) Remove upper TPS segments for NDE and visual inspection of the upper one-half area of the tank structure
- d. Thrust section structure
  - 1. Visual inspection every flight
    - (a) Forward bulkhead
      - (1) Frame segments for distortion, cracks and security of attachments
      - (2) Truss members for distortion, cracks and security of attachments
    - (b) Aft bulkhead
      - (1) Frame segments for distortion, cracks and security of attachments
      - (2) Truss members for distortion, cracks and security
    - (c) Thrust members
      - (1) Thrust beams for distortion and cracks
      - (2) Thrust posts for distortion and cracks
      - (3) Thrust tubes for distortion, cracks and security of attachment

(d) Intermediate frames

Frame segments for distortion and cracks

(e) Skin

Skin panels for distortion cracks and condition of skin stringers.

2. Phased inspections (five flight intervals)

(a) First phase

(1) NDE of six thrust posts

(2) NDE of one horizontal and one vertical thrust beam

(b) Second phase

(1) NDE of six thrust posts

(2) NDE of one horizontal and one vertical thrust beam

e. Vertical stabilizer

1. Visual inspection every flight

(a) Exterior

(1) Condition of surface for cracks and heat damage

(2) Access panels and doors for condition and security

(3) Surface areas for evidence of hydraulic leaks

(b) Interior

Stabilizer to body attach fittings for security and heat damage

2. Phased inspection (five flight intervals)

(a) First phase

(1) Remove all access provisions on left hand side and inspect internal structure for security, cracks, and distortion

(2) NDE rudder attach fittings

(b) Second phase

(1) Remove all access provisions on right hand side and inspect internal structure for security, cracks and distortion

(2) NDE stabilizer to body attach fittings

## 2.10 COSTS

The baseline configuration for program costs utilized in this study is shown at NASA work breakdown structure (WBS) level 4 in Table 2-13. The Convair-developed cost model that was used to generate these total program costs also served as the basis for calculating the various direct, cascaded, and growth cost penalties associated with the safe-life/fail-safe design concepts analyzed under this contract. The model calculates unit manufacturing costs based on parametric cost estimating relationships (e.g., cost as a function of sub-element weight) at various levels of detail down to NASA WBS level 6 which corresponds generally to the structural sub-components analyzed in this study such as the LH<sub>2</sub> tank, wing, and thrust structure. These calculated unit costs are introduced into the total program cost calculation wherever hardware requirements are identified (i.e., ground test articles, spares, flight test vehicles, production vehicles, etc.). In addition, engineering design and development, tooling, and test program costs are combined to give booster non-recurring program costs. Production hardware manufacture, and test article conversion activities are accumulated into total recurring production program costs. Recurring operations costs are then added to non-recurring and recurring production to obtain total program costs.

Table 2-13. Baseline B-9U Program — WBS Level 4 Summary  
Costs (\$ million)

	Nonrecurring	Recurring Production	Recurring Operations	Total Program
3-00 BOOSTER	3211	442	144	3797
-01 Structural Group	1294	227	14	1535
-02 Propulsion Group	552	88	31	671
-03 Avionics Group	364	46	59	469
-04 Power Group	276	38	26	340
-05 Environmental Control and Life Support	32	2	1	35
-06 Booster Vehicle Installation and Assembly	59	41	—	100
-07 Combined Subsystem Development Test	150	—	—	150
-08 System Engineering Integration	162	—	—	162
-09 Booster Facilities	12	—	—	12
-10 System Support Equipment and Services	273	—	13	286
-11 Booster Management	37	—	—	37

Table 2-14 is a cost calculation summary which breaks down the structural group line item. This breakdown identifies the structural sub-elements to WBS level 6 (LH<sub>2</sub> tank, thrust structure, etc.) and shows the distribution of total program cost by the various cost elements which comprise the non-recurring, recurring production, and recurring operations phases of the booster program. The aerodynamic surfaces (WBS 3.1.2), thermal protection system (WBS 3.1.3), and landing system (WBS 3.1.4) costs are similarly broken down and together with the body structure sum to the \$1.535 billion previously shown in Table 2-14. For analysis purposes the EDD and tooling level 5 sums were broken down to level 6 in proportion to the lower level TFU's.

Table 2-14. Baseline B-9U Structural Group Cost Calculation (\$ million)

WBS	Title	TFU	EDD	Tooling	GTH	FTH	FTS	Total Nonrecurring
3.1	Structural Group	160,688	286,761	277,080	388,885	121,377	20,132	1294,215
3.1.1	Body Structure	68,308	88,907	104,310	270,583	100,616	1,002	601,418
3.1.1.1	LH <sub>2</sub> Tank	18,031		39,472	72,124	36,062	0,180	147,818
3.1.1.2	LO <sub>2</sub> Tank	3,417		9,940	10,251	6,834	0,034	27,059
3.1.1.3	Cabin	1,176			2,152	2,152	0,035	4,719
3.1.1.4	Fwd Suppt Structure	1,697			5,091	6,594	0,051	8,536
3.1.1.5	Intertank	11,613			46,452	53,129	0,118	69,794
3.1.1.6	Thrust Str	23,092			96,986	40,184	0,241	143,401
3.1.1.7	Mating/Separation	1,381			4,143	2,062	0,276	7,181
3.1.1.8	Base Heat Shield	7,901			33,184	17,892	0,079	49,065
	Level 5 Sums		88,907	14,898				143,805
3.1.2	Aerosurfaces	44,202	78,126	105,344	61,325	58,437	4,420	337,619
3.1.2.1	Vertical Stabilizer							78,126
3.1.2.2	Canard	4,641		17,481	6,483	2,297	0,003	33,692
	Basic Structure	2,141		6,396	2,569	1,282	0,014	13,401
	TPS	0,847		2,741	0,776	2,69	0,065	4,876
3.1.2.3	Wing							
	Basic Structure	28,322		62,979	39,651	19,633	2,833	162,107
	TPS	8,461		15,745	11,845	14,407	0,846	45,158
3.1.3	Thermal Protection System	46,892	76,118	67,426	56,233	53,784	14,067	300,000
3.1.3.1	Center & Aft TPS	34,875		67,426	41,850	39,251	10,167	143,544
3.1.3.2	Nose TPS	12,017			14,420	14,634	3,666	122,062
3.1.4	Landing Gear	1,286	43,610		0,007	2,503	0,643	47,000

WBS	Title	Production Hardware	TAC	Total Recurring Production	Recurring Operations	Total Program
3.1	Structural Group	207,177	21,007	227,184	13,706	1535,125
3.1.1	Body Structure	68,308	20,492	88,800	1,555	691,774
3.1.1.1	LH <sub>2</sub> Tank	18,031	5,409	23,440	0,180	171,368
3.1.1.2	LO <sub>2</sub> Tank	3,417	1,025	4,442	0,034	31,518
3.1.1.3	Cabin	1,176	0,351	1,529	0,024	6,292
3.1.1.4	Fwd Suppt Structure	1,697	0,509	2,206	0,033	10,776
3.1.1.5	Intertank	11,613	3,484	15,097	0,232	85,121
3.1.1.6	Thrust Str	23,092	6,928	10,020	0,241	123,152
3.1.1.7	Mating/Separation	1,381	0,414	1,795	0,096	9,666
3.1.1.8	Base Heat Shield	7,901	2,370	10,271	0,243	59,574
	Level 5 Sums					143,805
3.1.2	Aerosurfaces	49,404	0,000	88,404	8,841	434,861
3.1.2.1	Vertical Stabilizer					78,126
3.1.2.2	Canard	4,267	0,000	9,262	0,929	33,880
	Basic Structure	4,282	0,000	4,282	0,128	18,171
	TPS	1,294	0,000	1,294	0,130	6,300
3.1.2.3	Wing					
	Basic Structure	56,644	0,000	56,644	5,301	254,415
	TPS	16,922	0,000	16,922	1,697	63,972
3.1.3	Thermal Protection System	46,892	0,000	46,892	2,345	156,907
3.1.3.1	Center & Aft TPS	34,875	0,000	34,875	1,344	143,544
3.1.3.2	Nose TPS	12,017	0,000	12,017	0,601	158,681
3.1.4	Landing Gear	1,286	0,515	3,087	0,965	51,585

TFU = Theoretical First Unit EDD = Engineering Design & Development GTH = Ground Test Hardware  
 FTH = Flight Test Hardware FTS = Flight Test Spares TAC = Test Article Conversion

SECTION 3  
ANALYSIS OF BASELINE BOOSTERS

3.1 STRUCTURAL SIZING FOR STATIC LOADS

This section presents the preliminary stress analysis of the structural components studied. Included are the analysis used to size the components for static limit and ultimate loads.

3.1.1 LO<sub>2</sub> TANK. The LO<sub>2</sub> tank is critical for the internal pressures and external loads presented in Section 2.6. Sizing of the various elements of the tank is shown in the following paragraphs.

3.1.1.1 LO<sub>2</sub> Tank End Domes. Upper and Lower LO<sub>2</sub> tank end domes have been sized for ultimate, yield, and proof test loads. Dome sizing and weight calculations were performed by a computer program that determines skin thickness requirements at five stations along the dome and calculates dome weight assuming a stepped thickness change.

The upper dome is not in contact with liquid oxygen during critical design times; consequently, the structure will be near room temperature. Proof testing of the upper dome will be performed at room temperature.

The lower dome is in contact with liquid oxygen during critical design times and will be proof tested with liquid nitrogen.

Dome structural material is 2219-T87 aluminum alloy with the following properties:

At room temperature

$$F_{tu} = 63 \text{ ksi}$$

$$F_{ty} = 52 \text{ ksi}$$

$$E_c = 10.8(10)^6$$

$$w = 0.102 \text{ lb/in}^3$$

At -297° F

$$F_{tu} = 75 \text{ ksi}$$

$$F_{ty} = 61 \text{ ksi}$$

$$E_c = 10.8 (10)^6$$

$$W = 0.102 \text{ lb/in}^3$$

At -320° F

$$F_{tu} = 78.0 \text{ ksi}$$

$$F_{ty} = 62.0 \text{ ksi}$$

$$E_c = 10.8(10)^6 \text{ psi}$$

$$w = 0.102 \text{ lb/in}^3$$

Design conditions are as follows:

#### Ultimate design

Upper dome pressure = 17.5 psi

Lower dome pressure = 40.0 psi ullage

Ultimate factor = 1.4

Yield factor = 1.1

#### Proof pressure test design

Upper dome pressure =  $17.5 (1.23) = 21.6 \text{ psi}$

Lower dome pressure =  $40 (1.23) = 49.1 \text{ psi}$

Results of this analysis are presented on the following pages.



# DCME SIZING PROGRAM

UPPER DOME L02 (PROOF DES)  
MATERIAL 2219-T87 ROOM TEMP

FTU = 63000 PSI FTY = 52000 PSI  
ECF = 10800000 PSI T MIN = .040 IN

GEOMETRY <

A/R = 1.41 A = 198.00 IN FUEL HEAD ABOVE ECTR = 0.00 IN

TYPE = 1 (TYPE 1 = UPPER DOME, TYPE 2 = LOWER DOME)

FACTORS <

ULTIMATE FS = 1.00 YIELD FS = 1.00 AXIAL LOAD FACTOR = 1.00

PRESSURES <

P ULLAGE = 21.6PSI P EQUATOR = 21.6PSI P APEX = 21.6PSI

OTHER CRITERIA <

DELTA T = .010IN BUCKLING COEFFICIENT = 5.531

DOME SIZES, YIELD DESIGN, COMPARE STRESS WITH FTY

	Y DOME	THICKNESS	F PHI	F THETA	WEIGHT	AREA
	(INCHES)	(INCHES)	(PSI)	(PSI)	(LB)	(SQ IN)
Y0	0.00	.044	48287	29	0.00	0.00
Y1	6.01	.044	52000	14364	322.99	71497.09
Y2	84.02	.044	52000	27540	191.72	38992.71
Y3	112.02	.057	52000	40590	228.57	42556.70
Y4	140.03	.068	52000	52000	278.12	46831.44

(Y0 IS AT EQUATOR, Y4 IS AT APEX)

TOTAL DOME WT = 1026.40 LB

FLUID WT (IN DOME) = 0.00 LB

DOME VOLUME = 6650.63 CU FT

WT EFFICIENCY = 0.0000

DOME WT / VOLUME = .1574 LB/CU FT

DOME WT / FLUID WT = 0 LB/LB

# DOME SIZING PROGRAM

UPPER DOME L02 (ULT DES)  
MATERIAL 2219-T87 ROOM TEMP

FTU = 63000 PSI FTY = 52000 PSI

EC= 10800000 PSI T MIN = .040 IN

GEOMETRY <

A/R = 1.41 A = 198.00 IN FUEL HEAD ABOVE EQTR = 0.00 IN

TYPE = 1 (TYPE 1 = UPPER DOME, TYPE 2 = LOWER DOME)

FACTORS <

ULTIMATE FS = 1.40 YIELD FS = 1.10 AXIAL LOAD FACTOR = 1.00

PRESSURES <

P ULLAGE = 17.5PSI P EQUATOR = 17.5PSI P APEX = 17.5PSI

OTHER CRITERIA <

DELTA T = .010IN BUCKLING COEFFICIENT = 5.63

DOME SIZES, ULTIMATE DESIGN, COMPARE STRESS WITH FTU

	Y DOME (INCHES)	THICKNESS (INCHES)	F PHI (PSI)	F THETA (PSI)	WEIGHT (LB)	AREA (SQ IN)
Y0	0.00	.041	58496	35	0.00	0.00
Y1	56.01	.041	63000	17403	302.38	71497.09
Y2	84.02	.045	63000	33366	178.56	38992.71
Y3	112.02	.049	63000	49176	213.99	42556.70
Y4	140.03	.054	63000	63000	260.38	46891.44

(Y0 IS AT EQUATOR, Y4 IS AT APEX)

TOTAL DOME WT = 955.31 LB

FLUID WT (IN DOME) = 0.00 LB

DOME VOLUME = 6650.63 CU FT

WT EFFICIENCY = 0.0000

DOME WT / VOLUME = .1436 LB/CU FT

DOME WT / FLUID WT = P LB/LB

# DOME SIZING PROGRAM

LOWER DOME LOT (PROOF DES)  
MATERIAL 2219-TA7 AT -320 F

FTU = 78000 PSI FTY = 62000 PSI

EC= 10800000 PSI T MIN = .040 IN

GEOMETRY <

A/R = 1.41 A = 198.00 IN FUEL HEAD ABOVE FCTR = 0.00 IN

TYPE = 2 (TYPE 1 = UPPER DOME, TYPE 2 = LOWER DOME)

FACTORS <

ULTIMATE FS = 1.00 YIELD FS = 1.00 AXIAL LOAD FACTOR = 1.00

PRESSURES <

P ULLAGE = 49.1PSI P EQUATOR = 51.9PSI P APEX = 53.3PSI

OTHER CRITERIA <

DELTA T = .010IN BUCKLING COEFFICIENT = 5.530

DOME SIZES, YIELD DESIGN, COMPARE STRESS WITH FTY

	Y DOME	THICKNESS	F PHI	F THETA	WEIGHT	AREA
	(INCHES)	(INCHES)	(PSI)	(PSI)	(LB)	(SQ IN)
Y0	0.00	.092	56056	34	0.00	0.00
Y1	56.01	.092	62000	17127	668.46	71497.09
Y2	84.02	.099	62000	32836	394.73	38992.71
Y3	112.02	.109	62000	48395	473.06	42556.70
Y4	140.03	.120	62000	62000	575.60	46891.44

(Y0 IS AT EQUATOR, Y4 IS AT APEX)

TOTAL DOME WT = 2111.85 LB

FLUID WT (IN DOME) = 344768.45 LB

DOME VOLUME = 6650.63 CU FT

WT EFFICIENCY = 163.2543

DOME WT / VOLUME = .3175 LB/CU FT

DOME WT / FLUID WT = .0061 LB/LB

# DOME SIZING PROGRAM

LOWER DOME LO2 (ULT DES)  
MATERIAL 2219-T87 AT -297 F

FTU = 75000 PSI FTY = 61000 PSI  
EC= 10800000 PSI T MIN = .040 IN

GEOMETRY <

A/R = 1.41 A = 198.00 IN FUEL HEAD ABOVE ENTR = 0.00 IN  
TYPE = 2 (TYPE 1 = UPPER DOME, TYPE 2 = LOWER DOME)

FACTORS <

ULTIMATE FS = 1.40 YIELD FS = 1.10 AXIAL LOAD FACTOR = 1.00

PRESSURES <

P ULLAGE = 40.0PSI P EQUATOR = 42.8PSI P APEX = 40.2PSI

OTHER CRITERIA <

DELTA T = .010IN BUCKLING COEFFICIENT = 5.533

DOME SIZES, ULTIMATE DESIGN, COMPARE STRESS WITH FTU

	Y DOME	THICKNESS	F PHI	F THETA	WEIGHT	AREA
	(INCHES)	(INCHES)	(PSI)	(PSI)	(LB)	(SQ IN)
Y0	0.00	.008	67433	41	0.00	0.00
Y1	56.01	.008	75000	20718	641.55	71497.09
Y2	84.02	.005	75000	39722	378.94	38992.71
Y3	112.02	.105	75000	59543	454.02	42556.70
Y4	140.03	.115	75000	75000	552.43	46891.44

(Y0 IS AT EQUATOR, Y4 IS AT APEX)

TOTAL DOME WT = 2026.83 LB

FLUID WT (IN DOME) = 344768.45 LB

DOME VOLUME = 6650.63 CU FT

WT EFFICIENCY = 170.1021

DOME WT / VOLUME = .3048 LB/CU FT

DOME WT / FLUID WT = .0059 LB/LB

3.1.1.2 LO<sub>2</sub> Tank Plate-Stringers. Plate-stringers for the LO<sub>2</sub> tank have been sized to carry tank pressures and fuselage external loads.

Plate-stringers were optimized by sizing the skin for pressure and then sizing longitudinal stiffeners (stringers) for axial loads.

Skins are critical for proof pressure, as shown on Page 92 , and stringers are sized for an axial load of 1000 lb/in compression.

Plate-stringer analysis is presented on Page 93 , and a plot of skin thickness and equivalent plate stringer thickness is presented in Figure 3-1.

Material: 2219-T87 plate three inches thick

Room temperature properties

$$F_{tu} = 63 \text{ ksi}$$

$$E_c = 10.8(10)^6 \text{ psi}$$

$$F_{ty} = 51 \text{ ksi}$$

$$w = 0.102 \text{ lb/in}^3$$

$$F_{su} = 38 \text{ ksi}$$

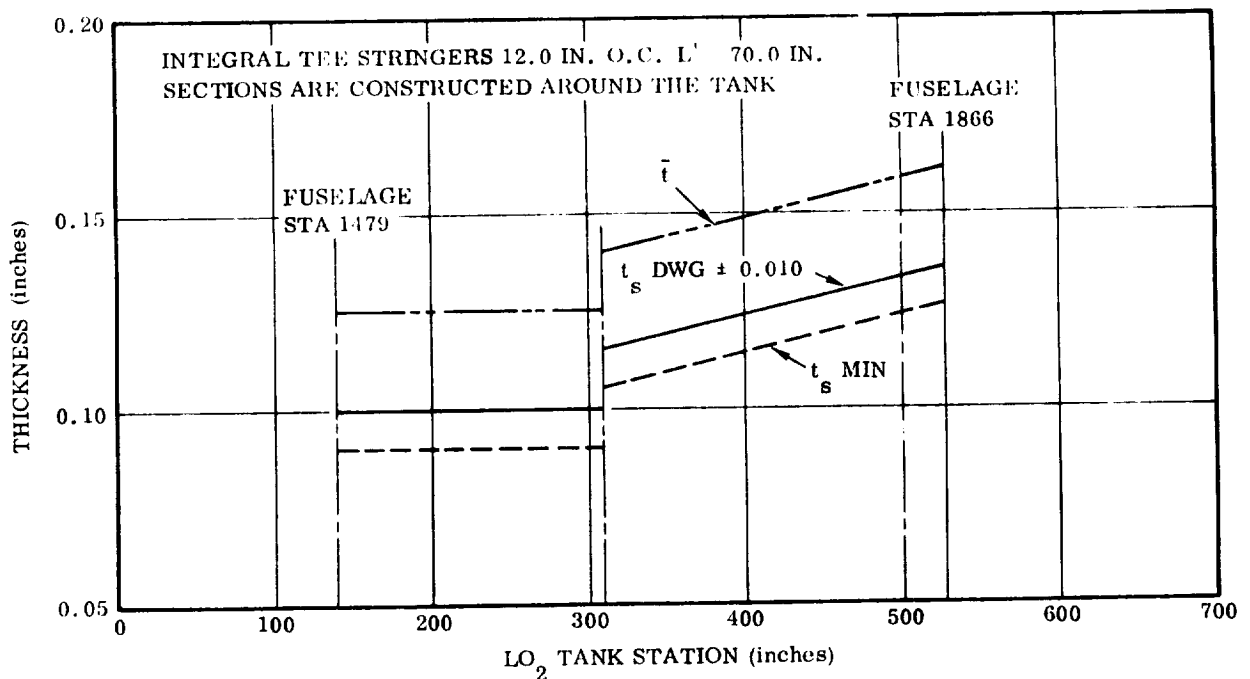


Figure 3-1. LO<sub>2</sub> Tank Plate-Stringer Sizing

Properties at -320° F

$$F_{tu} = 63(1.24) = 78 \text{ ksi}$$

$$F_{ty} = 51(1.19) = 61 \text{ ksi}$$

Allowable working tension stress at limit pressure

At room temperature

$$\text{Ultimate design } \frac{63}{1.4} = 45.0 \text{ ksi (1.4 ultimate factor)}$$

$$\text{Yield design } \frac{51}{1.1} = 46.4 \text{ ksi (1.1 yield factor)}$$

$$\text{Proof design } \frac{51}{1.23} = 41.5 \text{ ksi (1.23 proof factor)}$$

At -320° F

$$\text{Ultimate design } \frac{78}{1.4} = 55.5 \text{ ksi}$$

$$\text{Yield design } \frac{61}{1.1} = 55.5 \text{ ksi}$$

$$\text{Proof design } \frac{61}{1.23} = 49.5 \text{ ksi}$$

For pressure design the skins are proof test critical.

Tank skins from the lower dome to LO<sub>2</sub> tank Station 310 will be tested with LN<sub>2</sub> at -320° F.

Proof pressure at lower dome equator:  $p = 38.8 \text{ psi}$

$$\text{Minimum skin thickness} = \frac{38.8(198)}{61,000} = 0.126 \text{ (at lower dome equator)}$$

Proof pressure at LO<sub>2</sub> Station 310:  $p = 32.2 \text{ psi}$

$$\text{Minimum skin thickness} = \frac{32.2(198)}{61,000} = 0.105 \text{ (at Station 310)}$$

Tank skins from the upper dome to LO<sub>2</sub> tank Station 310 will be tested at room temperature.

Proof pressure:  $p = 21.5 \text{ psi}$

$$\text{Minimum skin thickness} = \frac{21.5(198)}{51,000} = 0.084$$

Drawing skin thickness tolerance is  $\pm 0.015$  inch for nominal thicknesses less than 0.100 inch and  $\pm 0.010$  inch for 0.100 and over. A minimum thickness of 0.084 minimum would require a callout of  $0.099 \pm 0.015$  because it is less than 0.100. A callout of  $0.100 \pm 0.010$  will be used, giving a minimum skin thickness of 0.090.

The maximum longitudinal compression load in the  $\text{LO}_2$  tank wall is  $N_x = -665 \text{ lb/in.}$

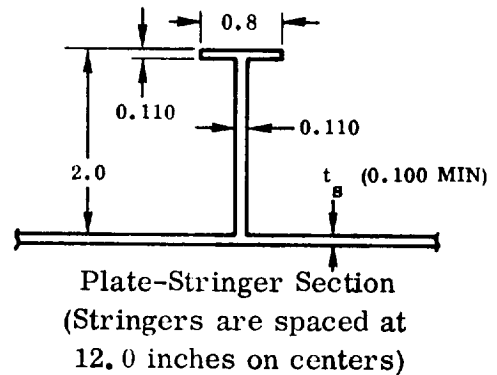
Section Data:

$$\text{Stringer } \Delta \bar{t} = 0.025 \text{ inch}$$

$$F_c = 8000 \text{ psi}$$

$$L' = 70$$

$$N_x = 980 \text{ lb/in minimum}$$



The same stringer section is used for all of the tank.

**3.1.2  $\text{LH}_2$  TANK.** The  $\text{LH}_2$  tank is critical for the pressure and axial loads presented in Section 2.5. Sizing of the various structural elements of the tank is presented in the following paragraphs.

**3.1.2.1  $\text{LH}_2$  Tank End Domes.** Upper and lower  $\text{LH}_2$  tank end domes have been sized for both ultimate design and proof test. Dome sizing and calculation of weights was performed by a computer program that determines skin thickness requirement of five stations along the dome and calculates the dome weight assuming a stepped thickness change.

Dome structural material is 2219-T87 aluminum alloy with the following properties at room temperature:

$$F_{tu} = 63,000 \text{ psi}$$

$$F_{ty} = 52,000 \text{ psi}$$

### Ultimate design

Upper dome pressure = 22.3 psi

Lower dome pressure = 26.4 psi

### Proof pressure test design

Upper and lower dome pressure = 26.4 (1.13) = 29.8 psi

Results of this analysis are presented on the following pages.

3.1.2.2 LH<sub>2</sub> Tank Plate-Stringers and Belt Frames. Plate-stringers for the LH<sub>2</sub> tank have been sized to carry tank pressures and fuselage external loads. The design criteria and loadings presented in Section 2 were followed in establishing factors of safety, minimum skin thickness for pressure design, and minimum thickness for stability design.

Plate-stringer and belt frame configurations were optimized for axial loads with the following constraints:

- a. Minimum skin required for pressure and/or shear.
- b. Minimum stringer spacing for machining.
- c. Maximum stringer height limited by available plate thickness.

Optimum frame spacing was determined for two basic integral stiffener configurations, tee and blade, by selecting average compressive load intensities and optimum stiffeners for various effective column lengths. Belt frame required moments of inertia were calculated by the Shanley criterion,

$$I_f = N_x \left( \frac{C_f \pi D^4}{4LE_f} \right)$$

Frame cross-sectional areas were calculated for 9.0 inch deep frames with truss webs that would have the required moment of inertia. Effective thickness ( $\bar{t}$ ) was calculated for each configuration and plotted as shown in Figure 3-2. As a result of this study, integral stiffeners with an effective column length of 60 inches were selected for detailed sizing.

Various sizes of integral stiffeners were analyzed to determine the effect of stringer spacing and height for several minimum skin thicknesses. Typical results of this study are shown in Figures 3-3 and 3-4. As a result of this study, a stiffener spacing of 4.0 inches was selected for the LH<sub>2</sub> tank.



# DOME SIZING PROGRAM

UPPER DOME LH2 (ULT DES)  
MATERIAL 2219-T87 ROOM TEMP

FTU = 63000 PSI FTY = 52000 PSI

EC= 10800000 PSI T MIN = .040 IN

GEOMETRY <

A/R = 1.41 A = 199.00 IN FUEL HEAD ABOVE EQTP = 0.00 IN

TYPE = 1 (TYPE 1 = UPPER DOME, TYPE 2 = LOWER DOME)

FACTORS <

ULTIMATE FS = 1.40 YIELD FS = 1.10 AXIAL LOAD FACTOR = 1.00

PRESSURES <

P ULLAGE = 22.3PSI P EQUATOR = 22.3PSI P APEX = 22.3PSI

OTHER CRITERIA <

DELTA T = .010IN BUCKLING COEFFICIENT = 5.530

DOME SIZES, ULTIMATE DESIGN, COMPARE STRESS WITH FTU

	Y DOME	THICKNESS	F PHI	F THETA	WIGHT	AREA
	(INCHES)	(INCHES)	(PSI)	(PSI)	(LB)	(SQ IN)
Y0	0.00	.053	58496	35	0.00	0.00
Y1	56.01	.053	63000	17403	385.32	71497.00
Y2	84.02	.057	63000	33366	227.53	38932.71
Y3	112.02	.063	63000	49176	272.69	42556.70
Y4	140.03	.069	63000	63000	331.90	46891.44

(Y0 IS AT EQUATOR, Y4 IS AT APEX)

TOTAL DOME WT = 1217.34 LB

FLUID WT (IN DOME) = 0.00 LB

DOME VOLUME = 6650.63 CU FT

WT EFFICIENCY = 0.0000

DOME WT / VOLUME = .1830 LB/CU FT

DOME WT / FLUID WT = 0 LB/LB

# DOME SIZING PROGRAM

UPPER DOME LH2 (PROOF DES)  
MATERIAL 2219-T87 ROOM TEMP

FTU = 63000 PSI FTY = 52000 PSI

EC 10000000 PSI T MIN = .040 IN

GEOMETRY <

A/R = 1.41 A = 198.00 IN FUEL HEAD ABOVE ENTR = 0.00 IN

TYPE = 1 (TYPE 1 = UPPER DOME, TYPE 2 = LOWER DOME)

FACTORS <

ULTIMATE FS = 1.00 YIELD FS = 1.00 AXIAL LOAD FACTOR = 1.00

PRESSURES <

P ULLAGE = 29.8PSI P EQUATOR = 29.8PSI P APEX = 29.8PSI

OTHER CRITERIA <

DELTA T = .010IN BUCKLING COEFFICIENT = 5.530

DOME SIZES, YIELD DESIGN, COMPARE STRESS WITH FTY

	Y DOME (INCHES)	THICKNESS (INCHES)	F PHI (PSI)	F THETA (PSI)	WEIGHT (LB)	AREA (SQ IN)
Y0	0.00	.061	48283	29	0.00	0.00
Y1	56.01	.061	52000	14364	445.60	71497.09
Y2	84.02	.066	52000	27540	263.13	38992.71
Y3	112.02	.073	52000	40590	315.35	42556.70
Y4	140.03	.080	52000	52000	383.79	46891.44

(Y0 IS AT EQUATOR, Y4 IS AT APEX)

TOTAL DOME WT = 1407.78 LB

FLUID WT (IN DOME) = 0.00 LB

DOME VOLUME = 6650.63 CU FT

WT EFFICIENCY = 0.0000

DOME WT / VOLUME = .2117 LB/CU FT

DOME WT / FLUID WT = R LB/LB

# DOME SIZING PROGRAM

LOWER DOME LH2 (ULT DES)  
MATERIAL 2219-T87 ROOM TEMP

FTU = 63000 PSI FTY = 52000 PSI

EC= 10800000 PSI T MIN = .040 IN

GEOMETRY <

A/R = 1.41 A = 198.00 IN FUEL HEAD ABOVE ENTR = 0.00 IN

TYPE = 2 (TYPE 1 = UPPER DOME, TYPE 2 = LOWER DOME)

FACTORS <

ULTIMATE FS = 1.40 YIELD FS = 1.10 AXIAL LOAD FACTOR = 1.00

PRESSURES <

P ULLAGE = 26.4PSI P EQUATOR = 26.4PSI P APEX = 26.4PSI

OTHER CRITERIA <

DELTA T = .010IN BUCKLING COEFFICIENT = 5.530

DOME SIZES, ULTIMATE DESIGN, COMPARE STRESS WITH FTU

	Y DOME	THICKNESS	F PHI	F THETA	WEIGHT	AREA
	(INCHES)	(INCHES)	(PSI)	(PSI)	(LB)	(SQ IN)
Y0	0.00	.063	58496	35	0.00	0.00
Y1	56.01	.063	63000	17403	456.17	71437.09
Y2	94.02	.068	63000	33366	269.37	38992.71
Y3	112.02	.074	63000	49176	322.82	42556.70
Y4	140.03	.082	63000	63000	392.80	46891.44

(Y0 IS AT EQUATOR, Y4 IS AT APEX)

TOTAL DOME WT = 1441.16 LB

FLUID WT (IN DOME) = 0.00 LB

DOME VOLUME = 6650.63 CU FT

WT EFFICIENCY = 0.0000

DOME WT / VOLUME = .2167 LB/CU FT

DOME WT / FLUID WT = 0 LB/LB

# DOME SIZING PROGRAM

LOWER DOME LH2 (PROOF DES)  
MATERIAL 2219-T87 ROOM TEMP

FTU = 63000 PSI FTY = 52000 PSI

EC= 10800000 PSI T MIN = .040 IN

GEOMETRY <

A/R = 1.41 A = 198.00 IN FUEL HEAD ABOVE ENTR = 0.00 IN

TYPE = 2 (TYPE 1 = UPPER DOME, TYPE 2 = LOWER DOME)

FACTORS <

ULTIMATE FS = 1.00 YIELD FS = 1.00 AXIAL LOAD FACTOR = 1.00

PRESSURES <

P ULLAGE = 29.8PSI P EQUATOR = 29.3PSI P APEX = 23.8PSI

OTHER CRITERIA <

DELTA T = .010IN BUCKLING COEFFICIENT = 5.531

DOME SIZES, YIELD DESIGN, COMPARE STRESS WITH FTY

	Y DOME	THICKNESS	F PHT	F THETA	WEIGHT	AREA
	(INCHES)	(INCHES)	(PSI)	(PSI)	(LB)	(SQ IN)
Y0	0.00	.061	48283	29	0.00	0.00
Y1	56.01	.061	52000	14364	445.50	71497.09
Y2	84.02	.066	52000	27540	263.13	38992.71
Y3	112.02	.073	52000	40590	315.35	42556.70
Y4	140.03	.080	52000	52000	383.70	46891.44

(Y0 IS AT EQUATOR, Y4 IS AT APEX)

TOTAL DOME WT = 1407.78 LB

FLUID WT (IN DOME) = 0.00 LB

DOME VOLUME = 6650.83 CU FT

WT EFFICIENCY = 0.0000

DOME WT / VOLUME = .2117 LB/CU FT

DOME WT / FLUID WT = R LB/LB

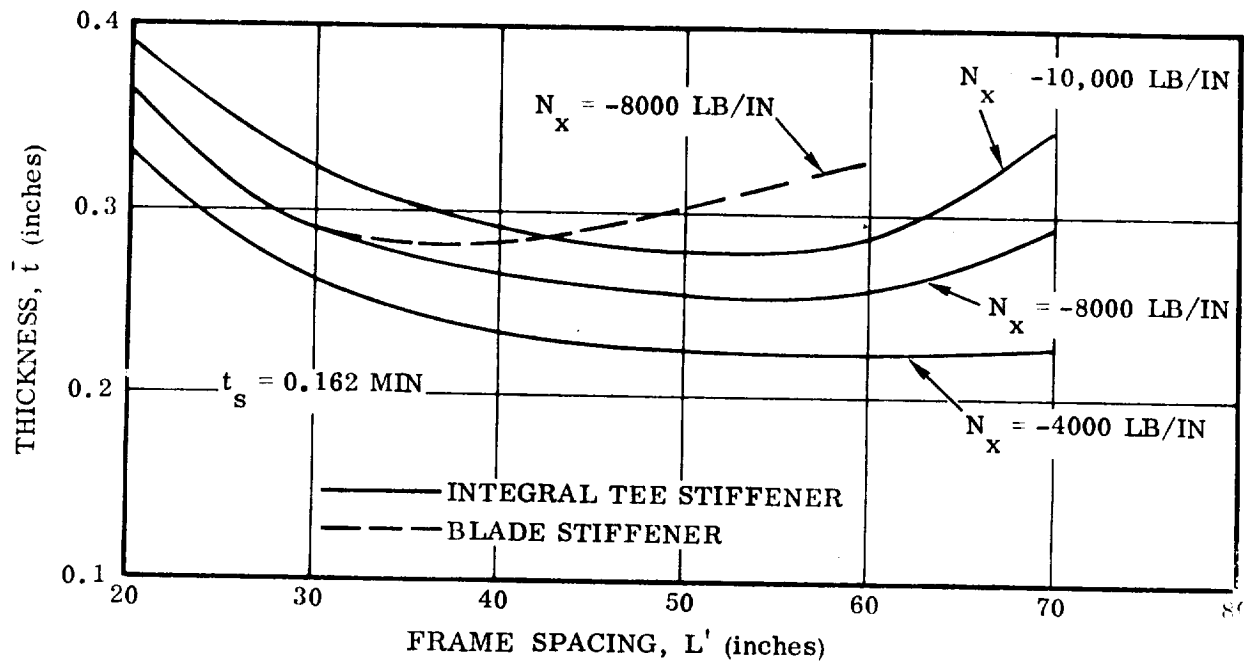


Figure 3-2. LH<sub>2</sub> Tank Plate-Stringer Effective Thickness Versus Frame Spacing

Detailed sizing of the plate-stringer includes the effects of internal pressure, axial load, and shear. Minimum skin thickness was determined for pressure design (ultimate, yield, and proof test), shear (principal stress), and axial load. Sizing of the skin is influenced by axial loads in determining optimum plate-stringer sizes for minimum weight to carry biaxial load and not exceed the allowable shear strength of the skin.

Four sections of the LH<sub>2</sub> tank were selected for detailed analysis of a clean structure. The effect of concentrated loads was calculated separately.

Loads for the selected stations are presented in Table 3-1. A typical analysis is presented on Page 102 and the final plate stringer sizes in Table 3-2.

Material: 2219-T87 plate 3 inches thick

Room temperature properties

$$F_{tu} = 63 \text{ ksi}$$

$$F_{ty} = 51 \text{ ksi}$$

$$F_{su} = 38 \text{ ksi}$$

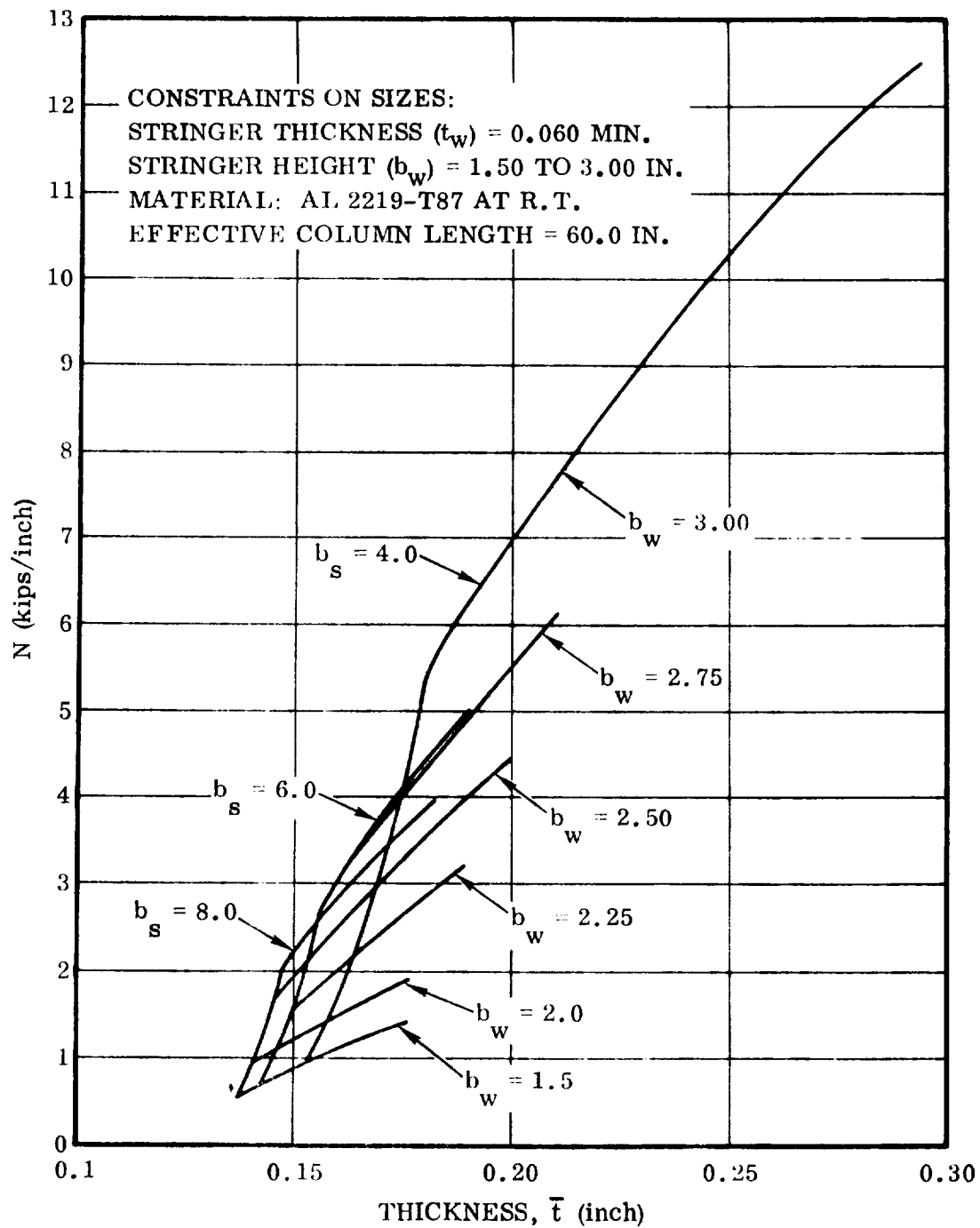


Figure 3-3. Integral Tee Plate-Stringer, Optimization of Stringer Spacing and Height — 0.122 Inch Skin Thickness

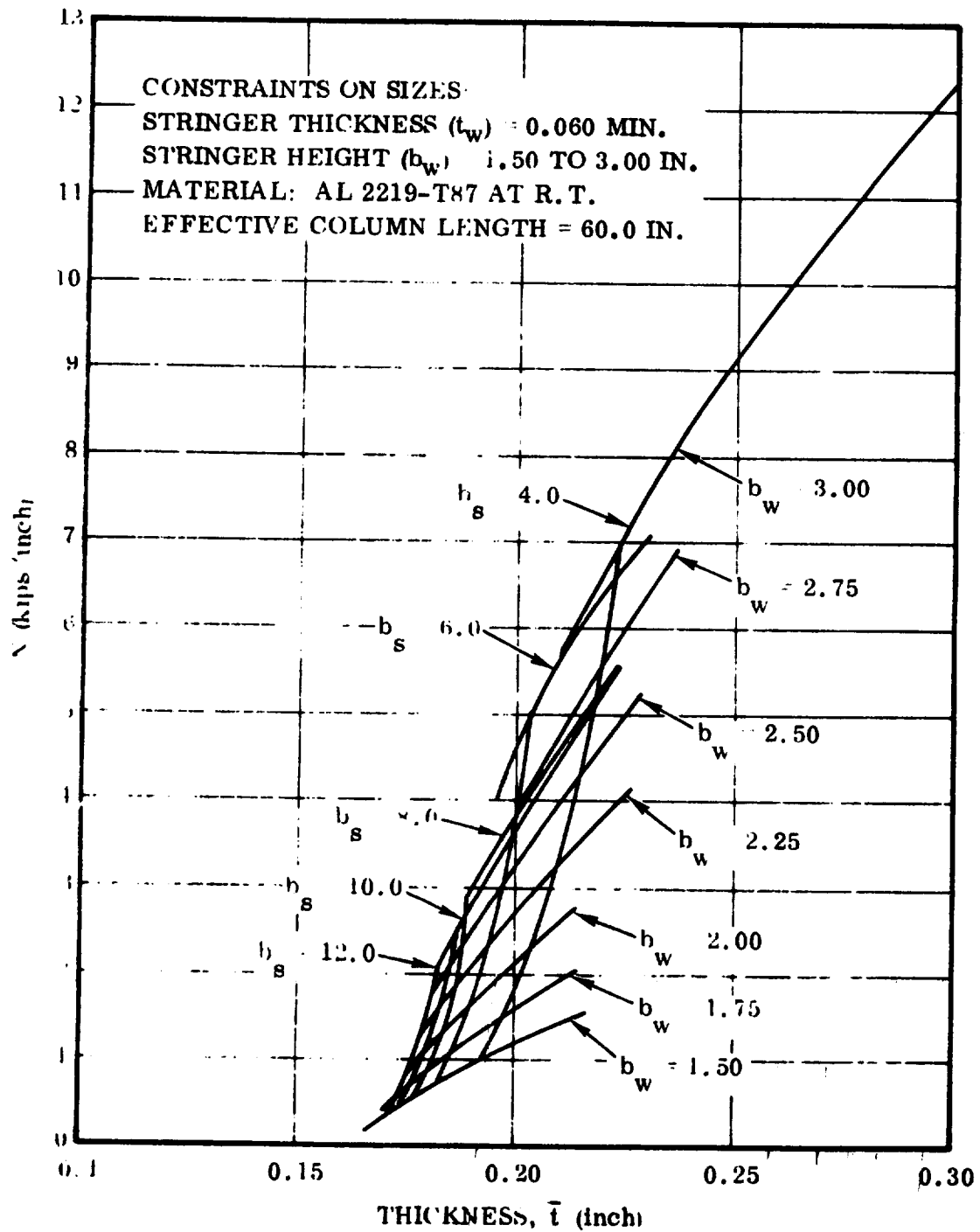


Figure 3-4. Integral Tee Plate-Stringer, Optimization of Stringer Spacing and Height — 0.162 Inch Skin Thickness

**Table 3-1. LH<sub>2</sub> Tank Critical Design Loads (Ultimate)**

Station	Bottom			Bottom Side			Side			Top Side			Top		
	N <sub>x</sub>	q	C*	N <sub>x</sub>	q	C*	N <sub>x</sub>	q	C*	N <sub>x</sub>	q	C*	N <sub>x</sub>	q	C*
<b>2400</b>	-4167	0	7	-4072	49	4	-6062	6	6	-8803	5	10	-10,923	0	10
<b>2800</b>	-6327	0	7	-5614	222	7	-6138	319	6	-8485	624	10	-10,412	0	10
<b>3161</b>	-7269	0	7	-6380	228	7	-6401	346	6	-7817	700	10	-9,206	0	10
<b>3377</b>	-8055	0	7	-7006	66	7	-6536	362	6	-7479	743	5	-8,349	0	10

Ultimate Radial Load Intensities

\*Condition number

Station	Condition 4		Condition 6		Condition 7		Condition 10	
	Press	N <sub>y</sub>	Press	N <sub>y</sub>	Press	N <sub>y</sub>	Press	N <sub>y</sub>
<b>2400</b>	11.9	2356	11.9	2356	27.3	5405	31.2	6178
<b>2800</b>	13.3	2633	13.3	2633	27.3	5405	31.2	6178
<b>3161</b>	15.4	3049	15.4	3049	28.7	5683	31.2	6178
<b>3377</b>	16.8	3326	16.8	3326	30.1	5960	32.2	6376

$$E_c = 10.8 (10)^6 \text{ psi}$$

$$w = 0.102 \text{ lb/in}^3$$

**Allowable working tension stress at limit pressure**

$$\text{Ultimate design } \frac{63}{1.4} = 45.0 \text{ ksi (1.4 ultimate factor)}$$

$$\text{Yield design } \frac{51}{1.1} = 46.4 \text{ ksi (1.1 yield factor)}$$

$$\text{Proof design } \frac{51}{1.13} = 45.1 \text{ ksi (1.13 proof test factor)}$$

**For pressure design the tank skins are ultimate critical.**

**Minimum skin thickness for the tank will be determined by ultimate design pressure and proof pressure.**

**The proof pressure is the maximum pressure in the tank multiplied by the proof test factor of 1.13.**



Maximum tank pressure is at the lower dome apex (26.4 psi).

$$\text{Proof pressure} = 26.4 (1.13) = 29.83 \text{ psi}$$

Maximum tank pressure in constant section:  $p = 25.5 \text{ psi}$ .

The tank constant section is proof test critical

$$\text{Minimum skin thickness} = \frac{29.83(198)}{51,000} = 0.116 \text{ inch}$$

$$\text{Drawing callout} = 0.126 \pm 0.010$$

$$\text{Stability design } t = 1.05 (0.116) = 0.122$$

Typical Plate Stringer Analysis — Section at Station 2800:

Tank Bottom Centerline:

$$\text{Ultimate loads: } N_x = -6327 \text{ lb/in; } N_y = 5405 \text{ lb/in; } q = 0.$$

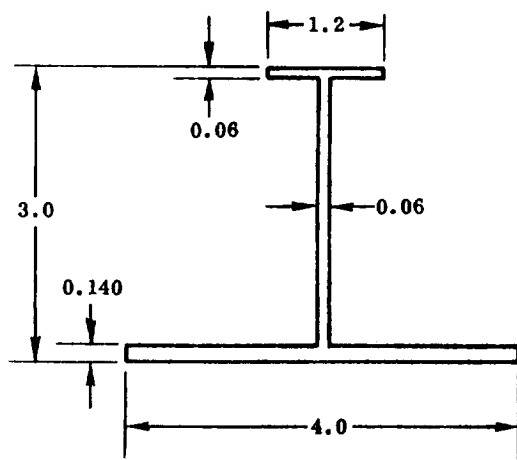


Plate-Stringer Section  
(Stringers are 4.0 inches on Centers)

Section Data:

$$t_s = 0.140$$

$$\bar{t} = 0.200$$

$$F_c = 33,500 \text{ psi } (L' = 60)$$

$$F_{su} = 38,000 \text{ psi}$$

Note: Thickness shown is for stability design:  $1.05 \times t_{min}$

$$\text{for pressure } t_s = \frac{0.140}{1.05} = 0.133$$

$$\text{Compressive stress: } f_c = \frac{6327}{0.200} = 31,630 \text{ psi}$$

$$\text{Tensile stress normal to compressive: } f_t = \frac{5405}{0.133} = 40,700 \text{ psi}$$

Maximum shear stress:

$$f_{sp} = \left[ \left( \frac{f_t + f_c}{2} \right)^2 + f_s^2 \right]^{1/2}$$

$$f_{sp} = 37,000 \text{ psi}$$

$$\text{M. S.} = \frac{33,500}{31,630} - 1 = +0.05 \text{ (compression)}$$

$$\text{M. S.} = \frac{38,000}{37,000} - 1 = +0.02 \text{ (shear)}$$

Typical Plate-Stringer Analysis - Station 2800 - Upper Side

Maximum compressive condition: 3g maximum thrust

$$N_x = -8485 \text{ lb/in ultimate}$$

$$q = 621 \text{ lb/in ultimate}$$

Internal pressure maximum ultimate:  $p = 22.3 (1.4) = 30.7 \text{ psi}$

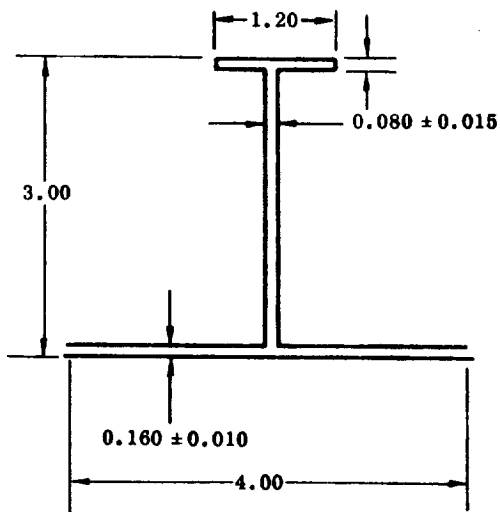
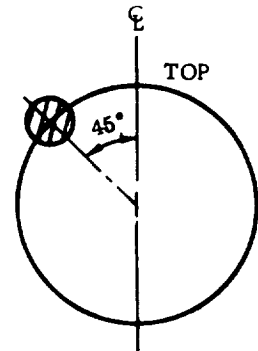


Plate Stringer Section

Nominal Section Properties

$$\bar{t} = 0.242$$

$$A = 0.9696/4 \text{ inch width}$$

$$\rho = 1.099$$

Section for Stability Design

$$\text{Skin } t = 0.150 (1.05) = 0.157$$

$$\text{Stringer } t = 0.065 (1.05) = 0.068$$

$$A = 0.9029$$

$$\bar{t} = 0.226$$

$$\rho = 1.014$$

Plate-stringer compression allowable:

Frame spacing is 66.7 inches

Column fixity is 1.5

Table 3-2. LH<sub>2</sub> Tank Plate Stringer Sizing

Material: 2219-T87; Stringer Spacing: 4.0 inches on centers;  
Stringer Height: 3.0 inches

Sta 2182	2400	2800	3161	3377	3681	
	$t_s = 0.122$ $\bar{t} = 0.175$	$t_s = 0.140$ $\bar{t} = 0.200$	$t_s = 0.150$ $\bar{t} = 0.220$	$t_s = 0.150$ $\bar{t} = 0.236$		Bottom $\phi$
	$t_s = 0.122$ $\bar{t} = 0.174$	$t_s = 0.130$ $\bar{t} = 0.192$	$t_s = 0.140$ $\bar{t} = 0.206$	$t_s = 0.150$ $\bar{t} = 0.212$		Bottom Side
	$t_s = 0.140$ $\bar{t} = 0.190$	$t_s = 0.140$ $\bar{t} = 0.193$	$t_s = 0.140$ $\bar{t} = 0.207$	$t_s = 0.150$ $\bar{t} = 0.204$		Side
	$t_s = 0.160$ $\bar{t} = 0.242$	$t_s = 0.160$ $\bar{t} = 0.240$	$t_s = 0.150$ $\bar{t} = 0.236$	$t_s = 0.150$ $\bar{t} = 0.223$		Top Side
	$t_s = 0.170$ $\bar{t} = 0.292$	$t_s = 0.170$ $\bar{t} = 0.276$	$t_s = 0.160$ $\bar{t} = 0.252$	$t_s = 0.160$ $\bar{t} = 0.246$		Top $\phi$

- Note: 1.  $t_s$  is skin thickness for stability design.  
2.  $\bar{t}$  is the equivalent thickness of skin and stringers.  
3. Thickness shown does not include effects of local loads.

$$L' = \frac{66.7}{\sqrt{1.5}} = 54.6$$

$$F_c = 37,600 \text{ psi}$$

$$f_c = \frac{8485}{0.226} = 37,500 \text{ psi}$$

$$M.S. = \frac{37,600}{37,500} - 1 = +0.0$$

Maximum skin shear: (nominal section)

$$f_t = \frac{pr}{t} = 38,000 \text{ psi}$$

$$f_c = \frac{N_x}{\bar{t}} = 35,000 \text{ psi}$$

$$f_s = \frac{q}{t} = 3880 \text{ psi}$$

$$f_{s_{\max}} = \left[ \left( \frac{f_t + f_c}{2} \right)^2 + f_s^2 \right]^{1/2} = 36,500 \text{ psi}$$

$$M. S. = \frac{38,000}{36,500} - 1 = +0.04$$

LH<sub>2</sub> Tank Belt Frames:

Frames sized by Shanley criterion:

$$I_f = N_x \left( \frac{C_f \pi D^4}{4LE_f} \right)$$

Typical frame analysis:

Design load intensity:  $N_x = -8000 \text{ lb/in}$

Frame spacing:  $L = 60 \text{ inches}$

Tank diameter:  $D = 396 \text{ inches}$

Coefficient:  $C_f = 62.5 (10)^{-6}$

$$\text{Solution: } I_f = \frac{8000(62.5)(10)^{-6} \pi (396)^4}{4(60)(10.3)(10)^6}; \quad I_f = 15.63 \text{ inches}^4$$

Frame section:

Frame depth:  $d = 9 \text{ inches}$

$$\text{Required cap area: } A = \frac{2I}{d_e^2}; \quad A = \frac{2(15.63)}{(8.75)^2} = 0.408 \text{ inch}^2/\text{cap}$$

Effective depth:  $d_e = 8.75$

Equivalent web thickness of the truss:  $t_w = 0.06$

$$\text{Frame } \Delta \bar{t}: \Delta \bar{t} = \frac{[2(0.408) + 9(0.060)]}{60} = 0.023 \text{ in.}$$

**3.1.3 VERTICAL TAIL BOX.** The vertical tail structural box is constructed of 6Al-4V titanium alloy, and has a three-spar arrangement with the front spar on the 10% chord line, the rear spar on the 60% chord line, and the mid spar on the 37% chord line as shown in Figure 3-5. Spars and ribs are of corrugated construction. Welding is used to attach spar and rib caps to the corrugated webs. Surface coverings are of integrally stiffened extruded "planks," welded together. The rear spar and mid spar transfer the bending moments and shear into the body bulkheads through fittings.

The vertical tail was simulated and analyzed by means of a Convair computer procedure that used the stiffness approach to obtain an internal load distribution. The spanwise bending moment distribution used for member sizing is shown in Figure 2-25. Another computer program was used to optimize the skin-stiffener configuration, with the resulting proportions shown on Page 109. The skins of the fin box are fully effective from the tip to the canted rib.

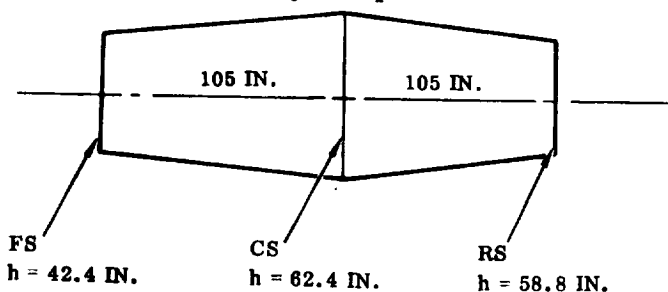
The section chosen for the fatigue calculations of the present study is at the canted rib, Section (A) - (A) of Figure 3-5. The spar cap sizing calculations for this section are shown below. Load distribution coefficients are determined by computer.

Section (A) - (A) of Figure 3-5

$$V = 352,800 \text{ lb (ultimate)}$$

$$M = 74.234 \times 10^6 \text{ in-lb}$$

$$T = 9.58 \times 10^6 \text{ in-lb}$$



$$q_{FS} = \frac{0.0176(352,800)}{42.4} = \frac{6209}{42.4} = 146 \text{ lb/in}$$

$$q_{CS} = \frac{0.123(352,800)}{62.4} = \frac{43,394}{62.4} = 695 \text{ lb/in}$$

$$q_{RS} = \frac{0.442(352,800)}{58.8} = \frac{155,938}{58.8} = 2652 \text{ lb/in}$$

Remainder of shear is carried in covers and caps, which are tapered.

Spar Cap Loads

$$\text{Forward } P_{cap} = \frac{0.013(74.234)10^6}{42.4} = 22,760$$

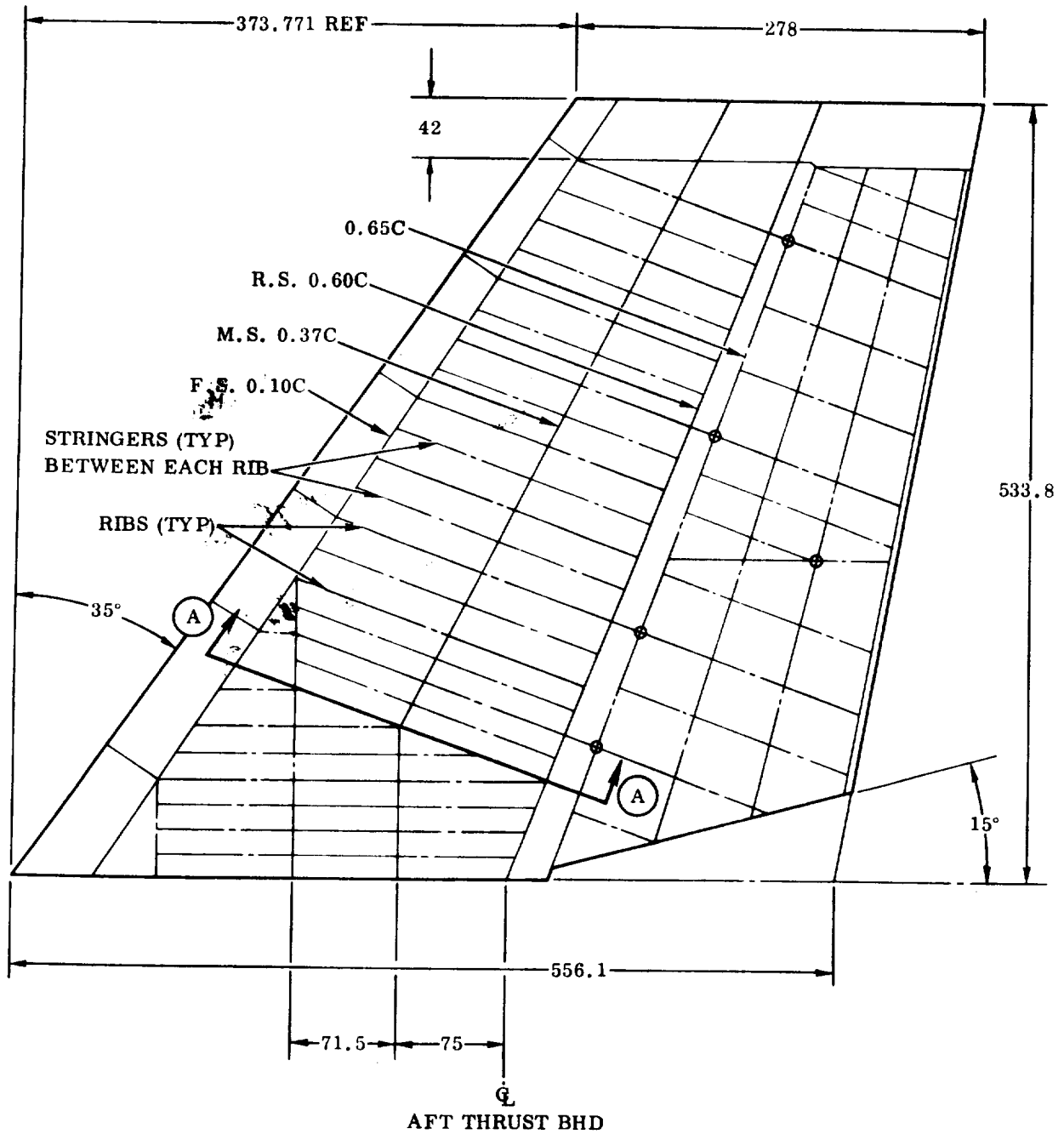


Figure 3-5. Vertical Tail Configuration

$$\text{Center } P_{\text{cap}} = \frac{0.032(74.234)(10^6)}{62.4} = 38,069$$

$$\text{Aft } P_{\text{cap}} = \frac{0.068(74.234) 10^6}{58.8} = 85,849$$

Cap Areas Choosing  $f = 34 \text{ ksi}$

$$\text{Forward } A = \frac{22,760}{34,000} = 0.670 \text{ in}^2$$

$$\text{Center } A = \frac{38,069}{34,000} = 1.12 \text{ in}^2$$

$$\text{Rear } A = \frac{85,849}{34,000} = 2.52 \text{ in}^2$$

Covers

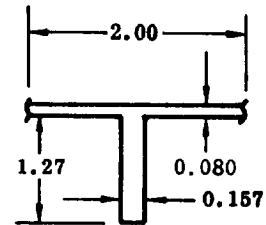
$$0.89 (74,234,000) = 66,068,260 \text{ in-lb}$$

$$P_x = \frac{66,068,260}{55 \text{ in.}} = 1,201,241 \text{ lb}$$

$$N_x = 1,201,241/210 = 5725 \text{ lb/in}$$

For the configuration with  $\bar{t} = 0.180$  we have  $\sigma_{\text{cr}} = 32,450 \text{ psi}$ .

This compares with  $\sigma_{\text{eff}} = \frac{5725 \text{ lb/in}}{0.180 \text{ in.}} = 31,805 \text{ psi}$



**3.1.4 THRUST STRUCTURE.** A finite element model was utilized to determine the theoretical weight of the thrust structure. The idealized model and geometry is shown in Figures 3-6 through 3-11 and Table 3-3. Figure 3-12 shows thrust structure model elements.

A total of 14 basic loading conditions were initially investigated, plus one or two engine failures for the flight conditions. By assuming an identical structural configuration in each 45-degree segment of the thrust structure model, the number of possible loading combinations with engine failure was reduced. For one engine failed, one of the four inner engines or one of the eight outer engines was considered failed — reducing the number of combinations from 12 to 2. For two engines failed the number of combinations was reduced from 66 to 12.

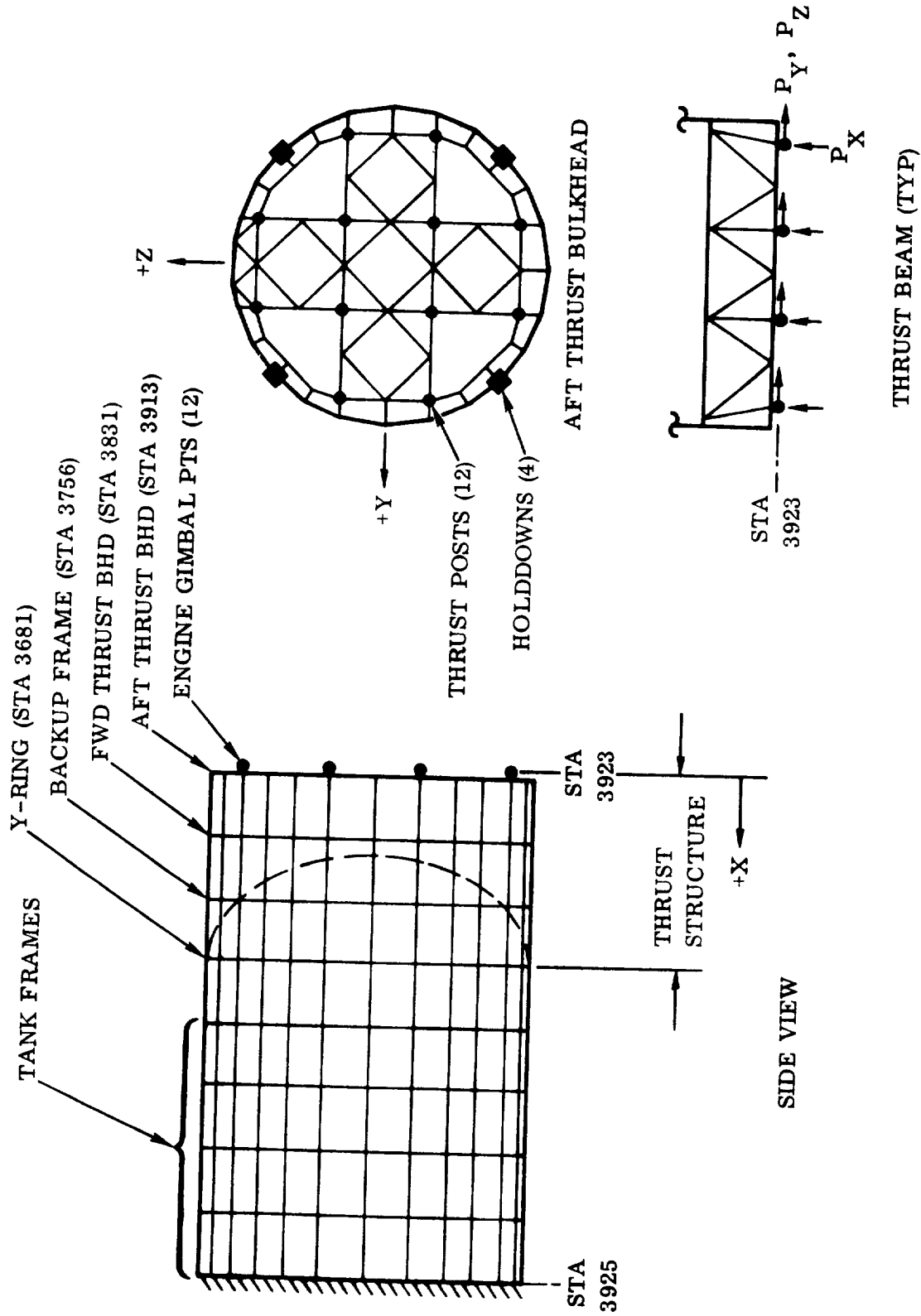
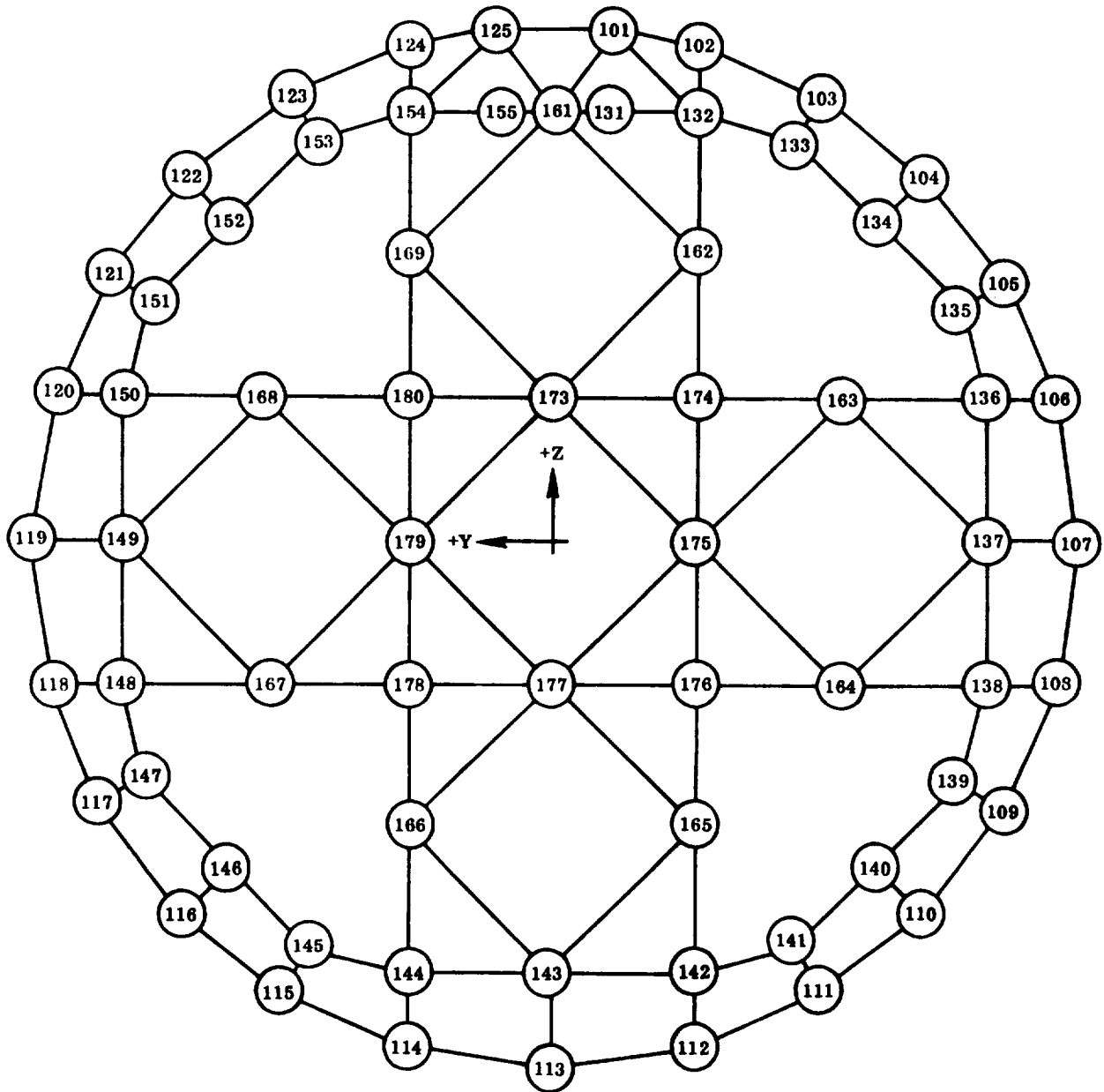


Figure 3-6. Thrust Structure Finite Element Model





(LOOKING FORWARD)

Figure 3-7. Aft Thrust Bulkhead Model, Station 3913

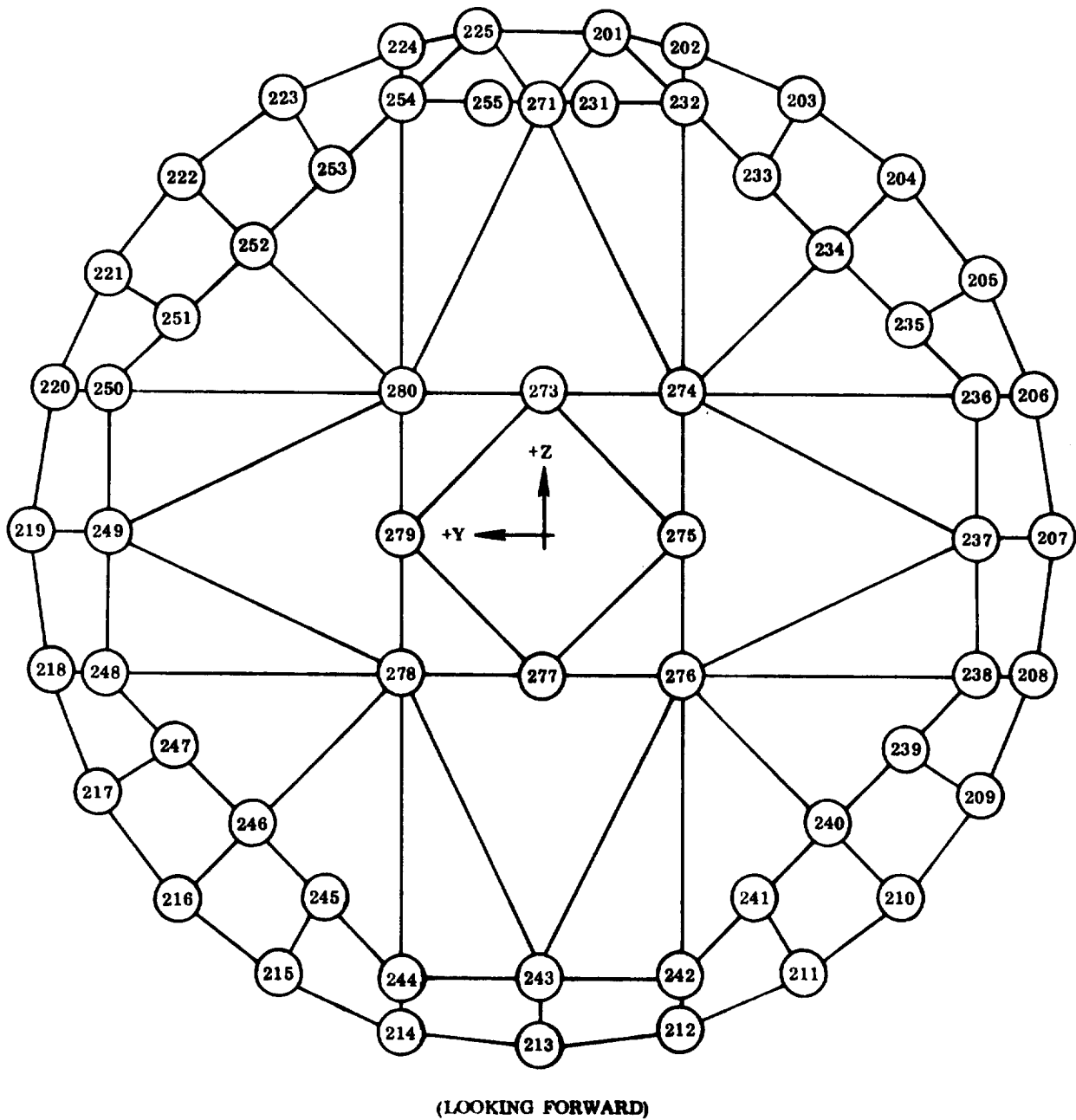
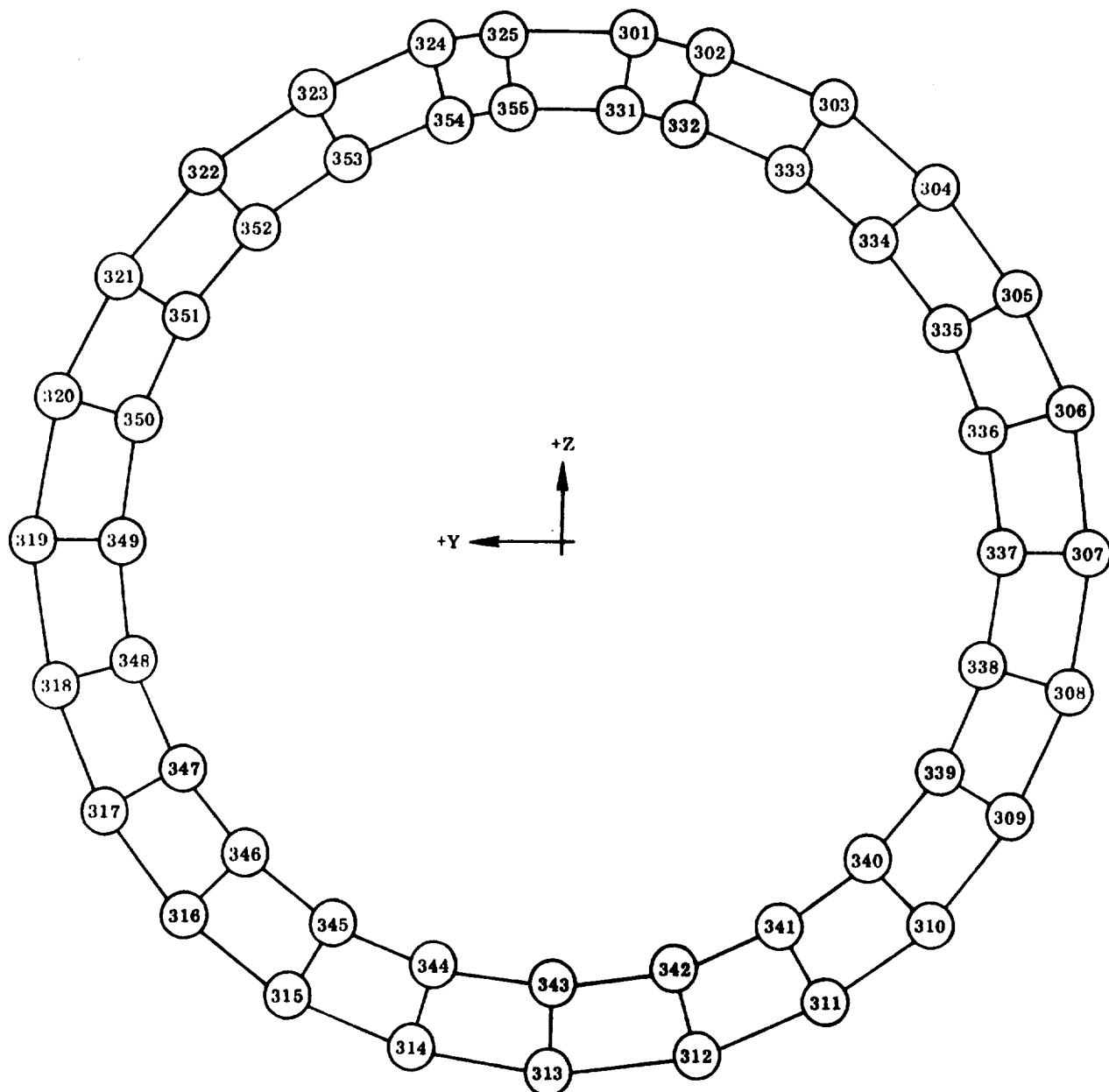
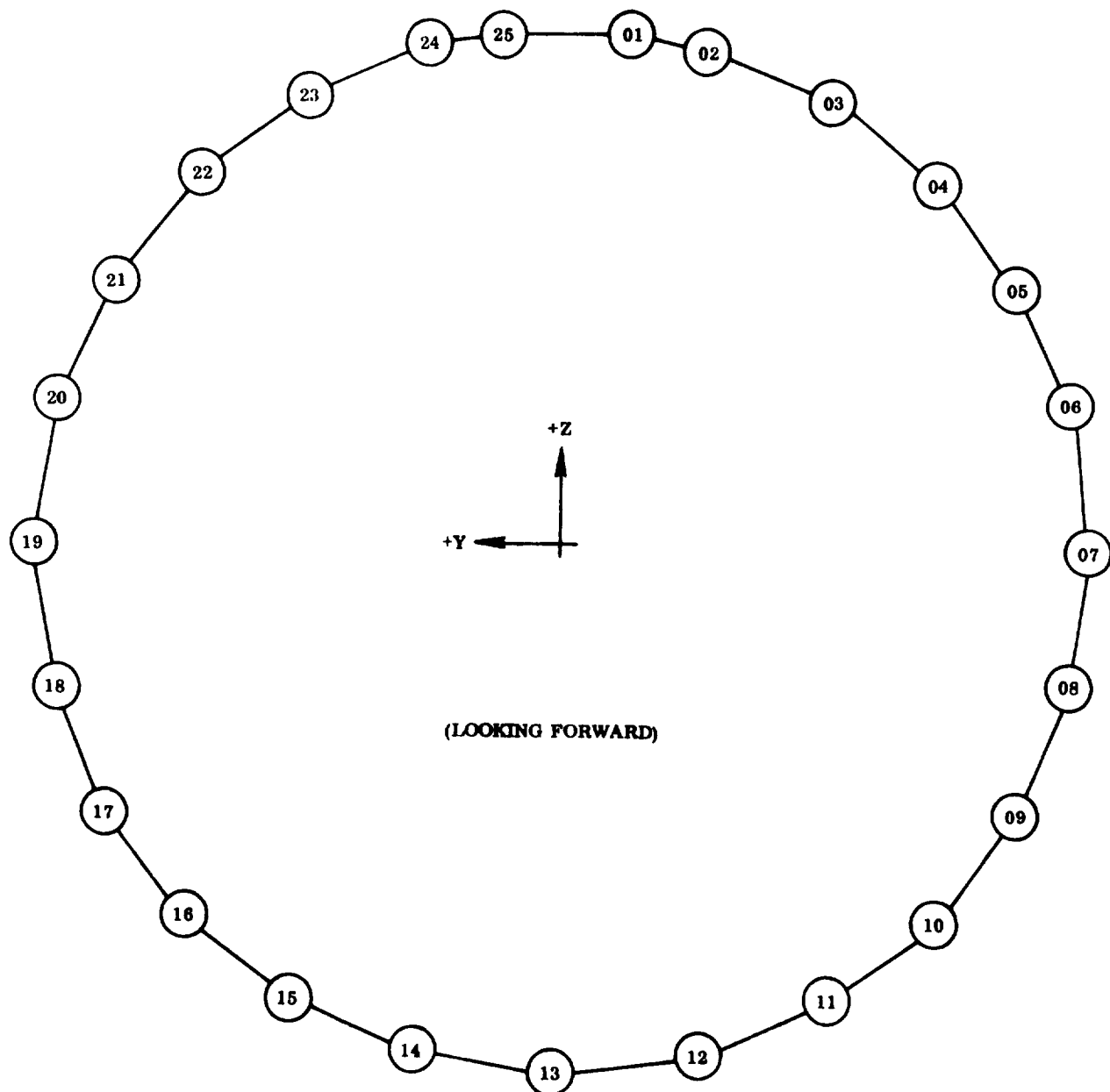


**Figure 3-8. Forward Thrust Bulkhead Model, Station 3831**



(LOOKING FORWARD)

Figure 3-9. Backup Frame Model, Station 3756



(STATION 3681, X=242, NODE 400s)	(STATION 3451, X=472, NODE 700s)
(STATION 3605, X=318, NODE 500s)	(STATION 3373, X=550, NODE 800s)
(STATION 3529, X=394, NODE 600s)	(STATION 3295, X=628, NODE 900s)

**Figure 3-10. Y-Ring Tank Frames Model**

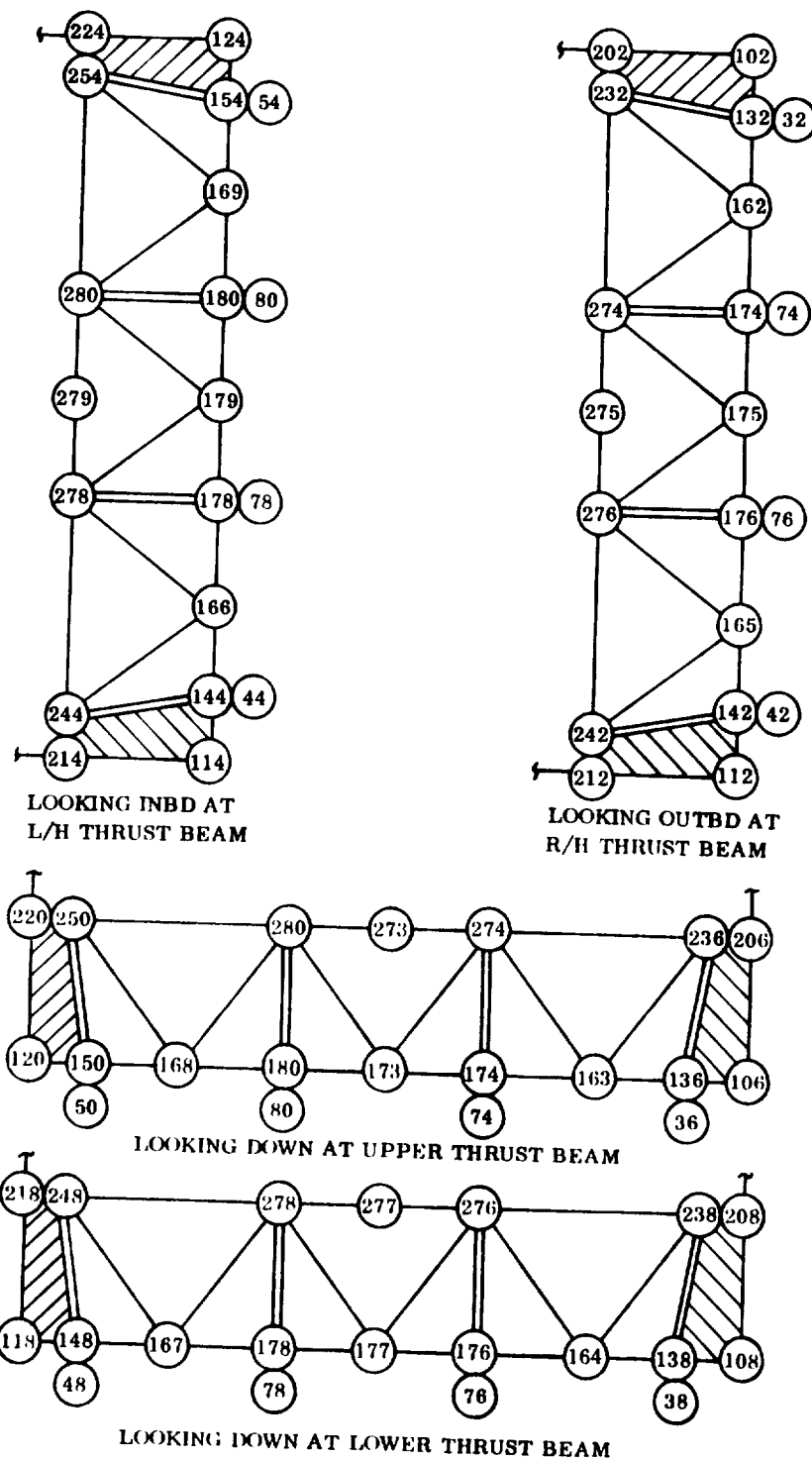


Figure 3-11. Thrust Beam Models

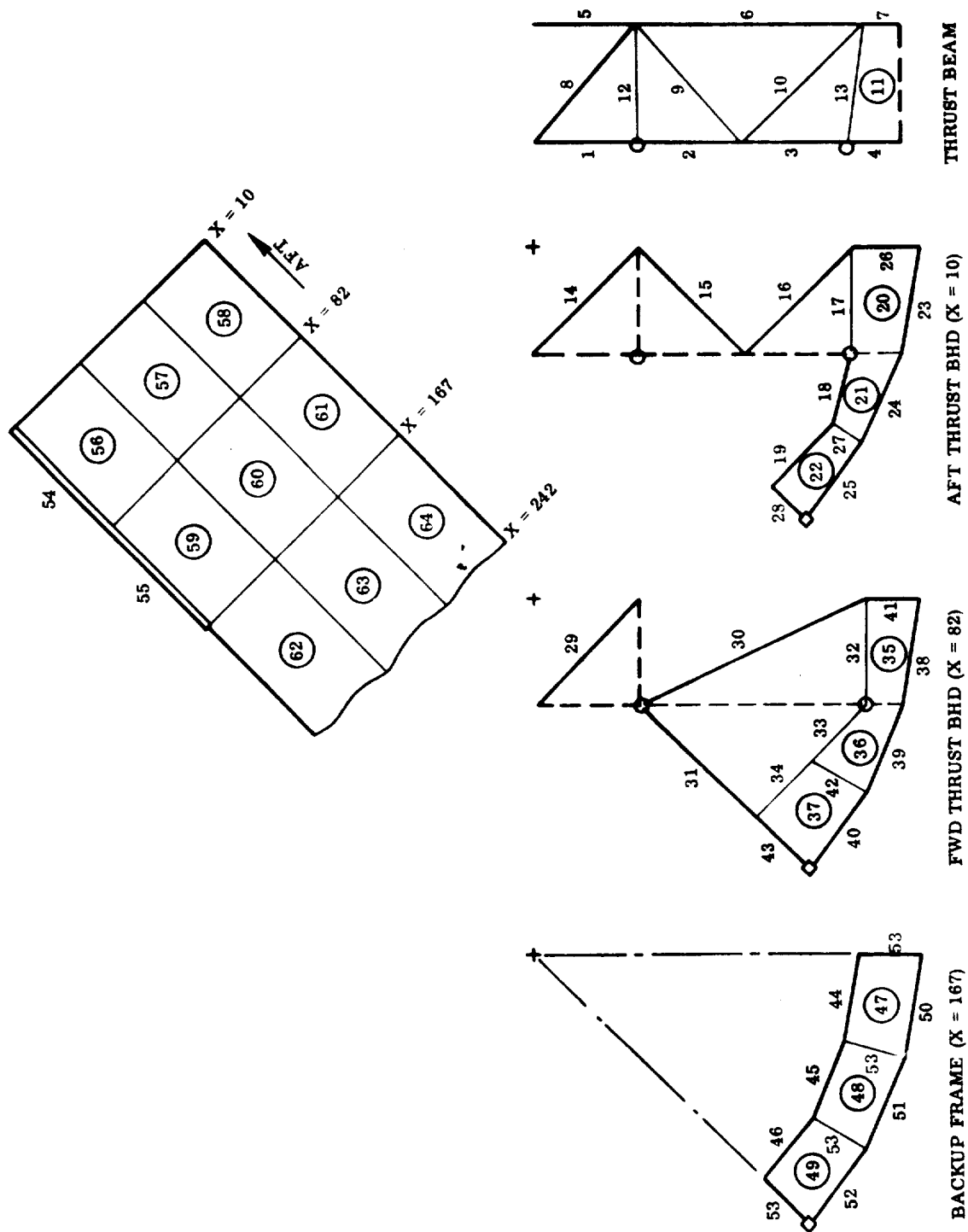


Figure 3-12. Thrust Structure Model Elements

Table 3-3. Thrust Structure Model Coordinates

Node	y	z	Node	y	z	Node	y	z
1	-25.00	196.42	146	122.43	-122.43	244	54.50	-180.00
2	-54.50	190.35	147	154.11	-90.74	245	86.90	-147.60
3	-100.46	170.62	148	163.50	-54.50	246	117.25	-117.25
4	-140.01	140.01	149	163.50	0	247	147.60	-86.90
5	-170.62	100.46	150	163.50	54.50	248	180.00	-54.50
6	-190.35	54.50	151	154.11	90.74	249	180.00	0
7	-198.00	0	152	122.43	122.43	250	180.00	54.50
8	-190.35	-54.50	153	90.74	154.11	251	147.60	86.90
9	-170.62	-100.46	154	54.50	163.50	252	117.25	117.25
10	-140.01	-140.01	155	19.20	163.50	253	86.90	147.60
11	-100.46	-170.62	161	0	163.50	254	54.50	180.00
12	-54.50	-190.35	162	-54.50	109.00	255	29.48	180.00
13	0	-198.00	163	-109.00	54.50	271	0	180.00
14	54.50	-190.35	164	-109.00	-54.50	331	-27.96	170.73
15	100.46	-170.62	165	-54.50	-109.00	332	-47.62	166.32
16	140.01	-140.01	166	54.50	-109.00	333	-87.78	149.08
17	170.62	-100.46	167	109.00	-54.50	334	-122.33	122.33
18	190.35	-54.50	168	109.00	54.50	335	-149.08	57.78
19	198.00	0	169	54.50	109.00	336	-166.32	47.62
20	190.35	54.50	x73	0	54.50	337	-173.00	0
21	170.62	100.46	x74	-54.50	54.50	338	-166.32	-47.62
22	140.01	140.01	x75	-54.50	0	339	-149.08	-87.78
23	100.46	170.62	x76	-54.50	-54.50	340	-122.33	-122.33
24	54.50	190.35	x77	0	-54.50	341	-87.78	-149.08
25	25.00	196.42	x78	54.50	-54.50	342	-47.62	-166.32
131	-19.20	163.50	x79	54.50	0	343	0	-173.00
132	-54.50	163.50	x80	54.50	54.50	344	47.62	-166.32
133	-90.74	154.11	231	-29.48	180.00	345	87.78	-149.08
134	-122.43	122.43	232	-54.50	180.00	346	122.33	-122.33
135	-154.11	90.74	233	-86.90	147.60	347	149.08	-87.78
136	-163.50	54.50	239	-117.25	117.25	348	166.32	-47.62
137	-163.50	0	235	-147.60	86.90	349	173.00	0
138	-163.50	-54.50	236	-180.00	54.50	350	166.32	47.62
139	-154.11	-90.74	237	-180.00	0	351	149.08	37.78
140	-122.43	-122.43	238	-180.00	-54.50	352	122.33	122.33
141	-90.74	-154.11	239	-147.60	-86.90	353	87.78	149.08
142	-54.50	-163.50	240	-117.25	-117.25	354	47.62	166.32
143	0	-163.50	241	-86.90	-147.60	355	27.96	170.73
144	54.50	-163.50	242	-54.50	-180.00			
145	90.74	-154.11	243	0	-180.00			

1. One hour ground headwinds
2. One hour ground tailwinds
3. One hour ground sidewinds

Conditions 4 through 11 were run with:

- a. No engines out.
- b. With one engine out.
- c. With two engines out.
4. Liftoff plus one hour ground headwinds
5. Liftoff plus one hour ground tailwinds
6. Liftoff plus one hour ground sidewinds
7. Maximum alpha q with headwinds
8. Maximum alpha q with tailwinds
9. Maximum beta q
10. Three g maximum thrust
11. Booster burnout
17. One day ground headwinds
18. One day ground tailwinds
19. One day ground sidewinds

A computerized analysis was made with these loading conditions. From the resulting internal loads it was determined that only seven loading conditions were critical for design. Conditions eliminated did not occur in the maximum/minimum search or were slightly critical in only a few areas; consequently, these conditions have a negligible effect on the overall results. The critical conditions are as follows:

- 7 Maximum alpha q headwinds
- 7 IE Maximum alpha q headwinds (inner engine failed)
- 7 OE Maximum alpha q headwinds (outer engine failed)
- 10 Three g maximum thrust
- 10 IE Three g maximum thrust (inner engine failed)
- 10 OE Three g maximum thrust (outer engine failed)
- 19 One day ground sidewinds



Ultimate applied loads are shown in Table 3-4. Table 3-5 lists the element number, maximum load, cross-sectional area and thickness, applied and allowable stress, and element weight based on the material properties given below.

As noted in Section 2.3, the structural members of the thrust structure are of Ti-6Al-4V annealed titanium, having the following room temperature properties:

$$F_{tu} = 130 \text{ ksi (Reference 14)}$$

$$F_t \text{ at limit load} = \frac{F_{tu}}{1.40} = \frac{130}{1.40} = 92.86 \text{ ksi}$$

$$F_{cy} = 126 \text{ ksi}$$

$$F_{su} = 76 \text{ ksi}$$

Table 3-4. Thrust Structure Ultimate Design Loads

		Ultimate Loads (pounds)			Locations
Conditions		P <sub>x</sub>	P <sub>y</sub>	P <sub>z</sub>	
19	1 Day Ground Sidewinds	1,065,367	-38,280	4,202	104
		1,065,537	-104,926	4,212	110
		2,467,059	-104,926	70,858	116
		2,466,889	-38,280	70,858	122
7	Maximum alpha-q Headwinds	809,000		-187,920	32,36,38,42,44,48,50,54,74,76,78,80
			185,610	508,470	109
			46,300		112
			-185,610	508,470	117
7 IE	Maximum alpha-q Headwinds (Inner Engine Out)	882,610		-205,000	32,36,38,42,44,48,50,54,74,78,80
			185,610	508,470	109
			46,300		112
			-185,610	508,470	117
7 OE	Maximum alpha-q Headwinds (Outer Engine Out)	882,610		-205,000	32,36,38,44,48,50,54,74,76,78,80
			185,610	508,470	109
			46,300		112
			-185,610	508,470	117
10	3g Maximum Thrust	920,990		-67,680	32,36,38,42,44,48,50,54,74,76,78,80
10 IE	3g Maximum Thrust (Inner Engine Out)	1,004,700		-73,832	32,36,38,42,44,48,50,54,74,78,80
10 OE	3g Maximum Thrust (Outer Engine Out)	1,004,700		-73,832	32,36,38,44,48,50,54,74,76,78,80

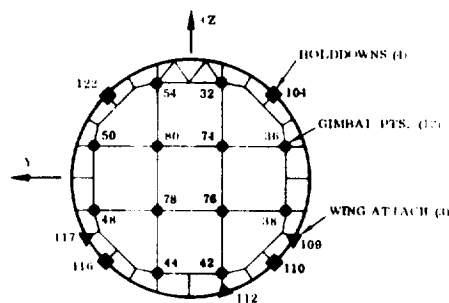


Table 3-5. Thrust Structure Model Element Loads, Areas, Thicknesses, Stresses, and Weights

THRUST BEAMS									
Element	A. L. (lb) q (lb/in)	A (sq in.) t (in.)	Comments	Stress (psi)		L (in.) A (sq in)	No. of Elements	Weight (lb)	
				Applied	Allowable				
1	-1,013,000	10.31	Cruciform 7 x 7 x 0.78	$f_c = 98,300$	99,000	54.50	8	719.2	
2	-998,400	10.19	Cruciform 7 x 7 x 0.77	$f_c = 97,800$	99,000	54.50	8	710.9	
3	-263,300	3.44	Cruciform 7 x 7 x 0.25	$f_c = 76,600$	79,000	54.50	8	240.0	
4	-205,900	2.34	Cruciform 5 x 5 x 0.24	$f_c = 87,800$	88,500	26.85	8	80.4	
						Aft Flange Weight = 1750			
5	776,000	6.10	Cruciform 7 x 7 x 0.45	$f_t = 127,200$	130,000	109.00	4	425.5	
6	476,300	3.71	Cruciform 7 x 7 x 0.27	$f_t = 128,400$	130,000	125.50	8	596.0	
7	-123,000	3.71	Cruciform (same as Element 6)		130,000	10.35	8	49.2	
						Fwd Flange Weight = 1071			
8	-392,000	4.48	Tube 7 O. D. x 0.21 wall	$f_c = 87,500$	89,500	98.46	8	564.6	
9	818,400	6.32	Tube 8 O. D. x 0.26 wall	$f_t = 129,500$	130,000	98.46	8	796.5	
10	-901,500	10.23	Tube 8 O. D. x 0.43 wall	$f_c = 88,100$	90,600	108.47	8	1420.3	
11	(17,160)	(0.300)	Web	$f_s = 57,200$	58,700	(1525)	8	585.6	
						Diagonal and Web Weight = 3367			
12	A. L. = -882,600 M = 2,050,000	14.14	Tube 9.5 O. D. x 0.50 wall	$f_c = 62,400$ $f_b = 67,800$	119,000 159,000	82.00	4	742.1	
13	A. L. = -882,600 M = 2,050,000	14.14	Tube 9.5 O. D. x 0.50 wall (aft end)	$f_c = 62,400$ $f_b = 67,800$	119,000 159,000	83.64	8	1050.3	
	A. L. = 635,000	5.47	Tube 8.9 O. D. x 0.20 wall (fwd end)	$f_t = 127,100$	130,000				Thrust Post Weight = 1792
									Thrust Beam Total Weight = 7980

Table 3-5. Thrust Structure Model Element Loads, Areas, Thicknesses, Stresses, and Weights, Contd

Element	A. L. (lb) q (lb/in)	A (sq in) t (in.)	Comments	Stress (psi)		L (in.) A (sq in)	No. of Elements	Weight (lb)
				Applied	Allowable			
14	-26,400	0.7014	Tube 3.5 O.D. x 0.065 wall	$f_c = 37,600$	40,000	77.07	4	34.6
15	-64,500	0.9567	Tube 4.75 O.D. x 0.065 wall	$f_c = 67,400$	73,500	77.07	8	94.4
16	-64,500	0.9567	Tube 4.75 O.D. x 0.065 wall	$f_c = 67,400$	73,500	77.07	8	94.4
Brace Weight = 223								
17	-320,000	2.54	Tee	$f_c = 126,000$	126,000	54.50	8	177.2
18	-356,000	2.83	Tee	$i_c = 126,000$	126,000	37.44	8	135.6
19	-256,900	2.04	Tee	$f_c = 125,900$	126,000	44.81	8	117.0
Inner Flange Weight = 430								
20	(4,466)	(0.077)	Web	$f_s = 58,000$	58,700	(1672)	8	164.8
21	(12,340)	(0.211)	Web	$f_s = 58,500$	58,700	(962)	8	259.8
22	(2,542)	(0.060)	Web (0.060 = assumed minimum t)	$f_s = 42,400$	58,700	(1032)	8	79.3
Web Weight = 504								
23	-330,100	2.62	Tee	$f_c = 126,000$	126,000	55.03	8	184.5
24	-413,500	3.28	Tee	$f_c = 126,000$	126,000	50.02	8	210.0
25	-150,400	2.62	Tee (same as Element 23)		126,000	50.01	8	167.7
Outer Flange Weight = 562								
26	38,900	0.50	Assumed minimum area			34.50	4	11.0
27	233,000	2.33		$f_c = 100,000$	100,000	19.16	8	57.1
28	30,000	0.50	Assumed minimum area			24.86	4	8.0
Stiffener Weight = 76								
Aft Thrust Bulkhead Total Weight = 1795								

**Table 3-5. Thrust Structure Model Element Loads, Areas, Thicknesses, Stresses, and Weights, Contd**

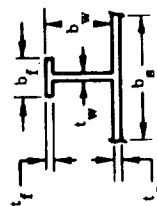
FORWARD THRUST BULKHEAD								
Element	A. L. (lb) q (lb/in)	A (sq in) t (in.)	Comments	Stress (psi)		L (in.) A (sq in)	No. of Elements	Weight (lb)
				Applied	Allowable			
29	69,300	0.534	Tube	$f_t = 129,800$	130,000	77.07	4	26.3
30	69,500	0.535	Tube	$f_t = 129,900$	130,000	136.82	8	93.7
31	-82,500	1.464	Tube 5.0 O. D. x 0.095 wall	$f_c = 56,400$	61,500	88.74	4	83.1
32	246,500	1.90	Tee	$f_t = 129,700$	130,000	54.50	8	132.5
33	353,500	2.72	Tee	$f_t = 130,000$	130,000	45.82	8	159.5
34	408,000	3.14	Tee	$f_t = 129,900$	130,000	42.92	8	172.5
35	(3693)	(0.063)	Web	$f_g = 58,600$	58,700	(773)	8	62.3
36	(3538)	(0.061)	Web	$f_s = 58,000$	58,700	(830)	8	64.8
37	(711)	(0.060)	Web (0.060 = assumed minimum t)			(1354)	8	104.0
38	352,500	2.72	Tee	$f_t = 129,600$	130,000	55.03	8	191.6
39	343,100	2.64	Tee	$f_t = 130,000$	130,000	50.02	8	169.0
40	129,700	2.00	Tee		130,000	50.01	8	128.0
41	-9,500	0.50	Assumed Minimum Area			Outer Flange Weight = 489		
42	13,500	0.50	Assumed Minimum Area			18.00	4	5.8
43	-73,300	0.73		$f_c = 100,000$	100,000	32.19	4	15.0
						Stiffener Weight = 38		
						Forward Thrust Bulkhead Total Weight = 1425		

Table 3-5. Thrust Structure Model Element Loads, Areas, Thicknesses, Stresses, and Weights, Contd

Element	A, L, (lb) q (lb/in)	A (sq in) t (in.)	Comments	Stress (psi)		L (in.) A (sq in)	No. of Elements	Weight (lb)
				Applied	Allowable			
44	-56,100	0.489	Tee 2 x 1 x 0.163	$f_c = 114,700$	115,000	48.09	8	30.1
45	19,200	0.468	Tee 2 x 1 x 0.156		130,000	43.70	8	26.2
46	58,400	0.450	Tee 2 x 1 x 0.150	$f_t = 129,800$	130,000	43.70	8	25.2
47	(594)	(0.040)	Web (0.040 = assumed minimum t)			Inner Flange Weight = 81		
48	(1302)	(0.040)	Web			(1277)	8	65.4
49	(983)	(0.040)	Web			(1162)	8	59.5
						(1162)	8	59.5
							Web Weight = 185	
50	-28,700	0.342	Tee 2 x 1 x 0.114	$f_c = 83,900$	84,500	55.03	8	24.1
51	-20,900	0.316	Tee 2 x 1 x			50.02	8	20.2
52	37,800	0.291	Tee 2 x 1 x 0.097	$f_t = 129,900$	130,000	50.01	8	18.6
						Outer Flange Weight = 63		
53	6,300	0.500	Assumed minimum area.			25.00	24	48.0
						Stiffener Weight = 48.0		
						Backup Frame Total Weight = 377		
HOLDDOWN								
54	-1,916,300	15.21	H-section	$f_c = 126,000$	126,000	82.0	4	798.2
55	-1,113,100	8.84	H-section	$f_c = 125,900$	126,000	75.0	4	424.3
						Holddown Fittings Total Weight = 1223		

Table 3-5. Thrust Structure Model Element Loads, Areas, Thicknesses, Stresses, and Weights, Contd

SKIN PANELS											
Element	Loads (lb/in)		$\bar{t}$ (in.)	Comments*	Stress (psi)				A (sq in)	No. of Elements	Weight (lb)
					Applied		Allowable				
	$N_x$	q			$f_c$	$f_s$	$F_c$	$F_s$			
56	20,334	7520	0.3021	$t_s^{**} = 0.160, t_w^{**} = t_f = 0.140$	67,309	47,000	108,870	80,000	4102	8	1586.2
57	4,752	6905	0.1821	$t_s = 0.120, t_w = t_f = 0.060$	26,100	57,540	63,270	80,000	4102	8	956.1
58	4,358	3167	0.1421	$t_s = 0.080, t_w = t_f = 0.060$	30,810	39,590	55,540	80,000	4512	8	820.7
Aft Bay Skin Panel Weight = 3363											
59	14,106	3910	0.2221	$t_s = 0.160, t_w = t_f = 0.060$	63,510	24,440	71,370	80,000	3751	8	1066.4
60	10,947	5372	0.2221	$t_s = 0.160, t_w = t_f = 0.060$	49,290	33,580	71,370	80,000	3752	8	1066.5
61	10,862	4033	0.2021	$t_s = 0.140, t_w = t_f = 0.060$	53,750	28,810	67,300	80,000	4127	8	1067.6
Center Bay Skin Panel Weight = 3201											
62	12,175	2719	0.2021	$t_s = 0.140, t_w = t_f = 0.060$	60,240	19,420	67,300	00,000	3751	8	970.4
63	11,567	3756	0.2021	$t_s = 0.140, t_w = t_f = 0.060$	57,230	26,830	67,300	80,000	3752	8	970.6
64	11,539	3675	0.2021	$t_s = 0.140, t_w = t_f = 0.060$	57,100	26,250	67,300	80,000	4127	8	1067.7
Forward Bay Skin Panel Weight = 3009											
Skin Panels Total Weight = 9573											



\*  $b_s = 4, b_w = 3, b_f = 1.2$

\*\*  $t_s$  and  $t_w$  were determined through the utilization of a plate-stringer optimization program.

**3.1.5 AFT ORBITER SUPPORT FRAME.** The principal aft support point of the orbiter to the booster is located at Station 2666. A substantial body frame is provided at this station to distribute orbiter loads to the booster body shell. Figure 3-13 shows the critical applied loads (ultimate), and Figure 3-14 shows the element identification.

A finite element computer solution was used to size the frame, and the model, geometry, applied loads, section properties and internal loads are shown on the following pages. The material of the frame is 2219 aluminum alloy, largely in the T851 plate temper. The room temperature properties of this material are as follows:

$$F_{tu} = 62 \text{ ksi}$$

$$F_t \text{ at limit load} = \frac{F_{tu}}{1.40} = \frac{62}{1.40} = 44.29 \text{ ksi}$$

$$F_{cy} = 48 \text{ ksi}$$

$$F_{su} = 36 \text{ ksi}$$

To allow for the effects of fastener holes, welds, and other stringer reducers, these properties were reduced for member sizing to the following values for use with ultimate loads.

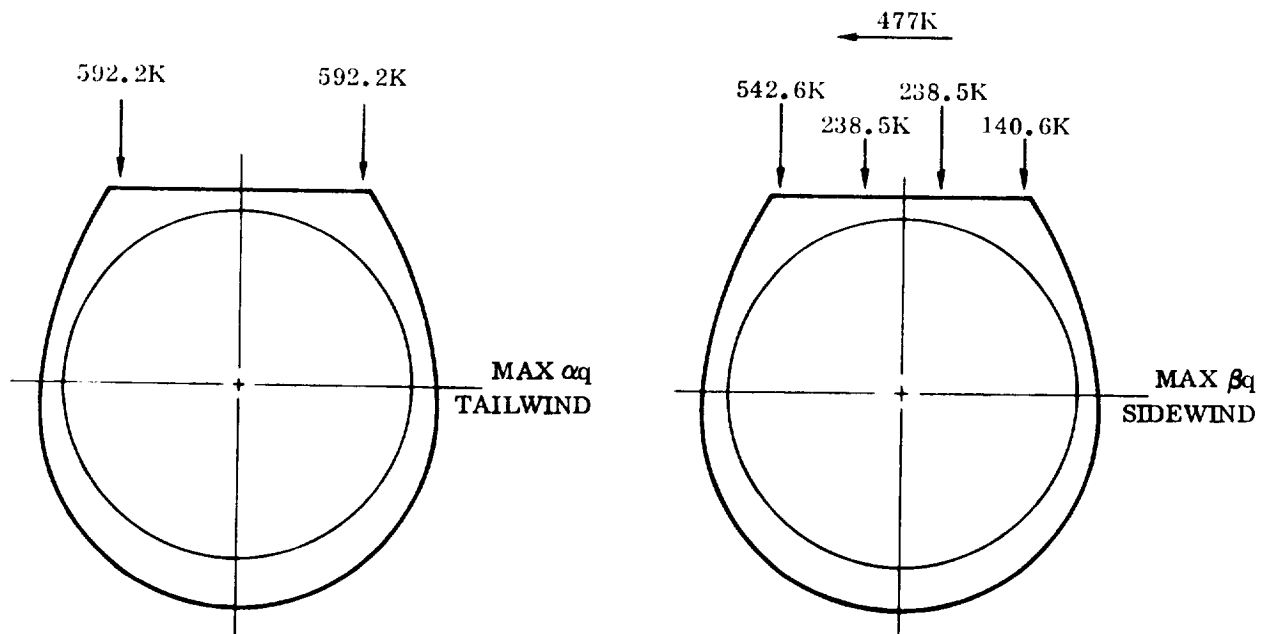


Figure 3-13. Critical Applied Loads (Ultimate),  
Aft Orbiter Attachment Frame

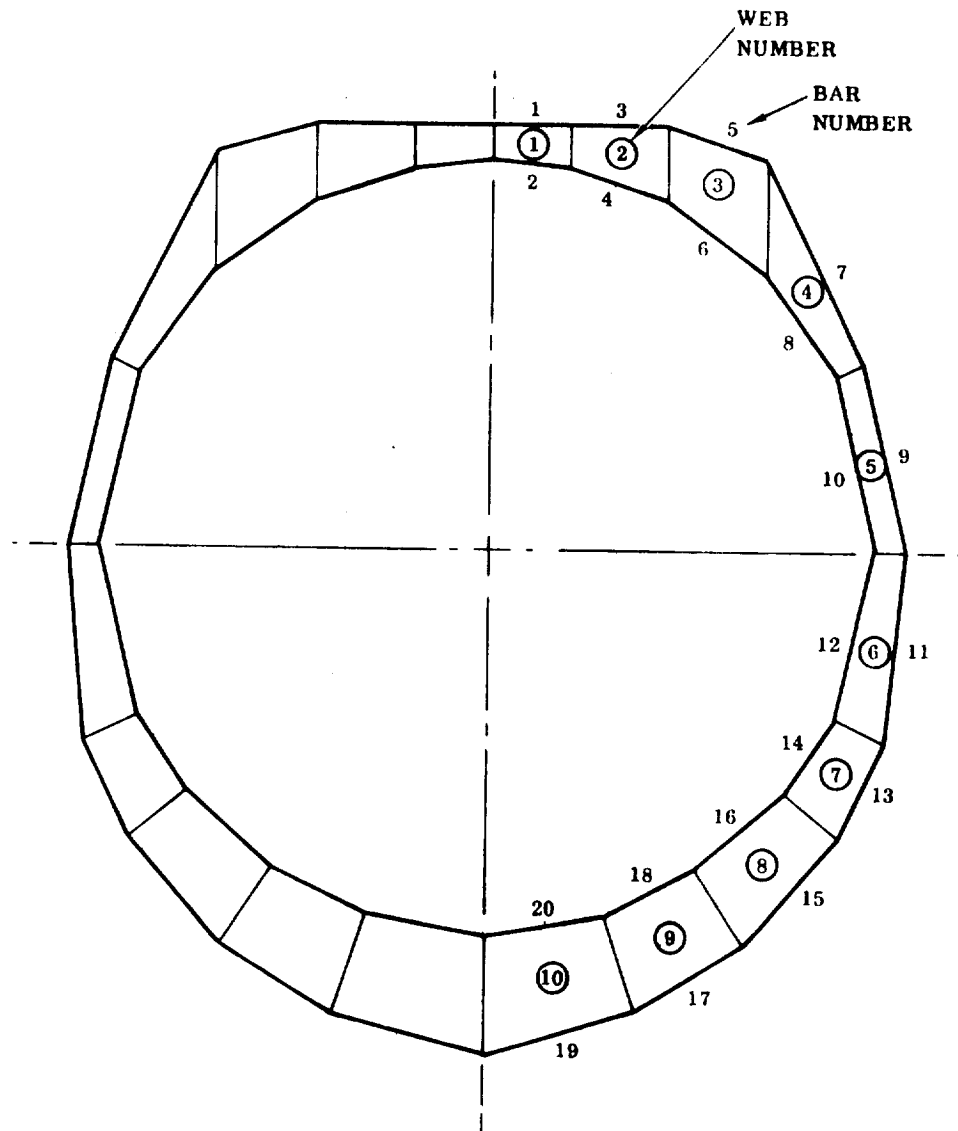


Figure 3-14. Aft Orbiter Attachment Frame Element Identification

$$F_t = F_c = 50 \text{ ksi}$$

$$F_s = 20 \text{ ksi}$$

Table 3-6 lists cap axial loads and cross-sectional areas, and Table 3-7 lists the web shear flows and thicknesses.



**Table 3-6. Aft Orbiter Attachment Frame, Cap Axial  
Loads and Cross-Sectional Areas**

Bar	Length (inches)	Ultimate Axial Loads (kips)			Area* (in <sup>2</sup> )
		Max. $\alpha_q$	Max. $\beta_q$		
			Left	Right	
1	40	-56	302	-375	7.5
2	40	-227	-234	-11	4.6
3	50	-125	220	-376	7.5
4	53	-130	-180	87	3.6
5	52	-223	-1	-260	5.2
6	62	44	30	74	1.5
7	117	-424	-106	-373	8.5
8	64	63	87	-161	3.2
9	98	-110	-52	-62	2.2
10	91	-120	25	-185	3.7
11	102	19	-5	33	0.5
12	91	-82	-14	-87	1.7
13	55	1	1.7	0	0.5
14	47	3	-7.5	12	0.5
15	69	-5	0.6	-6.3	0.5
16	57	15	-0.5	22	0.5
17	67	-6	-0.9	-6.4	0.5
18	53	12	0.8	14.1	0.5
19	80	-6	-2.2	-4.2	0.5
20	62	6	1.1	5.6	0.5

\* Assume  $F_T = F_C = 50$  ksi ultimate

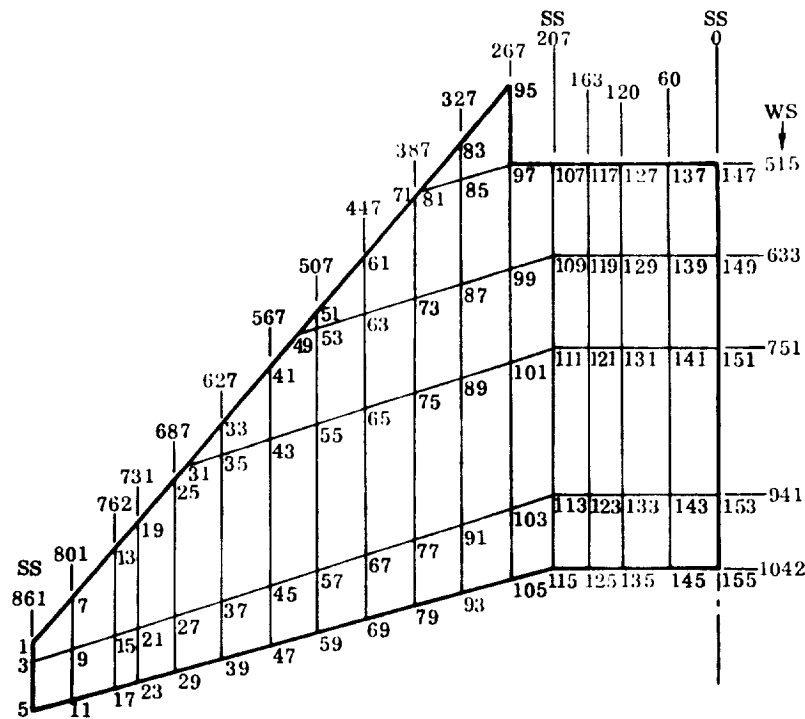
**Table 3-7. Aft Orbiter Attachment Frame, Web  
Shear Flows and Thicknesses**

Web	Area (in <sup>2</sup> )	Ultimate Shear Flow (kips/in)			t* (in. )
		Max. $\alpha_q$	Max. $\beta_q$		
			Left	Right	
1	722	1.1	4.3	5.7	0.29
2	1493	1.9	6.7	4.7	0.34
3	2441	1.8	2.1	0.11	0.11
4	2048	7.5	0.57	8.4	0.42
5	1471	3.5	1.00	2.9	0.50
6	2103	0.32	0.16	0.66	0.33
7	1631	0.21	0	0.26	0.13
8	2483	0.06	0	0.01	0.04
9	2854	0.01	0	0	0.04
10	3947	0	0	0.01	0.04

\* Assume  $F_S = 20$  ksi ultimate

**3.1.6 B-9U DELTA WING BOX.** Primary structural components such as spars and ribs are sized by maximum  $\alpha q$  loads during boost (Condition W1). This condition is critical because it combines high air loads and low relieving inertia loads. A finite element solution was programmed for the IBM 360, Model 65 computer, using a structural simulation model consisting of 156 nodes and 1073 constant stress elements, as shown in Figure 3-15. Skin corrugations were simulated in shear with quadrilateral plate elements. Orthotropic triangles with negligible shear stiffness were superimposed to simulate the unidirectional extensional stiffness of the skins.

Spar cap loads obtained from the computer solution are tabulated in Table 3-8 for Condition W1. These loads, as well as the spar sizing data of Tables 3-9 through 3-13, are based on preliminary analysis. However, it is believed that the data shown are sufficiently refined for the present purposes.



B-9U space shuttle wing box simulation node points for upper surface. Add "1" to the upper surface nodes to obtain the node numbering for the lower surface.

**Figure 3-15. B-9U Wing Structural Simulation Model**

Table 3-8. Spar Cap Loads, B-9U Wing

S. STA.	P <sub>LE</sub>	P <sub>1</sub>	P <sub>2</sub>	P <sub>3</sub>	P <sub>4</sub>	P <sub>5</sub>		ΣP <sub>1</sub> -P <sub>5</sub>
	(KIPs)	(KIPs)	(KIPs)	(KIPs)	(KIPs)	(KIPs)		(KIPs)
861						-		
						-		
801	-3.2					-10.		-10
	+2.0				-	-		-
762	+1.0				-50	-25		-75
	-1.0				+20	+10		+30
731	+1.0				-105	-47		-152
	0.0				+50	+18		+68
637	-29.0			-75	-200	-85		-360
	+7.0			-	+100	+40		+140
627	-16.0			-235	-300	-120		-655
	+43.0			+110	+150	+80		+340
567	-51.0			-395	-360	-145		-900
	+33.0			+310	+170	+135		+615
507	-12.0		-145	-525	-430	-175		-1275
	+37.0		+90	+500	+240	+180		+1010
447	-15.0		-280	-650	-520	-240		-1690
	+33.0		+245	+415	+625	+220		+1505
337	-12.0		-425	-825	-650	-330		-2230
	+30.0		+385	+700	+660	+245		+1990
327	-4.0	-100	-480	-1000	-810	-410		-2800
	+8.0	+110	+440	+795	+935	+275		+2555
267	-2.0	-220	-595	-1250	-1035	-505		-3605
	+2.0	+255	+530	+880	+945	+320		+2930
207		-295	-730	-1385	-1180	-460		-4050
		+375	+670	+1020	+1245	+445		+3755
163		-315	-735	-1375	-1190	-465		-4080
		+415	+715	+1105	+1265	+500		+4000
120		335	-755	-1400	-1215	-482		-4187
		+420	+540	+1150	+1290	+480		+3880
60		-365	-790	-1465	-1240	-480		-4340
		+440	+760	+1225	+1330	+515		+4270
0		-400	-830	-1555	-1360	-495		-4640
		+460	+765	+1305	+1360	+510		+4420

Table 3-9. Sizing Data — Spar No. 1 (WS 515), B-9U Wing

Based on Initial Loads

SS	$A_c$	$W_c$	$t_c$	$W_u$	$t_u$	$W_d$	$t_d$
327	3.56	4.08	0.218	2.09	0.074	4.14	0.036
267	5.19	4.54	0.285	2.64	0.099	4.39	0.055
207	6.56	4.86	0.338	3.88	0.18	4.62	0.075
163	6.84	3.90	0.44	3.25	0.107	3.77	0.034
120	7.06	3.93	0.45	3.50	0.11	3.68	0.023
60	7.30	4.81	0.38	2.96	0.081	4.23	0.016
0	7.50	4.84	0.387	2.48	0.060	4.14	0.016

$A_c$  = Spar cap area (in<sup>2</sup>)

$t_d$  = Spar diagonal gage (in. )

$W_c$  = Spar cap width (in. )

$t_w$  = Spar shear web gage

$t_c$  = Spar cap gage

$R$  = Spar shear web corrugation radius (in. )

$W_u$  = Spar upright width (in. )

$t_f$  = Spar shear web support cap gage (in. )

$t_u$  = Spar upright gage (in. )

SS = Spanwise station

$W_d$  = Spar diagonal width (in. )

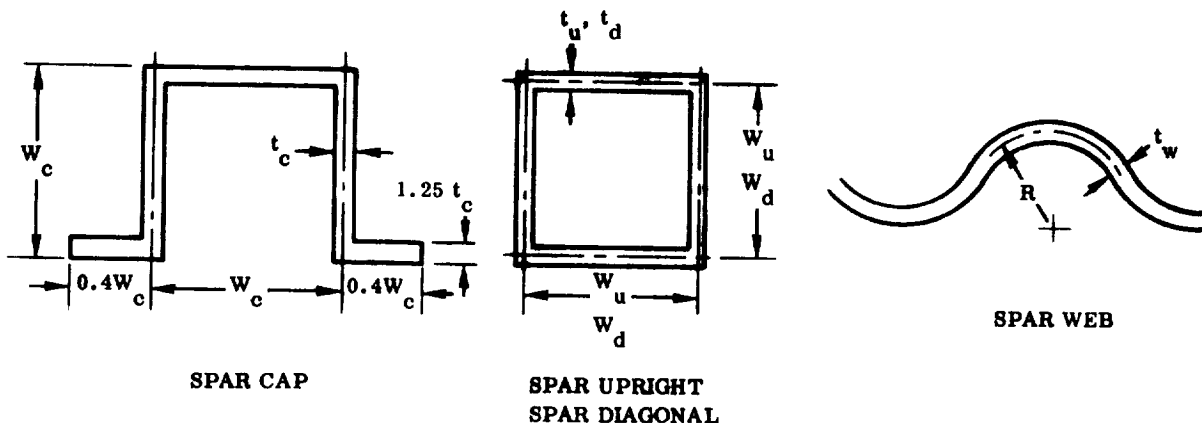


Table 3-10. Sizing Data — Spar No. 2 (WS 633), B-9U Wing

Based on Initial Loads							
SS	A <sub>c</sub>	W <sub>c</sub>	t <sub>c</sub>	W <sub>u</sub>	t <sub>u</sub>	W <sub>d</sub>	t <sub>d</sub>
507	2.35	3.80	0.153	2.50	0.093	4.04	0.041
447	4.05	4.37	0.232	2.61	0.103	4.29	0.067
387	5.92	4.82	0.307	3.15	0.129	4.54	0.095
327	7.45	5.10	0.365	3.5	0.144	4.73	0.109
267	8.78	5.32	0.411	3.81	0.158	4.90	0.122
207	9.44	5.42	0.437	5.05	0.210	5.03	0.129
163	9.62	4.32	0.555	4.13	0.147	4.20	0.056
120	9.75	4.33	0.562	4.40	0.145	4.07	0.038
60	9.86	5.26	0.467	3.64	0.107	4.52	0.019
0	9.87	5.26	0.467	3.00	0.075	4.37	0.016

Table 3-11. Sizing Data — Spar No. 3 (WS 751), B-9U Wing

Based on Initial Loads										
SS	A <sub>c</sub>	W <sub>c</sub>	t <sub>c</sub>	W <sub>u</sub>	t <sub>u</sub>	W <sub>d</sub>	t <sub>d</sub>	t <sub>w</sub>	R	t <sub>f</sub>
627	2.54	3.92	0.162	1.98	0.085	4.07	0.124			
567	3.64	4.42	0.206	2.82	0.125	4.24	0.118			
507	5.09	4.80	0.264	4.27	0.187	4.42	0.101	0.095	3.18	0.238
447	6.83							0.106	3.50	0.25
387	8.48							0.115	3.76	0.25
327	9.92							0.12	3.98	0.25
267	11.02	5.69	0.485	4.46	0.194	5.19	0.172	0.124	4.16	0.25
207	11.68	5.78	0.505	5.85	0.254	5.33	0.177			
163	11.80	4.59	0.643	4.77	0.177	4.51	0.077			
120	12.07	4.61	0.654	5.1	0.177	4.38	0.052	0.040	2.78	0.10
60	12.17							0.032	2.45	0.08
0	12.22							0.020	2.00	0.05

Table 3-12. Sizing Data — Spar No. 4 (WS 941), B-9U Wing

Based on Initial Loads										
SS	A <sub>c</sub>	W <sub>c</sub>	t <sub>c</sub>	W <sub>u</sub>	t <sub>u</sub>	W <sub>d</sub>	t <sub>d</sub>	t <sub>w</sub>	R	t <sub>f</sub>
861	0.12	1.05	0.029	1	0.025	1	0.025			
801	0.22	1.61	0.034	1.5	0.062	3.01	0.029			
762	1.41	3.01	0.117	1.9	0.049	3.12	0.064			
731	1.82	2.42	0.188	2.08	0.096	2.17	0.085			
687	2.30	3.54	0.163	2.21	0.113	3.32	0.133			
627	3.50	4.36	0.200	2.53	0.117	4.07	0.124			
567	3.66	4.41	0.205	2.81	0.124	4.24	0.116			
507	4.26	4.55	0.234	2.43	0.090	4.42	0.101	0.080	2.82	0.199
447	5.17							0.080	2.90	0.200
387	6.02							0.081	3.00	0.203
327	6.79							0.082	3.09	0.205
267	7.49	5.07	0.37	3.41	0.137	4.72	0.096	0.084	3.21	0.211
207	7.86	5.13	0.383	4.40	0.176	4.81	0.098			
163	8.27	4.13	0.50	3.72	0.127	4.0	0.045			
120	8.89	4.21	0.52	4.12	0.133	3.95	0.033	0.032	2.31	0.080
60	9.86							0.025	2.12	0.062
0	10.96							0.020	1.95	0.050

Table 3-13. Sizing Data — Spar No. 5 (WS 1042), B-9U Wing

Based on Initial Loads							
SS	A <sub>c</sub>	W <sub>c</sub>	t <sub>c</sub>	W <sub>u</sub>	t <sub>u</sub>	W <sub>d</sub>	t <sub>d</sub>
861	0.16	1.14	0.034	1	0.025	1	0.025
801	0.16	1.42	0.029	1	0.050	2.96	0.016
762	0.82	2.51	0.082	1.25	0.050	3.01	0.026
731	1.00	2.00	0.125	1.36	0.056	1.96	0.035
687	1.30	2.93	0.110	1.42	0.061	3.11	0.051
627	1.90	3.57	0.134	1.59	0.064	3.81	0.046
567	2.04	3.63	0.139	1.78	0.069	3.91	0.044
507	2.07	3.77	0.15	2.42	0.090	4.02	0.039
447	2.87	3.95	0.181	2.50	0.095	4.08	0.040
387	3.50	4.11	0.21	2.50	0.10	4.15	0.043
327	4.13	4.27	0.24	2.50	0.10	4.23	0.045
267	4.65	4.39	0.265	2.50	0.10	4.30	0.047
207	4.72	4.40	0.268	3.09	0.11	4.34	0.045
163	4.99	3.55	0.35	2.60	0.081	3.45	0.021
120	5.29	3.60	0.37	2.87	0.084	3.45	0.020
60	5.72	4.47	0.319	2.50	0.066	4.05	0.020
0	6.20	4.58	0.338	2.16	0.051	4.01	0.020

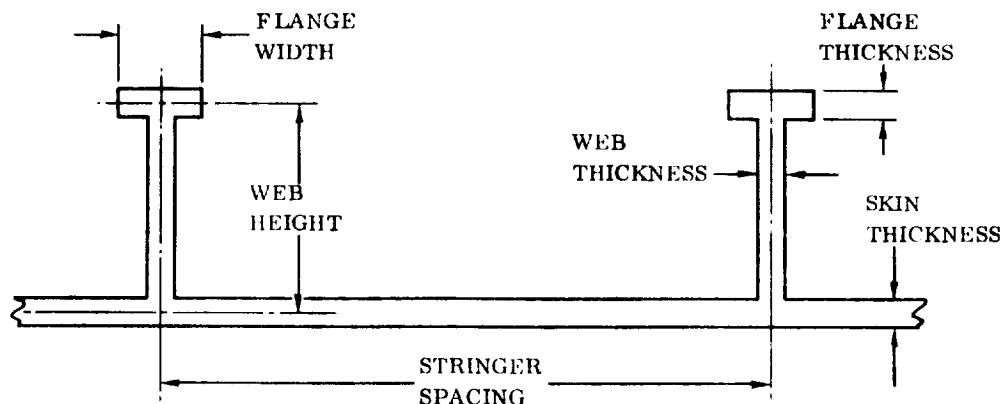
### 3.1.7 B-16B SWEPT WING BOX

**3.1.7.1 Three-Spar Configuration.** The three-spar, safe-life wing with the integrally stiffened skin was sized using a computer program written at Convair. The program is a multiweb, multirib, multistation synthesis of a wing box that sizes the wing box covers, webs, and ribs for the bending, shear, and crushing loads that occur at various stations along the span. The upper and lower covers are considered to be skin-stringer wide columns and are sized as such, using as a basis the structural efficiency equations developed by Emero & Spunt (Reference 5). The spar webs are also sized using structural efficiency equations developed in Reference 5. The ribs are sized for crushing loads due to overall wing bending and as such yield good results for corrugated web ribs acting merely as formers with no concentrated loads acting upon them. It is necessary for the user to specify minimum gages and maximum allowable stress levels for this synthesis procedure.

Using skin and stringer proportions input by the user, the program starts with a base rib spacing in the first bay outboard of the wing root and optimizes the stringer spacing and thickness for the specified load. Stringer height and spacing are then maintained constant along the span by means of variable rib spacing, which is accomplished by making the rib spacing inversely proportional to the cubic root of the edgewise load intensity. By making this stipulation, only the skin and stringer thicknesses have to be varied along the span to accommodate the variable load intensity.

In the computer printout (Tables 3-14 and 3-15), it can be seen that one of the pages contains a weight breakdown of the wing as calculated in the program. It should be noted here that none of the weights as calculated in the program, with the exception of the upper and lower structural box covers, was used in the calculation of the wing weights.

Figure 3-16 shows the idealized integrally stiffened skin elements.



NOTE: FLANGE THICKNESS IS ALWAYS ASSUMED TO BE EQUAL TO THE WEB THICKNESS

Figure 3-16. Idealized Integrally Stiffened Skin Elements  
(Three-Spar, Swept-Wing B-16B Booster)



### THREE SPAR SAFE LIFE WING BOX SIZING

#### DEFINITION OF INPUT PARAMETERS

ALPHAC	= Structural concept parameter*
ALPHAT	= Structural concept parameter*
B	= Wing structural span (inches)
BETAC	= Structural concept parameter*
BETAT	= Structural concept parameter*
BTAB (N)	= Table of wing bending moments utilized when the bending moments are to be specified at predetermined wing span stations (this option was not preferred here so BTAB (1) was defined as zero to implement alternative method of determining the wing bending moments)
CTAB (N)	= Table of wing chords utilized when the cords are to be specified at predetermined wing span stations (this option was not preferred here so CTAB (1) was defined as zero to implement alternative method of determining the wing chords)
CY (1)	= Wing root chord (inches)
DENS	= Material density for the wing covers (lb/in <sup>3</sup> )
DENSR	= Material density for the wing ribs (lb/in <sup>3</sup> )
DENSW	= Material density for the wing spar webs (lb/in <sup>3</sup> )
DPIVOT	= Distance between wing pivot points (parameter necessary weights portion of computer program which was relied upon for this study)
E	= Modulus of elasticity for the covers (lb/in <sup>2</sup> )
ER	= Modulus of elasticity for the ribs (lb/in <sup>2</sup> )
EW	= Modulus of elasticity for the webs (lb/in <sup>2</sup> )
EFFCC	= Efficiency of the compression cover*
EFFRC	= Efficiency of the ribs in compression
EFFTC	= Efficiency of the tension cover*
EFFWS	= Efficiency of the webs in shear

\*For further definition of terms, see Reference 5.

<b>FNOPCC</b>	= Non-optimum factor for the compression cover
<b>FNOPL</b>	= Non-optimum factor for the leading edge
<b>FNOPTC</b>	= Non-optimum factor for the tension cover
<b>FNOPT</b>	= Non-optimum factor for the trailing edge
<b>FNOPTR</b>	= Non-optimum factor for the ribs
<b>FNOPTW</b>	= Non-optimum factor for the webs
<b>FCALL</b>	= Maximum allowable compression stress (lb/in <sup>2</sup> )
<b>FSALLW</b>	= Maximum allowable working shear stress (lb/in <sup>2</sup> )
<b>FTALL</b>	= Maximum allowable tension stress (lb/in <sup>2</sup> )
<b>G</b>	= Shear modulus for the computation of GJ (lb/in <sup>2</sup> )
<b>GAMC</b>	= Structural concept parameter*
<b>GAMT</b>	= Structural concept parameter*
<b>HEFFR</b>	= Effective height ratio for covers at wing root
<b>HEFFT</b>	= Effective height ratio for covers at wing tip
<b>HPIVOT</b>	= Distance between pivot bearings (unimportant to sizing routine)
<b>IPRINT</b>	= Option to print secondary output (if IPRINT = 0, option is not exercised)
<b>ITAB</b>	= Number of data points in data tables (tables not
<b>KAREA</b>	= Wing box cross sectional area factor
<b>KB</b>	= Wing box chord/wing chord
<b>KCARRY</b>	= Constant for wing carry through weight equation (unimportant to sizing routine)
<b>KL</b>	= Lift on one wing panel, fraction of total lift
<b>KLE</b>	= Leading edge chord/wing chord (average value)
<b>KPIVOT</b>	= Constant in pivot weight equation (unimportant to sizing routine)
<b>KTE</b>	= Trailing edge chord/wing chord (average value)
<b>KTIP</b>	= Constant in wing tip weight equation (unimportant to sizing routine)

\*For further definition of terms, see Reference 5.

KWR	= Average web height at the wing root divided by the root chord
KWT	= Average web height at the wing tip divided by the tip chord
L(1)	= Rib spacing in the bay just outboard of station one
LANDAW	= Wing taper ratio
LVAR	= Non-operable option key parameter
NW	= Number of spar webs (number of spars)
NZL	= Ultimate load factor at critical negative load condition
NZU	= Ultimate load factor at critical positive load condition
QTAB (N)	= Table of wing shear loads utilized when the shears are to be specified at predetermined wing span stations (this option was not preferred here so QTAB (1) was defined as zero to implement alternative method of determining the wing shear loads)
RBFC	= Flange width/web height (for compression cover stringer)
RBFT	= Flange width/web height (for tension cover stringer)
RBWC	= Stringer web height/stringer spacing (for compression cover stringer)
RBWT	= Stringer web height/stringer spacing (for tension cover stringer)
RTWC	= Stringer thickness/skin thickness (for compression cover stringer)
RTWT	= Stringer thickness/skin thickness (for tension cover stringer)
TBLE	= Leading edge T bar (inches)
TBMG	= T bar for minimum gage covers (inches)
TBMGR	= T bar for minimum gage <sup>8</sup> ribs (inches)
TBMGW	= T bar for minimum gage webs (inches)
TBTE	= Trailing edge T bar (inches)
TOCR	= Airfoil thickness ratio at the wing root
TOCT	= Airfoil thickness ratio at the wing tip
UWAIL	= Unit weight of aileron (lb/ft <sup>2</sup> )
UWFLAP	= Unit weight of flap (lb/ft <sup>2</sup> )

WAREA = Wing reference area (ft<sup>2</sup>)  
 WTD = Vehicle design weight at critical design condition (lb)  
 YFLAPI = Station of inboard flap rib (inches)  
 (unimportant to sizing routine)  
 YFLAPO = Station of outboard flap rib (inches)  
 (unimportant to sizing routine)

#### DEFINITION OF SELECTED OUTPUT TERMS

BFLANG = Flange width of stringer  
 BSKIN = Stringer spacing  
 BSTR = Stringer height  
 TBC = T bar of compression cover  
 TBR = Rib thickness  
 TBT = T bar of tension cover  
 TBW = Web thickness  
 TSKIN = Skin thickness  
 TSTR = Stringer thickness

Table 3-14. Input, Wing Box Multiple Station Sizing Program, B-16B Three-Spar Wing

TITLE = 604 THREE SPAR -- SAFE LIFE WING		FINAL SIZING RUN
ALPHAC = 1.4960,	ALPHAT = 1.4960,	R = 775.90,
REFAC = 0.49240,	REFAT = 0.49240,	RTAR(1) = 0.00,
CTAR(1) = 0.00,	CV(1) = 56A.80,	DFNS = 0.160,
DFNSP = 0.160,	DFNSW = 0.160,	DPivot = 0.00,
E = 16.0E+6,	EP = 16.0E+6,	EW = 15.0E+6,
EFFCC = 0.760,	EFFRC = 0.500,	EFFTC = 0.760,
EFEX = 1.000,	FNOPCC = 1.000,	FNOPLF = 1.000,
FNOPIC = 1.000,	FNOPYC = 1.000,	FNOPYR = 1.000,
FNOPTH = 1.000,	FCALL = 112000.0,	FSALLW = 50000.0,
FTALL = 100500.0,	G = 6.2E+6,	GAMC = 0.33440,
GAMT = 0.33440,	HFFFR = 0.850,	HEFFT = 0.850,
HPivot = 1.00,	ICRINT = 0,	ITAB = 0,
KAPFA = 0.750,	KP = 0.640,	KCAPRY = 0.00,
KL = 0.450,	KL = 0.150,	KPIVOT = 0.00,
KT = 0.790,	KTIP = 0.001450,	KWR = 0.090,
KWT = 0.090,	L(1) = 52.00,	LAMBDAW = 0.240,
LVAP = 1,	NW = 7.0,	N7L = 0.50,
N7U = 1.40,	QATAR(1) = 0.00,	PARC = 0.500,
PACT = 0.500,	QRWC = 0.500,	R2WT = 0.500,
PTWC = 1.000,	RTWT = 1.000,	TALF = 0.040,
THWC = 0.050,	THWGR = 0.030,	TANGW = 0.040,
TOTE = 0.040,	TOCR = 0.100,	TOCT = 0.100,
UMAIL = 0.00,	UMFLAP = 0.00,	WAPFA = 2307.00,
WTD = 1567440.0,	YFLAPI = 100.0,	YFLAPO = 600.0

Table 3-15. Output, Final Sizing Run, B-16B Three-Spar Wing

STATION	CHORD	210 SPC	SHEAR	POS. D. MOM.	MY (+M)	SIGL	NEG. D. MOM.	MYNI (-M)	PER (N)	KH (N)	KW (N)
(IN)	(IN)	(IN)	(LBS)	(IN-LBS)	(LBS/IN)	(PSI)	(IN-LBS)	(LBS/IN)	(IN)	(IN)	(IN)
0.00	858.40	40.31	987764	311152599	12796	56173	111197357	4570	976.45	.0850	.0900
49.31	838.20	40.43	891973	265027141	11961	53704	94652550	4272	931.77	.0850	.0900
98.74	808.90	41.70	798547	222470933	11101	51095	79436047	3964	886.07	.0850	.0900
151.44	576.81	57.16	707688	143504363	10209	47323	65437273	3646	819.23	.0850	.0900
204.61	541.83	54.84	619405	114250066	9283	44354	52946457	3315	791.05	.0850	.0900
256.49	507.76	56.93	533771	916634367	8316	41447	41655131	2970	741.33	.0850	.0900
311.41	477.47	59.45	459777	78639682	7301	38142	31657029	2607	689.75	.0850	.0900
370.87	446.63	62.69	378497	64258679	6227	34755	22949524	2224	635.88	.0850	.0900
434.66	416.63	67.08	299098	43502089	5083	30357	15536460	1815	579.07	.0850	.0900
500.63	386.00	74.67	217944	26414941	3853	25236	9433908	1376	518.30	.0850	.0900
570.70	356.74	84.74	149263	13115969	2520	19013	4684275	900	451.64	.0850	.0900
643.94	326.74	111.05	71917	3921200	1094	10899	1400429	391	374.84	.0850	.0900
725.00	187.76	0.00	-2	0	0	0	0	0	273.40	.0850	.0900

COMPRESSION COVER OUTPUT DATA												
STATION	TRF	TRFC	TRC	AY1	AY0	OWTFC	SIGC	PHOROC	TSKIN	ASKIN	TSTR	RSTR
(IN)	(IN)	(IN)	(IN)	(IN2)	(IN2)	(LBS)	(PSI)	(IN)	(IN)	(IN)	(IN)	(IN)
0.00	.1273	.0000	.1273	59.27	55.80	449.13	93906	.719	.0718	2.18	.0718	1.09
49.31	.1190	.0000	.1190	54.37	51.70	427.97	89815	.719	.0702	2.18	.0702	1.09
98.74	.1105	.0000	.1105	49.47	47.76	406.14	85499	.719	.0685	2.18	.0685	1.09
151.44	.1021	.0000	.1021	44.55	43.74	383.77	80880	.719	.0668	2.18	.0668	1.09
204.61	.1024	.0000	.1024	44.55	43.74	383.77	76902	.719	.0668	2.18	.0668	1.09
256.49	.1027	.0000	.1027	44.55	43.74	383.77	72925	.719	.0662	2.18	.0662	1.09
311.41	.1029	.0000	.1029	44.55	43.74	383.77	68948	.719	.0655	2.18	.0655	1.09
370.87	.1031	.0000	.1031	44.55	43.74	383.77	64971	.719	.0648	2.18	.0648	1.09
434.66	.1032	.0000	.1032	44.55	43.74	383.77	60994	.719	.0641	2.18	.0641	1.09
500.63	.1033	.0000	.1033	44.55	43.74	383.77	57017	.719	.0634	2.18	.0634	1.09
570.70	.1034	.0000	.1034	44.55	43.74	383.77	53040	.719	.0627	2.18	.0627	1.09
643.94	.1035	.0000	.1035	44.55	43.74	383.77	49063	.719	.0620	2.18	.0620	1.09
725.00	.1036	.0000	.1036	44.55	43.74	383.77	45086	.719	.0613	2.18	.0613	1.09

TENSION COVER OUTPUT DATA												
STATION	TRF	TRFC	TRC	AY1	AY0	OWTFC	SIGC	PHOROC	TSKIN	ASKIN	TSTR	RSTR
(IN)	(IN)	(IN)	(IN)	(IN2)	(IN2)	(LBS)	(PSI)	(IN)	(IN)	(IN)	(IN)	(IN)
0.00	.1436	.1094	.1436	59.27	55.80	449.13	93906	.719	.0718	2.18	.0718	1.09
49.31	.1367	.1035	.1367	54.37	51.70	427.97	89815	.719	.0702	2.18	.0702	1.09
98.74	.1298	.0975	.1298	49.47	47.76	406.14	85499	.719	.0685	2.18	.0685	1.09
151.44	.1214	.0912	.1214	44.55	43.74	383.77	80880	.719	.0668	2.18	.0668	1.09
204.61	.1176	.0847	.1176	44.55	43.74	383.77	76902	.719	.0662	2.18	.0662	1.09
256.49	.1138	.0782	.1138	44.55	43.74	383.77	72925	.719	.0655	2.18	.0655	1.09
311.41	.1100	.0717	.1100	44.55	43.74	383.77	68948	.719	.0648	2.18	.0648	1.09
370.87	.1062	.0652	.1062	44.55	43.74	383.77	64971	.719	.0641	2.18	.0641	1.09
434.66	.1024	.0587	.1024	44.55	43.74	383.77	60994	.719	.0634	2.18	.0634	1.09
500.63	.1012	.0522	.1012	44.55	43.74	383.77	57017	.719	.0627	2.18	.0627	1.09
570.70	.1000	.0457	.1000	44.55	43.74	383.77	53040	.719	.0620	2.18	.0620	1.09
643.94	.0988	.0392	.0988	44.55	43.74	383.77	49063	.719	.0613	2.18	.0613	1.09
725.00	.0976	.0327	.0976	44.55	43.74	383.77	45086	.719	.0606	2.18	.0606	1.09

SPR OUTPUT DATA												
STATION	TRF	TRFC	TRC	AY1	AY0	OWTFC	SIGC	PHOROC	TSKIN	ASKIN	TSTR	RSTR
(IN)	(IN)	(IN)	(IN)	(IN2)	(IN2)	(LBS)	(PSI)	(IN)	(IN)	(IN)	(IN)	(IN)
0.00	.0333	.0333	.0333	179.17	.22	.22	.22	.22	.22	.22	.22	.22
49.31	.0314	.0314	.0314	179.17	.22	.22	.22	.22	.22	.22	.22	.22
98.74	.0295	.0295	.0295	179.17	.22	.22	.22	.22	.22	.22	.22	.22
151.44	.0276	.0276	.0276	179.17	.22	.22	.22	.22	.22	.22	.22	.22
204.61	.0257	.0257	.0257	179.17	.22	.22	.22	.22	.22	.22	.22	.22
256.49	.0238	.0238	.0238	179.17	.22	.22	.22	.22	.22	.22	.22	.22
311.41	.0219	.0219	.0219	179.17	.22	.22	.22	.22	.22	.22	.22	.22
370.87	.0200	.0200	.0200	179.17	.22	.22	.22	.22	.22	.22	.22	.22
434.66	.0181	.0181	.0181	179.17	.22	.22	.22	.22	.22	.22	.22	.22
500.63	.0162	.0162	.0162	179.17	.22	.22	.22	.22	.22	.22	.22	.22
570.70	.0143	.0143	.0143	179.17	.22	.22	.22	.22	.22	.22	.22	.22
643.94	.0124	.0124	.0124	179.17	.22	.22	.22	.22	.22	.22	.22	.22
725.00	.0105	.0105	.0105	179.17	.22	.22	.22	.22	.22	.22	.22	.22

Table 3-15. Output, Final Sizing Run, B-16B Three-Spar Wing, Contd

WING WEIGHT SUMMARY

WT. COVER = 17704 (1.691)	WT. L. EDGE = 1754 (1.051)
WT. T. COVER = 7591 (1.270)	WT. T. EDGE = 7781 (1.226)
WT. WIRS = 2421 (1.044)	WT. FLAPS = 0 (0.000)
WT. PING = 1696 (1.047)	WT. PIVOTS = 0 (0.000)
WT. TIES = 102 (1.003)	WT. AILERONS = 0 (0.000)
WT. WING BOX = 24795 (1.720)	

TOTAL WING WEIGHT = 34443 LB WING CG LOC. = 282.71 IN

TOTAL EXPOSED WING AREA = 2107 FT<sup>2</sup>

UNIT WING WEIGHT = 14.93 LB/FT<sup>2</sup>

WT OF CARRY THRU STRUTS = 0 LB

STATION	TOP	AIC	HC	BIT	WT	SOSOT	GJIN	FIIN
(IN)	(-)	(IN2)	(IN)	(IN2)	(IN)	(-)	(LR-IN2)	(LR-IN2)
0.00	.1000	97.90	21.26	58.27	15.58	10163	2497102078934	1445873116148
49.11	.1000	70.97	21.20	54.37	11.95	10138	2282717413638	1402227116615
98.24	.1000	44.78	17.10	50.41	32.20	9909	1909900724789	1341949946917
147.34	.1000	27.77	14.24	46.45	10.51	9678	1577612097179	1110472480281
204.61	.1000	10.04	17.23	42.47	28.83	9446	1277770114538	900139614477
259.49	.1000	64.17	10.14	38.37	27.01	9215	1001798723829	714408137159
316.41	.1000	27.17	15.87	34.14	25.14	8989	773040213641	55130740097
375.87	.1000	19.94	17.81	29.85	11.17	8778	571849210523	409110845315
438.55	.1000	42.51	17.61	25.40	21.10	8597	401544916786	281110994583
505.63	.1000	14.64	11.20	20.71	18.89	8491	268929848215	169873601638
579.20	.1000	26.24	9.84	15.68	16.46	8584	148802011115	108512685532
663.96	.1000	16.49	8.16	9.85	13.65	9478	61941394315	46990784546
775.90	.1000	5.99	7.96	5.99	7.96	10213	16791682661	12145716747

**3.1.7.2 Five-Spar Configuration.** The five-spar, fail-safe wing structural box was sized for the same critical shear and bending moment loads as the three-spar, safe-life wing structural box. The method of sizing was different, however. The five-spar box was sized by a hand analysis method, which, it was felt, yielded good results.

Since the sizing procedure was accomplished by hand, only two stations, one near the root and one near the tip, were completely sized. The areas and gages resulting from the sizing procedure at these two stations were then linearly extrapolated to root and tip values, and these were linearly interpolated to obtain values over the length of the span.

The basic sizing procedure consisted of first determining the moment and shear loads along the span and then distributing the moment to the spars. The moment was proportioned to the spars on the basis of percent of effective heights i. e. ,

$$M \text{ (per spar)} = M_{\text{total}} \times \frac{(h_{\text{eff}})_{\text{spar}}^2}{\sum (h_{\text{eff}})^2}$$

After determining the moment at each of the five spars, the upper and lower cap areas were determined using the following equations:

$$A_{\text{tension}} = \frac{M_{\text{spar}}}{h_{\text{eff}}} \times \frac{1}{\text{tension allowable}}$$

$$A_{\text{compression}} = \frac{M_{\text{spar}}}{h_{\text{eff}}} \times \frac{1}{\text{compression allowable}}$$

The allowables were chosen such that the tension allowable was equal to 75% of  $F_{tu}$  at both the inboard and outboard stations and the compression allowable was equal to  $F_{cy}$  at the inboard station and 50% of  $F_{cy}$  at the outboard station.

The spar webs were sized by assuming a generalized allowable working shear stress of 30,000 psi and then assuming that the webs reacted the shear load in such a manner that all the gages were equal at any particular station. Web gages were then interpolated between the two sized stations to obtain gages over the length of the span.

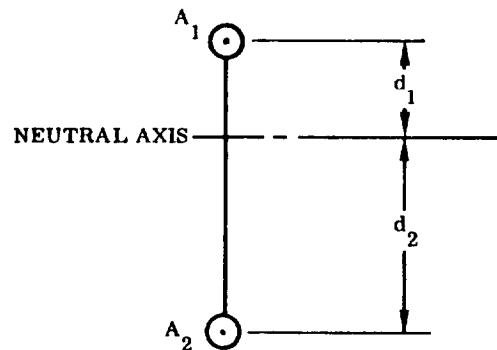
For the maximum stress in the upper caps use  $F_c = F_{cy} = 132$  ksi ultimate at Station 102.16,  $F_c = 0.5 F_{cy} = 66$  ksi ultimate at Station 604.07.

For the maximum stress in the lower caps use  $F_T = 0.75 F_{tu} = 100.5$  ksi ultimate.

The method of distributing moment to spars is to assume that the load is reacted in proportion to the stiffness.

$$I = A_1 d_1^2 + A_2 d_2^2$$

$$M_{(\text{per spar})} = M_{(\text{total})} \left( \frac{I_{(\text{per spar})}}{I_{(\text{total})}} \right)$$



At the wing root,

Chord = 668.80 inches

$\frac{t}{c} = 0.1 = \text{thickness ratio}$

$t = 66.88$  inches = maximum height or  $t$  at Spar 2

Express height of Spars 1, 3, 4, and 5 as a percent of Spar 2

<u>Spar No.</u>	<u>% of Spar 2 height</u>
1	0.9545
3	0.9785
4	0.9083
5	0.7662

Taper ratio = 0.28

Tip chord =  $668.8 \times 0.28 = 187.264$

<u>Spar No.</u>	<u>Total Height at Root (Station 0)</u>	<u>Total Height at Tip (Station 775.90)</u>
1	63.84	17.88
2	66.88	18.73
3	65.44	18.33
4	60.75	17.01
5	51.24	14.35

Total box heights (including skin) at Station 102.16:

<u>Spar No.</u>	<u>Height</u>	
1	57.79	} Interpolated values
2	60.54	
3	59.24	
4	54.99	
5	46.39	

At Station 604.07

<u>Spar No.</u>	<u>Height</u>	
1	28.06	} Interpolated values
2	29.39	
3	28.76	
4	26.70	
5	22.52	

Station 102.16:  $M = 220,497,489 \text{ in-lb}^*$ ;  $S = 794,191 \text{ pounds}^*$

Station 604.07:  $M = 9,782,892 \text{ in-lb}^*$ ;  $S = 122,951 \text{ pounds}^*$

Station 102.16

The effective section depth,  $h_{\text{eff}}$ , of a wing spar will be taken as the contour depth at that spar,  $h_{\text{total}}$ , less the sum of the distances from contour to each spar cap centroid. Assuming the thickness of each corrugated cover to be one inch and the distance from the inside of the cover to each spar cap centroid to be two inches,

\* Moment and shear values from computer run on three-spar wing.



$$h_{\text{eff}} = h_{\text{total}} - 2(1.0 + 2.0) = h_{\text{total}} - 6.0$$

At Station 102.16,

<u>Spar No.</u>	<u><math>h_{\text{eff}}</math></u>	<u><math>(h_{\text{eff}})^2</math></u>
1	51.79	2682.2041
2	54.54	2974.6116
3	53.24	2834.4976
4	48.99	2400.0201
5	40.39	1631.3521

$$\Sigma(h_{\text{eff}})^2 = 12,522.6855$$

<u>Spar No.</u>	<u><math>(h_{\text{eff}})^2 / \Sigma(h_{\text{eff}})^2</math></u> <u>% of Moment Reacted</u>
1	0.2142
2	0.2375
3	0.2263
4	0.1917
5	0.1303

Distributing total moment at spars on basis of percent of  $(h_{\text{eff}})^2$ ,

<u>Spar No.</u>	<u>%</u>	<u>Moment (in-lb)</u>
1	21.42	47,230,562
2	23.75	52,368,154
3	22.63	49,898,582
4	19.17	42,269,369
5	13.03	28,730,822

Total moment = 220,497,489 in-lb

$$A_{\text{tension}} = \frac{M}{(h_{\text{eff}})} \cdot \frac{1}{F_T}$$

$$A_{\text{compression}} = \frac{M}{(h_{\text{eff}})} \cdot \frac{1}{F_{\text{cy}}}$$

Spar 1:

$$A_T = \frac{47,230,562}{51.79} \cdot \frac{1}{100,500} = 9.074 \text{ in}^2$$

$$A_C = \frac{47,230,562}{51.79} \cdot \frac{1}{132,000} = 6.909 \text{ in}^2$$

Spar 2:

$$A_T = \frac{52,368,154}{54.54} \cdot \frac{1}{100,500} = 9.554 \text{ in}^2$$

$$A_C = \frac{52,368,154}{54.54} \cdot \frac{1}{132,000} = 7.274 \text{ in}^2$$

Spar 3:

$$A_T = \frac{49,898,582}{53.24} \cdot \frac{1}{100,500} = 9.326 \text{ in}^2$$

$$A_C = \frac{49,898,582}{53.24} \cdot \frac{1}{132,000} = 7.100 \text{ in}^2$$

Spar 4:

$$A_T = \frac{42,269,369}{48.99} \cdot \frac{1}{100,500} = 8.585 \text{ in}^2$$

$$A_C = \frac{42,269,369}{48.99} \cdot \frac{1}{132,000} = 6.536 \text{ in}^2$$

Spar 5:

$$A_T = \frac{28,730,822}{40.39} \cdot \frac{1}{100,500} = 7.078 \text{ in}^2$$

$$A_C = \frac{28,730,822}{40.39} \cdot \frac{1}{132,000} = 5.389 \text{ in}^2$$

Station 604.07

The spar effective depth,  $h_{eff}$ , will be computed in the same manner as at Station 102.16, except that the distance from the inside of the cover to the spar cap centroid will be taken as 1-1/2 inches. Therefore

$$h_{eff} = h_{total} - 2(1.0 + 1.5) = h_{total} - 5.0$$

At Station 604.07

<u>Spar No.</u>	<u><math>h_{eff}</math></u>	<u><math>(h_{eff})^2</math></u>
1	23.06	531.7636
2	24.39	594.8721
3	23.76	564.5376
4	21.70	470.8900
5	17.52	306.9504

$$\Sigma (h_{eff})^2 = 2469.0137$$

<u>Spar No.</u>	<u><math>(h_{eff})^2 / \Sigma (h_{eff})^2</math></u>
1	0.2154
2	0.2409
3	0.2287
4	0.1907
5	0.1243

Distributing total moment to spars on basis of percent of  $(h_{eff})^2$ ,

<u>Spar No.</u>	<u>%</u>	<u>Moment (in-lb)</u>
1	21.54	2,107,235
2	24.09	2,356,699
3	22.87	2,237,347
4	19.07	1,865,598
5	12.43	1,216,013

Total moment = 9,782,892

$$A_{tension} = \frac{M}{(h_{eff})} \cdot \frac{1}{F_T}$$

$$A_{\text{compression}} = \frac{M}{(h_{\text{eff}})} \cdot \frac{1}{F_T}$$

Spar 1:

$$A_T = \frac{2,107,235}{23.06} \cdot \frac{1}{100,500} = 0.9093 \text{ in}^2$$

$$A_C = \frac{2,107,235}{23.06} \cdot \frac{1}{66,000} = 1.385 \text{ in}^2$$

Spar 2:

$$A_T = \frac{2,356,699}{24.39} \cdot \frac{1}{100,500} = 0.9614 \text{ in}^2$$

$$A_C = \frac{2,356,699}{24.39} \cdot \frac{1}{66,000} = 1.464 \text{ in}^2$$

Spar 3:

$$A_T = \frac{2,237,347}{23.76} \cdot \frac{1}{100,500} = 0.937 \text{ in}^2$$

$$A_C = \frac{2,237,347}{23.76} \cdot \frac{1}{66,000} = 1.427 \text{ in}^2$$

Spar 4:

$$A_T = \frac{1,865,598}{21.70} \cdot \frac{1}{100,500} = 0.8554 \text{ in}^2$$

$$A_C = \frac{1,865,598}{21.70} \cdot \frac{1}{66,000} = 1.303 \text{ in}^2$$

Spar 5:

$$A_T = \frac{1,216,013}{17.52} \cdot \frac{1}{100,500} = 0.691 \text{ in}^2$$

$$A_C = \frac{1,216,013}{17.52} \cdot \frac{1}{66,000} = 1.052 \text{ in}^2$$

Spar No.	Upper Cap		Lower Cap	
	Cross-Sectional Area (in <sup>2</sup> )		Cross-Sectional Area (in <sup>2</sup> )	
	Station 102.16	Station 604.07	Station 102.16	Station 604.07
1	6.909	0.692	6.806	0.682
2	7.274	0.732	7.166	0.721
	7.100	0.713	6.994	0.703
	6.536	0.651	6.439	0.642
5	5.389	0.526	5.308	0.518

Let the minimum cap cross sectional area be 0.20 in<sup>2</sup>.

For spar webs, assume a generalized allowable working shear stress of 30,000 psi, and assume spar heights =  $h_{eff}$

At Station 102.16

<u>Spar No.</u>	<u><math>h_{eff}</math></u>	$\Sigma h_{eff} = 248.95$
1	51.79	
2	54.54	
3	53.24	
4	48.99	
5	40.39	

Shear at Station 102.16 = 794,191 pounds

Spar web thickness = 0.110 inch

At Station 604.07

<u>Spar No.</u>	<u><math>h_{eff}</math></u>	$\Sigma h_{eff} = 110.43$
1	23.06	
2	24.39	
3	23.76	
4	21.70	
5	17.52	

Shear at Station 604.07 = 122,951 pounds

Spar web thickness = 0.037 inch

Let minimum spar web thickness = 0.030 inch

### 3.2 FATIGUE ANALYSIS

On the following pages, a cumulative fatigue damage analysis is made for each of the baseline components to determine the safe-life number of missions to initiation of fatigue cracks, assuming initially flawless material. The service load spectra shown in Figures 2-31 through 2-39 are used.

Material information used in classical fatigue analysis is usually in the form of S-N curves, constant life diagrams, or some such presentation of stress versus cycles-to-failure of test specimens. Although this information is in terms of complete failure rather than fatigue crack initiation, S-N curves are being used as indicating crack initiation for purposes of this study. This interpretation is justified by the fact that the standard test specimen configuration used to generate S-N data has a small cross-section compared to space shuttle booster structural members. The specimen is therefore more sensitive to a given amount of fatigue damage, and progression of fatigue damage to complete failure is rapid. The fatigue curves of Figures 3-17, 3-18, and 3-19 provide S-N data for 2219-T87 aluminum alloy at room temperature, and Ti-6Al-4V annealed titanium alloy at room temperature and 650°F, respectively.

The service loading spectra and fatigue damage analyses for the selected components are shown in Tables 3-16 through 3-25.

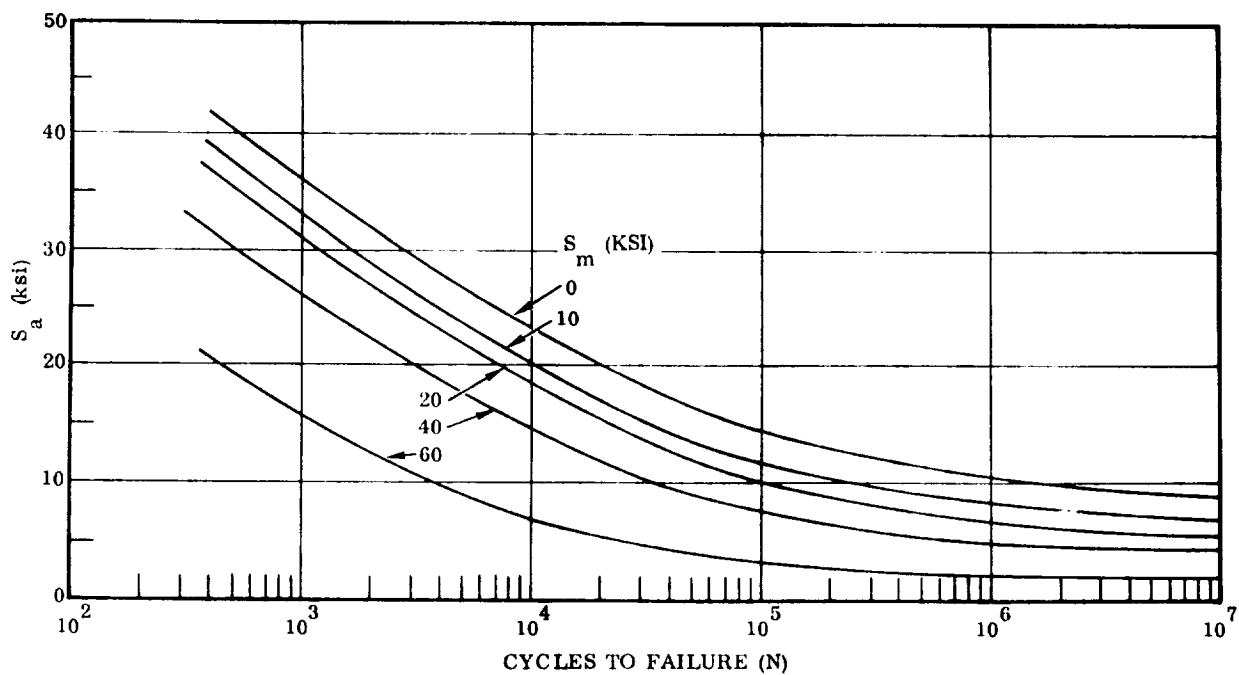


Figure 3-17. Estimated Fatigue Curves for 2219-T87 Aluminum Alloy at Room Temperature with  $K_t = 3.0$

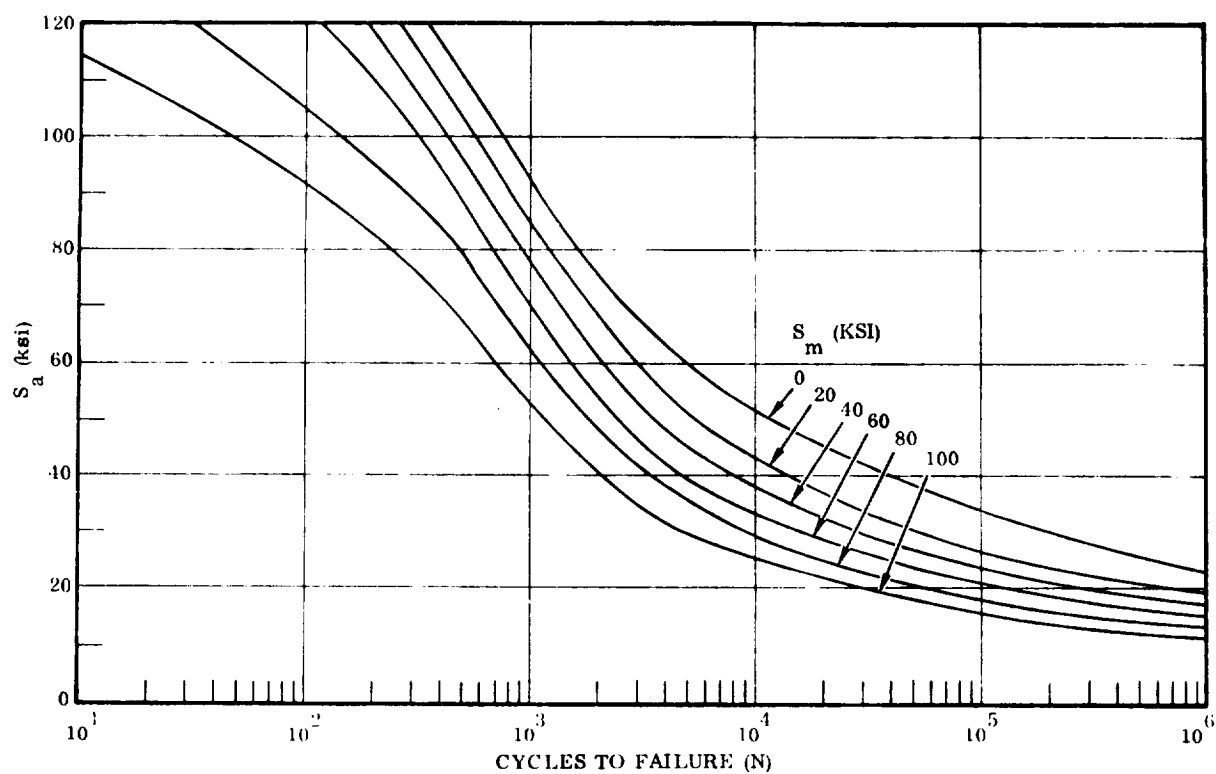


Figure 3-18. Fatigue Curves for Annealed Ti-6Al-4V at Room Temperature with  $K_t = 3.0$

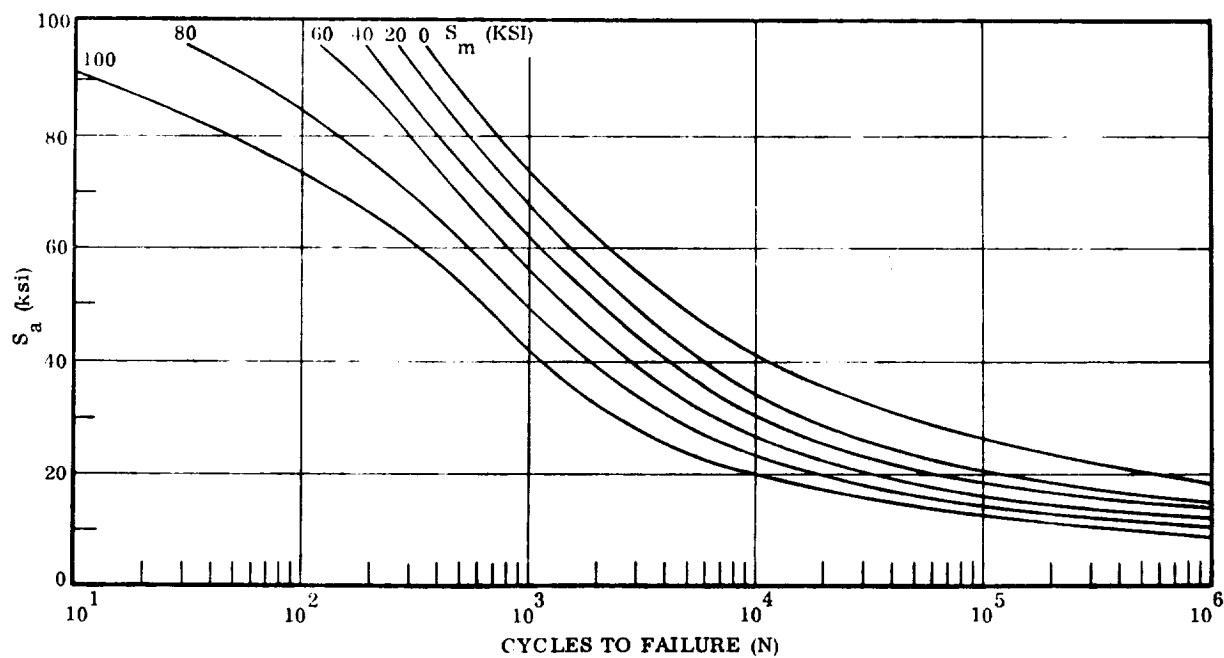


Figure 3-19. Fatigue Curves for Annealed Ti-6Al-4V at 650°F with  $K_t = 3.0$

Table 3-21. B-9U Wing Spar Caps Fatigue Damage Analysis

Mission Phase	T Deg. F	$\sigma_{limit}$ ksi	$\frac{\sigma_{mean}}{\sigma_{limit}}$ (1)	$\frac{\sigma_{alt}}{\sigma_{limit}}$ (1)	$\sigma_{mean}$ ksi	$\sigma_{alt}$ ksi	$K_t$	N	n	$\frac{n}{N}$
cent	RT	91.2	0	.015	0	1.37	3.0	$\infty$	90,000	0
			0	.025	0	2.28			9,000	0
			0	.035	0	3.19			900	0
			0	.045	0	4.10			90	0
			0	.055	0	5.01			9	0
			.15	.035	13.7	3.2			90,000	0
			.15	.05	13.7	4.6			9,000	0
			.15	.065	13.7	5.9			900	0
			.15	.08	13.7	7.3			90	0
			.15	.09	13.7	8.2			9	0
			0	.055	0	5.0			90,000	0
			0	.09	0	8.2			9,000	0
			0	.125	0	11.4			900	0
			0	.155	0	14.1			90	0
			0	.185	0	16.9			9	0
			.40	.08	36.5	7.3			90,000	0
			.40	.145	36.5	13.2			9,000	0
			.40	.21	36.5	19.2		500,000	900	.0018
			.40	.27	36.5	24.6		90,000	90	.0010
			.40	.33	36.5	30.1		30,000	9	.0003
			.10	.105	9.1	9.6		$\infty$	90,000	0
			.10	.185	9.1	16.9		$\infty$	9,000	0
			.10	.30	9.1	27.4		170,000	900	.0052
			.10	.45	9.1	41.0		20,000	90	.0045
			.10	.605	9.1	55.1		5,500	9	.0016
			.15	.135	13.7	12.3		$\infty$	90,000	0
			.15	.20	13.7	18.2		$4 \times 10^6$	9,000	.0022
			.15	.37	13.7	33.7		50,000	900	.0180
			.15	.61	13.7	55.6		5,000	90	.0180
cent	RT	91.2	.15	.80	13.7	72.9	3.0	1,900	9	.0047

3  
5  
2



Table 3-21. B-9U Wing Spar Caps Fatigue Damage Analysis, Contd.

Mission Phase	T Deg. F	$\sigma_{limit}$ ksi	$\frac{\sigma_{mean}}{\sigma_{limit}}$ (1)	$\frac{\sigma_{alt}}{\sigma_{limit}}$ (1)	$\sigma_{mean}$ ksi	$\sigma_{alt}$ ksi	$K_t$	N	n	$\frac{n}{N}$
Entry	650°	91.2	.075 .135 .185	.075 .135 .185	0.8 12.3 16.9	6.8 12.3 16.9	3.0	$\infty$ $\infty$ $1 \times 10^4$	90,000 9,000 500	0 0 .0005
Entry	650°		.23 .37 .47	.23 .37 .47	21.0 33.7 42.9	21.0 33.7 42.9		$8 \times 10^3$ $8 \times 10^3$ $3 \times 10^3$	250 150 100	.0031 .0188 .0333
Cruise/Landing (2)	RT	91.2	.50 .20	.50 .20	45.6 18.2	45.6 6.4		$2.5 \times 10^3$ $\infty$	1 180,000	.0004 0
Cruise/Landing (2)			.17 .27 .36	.17 .27 .36	15.5 24.6 32.8	15.5 24.6 32.8		$\infty$ $1.5 \times 10^5$ $3.0 \times 10^4$	18,000 1,800 180	0 .0120 .0060
Taxi (2)			.43	.43	39.2	39.2		$1.5 \times 10^4$	18	.0012
Taxi (2)	RT	91.2	-.021	-.021	-1.9	3.6		$\infty$	180,000	0
GAG (2)	RT	91.2			5.5 7.3 8.7	5.5 7.3 8.7			18,000 1,800 180	0 0 0
					10.0	10.0		$\infty$	18	0
			-	-	23.2	35.1	3.0	$2 \times 10^4$	200	.0100

Note: Safe Life for fatigue crack initiation in B-16B 3- and 5-spar swept wings assumed same as for B-9U delta wing, since spectrum, material, stress levels and environment are the same.

Table 3-21. B-9U Wing Spar Caps Fatigue Damage Analysis, Contd.

Mission Phase	$n/N$
Ascent	.0573
Entry	.0561
Cruise/Landing	.0192
Taxi	0
GAG	.0100

$$\Sigma (n/N) = .1426$$

$$\text{Fatigue life} = \frac{100}{4(.1426)} = 175 \text{ missions, based on a scatter factor of 4.}$$

## NOTES:

- (1) Spectrum information from Table 3-20.
- (2) To provide for one ferry flight per mission, the number of cycles for the cruise/landing and taxi phases has been increased by a factor of 2.0, and two GAG cycles per mission added, using a minimum stress from the taxi phase and a maximum stress from the cruise/landing phase.
- (3) Material: Ti-6Al -4V annealed.

Table 3-21. B-9U Wing Spar Caps Fatigue Damage Analysis, Contd.

Mission Phase	T Deg. F	$\sigma_{limit}$ ksi	$\frac{\sigma_{mean}}{\sigma_{limit}}$ (1)	$\frac{\sigma_{alt}}{\sigma_{limit}}$ (1)	$\sigma_{mean}$ ksi	$\sigma_{alt}$ ksi	$K_t$	N	n	$\frac{n}{N}$
Entry	650°	91.2	.075 .135 .185 .23 .37 .47 .50	.075 .135 .185 .23 .37 .47 .50	5.8 12.3 15.9 21.0 33.7 42.9 45.6	6.8 12.3 16.9 21.0 33.7 42.9 45.6	3.0	$\infty$ $\infty$ $1 \times 10^6$ $8 \times 10^3$ $8 \times 10^3$ $3 \times 10^3$ $2.5 \times 10^3$	90,000 9,000 500 250 150 100 1	0 0 .0005 .0031 .0188 .0333 .0004
Entry	650°	91.2								
Cruise/Landing (2)	RT	91.2	.20	.07 .17 .27 .36 .43	18.2	6.4 15.5 24.6 32.8 39.2		$\infty$ $\infty$ $1.5 \times 10^5$ $3.0 \times 10^4$ $1.5 \times 10^4$	180,000 18,000 1,800 180 18	0 0 .0120 .0060 .0012
Taxi (2)			-.021	.040 .060 .080 .095 .110	-1.9	3.6 5.5 7.3 8.7 10.0		$\infty$	180,000 18,000 1,800 180 18	0 0 0 0 0
Taxi (2)	RT	91.2	-.021		-1.9			$\infty$		0
GAG (2)	RT	91.2	-	-	23.2	35.1	3.0	$2 \times 10^4$	200	.0100

Note: Safe Life for fatigue crack initiation in B-16B 3- and 5-spar swept wings assumed same as for B-9U delta wing, since spectrum, material, stress levels and environment are the same.

Table 3-21. B-9U Wing Spar Caps Fatigue Damage Analysis, Contd.

Mission Phase	n/N
Ascent	.0573
Entry	.0561
Cruise/Landing	.0192
Taxi	0
GAG	.0100

$$\Sigma (n/N) = .1426$$

$$\text{Fatigue life} = \frac{100}{4(.1426)} = 175 \text{ missions, based on a scatter factor of 4.}$$

## NOTES:

- (1) Spectrum information from Table 3-20.
- (2) To provide for one ferry flight per mission, the number of cycles for the cruise/landing and taxi phases has been increased by a factor of 2.0, and two GAG cycles per mission added, using a minimum stress from the taxi phase and a maximum stress from the cruise/landing phase.
- (3) Material: Ti-6AL -4V annealed.

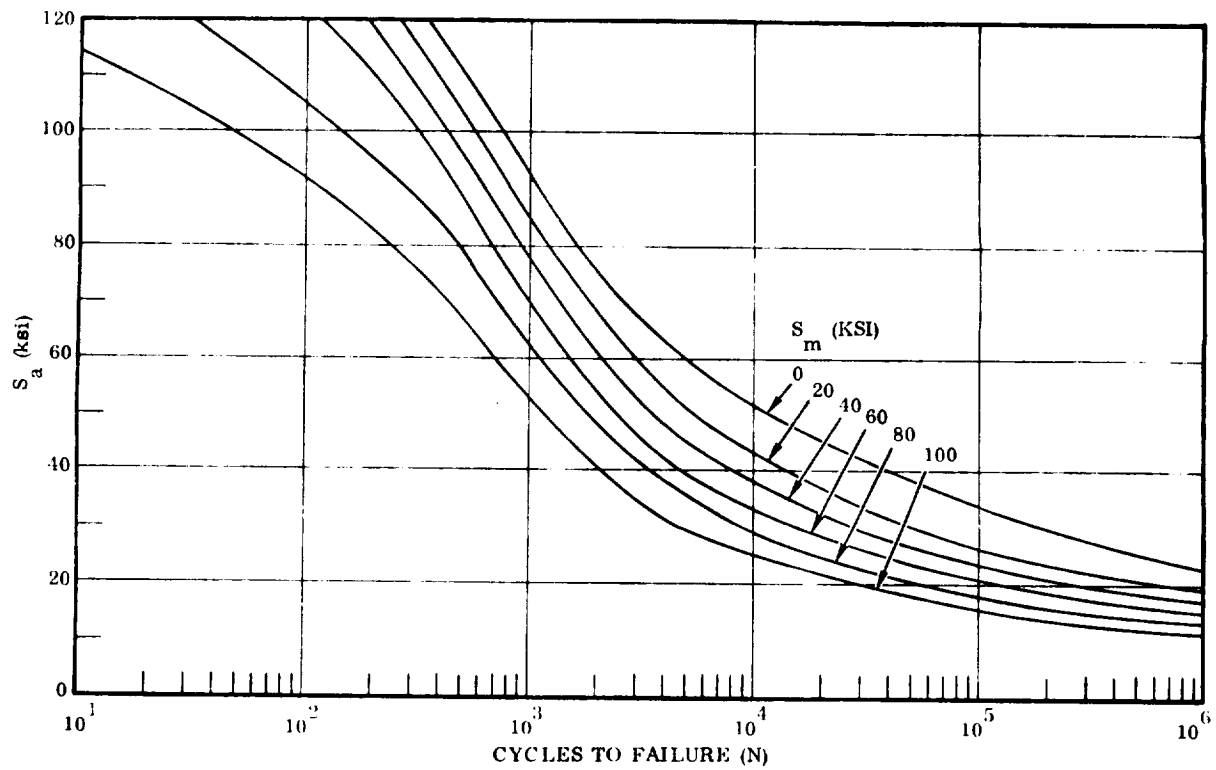


Figure 3-18. Fatigue Curves for Annealed Ti-6Al-4V at Room Temperature with  $K_t = 3.0$

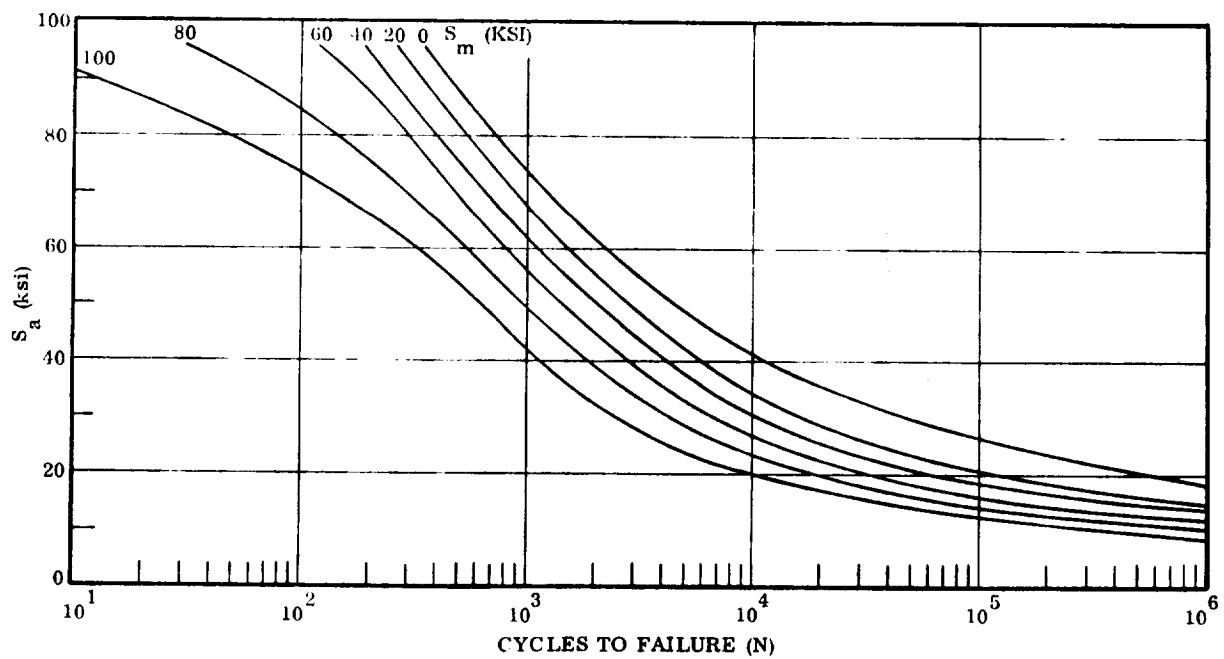


Figure 3-19. Fatigue Curves for Annealed Ti-6Al-4V at 650°F with  $K_t = 3.0$

Table 3-16. LO<sub>2</sub> Tank Pressure Spectrum and Damage Analysis at Upper Dome Equator

PHASE	CONDITION	P <sub>max</sub> (psig)	P <sub>min</sub> (psig)	σ <sub>max</sub> (1) (ksi)	σ <sub>min</sub> (1) (ksi)	n (2) (cycles)	σ <sub>mean</sub> (ksi)	σ <sub>alt</sub> (ksi)	K <sub>t</sub>	N (cycles)	n/N
Manufacture	Proof Test	21.6	0	47.3	0	1	23.6	23.6	3.0	3 × 10 <sup>3</sup>	.0003
Pre-Flight	Fueling	5.0	0	11.0	0	100	5.5	5.5	↑	∞	0
Flight	Nominal Ullage Pressure	18.0 (3)	0	39.6	0	95	19.8	19.8	↑	7 × 10 <sup>3</sup>	.0136
Flight	Max. Relief Valve Pressure	20.0 (3)	0	44.0	0	5	22.0	22.0	↑	4 × 10 <sup>3</sup>	.0012

$$\Sigma \left( \frac{n}{N} \right) = .0151 \text{ for one design lifetime of 100 missions}$$

$$\text{Fatigue life} = \frac{100}{4} \left( 1 + \frac{1 - .0151}{.0151 - .0003} \right) = 1687 \text{ missions, based on a scatter factor of 4.}$$

NOTES:

$$(1) \sigma - \frac{Pr}{t} = \frac{P(198)}{.090}$$

(2) n is cycles for one design lifetime of 100 missions

(3) Proof test pressure from Figure 2-22, flight pressures from Figure 2-39. A pressure regulator malfunction is assumed to occur in 5% of the flights.

(4) Material: 2219-T87 aluminum alloy

Table 3-17. LH<sub>2</sub> Tank Pressure Spectrum and Damage Analysis at Upper Dome Equator

PHASE	CONDITION	P <sub>max</sub> (psig)	P <sub>min</sub> (psig)	σ <sub>max</sub> (1) (ksi)	σ <sub>min</sub> (1) (ksi)	n (2) (cycles)	σ <sub>mean</sub> (ksi)	σ <sub>alt</sub> (ksi)	K <sub>t</sub>	N (cycles)	n/N
Manufacture	Proof Test	29.8	0	50.9	0	1	25.4	25.4	3.0	2 x 10 <sup>3</sup>	.0005
Pre-Flight	Fueling	5.0	0	8.5	0	100	4.2	4.2	↑	∞	0
Flight	Nominal Ullage Pressure	22.0 (3)	0 (3)	37.5	0	95	18.8	18.8	↑	10 <sup>4</sup>	.0095
Flight	Max. Relief Valve Pressure	23.5 (3)	0 (3)	40.1	0	5	20.0	20.0	↓	7 x 10 <sup>3</sup>	.0007

$$\Sigma \left( \frac{n}{N} \right) = .0107 \text{ for one lifetime of 100 missions}$$

$$\text{Fatigue life} = \frac{100}{4} \left( 1 + \frac{1 - .0107}{.0107 - .0005} \right) = 2450 \text{ missions, based on a scatter factor of 4.}$$

NOTES:

$$(1) \sigma = \frac{P_r}{t} = \frac{P(198)}{.116}$$

(3) Proof test pressure from Figure 2-22, flight pressures from Figure 2-38.

(2) n is cycles for one design lifetime of 100 missions.

(4) Material: 2219-T87 aluminum alloy.

Table 3-18. Fuselage Load Spectrum - Station 2600 Bottom Centerline

(1) Mission Phase	(2) $M_{\text{mean}}$ (in. lb. $\times 10^6$ ) (1)	(3) $M_{\text{alt}}$ (in. lb. $\times 10^6$ ) (1)	(4) Limit Tank Press. (psi)	(5) $\frac{Pr}{2}$ (lb/in) (2)	(6) $n_e$ (cycles) (2)	(7) $n$ (cycles)	(8) $M_{\text{mean}}$ (in. lb. $\times 10^6$ )	(9) $M_{\text{alt}}$ (in. lb. $\times 10^6$ )	(10) $\frac{-M_{\text{mean}}}{\pi r^2}$ (lb/in)	(11) $N_{x_{\text{mean}}}$ $= (5) + (10)$ (lb/in)	(12) $N_{x_{\text{alt}}}$ $= (9) / \pi r^2$ (lb/in)
Max. Thrust	-340	340	22.30	2210	100	100	-340	340	2761	4971	2761
Ascent	-348	28	22.30	2210	100,000	90,000	-348	44.5	2826	5036	361
		61			10,000	9,000		77			625
		93			1,000	900		109			885
		125			100	90		141.5			1149
		158			10	9		174			1413
Ascent	-348	190	22.30	2210	1		-348		2826	5036	
Entry	-9.5	9.5	18.70	1851	100,000	90,000	-12.75	12.75	104	1955	104
	-16	16			10,000	9,000	-19.75	19.75	160	2011	160
Entry	-23.5	23.5	18.70	1851	1,000	900	-42.75	42.75	347	2198	347

NOTES: (1) Bending moments from Figure 2-33

(2)  $r = 198$  inches;  $\pi r^2 = 123,163$



Table 3-18. Fuselage Load Spectrum - Station 2600 Bottom Centerline, Contd.

①	②	③	④	⑤	⑥	⑦	⑧	⑨	⑩	⑪	⑫
Mission Phase	$M_{\text{mean}}$ (in. lb. $\times 10^6$ ) (1)	$M_{\text{alt}}$ (in. lb. $\times 10^6$ ) (1)	Limit Tank Press. (psi)	$\frac{P r}{2}$ (lb/in) (2)	$n_c$ (cycles)	$n$	$M_{\text{mean}}$ (in. lb. $\times 10^6$ )	$M_{\text{alt}}$ (in. lb. $\times 10^6$ )	$\frac{-M_{\text{mean}}}{\pi r^2}$ (lb/in)	$\frac{-M_{\text{alt}}}{\pi r^2}$ (lb/in)	$N_{x_{\text{alt}}}$ # $= \frac{9}{\pi} r^2$ (lb/in)
Entry	-62	-26	18.70	1851	100	99	-62	62	503	2354	503
Entry	-62	-62	18.70	1851	1						
Cruise/Lndg	-10	15	10.20	1010	100,000	90,000	-10	19.5	81	1091	158
		24			10,000	9,000		28.5			231
		33			1,000	900		37.5			304
		42			100	90		46.5			378
		51			10	9		55.5			451
Cruise/Lndg	-10	60	10.20	1010	1		-10			1091	

NOTES: (1) Bending moments from Figure 2-33

(2)  $r = 198$  inches;  $\pi r^2 = 123,163$

Table 3-18. Fuselage Load Spectrum - Station 2600 Bottom Centerline, Contd.

(1) Mission Phase	(2) $M_{\text{mean}}$ (in. lb. $\times 10^6$ ) (1)	(3) $M_{\text{alt}}$ (in. lb. $\times 10^6$ ) (1)	(4) Limit Tank Press. (psi)	(5) $\frac{P r}{2}$ (lb/in) (2)	(6) $n_e$ (cycles)	(7) $n$ (cycles)	(8) $M_{\text{mean}}$ (in. lb. $\times 10^6$ )	(9) $M_{\text{alt}}$ (in. lb. $\times 10^6$ )	(10) $\frac{-M_{\text{mean}}}{\pi r}$ (lb/in)	(11) $N_{\text{mean}} \times$ $= \frac{5}{\pi r} + \frac{10}{\pi r}$ (lb/in)	(12) $N_{\text{alt}} \times$ $= \frac{9}{\pi r}$ (lb/in)
Taxi	-10	12	4.00	396	100,000	90,000	-10	14.5	81	477	118
		17			10,000	9,000		20.0			162
		23			1,000	900		25.5			207
		28			100	90		31.0			252
		34			10	9		37.0			300
Taxi	-10	40	4.00	396	1		-10		81	477	

NOTES: (1) Bending moments from Figure 2-33

(2)  $r = 198$  inches;  $\pi r^2 = 123,163$

Table 3-19. Fuselage Damage Analysis - Station 2600 Bottom Centerline

Mission Phase	T Deg. F (i)	$\bar{N}_x$ mean lb/in	$\bar{N}_x$ alt lb/in	$\bar{t}$ in	$\sigma_{mean}$ ksi	$\sigma_{alt}$ ksi	$K_t$	n cycles	N cycles	n/N
Maximum Thrust	RT	4971	2761	.188	26.4	14.7	3.0	100	$2.6 \times 10^4$	.0038
Ascent		5036	361		26.8	1.9		90,000	$\infty$	0
			625			3.3		9,000	$\infty$	0
Ascent			885			4.7		900	$\infty$	0
			1149			6.1		90	$7 \times 10^5$	.0001
			1413		26.8	7.5		9	$2.5 \times 10^5$	0
Entry		1955	104		10.4	0.5		90,000	$\infty$	0
		2011	160		10.7	0.9		9,000	$\infty$	0
Entry		2198	347		11.7	1.8		900	$\infty$	0
		2354	503		12.5	2.7		99	$\infty$	0
Cruise/Landing (1)		1091	158		5.8	0.8		180,000	$\infty$	0
			231			1.2		18,000	$\infty$	0
			304			1.6		1,800	$\infty$	0
Cruise/Landing (1)		1091	378		5.8	2.0		180	$\infty$	0
			451			2.4		18	$\infty$	0
Taxi (1)		477	118		2.5	0.6		180,000	$\infty$	0
			162			0.9		18,000	$\infty$	0
			207			1.1		1,800	$\infty$	0
Taxi (1)		477	252		2.5	1.3		180	$\infty$	0
			300	.188		1.6	3.0	18	$\infty$	0
GAG (1)	RT				4.1	4.1	3.0	200	$\infty$	0

Table 3-19. Fuselage Damage Analysis - Station 2600 Bottom Centerline, **Contd.**

Mission Phase	$n/N$
Maximum Thrust	.0038
Ascent	.0001
Entry	0
Cruise/Landing	0
Taxi	0
GAG	0
$\Sigma (n/N)$	.0039

Fatigue life =  $\frac{100}{S.F. (\Sigma n/N)} = \frac{100}{4 (.0039)} = 6410$  missions, based on a scatter factor of 4

NOTES:

- (1) To provide for one ferry flight per mission, the number of cycles for cruise/landing and taxi phases has been increased by a factor of 2.0, and two GAG cycles per mission added, using a minimum stress from the taxi phase and a maximum stress from the cruise/landing phase.
- (2) Material: 2219-T87 plate

Table 3-20. B-9U Wing Load Spectrum

Flight Phase	Wing Root M <sub>Design</sub> (in. kips limit)	$\bar{M}$ (%)	MA (%)	$\bar{M}_A$ (%)	$\bar{M}$ (in. kips) ( $\times 10^{-3}$ )	$\bar{M}_A$ (in. kips) ( $\times 10^{-3}$ )	n <sub>e</sub> (Cycles)	n (Cycles)	$\sigma_{Mean}/$ $\sigma_{Limit}$ (1)	$\sigma_{Alt}/$ $\sigma_{Limit}$ (2)
Ascent	189.1 $\times 10^3$ ( $\sigma_{Limit} = 91.2$ ksi)	0	1.0	1.5	0	2.84	100,000	90,000	0	.015
		0	2.0	2.5	0	4.73	10,000	9,000	0	.025
		0	3.0	3.5	0	6.62	1,000	900	0	.035
		0	4.0	4.5	0	8.51	100	90	0	.045
		0	5.0	5.5	0	10.40	10	9	0	.055
		0	6.0				1			
		15	3.0	3.5	28.37	6.62	100,000	90,000	.15	.035
		15	4.0	5.0	28.37	9.46	10,000	9,000	.15	.05
		15	6.0	6.5	28.37	12.29	1,000	900	.15	.065
		15	7.0	7.8	28.37	14.75	100	90	.15	.08
		15	8.5	9.3	28.37	17.59	10	9	.15	.09
		15	10.0				1			
		0	4.0	5.5	0	10.40	100,000	90,000	0	.055
		0	7.0	9.0	0	17.02	10,000	9,000	0	.09
		0	11.0	12.5	0	23.64	1,000	900	0	.125
		0	14.0	15.5	0	29.31	100	90	0	.155
		0	17.0	18.5	0	34.98	10	9	0	.185
		0	20.0							
		40	5.0	8.3	75.64	15.70	100,000	90,000	.40	.08
		0	11.5	14.5	75.64	27.42	10,000	9,000	.40	.145
		40	17.5	20.8	75.64	39.33	1,000	900	.40	.21
		40	24.0	27.0	75.64	51.06	100	90	.40	.27
Ascent	189.1 $\times 10^3$	40	24.0	27.0	75.64	51.06	100	90	.40	.27

Table 3-20. B-9U Wing Load Spectrum, Contd

Flight Phase	Wing Root M <sub>Design</sub> (in. kips limit)	$\bar{M}$ (%)	MA (%)	$\bar{MA}$ (%)	$\bar{M}$ (in. kips) ( $\times 10^{-3}$ )	$\bar{MA}$ (in. kips) ( $\times 10^{-3}$ )	$n_e$ (Cycles)	n (Cycles)	$\sigma_{Mean}/\sigma_{Limit}$ (1)	$\sigma_{Alt}/\sigma_{Limit}$ (2)
Ascent (Cont)	$189.1 \times 10^3$	40	30.0				10			
				33.3	75.64	62.97		9	.40	.33
		40	36.5				1			
		10	6.5				100,000			
				10.5	18.91	19.86		90,000	.10	.105
		10	14.5				10,000			
				18.5	18.91	34.98		9,000	.10	.185
		10	22.5				1,000			
				30.0	18.91	56.73		900	.10	.30
		10	37.5				100			
				45.3	18.91	85.66		90	.10	.45
		10	53.0				10			
				60.5	18.91	114.41		9	.10	.605
		10	68.0				1			
		15	8.5				100,000			
				13.5	28.36	25.53		90,000	.15	.135
		15	18.5				10,000			
				20.0	28.36	37.82		9,000	.15	.20
		15	21.5				1,000			
				36.8	28.36	69.58		900	.15	.37
		15	52.0				100			
				61.0	28.36	115.35		90	.15	.61
		15	70.0				10			
				79.5	28.36	150.33		9	.15	.80
Ascent	$189.1 \times 10^3$	15	89.0				1			
Entry	$189.1 \times 10^3$	5.0	5.0				100,000			
				7.5	9.5	14.2		90,000	.075	.075
		10.0	10.0				10,000			
				13.5	18.9	25.5		9,000	.135	.135
		17.0	17.0				1,000			
				18.5	32.1	35.0		500	.185	.185
		20.0	20.0				500			
				23.0	37.8	43.5		250	.23	.23
		26.0	26.0				250			
				36.8	49.2	69.6		150	.37	.37
		47.5	47.5				100			
				47.5	89.8	89.8		100	.47	.47
		47.5	47.5				0			
Entry	$189.1 \times 10^3$	50.0	50.0	50.0	94.6	94.6		1	.50	.50

Table 3-20. B-9U Wing Load Spectrum, Contd

Flight Phase	Wing Root M <sub>Design</sub> (in. kips limit)	$\bar{M}$ (%)	MA (%)	$\bar{M}_A$ (%)	$\bar{M}$ (in. kips) ( $\times 10^{-3}$ )	$\bar{M}_A$ (in. kips) ( $\times 10^{-3}$ )	n <sub>e</sub> (Cycles)	n (Cycles)	$\frac{\sigma_{Mean}}{\sigma_{Limit}}$ (1)	$\frac{\sigma_{Alt}}{\sigma_{Limit}}$ (2)
Cruise/ Landing	$189.1 \times 10^3$	20	2	7	37.8	13.2	100,000	90,000	.20	.07
		20	12	17	37.8	32.1	10,000	9,000	.20	.17
		20	22	27	37.8	51.1	1,000	900	.20	.27
		20	32	36	37.8	68.1	100	90	.20	.36
		20	40	43	37.8	81.3	10	9	.20	.43
		20	46				1			
Cruise/ Landing	$189.1 \times 10^3$	20	46				1			
Taxi	$189.1 \times 10^3$	-2.1	3.0	4.0	-4.0	7.6	100,000	90,000	-.021	.040
		-2.1	5.0	6.0	-4.0	11.3	10,000	9,000	-.021	.060
		-2.1	7.0	8.0	-4.0	15.1	1,000	900	-.021	.080
		-2.1	9.0	9.5	-4.0	18.0	100	90	-.021	.095
		-2.1	10.0	11.0	-4.0	20.8	10	9	-.021	.110
		-2.1	12.0				1			
Taxi	$189.1 \times 10^3$	-2.1	12.0				1			

$$(1) \frac{\sigma_{mean}}{\sigma_{limit}} = \frac{\bar{M}}{189.1}$$

$$(2) \frac{\sigma_{alt}}{\sigma_{limit}} = \frac{M_a}{189.1}$$

Table 3-21. B-9U Wing Spar Caps Fatigue Damage Analysis

Mission Phase	T Deg. F	$\sigma_{\text{limit}}$ ksi	$\frac{\sigma_{\text{mean}}}{\sigma_{\text{limit}}}$ (1)	$\frac{\sigma_{\text{alt}}}{\sigma_{\text{limit}}}$ (1)	$\sigma_{\text{mean}}$ ksi	$\sigma_{\text{alt}}$ ksi	$K_t$	N	n	$\frac{n}{N}$
Ascent	RT	91.2	0	.015	0	1.37	3.0	$\infty$	90,000	0
									9,000	0
			0	.025	0	2.28			9,900	0
									90	0
			0	.035	0	3.19			90	0
									9	0
			0	.045	0	4.10			90	0
									9	0
			0	.055	0	5.01			90,000	0
									9,000	0
			.15	.035	13.7	3.2			90,000	0
									9,000	0
			.15	.05	13.7	4.6			90,000	0
									9,000	0
			.15	.065	13.7	5.9			90	0
									9	0
			.15	.08	13.7	7.3			90	0
									9	0
			.15	.09	13.7	8.2			90,000	0
									9,000	0
			0	.055	0	5.0			90,000	0
									9,000	0
			0	.09	0	8.2			90,000	0
									9,000	0
			0	.125	0	11.4			90	0
									9	0
			0	.155	0	14.1			90	0
									9	0
			0	.185	0	16.9			90,000	0
									9,000	0
			.40	.08	36.5	7.3			90,000	0
									9,000	0
			.40	.145	36.5	13.2			500,000	.0018
									90,000	.0010
			.40	.21	36.5	19.2			30,000	.0003
									9	0
			.40	.27	36.5	24.6			90,000	0
									9	0
			.40	.33	36.5	30.1			90,000	0
									9,000	0
			.10	.105	9.1	9.6			170,000	.0052
									20,000	.0045
			.10	.185	9.1	16.9			5,500	.0016
									9	0
			.10	.30	9.1	27.4			90,000	0
									9,000	0
			.10	.45	9.1	41.0			4 x 10 <sup>6</sup>	.0022
									50,000	.0180
			.10	.605	9.1	55.1			5,000	.0180
									9	.0047
			.15	.135	13.7	12.3			90,000	0
									9,000	.0022
			.15	.20	13.7	18.2			50,000	.0180
									90	.0180
			.15	.37	13.7	33.7			90	.0180
									9	.0047
			.15	.61	13.7	55.6			90,000	0
									9,000	.0022
			.15	.80	13.7	72.9			50,000	.0180
									1,900	.0047
Ascent	RT	91.2	.15	.80	13.7	72.9	3.0			



Table 3-22. B-9U Vertical Tail Load Spectrum

Phase	Segment	Tail Root M <sub>Design</sub> (in. kips limit)	M %	MA %	M <sub>A</sub> %	M (in. kips x 10 <sup>3</sup> )	M <sub>A</sub> (in. kips x 10 <sup>3</sup> )	M <sub>max</sub> (in. kips x 10 <sup>3</sup> )	n <sub>e</sub> (Cycles)	n (Cycles)	σ <sub>Max</sub> / σ <sub>Limit</sub>	σ <sub>Mean</sub> / σ <sub>Limit</sub>	σ <sub>Alt.</sub> / σ <sub>Limit</sub>
Ascent	(1)	78.8 x 10 <sup>3</sup> (σ <sub>Limit</sub> = 34)	0	2.1					100,000				
					4.0	0	3.2	43.2		90,000	0.041	0	0.041
			0	6.0					10,000				
					7.6	0	6.0	6.0		9,000	.076	0	.076
			0	9.2					1,000				
					11.1	0	8.7	8.7		900	.110	0	.110
			0	13					100				
					14.5	0	11.4	11.4		90	.145	0	.145
Ascent	(2)	78.8 x 10 <sup>3</sup> (σ <sub>Limit</sub> = 34)	0	16					10				
					18.0	0	14.2	14.2		9	.180	0	.180
			0	20					1				
					6.0	0	8.9	48.9	100,000	90,000	.113	0	.113
			0	16.6					10,000				
					21.9	0	17.3	17.3		9,000	.220	0	.220
			0	27.2					1,000				
					32.6	0	25.7	25.7		900	.326	0	.326
Ascent	(3)	78.8 x 10 <sup>3</sup> (σ <sub>Limit</sub> = 34)	0	38.0					100				
					43.5	0	34.3	34.3		90	.435	0	.435
			0	49.0					10				
					54.5	0	42.9	42.9		9	.545	0	.545
			0	60.0					1				
					10.0	0	15.0	15.0	100,000	90,000	.190	0	.190
			0	28.0					10,000				
					37.0	0	29.2	29.2		9,000	.371	0	.371
Ascent	(4)	78.8 x 10 <sup>3</sup> (σ <sub>Limit</sub> = 34ksi)	0	46.0					1,000				
					55.0	0	43.3	43.3		900	.550	0	.550
			0	64.0					100				
					73.0	0	57.5	57.5		90	.730	0	.730
			0	82.0					10				
					91.0	0	71.7	71.7		9	.910	0	.910
			0	100.0					1				
					7.5	0	10.9	10.9	100,000	90,000	.138	0	.138
Ascent	(4)	78.8 x 10 <sup>3</sup> (σ <sub>Limit</sub> = 34ksi)	0	20.0					10,000				
					26.2	0	20.6	20.6		9,000	.262	0	.262
			0	32.5					1,000				
					38.8	0	30.6	30.6		900	.388	0	.388
			0	45.0					100				
					51.2	0	40.3	40.3		90	.511	0	.511
			0	57.5					10				
					63.8	0	50.3	50.3		9	.639	0	.639
Ascent	(4)	78.8 x 10 <sup>3</sup> (σ <sub>Limit</sub> = 34ksi)	0	70.0					1				

Table 3-22. B-9U Vertical Tail Load Spectrum, Contd

Phase	Segment	Tail Root M <sub>Design</sub> (in. kips limit)	M % (1)	MA % (1)	M <sub>A</sub> %	M (in. kips x 10 <sup>3</sup> )	M <sub>A</sub> (in. kips x 10 <sup>3</sup> )	M <sub>max</sub> (in. kips x 10 <sup>3</sup> )	n <sub>e</sub> (Cycles)	n (Cycles)	σ <sub>Max</sub> / σ <sub>I limit</sub>	σ <sub>Mean</sub> / σ <sub>I limit</sub>	σ <sub>Alt.</sub> / σ <sub>I limit</sub>
Ascent	(5)	78.8 x 10 <sup>3</sup> (σ limit = 34ksi)	0	4.3					100,000				
				9.1	0	7.2	±7.2			90,000	.091	0	.091
			0	13.9					10,000				
				18.4	0	14.5	14.5			9,000	.184	0	.184
			0	23.0					1,000				
				27.5	0	21.7	21.7			900	.276	0	.276
			0	32.0					100				
				36.5	0	28.8	28.8			90	.366	0	.366
			0	41.0					10				
				45.5	0	35.9	35.9			9	.455	0	.455
Ascent	(6)	78.8 x 10 <sup>3</sup> (σ limit = 34ksi)	0	50.0					1				
				3.0					100,000				
				5.9	0	4.6	±4.6			90,000	.058	0	.058
			0	8.8					10,000				
				11.4	0	9.0	9.0			9,000	.114	0	.114
			0	14.0					1,000				
				16.6	0	13.1	13.1			900	.166	0	.166
			0	19.3					100				
				21.6	0	17.0	17.0			90	.216	0	.216
			0	24.0					10				
Ascent	(7)	78.8 x 10 <sup>3</sup> (σ limit = 34ksi)		27.0	0	21.3	21.3			9	.270	0	.270
			0	30.0					1				
				1.5					100,000				
				2.2	0	1.7	1.7			90,000	.026	0	.026
			0	3.0					10,000				
				3.6	0	2.8	2.8			9,000	.036	0	.036
			0	4.2					1,000				
				5.0	0	3.9	3.9			900	.050	0	.050
			0	5.9					100				
				6.5	0	5.1	5.1			90	.065	0	.065
Cruise/ Lndg.		78.8 x 10 <sup>3</sup> (σ limit = 34ksi)	0	7.1					10				
				7.9	0	6.2	6.2			9	.079	0	.079
			0	8.7					1				
				18.0					100,000				
				21.0	0	16.5	16.5			90,000	.210	0	.210
			0	23.9					10,000				
				26.7	0	21.0	21.0			9,000	.267	0	.267
			0	29.5					1,000				
				32.2	0	25.4	25.4			900	.322	0	.322
			0	35.0					100				
				38.0	0	30.0	30.0			90	.380	0	.380
			0	41.0					10				
				43.7	0	34.4	34.4			9	.436	0	.436
			0	46.4					1				

(1) Mean and alternating bending moments in percent of design bending moment, from Figure 2-32.

Table 3-23. B-9U Vertical Tail Fatigue Damage Analysis

Mission Phase	T (°F)	$\sigma_{limit}$ ksi	$\frac{\sigma_{mean}}{\sigma_{limit}}$	$\frac{\sigma_{alt}}{\sigma_{limit}}$	$\sigma_{mean}$ (ksi)	$\sigma_{alt}$ (ksi)	$K_t$	N	n	n/N
Ascent - Segment (1)	RT	34	0	0.041	0	1.4	3.0	$\infty$	90,000	0
		34	0	.076	0	2.6	3.0		9,000	0
		34	0	.110	0	3.7	3.0		900	0
		34	0	.145	0	4.9	3.0		90	0
		34	0	.180	0	6.1	3.0		9	0
Ascent - Segment (2)	RT	34	0	.113	0	3.8	3.0		90,000	0
		34	0	.220	0	7.5	3.0		9,000	0
		34	0	.326	0	11.1	3.0		900	0
		34	0	.435	0	14.8	3.0	$\infty$	90	0
		34	0	.545	0	18.5	3.0	$10^7$	9	0
Ascent - Segment (3)	RT	34	0	.190	0	6.5	3.0	$\infty$	90,000	0
		34	0	.371	0	12.6	3.0	$\infty$	9,000	0
		34	0	.550	0	18.7	3.0	$10^7$	900	0
		34	0	.730	0	24.8	3.0	$6 \times 10^5$	90	0
		34	0	.910	0	30.9	3.0	$1.8 \times 10^5$	9	0
Ascent - Segment (4)	RT	34	0	.138	0	4.7	3.0	$\infty$	90,000	0
		34	0	.262	0	8.9	3.0	$\infty$	9,000	0
		34	0	.388	0	13.2	3.0	$\infty$	900	0
		34	0	.511	0	17.4	3.0	$\infty$	90	0
		34	0	.639	0	21.7	3.0	$1.9 \times 10^6$	9	0
Ascent - Segment (5)	RT	34	0	.091	0	3.1	3.0	$\infty$	90,000	0
		34	0	.184	0	6.3	3.0		9,000	0
		34	0	.276	0	9.4	3.0		900	0
		34	0	.366	0	12.4	3.0		90	0
		34	0	.455	0	15.5	3.0		9	0
Ascent - Segment (6)	RT	34	0	.058	0	2.0	3.0		90,000	0
		34	0	.114	0	3.9	3.0		9,000	0
		34	0	.166	0	5.6	3.0		900	0
		34	0	.216	0	7.3	3.0		90	0
		34	0	.270	0	9.2	3.0		9	0
Ascent - Segment (7)	RT	34	0	.026	0	0.9	3.0		90,000	0
		34	0	.036	0	1.2	3.0		9,000	0
		34	0	.050	0	1.7	3.0		900	0
		34	0	.065	0	2.2	3.0		90	0
		34	0	.079	0	2.7	3.0	$\infty$	9	0

Table 3-23. B-9U Vertical Tail Fatigue Damage Analysis, Contd

Mission Phase	T (°F)	$\sigma_{\text{limit}}$ (ksi)	$\frac{\sigma_{\text{mean}}}{\sigma_{\text{limit}}}$	$\frac{\sigma_{\text{alt}}}{\sigma_{\text{limit}}}$	$\sigma_{\text{mean}}$ (ksi)	$\sigma_{\text{alt}}$ (ksi)	$K_t$	N	n	n/N
Cruise/Landg	RT	34	0	.210	0	7.1	3.0	$\infty$	180,000	0
		34	0	.267	0	9.1	3.0		18,000	0
		34	0	.322	0	11.0	3.0		1,800	0
		34	0	.380	0	12.9	3.0		180	0
		34	0	.436	0	14.8	3.0		18	0

Summary

Mission Phase	n/N
Ascent	.0002
Cruise/Landg	0
$\Sigma(n/N)$	.0002

$$\text{Fatigue life} = \frac{100}{S.F. \times \Sigma(n/N)} = \frac{100}{4(.0002)} = \frac{125,000 \text{ missions,}}{\text{based on a scatter factor of 4.}}$$

NOTES:

- 1) To provide for one ferry flight per mission, the number of cycles for the cruise/landing phase has been increased to a factor of 2.
- 2) Material is Ti-6Al - 4V annealed.

Table 3-24. Thrust Beam Cap Fatigue Damage Analysis

Design $\sigma_{\text{limit}}$ (ksi)	T (°F)	$K_t$	$T_m$ (%)	$T_a$ (%) (1)	$\sigma_m$ (ksi)	$\sigma_a$ (ksi)	$n_e$ (cycles) (2)	n (cycles) (2)	$\bar{\sigma}_a$ (ksi)	N (cycles)	n/N
92.9	RT	3.0	96.8	0.05	89.9	0.05	15,000			$\infty$	
								5,000	0.195		0
92.9	RT	3.0	96.8	0.37	89.9	0.34	10,000				
								9,000	0.67		0
92.9	RT	3.0	96.8	1.08	89.9	1.00	1,000				
								900	1.33		0
92.9	RT	3.0	96.8	1.79	89.9	1.66	100				
								90	1.99		0
92.9	RT	3.0	96.8	2.50	89.9	2.32	10				
								9	2.64		0
92.9	RT	3.0	96.8	3.20	89.9	2.97	1			$\infty$	
92.9	RT	3.0	50	50	46.4	46.4	1	1	47.4	$3.5 \times 10^3$	0.000285

$$\Sigma\left(\frac{n}{N}\right)_{\text{thrust beam cap}} = 0.000285 \text{ for one flight}$$

$$\text{Fatigue life} = \frac{1}{4(0.000285)} = 887 \text{ missions}$$

NOTES:

- (1) Alternating thrust in percent of design thrust from Figure 2-37.
- (2) Cycles for one flight.
- (3) Material: Ti-6Al-4V annealed.

Table 3-25. Aft Orbiter Support Frame Load Spectrum and Damage Analysis

$A_z$ mean % (2)	$A_z$ alt % (2)	$A_y$ mean % (2)	$A_y$ alt % (2)	$A_z$ mean (kips) (3)	$A_z$ alt (kips) (3)	$A_y$ mean (kips) (4)	$A_y$ alt (kips) (4)	$\sigma_z$ mean (ksi) (5)	$\sigma_z$ alt (ksi) (5)	$\bar{y}$ mean (ksi) (6)	$\sigma_y$ alt (ksi) (6)	Total mean (ksi)	Total alt (ksi)	$\bar{\sigma}_{alt}$ (ksi)	$n_e$ (Cycles)	$n$ (Cycles)	N (Cycles) (7)	n/N
Max. $\alpha$ -q Condition																		
63	2.9	0	0	488	22	0	0	12	1	0	0	12	1	1	100,000	1,000	∞	0
63	5.1	0	0	488	40	0	0	12	1	0	0	12	1	2	10,000	9,000	∞	0
63	7.9	0	0	488	61	0	0	12	2	0	0	12	2	2	1,000	900	∞	0
63	17	0	0	488	132	0	0	12	3	0	0	12	3	4	100	90	∞	0
63	27	0	0	488	209	0	0	12	5	0	0	12	5	6	10	9	∞	0
63	37	0	0	488	287	0	0	12	7	0	0	12	7	1	1	1	∞	0
Max. $\beta$ -q Condition																		
63	0	0	7.5	488	0	0	26	12	0	0	2	12	2	3	100,000	90,000	∞	0
63	0	0	17	488	0	0	58	12	0	0	4	12	4	5	10,000	9,000	∞	0
63	0	0	27	488	0	0	92	12	0	0	6	12	6	9	1,000	900	$4 \times 10^5$	.0022
63	0	0	51	488	0	0	174	12	0	0	12	12	12	14	100	90	$4 \times 10^4$	.0022
63	0	0	75	488	0	0	256	12	0	0	17	12	17	20	10	9	$9 \times 10^3$	.0010
63	0	0	100	488	0	0	341	12	0	0	23	12	23	1	1	1	∞	∞

Table 3-25. Aft Orbiter Support Frame Load Spectrum and Damage Analysis, Contd

NOTES:

1. Critical member judged to be Bar 6 (see Figure 3-14 and Table 3-6).
2. Percent of design values, from spectrum curves, Figure 2-35.
3. Design value of  $A_z = 775$  kips.  $A_z = \frac{\% A_z}{100}$  (775)
4. Design value of  $A_y = 341$  kips.  $A_y = \frac{\% A_y}{100}$  (341)
5. For a unit  $A_z$  of 1000 kips,  $\sigma_z$  in Bar 6 = 24.7 ksi
6. For a unit  $A_y$  of 1000 kips,  $\sigma_y$  in Bar 6 = 68.0 ksi
7. Cycles to failure (crack initiation) from Figure 3-17.
8. Material is 2219-T81 aluminum alloy.
9. Operating temperature for above conditions assumed to be RT.

Fatigue Life Computation:

$$\sum \frac{n}{N} = 0.0054 \text{ for 100 missions}$$

Fatigue Life

$$= \frac{100}{S.F. \times \sum (n/N)} = \frac{100}{4(0.0054)} = 4630 \text{ missions}$$

### 3.3 SAFE-LIFE ANALYSIS

This section presents the results of crack growth studies when the structural components are assumed to contain crack-like flaws. Flights to failure are calculated for all components.

The crack growth analyses are based on a Convair crack growth computer program called CRACKPROP, which calculates crack growth for both cyclic and sustained loads. Initial flaws are assumed to be elliptical surface flaws or through-cracks for the LO<sub>2</sub> and LH<sub>2</sub> propellant tank walls and the vertical stabilizer skin. Corner cracks emanating from flange edges are assumed for the thrust structure, orbiter support bulkhead, and wing spar caps. An analysis is also made assuming a crack initiating at a fastener hole in those components where mechanical fasteners may be used, i.e., the wing structure, thrust structure, and the orbiter aft support bulkhead.

For the LO<sub>2</sub> and LH<sub>2</sub> propellant tanks the initial flaw size is assumed to be that flaw screened by proof test using a plain strain fracture toughness ( $K_{IC}$ ) value. When the calculated elliptical surface flaw screened by the proof test is greater than the tank wall thickness an equivalent through-crack of an area equal to the area of a surface flaw on the verge of leakage is assumed.

Minimum fracture toughness values were used for all calculations of initial and critical flaw sizes. Because of this, the safe-lives calculated for the tanks should be treated with caution. However, where the initial flaw size was not dependent on material toughness the use of the minimum toughness in determining the critical flaw size does give the shortest life.

**3.3.1 CYCLIC AND SUSTAINED FLAW GROWTH RATE CURVES.** Figures 3-20 through 3-25 present crack growth rate curves of  $da/dn$  versus  $\Delta K_I$  and  $da/dt$  vs  $\Delta K_I$ , which are used in the safe-life analysis of structural components containing flaws in this section.

The cyclic growth rate curves ( $da/dn$  versus  $\Delta K_I$ ) for the 2219-T87 aluminum base metal at room temperature and at -320°F were derived from data found in Reference 6. The sustained growth rate curves ( $da/dt$  versus  $\Delta K_I$ ) for the 2219-T87 aluminum base metal at room temperature and at -320°F were derived from data found in Reference 7.

The cyclic growth rate curve ( $da/dn$  versus  $\Delta K_I$ ) for the Ti-6Al-4V annealed titanium base metal at room temperature was derived from data found in Reference 8. The sustained growth rate curve for the same material and temperature was derived from data found in References 8 and 9.

**3.3.2 LO<sub>2</sub> TANK SAFE LIFE-ANALYSIS.** The LO<sub>2</sub> propellant tank is assumed to contain two distinct types of flaws. These are an elliptical surface flaw and a through crack, for which the initial size of each flaw is propagated to a specified failure criterion under the influence of the applied pressure spectrum loading. The critical crack lengths for both types of flaws are also developed here.

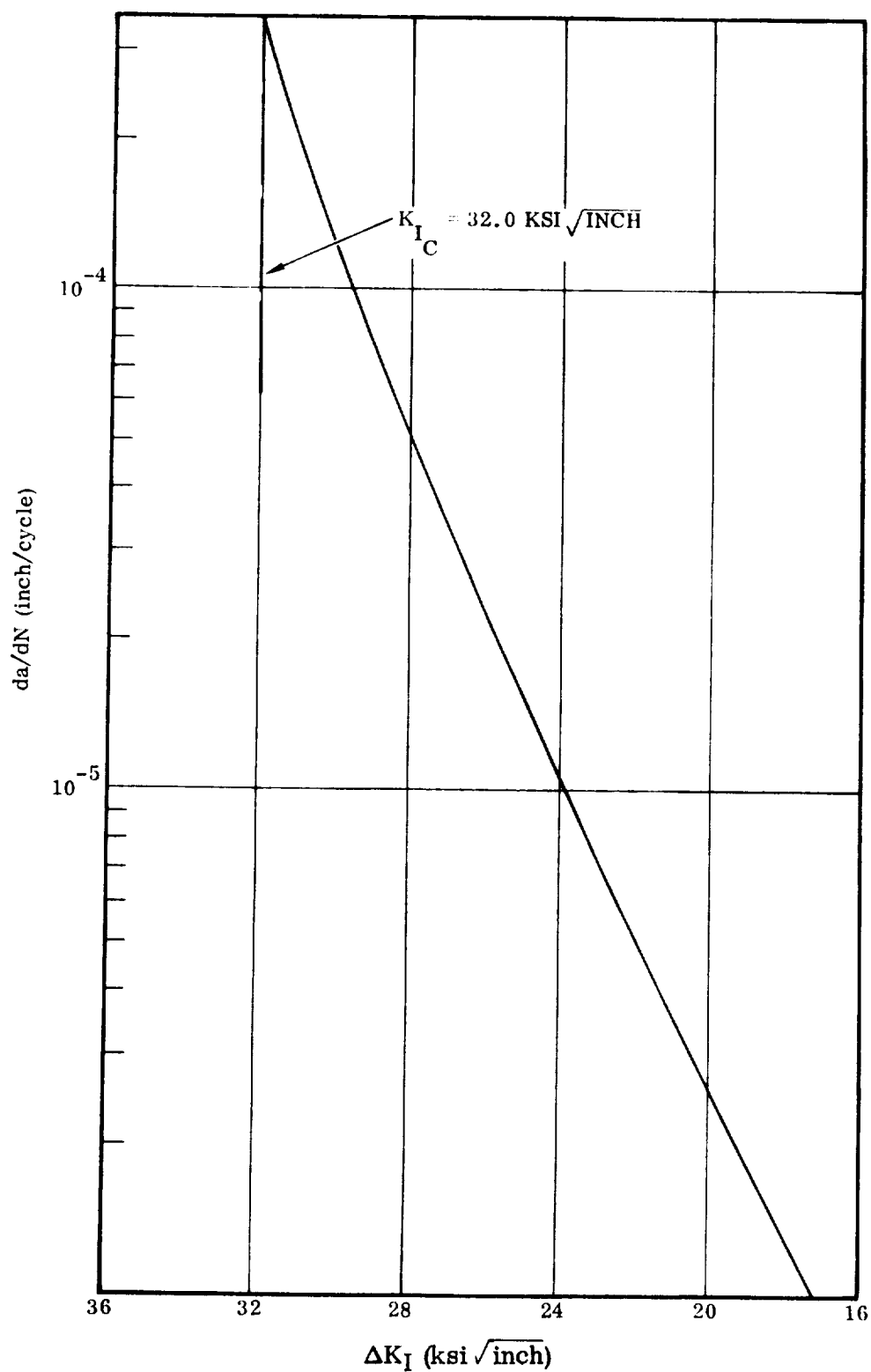


Figure 3-20. Cyclic Flaw Growth Rate for 2219-T87 Aluminum Alloy at Room Temperature



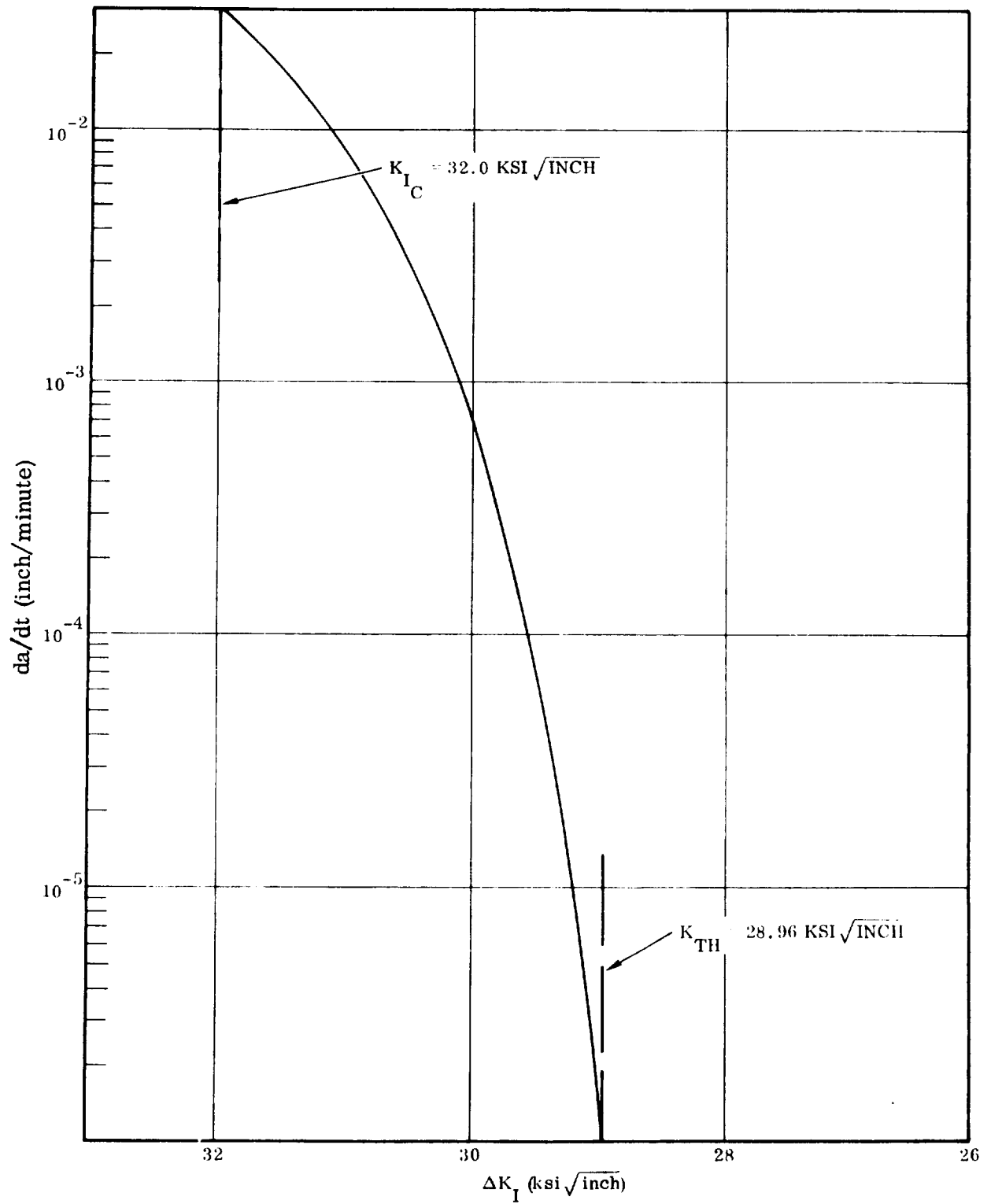


Figure 3-21. Sustained Flaw Growth Rate for 2219-T87 Aluminum Alloy at Room Temperature

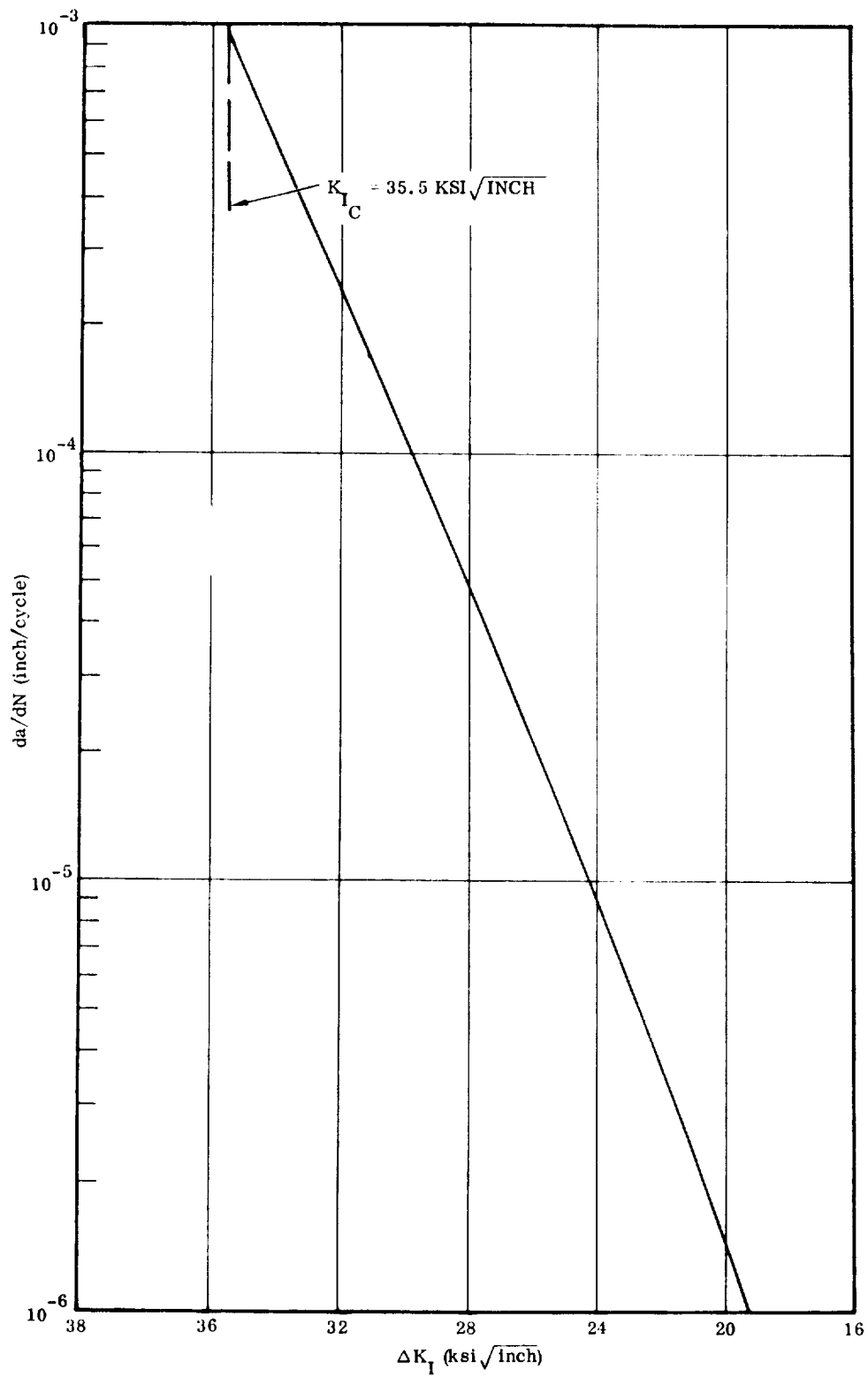


Figure 3-22. Cyclic Flaw Growth Rate for 2219-T87 Aluminum Alloy at -320°F

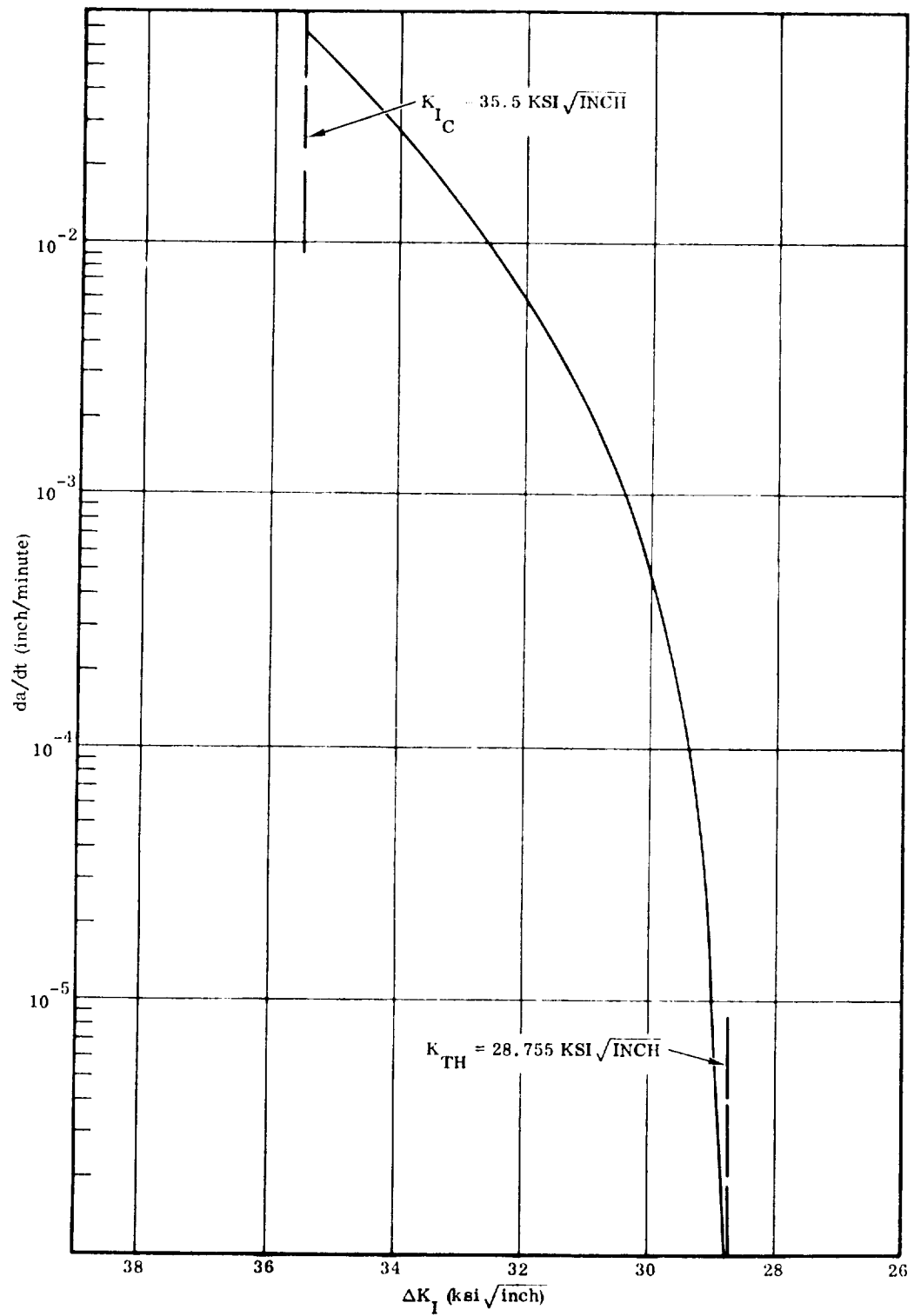


Figure 3-23. Sustained Flaw Growth Rate for 2219-T87 Aluminum Alloy at -320°F

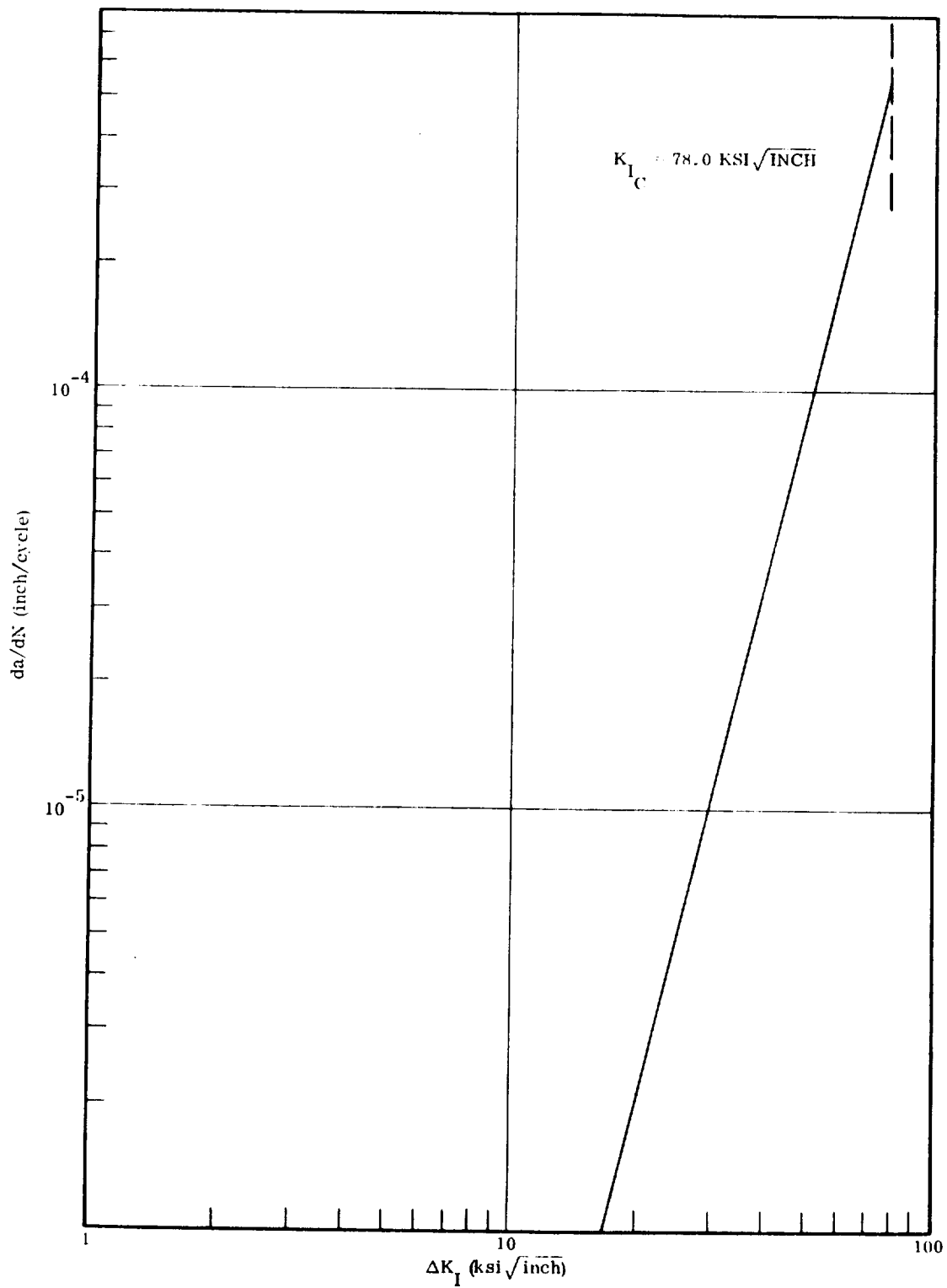


Figure 3-24. Cyclic Flaw Growth Rate for Ti-6Al-4V(ELI) Annealed Titanium Alloy at Room Temperature

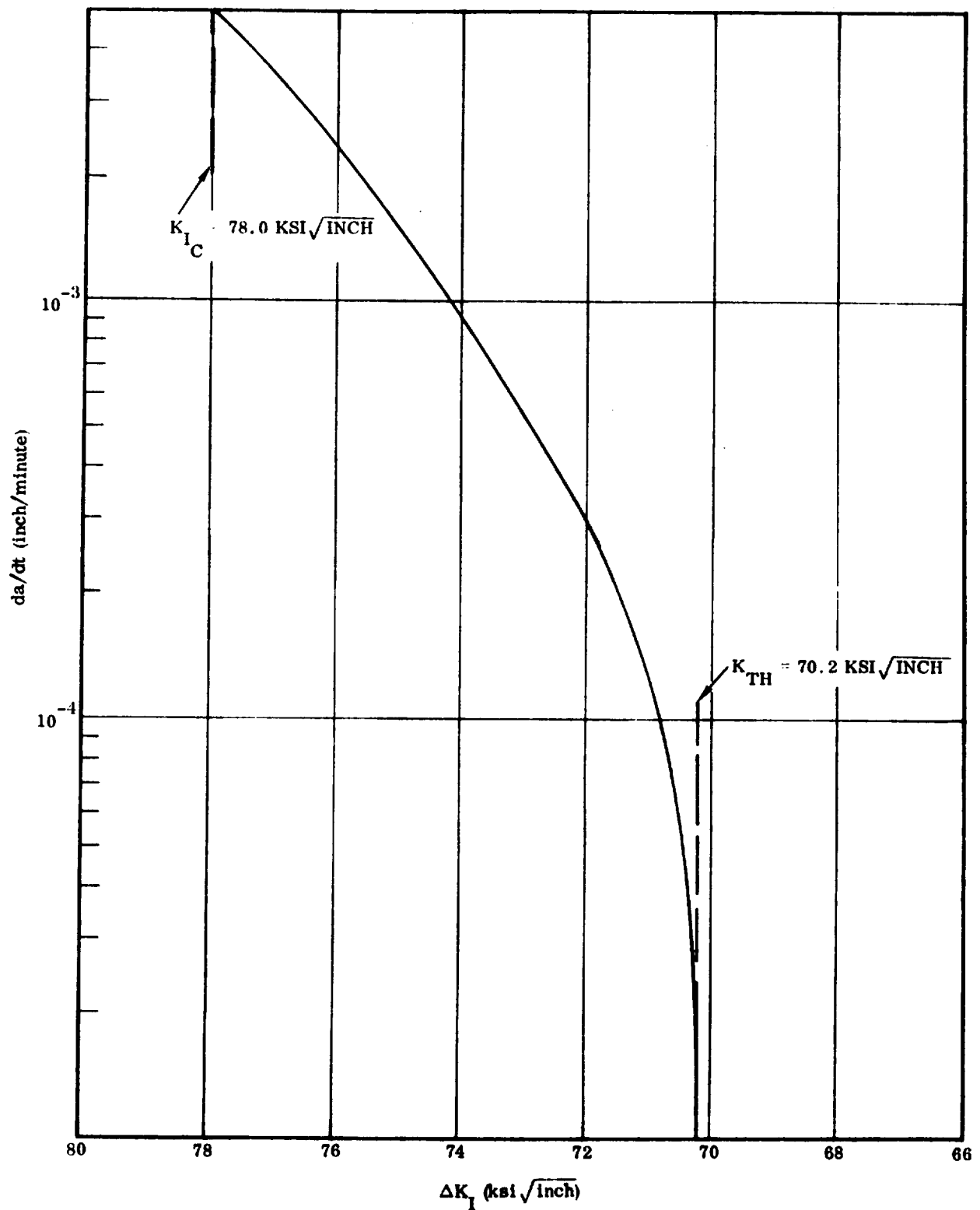


Figure 3-25. Sustained Flaw Growth Rate for Ti-6Al-4V(ELI) Annealed Titanium Alloy at Room Temperature

The applied pressure spectrum loading for the LO<sub>2</sub> tank was developed from the curve of Figure 2-39. Only those portions of the total loading spectrum that could contribute to the growth of the flaws was included in the spectrum for the tank. It should be noted here that it was necessary to take average pressures over a given time span to truly approximate the curve. The pressures used in developing the final spectrum are as follows:

LO<sub>2</sub> Tank Upper Dome Equator Pressures

Pressure (psi)	Time at Pressure (minutes)	Description
18.0	4.0	Nominal ullage pressure
12.0	6.0	Vent after staging pressure
20.0	4.0	Pressure regulator malfunction stress (assumed to occur once every 20 flights)

The tensile stresses in the LO<sub>2</sub> tank at the upper dome equator were developed from the pressures in the preceding list through the use of the following formula.

$$\sigma = \frac{PR}{t} = \frac{P (198 \text{ in.})}{(0.090 \text{ in.})}$$

P = internal pressure (psi)

R = 198 in. = tank radius

t = 0.090 in. = tank wall thickness at the upper dome equator.

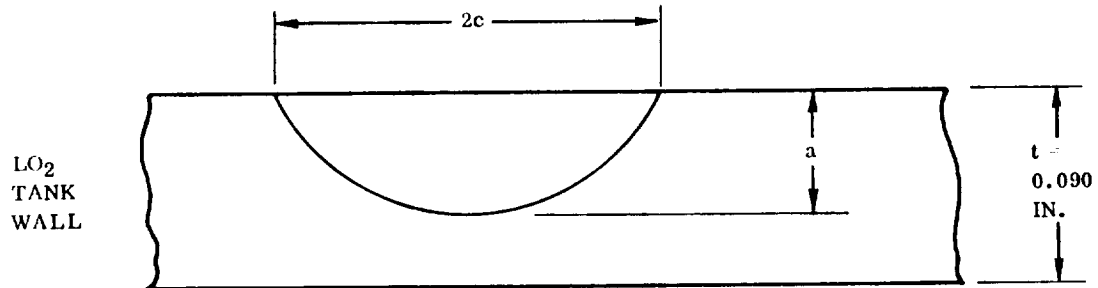
The results of this calculation and the final form of the pressure loading spectrum is as follows:

LO<sub>2</sub> Tank Pressure Loading Spectrum

Minimum Stress (ksi)	Maximum Stress (ksi)	Cycles per Flight	Time per Flight (minutes)
0.000	39.600*	1	
0.000	39.600*		4.0
0.000	26.400		6.0

\*Once every 20 flights, this nominal ullage pressure stress is replaced with the pressure regulator malfunction stress of 44.0 ksi.

The elliptical surface flaw is assumed to have two different initial aspect ratios,  $a/2c$  (see sketch below). These two aspect ratios are  $a/2c = 0.1$  and  $a/2c = 0.4$ .



The initial flaw size, which is calculated here for both the 0.1 and 0.4 aspect ratios, is the maximum flaw size that would be screened by a proof test of the tank, using a minimum value for the material toughness parameter,  $K_{Ic}$ , to be consistent with the value used in the crack growth analysis, and using the yield stress for the maximum stress developed in the tank wall during a proof test.

The equation for the maximum stress intensity factor for the elliptical surface flaw, which is used to calculate the maximum flaw size screened by a proof test, is as follows:

$$K_I = \frac{1.1 \sigma \sqrt{\pi} \sqrt{a} (M_K)}{\sqrt{\phi^2 - 0.212 (\sigma/\sigma_Y)^2}} \quad (\text{Reference 3, Equation IX-8})$$

where

$\sigma$  = applied stress (ksi)

$\sigma_Y$  = tensile yield stress (ksi)

$a$  = flaw size (inch)

$\phi^2$  = a function depending upon the value of  $a/2c$

for  $a/2c = 0.1$ ,  $\phi^2 = 1.10355$

for  $a/2c = 0.4$ ,  $\phi^2 = 2.01096$

$M_K$  is a function depending upon the value of  $a/t$ , (deep flaw correction factor) defined in the following list:

<u><math>a/2c = 0.1</math></u>		<u><math>a/2c = 0.4</math></u>	
<u><math>a/t</math></u>	<u><math>M_K</math></u>	<u><math>a/t</math></u>	<u><math>M_K</math></u>
0	1.000	0	1.000
0.1	1.010	0.1	1.005
0.2	1.030	0.2	1.010
0.3	1.065	0.3	1.015
0.4	1.110	0.4	1.020
0.5	1.185	0.5	1.035
0.6	1.290	0.6	1.055
0.7	1.430	0.7	1.085
0.8	1.565	0.8	1.130
0.9	1.680	0.9	1.180
1.0	1.770	1.0	1.210

(From Reference 10, Page 135)

The LO<sub>2</sub> tank is proof tested at room temperature so that the value of  $K_{IC}$  used in the following calculations will be the minimum value of  $K_{IC}$  at room temperature. This value is  $K_{IC} = 32.0 \text{ ksi } \sqrt{\text{inch}}$  (Reference 6, Figure 52, lower curve). Substituting this value of  $K_{IC}$  into the equation for the stress intensity factor and using  $\sigma_Y = 51.0 \text{ ksi}$  (2219-T87 aluminum base metal at room temperature) as the proof test stress, we can arrive at a value of 'a' from the following equation:

$$32.0 = \frac{1.1 (51.0) \sqrt{\pi} \sqrt{a} (M_K)}{\sqrt{\phi^2 - 0.212 (51.0/51.0)^2}}$$

Note in the above equation that the variable  $M_K$  is a function of the flaw size, 'a', and that a trial and error solution is necessary to find the correct value of 'a'. The results of this solution for both aspect ratios of 0.1 and 0.4 are shown below.

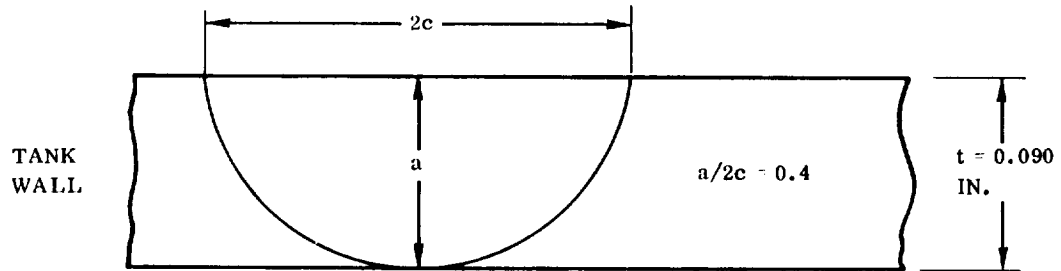
For  $a/2c = 0.1$ , the maximum flaw size that would be screened by a proof test is:

$$a_i = 0.05464 \text{ inch}$$



For  $a/2c = 0.4$ , the maximum flaw size that would be screened by a proof test resulted in a flaw size, 'a', which was larger than the thickness of the tank wall,  $t = 0.090$  inch.

Since the 0.4 aspect ratio results in an initial flaw size greater than the thickness, an equivalent through crack, with an area equal to the area of a surface flaw of aspect ratio  $a/2c = 0.4$  on the verge of leakage, is calculated here.



Cross-sectional area of flaw -  $A_c$

$$A_c = \frac{\pi (a) (c)}{2} = 0.01590 \text{ in}^2$$

For a through crack, the area would be calculated by

$$A_c = (2c) \times t \text{ or } (2c) = \frac{A_c}{t}$$

Therefore the equivalent through crack would have a  $(2c)_i$  dimension of

$$(2c)_i = \frac{A_c}{t} = \frac{0.01590}{0.090} = 0.17671 \text{ inch}$$

The elliptical surface flaw of initial size  $a_i = 0.05464$  inch and the through crack of initial size  $(2c)_i = 0.17671$  inch are propagated to failure. The run to failure is made using material properties and growth rate curves for 2219-T87 aluminum base metal at  $-320^\circ\text{F}$ . The  $-320^\circ\text{F}$  temperature is used because growth rates at this temperature are more critical than those at room temperature, and the  $\text{LO}_2$  tank at the upper dome equator is assumed to be prechilled to  $-320^\circ\text{F}$ . The critical flaw sizes must therefore be calculated from the properties of the material at  $-320^\circ\text{F}$ .

The minimum value of  $K_{Ic}$  is used to calculate critical flaw sizes, and for the  $-320^{\circ}\text{F}$  temperature this value is  $35.5 \text{ ksi} \sqrt{\text{inch}}$  (Reference 6, Figure 52, lower curve at  $-320^{\circ}\text{F}$ ). The tensile yield at this temperature is taken to be  $\sigma_Y = 61.0 \text{ ksi}$ . The maximum stress in the spectrum, on which the critical flaw sizes must be based, is  $\sigma = 44.0 \text{ ksi}$ .

For the elliptical flaw of aspect ratio  $a/2c = 0.1$ , the critical flaw size,  $a_{cr}$ , is calculated from the equation

$$35.5 = \frac{1.1 (44.0) \sqrt{\pi} \sqrt{a_{cr}} (M_K)}{\sqrt{1.10355 - 0.212 (44.0/61.0)^2}}$$

which results in a value of  $a_{cr} = 0.07091 \text{ inch}$ .

For the through crack the equation for the stress intensity factor is

$$K_I = \frac{\sigma \sqrt{\pi} \sqrt{2c}}{\sqrt{2 - (\sigma/\sigma_Y)^2}} \quad (\text{Reference 10, Page 28})$$

Substituting the critical values into this equation results in

$$35.5 = \frac{44.0 \sqrt{\pi} \sqrt{(2c)_{cr}}}{\sqrt{2 - (44.0/61.0)^2}}$$

or  $(2c)_{cr} = 0.30660 \text{ inch}$ .

Results of flaw growth calculations:

Carrying out the analysis described above by use of a computer program, the following results were obtained.

Elliptical Surface Flaw,  $a/2c = 0.1$  (See Figure 3-26)

Starting with an initial flaw size of  $a_i = 0.05464 \text{ inch}$ , it took 294 flights for the flaw to grow to the critical size of  $a_{cr} = 0.07091 \text{ inch}$  (see sketch below). Note that a scatter factor of 1.5 was used on the number of flights to failure.

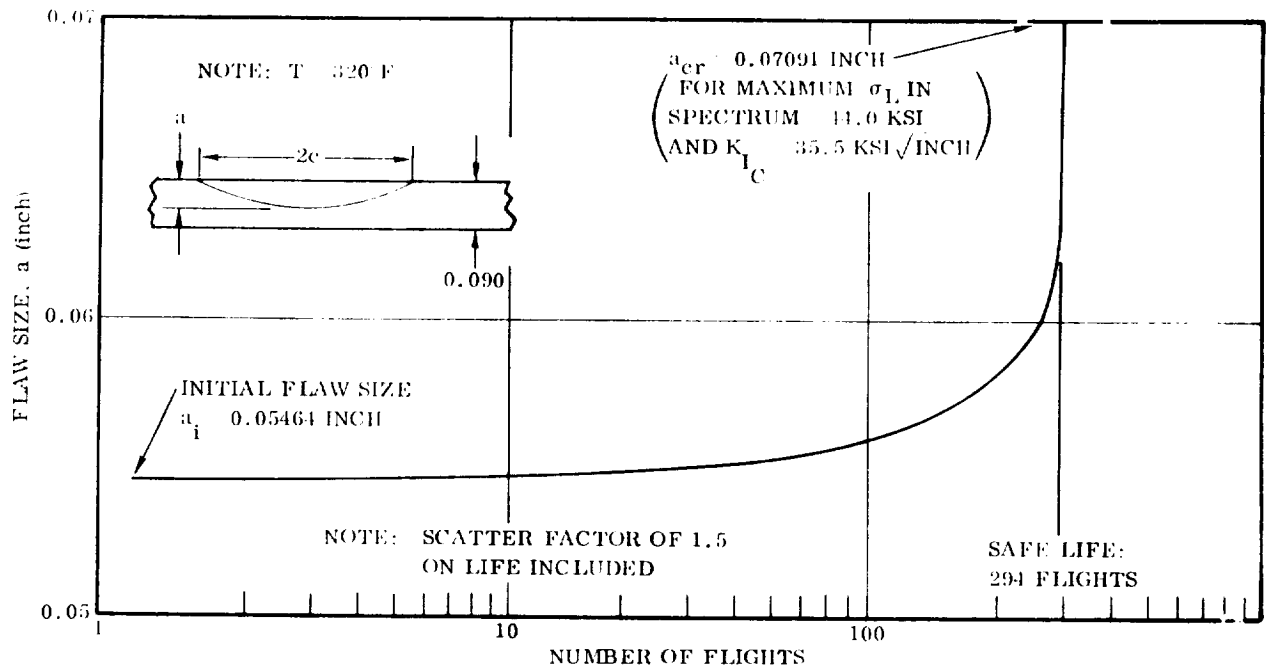
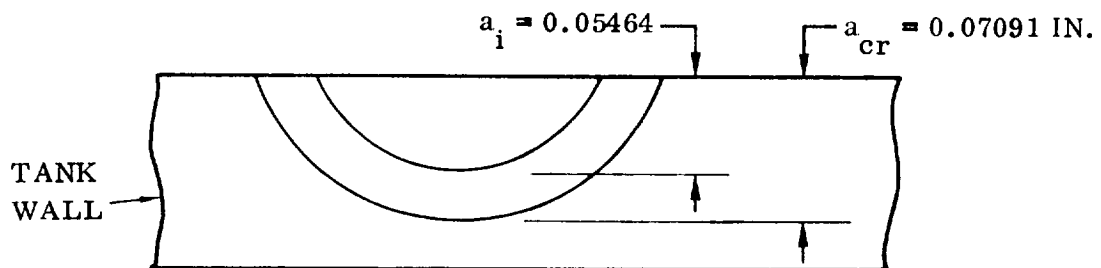


Figure 3-26. Crack Growth in LO<sub>2</sub> Tank for Pressure Load Spectrum  
(Surface Flaw,  $a/2c = 0.1$ )



Through Crack (See Figure 3-27)

Starting with an initial flaw size of  $(2c)_i = 0.17671$  inch, it took 867 flights for the flaw to grow to the critical size of  $(2c)_{cr} = 0.30660$  inch. Again a scatter factor of 1.5 was used on the flights to failure.

**3.3.3 LH<sub>2</sub> TANK SAFE LIFE ANALYSIS.** The LH<sub>2</sub> propellant tank is assumed to contain two distinct types of flaws. These are an elliptical surface flaw and a through crack, for which the initial size of each is developed in this section. These flaws are

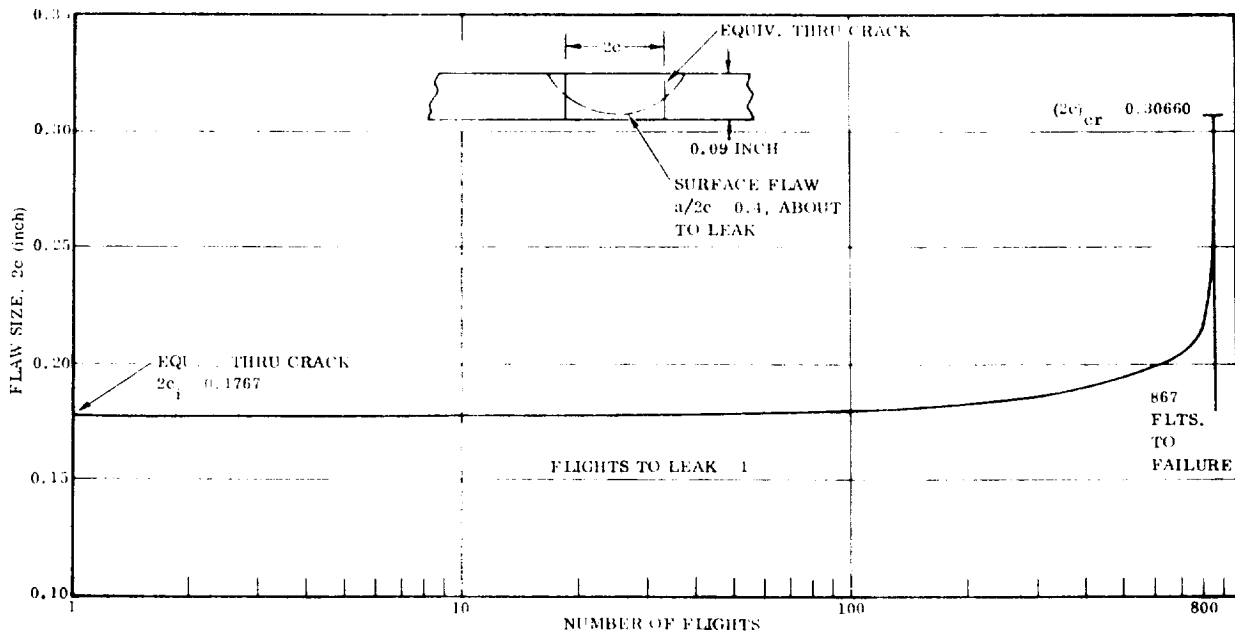


Figure 3-27. Crack Growth in LO<sub>2</sub> Tank for Pressure Load Spectrum (Surface Flaw,  $a/2c = 0.4$  and Equivalent Through Crack)

propagated to a specified failure criterion under the influence of the applied pressure spectrum loading. The critical crack lengths for both types of flaws are also developed here.

The applied pressure loading spectrum for the LH<sub>2</sub> tank was developed from the curve of Figure 2.38. Only those portions of the complete loading spectrum that could contribute to the growth of the flaws was included in the spectrum for the tank. The pressures used in developing the final spectrum are:

#### LH<sub>2</sub> Tank Upper Dome Equator Pressures

Pressure (psi)	Time at Pressure (minutes)	Description
15.0	2.5	Tank lockup pressure
22.0	3.5	Nominal ullage pressure
16.0	6.0	Vent after staging pressure
23.5	3.5	Pressure regulator
		Malfunction pressure - assumed to occur once every 20 flights

Stresses in the tank at the upper dome equator were developed from these pressures through the use of the formula

$$\sigma = \frac{PR}{t} = \frac{P (198)}{0.116}$$

where

P = pressure (psi)

R = 198 inches = tank radius

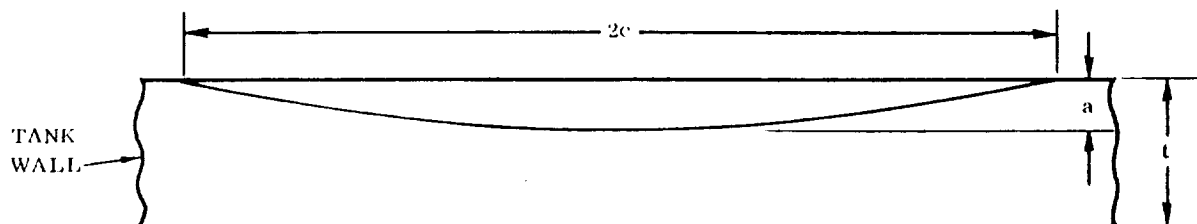
t = 0.116 inch = tank thickness at the upper dome equator

The calculated stresses and the final form of the pressure loading spectrum is shown below

Minimum Stress (ksi)	Maximum Stress (ksi)	Cycles per Flight	Time per Flight (minutes)
0.000	25.603	1	2.5
0.000	37.552*		
0.000	37.552*		3.5
0.000	27.310		6.0

\*Every 20 flights, this stress is replaced with the pressure regulator malfunction stress, which is 40.112 ksi.

The elliptical surface flaw is assumed to initially have aspect ratios,  $a/2c$ , of 0.1 and 0.4 (see sketch below).



The initial flaw size for each of these aspect ratios is calculated here, based on the maximum flaw size that would be screened by the proof test, using a minimum value for the material toughness parameter  $K_{IC}$  for consistency with the crack growth analysis.

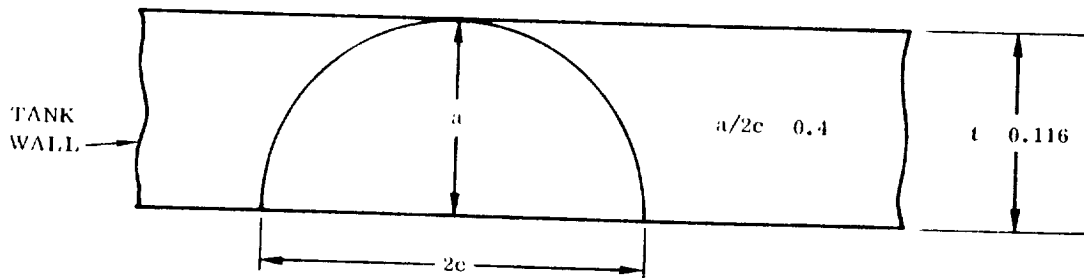
For 2219-T87 aluminum base metal at room temperature the minimum value of the material toughness parameter,  $K_{IC}$ , is 32.0 ksi  $\sqrt{\text{inch}}$  (Reference 6, Figure 52, lower curve). Using this value of  $K_{IC}$  in the equation for the stress intensity factor, and substituting  $\sigma = \sigma_Y$  for the proof test stress, the equation becomes

$$32.0 = \frac{1.1 (51.0) \sqrt{\pi} \sqrt{a} (M_K)}{\sqrt{\phi^2 - 0.212 (51.0/51.0)^2}}$$

This equation can now be solved for 'a', which is the maximum flaw size that would be screened by a proof test. It should be noted that  $M_K$  is dependent upon the value of 'a' so that a trial and error solution is necessary. This equation was solved for both aspect ratios of 0.1 and 0.4 and the results are shown below.

For  $a/2c = 0.1$ , the flaw screened by a proof test,  $a = 0.06195$  inch. This value becomes the initial flaw size,  $a_i$ , for the flaw propagation studies.

For  $a/2c = 0.4$ , the flaw that would be screened by a proof test turned out to be greater than the thickness of the tank wall,  $t = 0.116$  inch. An equivalent through crack with an area equal to the area of a surface flaw of aspect ratio,  $a/2c = 0.4$  on the verge of leakage is calculated here.



$$\text{Area of flaw} = \frac{\pi a c}{2} \quad a = 0.116 \text{ inch} \quad \text{Area} = 0.02642 \text{ in}^2$$

The equation for the stress intensity factor  $K_I$ , for the elliptical surface flaw, is as follows:

$$K_I = \frac{1.1 \sigma \sqrt{\pi} \sqrt{a} (M_K)}{\sqrt{\phi^2 - 0.212 (\sigma/\sigma_Y)^2}} \quad (\text{Reference 3, Equation IX-8})$$

$\sigma$  = applied stress (ksi)

$\sigma_Y$  = tensile yield stress = 51 ksi

$a$  = flaw size (inch)

$\phi^2$  = is a function which depends on the value of  $a/2c$

For

$$a/2c = 0.1, \quad \phi^2 = 1.10355$$

$$a/2c = 0.4, \quad \phi^2 = 2.01096$$

$M_K$  is a function which depends on both the value of  $a/2c$  and  $a/t$

<u>For <math>a/2c = 0.1</math></u>		<u>For <math>a/2c = 0.4</math></u>	
<u><math>a/t</math></u>	<u><math>M_K</math></u>	<u><math>a/t</math></u>	<u><math>M_K</math></u>
0	1.000	0	1.000
0.1	1.010	0.1	1.005
0.2	1.030	0.2	1.010
0.3	1.065	0.3	1.015
0.4	1.110	0.4	1.020
0.5	1.185	0.5	1.035
0.6	1.290	0.6	1.055
0.7	1.430	0.7	1.085
0.8	1.565	0.8	1.130
0.9	1.680	0.9	1.180
1.0	1.770	1.0	1.210

(From Reference 10, Page 135.)

An equivalent through crack would have an area of  $(2c) \times t$

$$(2c) \times t = 0.02642 \text{ in}^2 \quad 2c = 0.2278 \text{ inch}$$

This value becomes the initial size of the through crack in the flaw propagation studies.

The critical flaw size of the elliptical surface flaw of aspect ratio  $a/2c = 0.1$  is calculated in a manner similar to that in which the initial flaw size was calculated. Obtaining the minimum value of the material toughness parameter,  $K_{Ic}$ , from the minimum curve of Figure 52 of Reference 6,  $K_{Ic} = 32.0 \text{ ksi } \sqrt{\text{inch}}$  and the applied stress becomes the maximum stress from the applied pressure loads spectrum ( $\sigma = 40.112 \text{ ksi}$ ). The stress intensity factor equation then becomes

$$32.0 = \frac{1.1 (40.112) \sqrt{\pi} \sqrt{a_{cr}} (M_K)}{\sqrt{\phi^2 - 0.212 (40.112/51.0)^2}}$$

Solving for  $a_{cr}$ , we find  $a_{cr} = 0.08053 \text{ inch}$ . The critical flaw size for the through flaw is found by using the same minimum  $K_{Ic}$  value of  $32.0 \text{ ksi } \sqrt{\text{inch}}$  and the same applied stress of  $40.112 \text{ ksi}$ . However, the equation for the through crack now becomes

$$K_I = \frac{\sigma \sqrt{\pi} \sqrt{(2c)_{cr}}}{\sqrt{2 - (\sigma/\sigma_Y)^2}}$$

or

$$32.0 = \frac{40.112 \sqrt{\pi} \sqrt{(2c)_{cr}}}{\sqrt{2 - (40.112/51.0)^2}}$$

Solving this equation for  $(2c)_{cr}$ , we find  $(2c)_{cr} = 0.2798 \text{ inch}$ .

Results of flaw growth calculations:

Elliptical Surface Flaw,  $a/2c = 0.1$  (see Figure 3-28)

Starting with  $a_i = 0.06195 \text{ inch}$ , it took 626 flights for the flaw to grow to  $a_{cr} = 0.08053 \text{ inch}$  (scatter factor of 1.5 used on flights) as shown in Figure 3-28.

Through Flaw (see Figure 3-29)

Starting with  $2c_i = 0.2278 \text{ inch}$ , it took 160 flights for the flaw to grow to  $(2c)_{cr} = 0.2798 \text{ inch}$  (scatter factor of 1.5 used on flights).



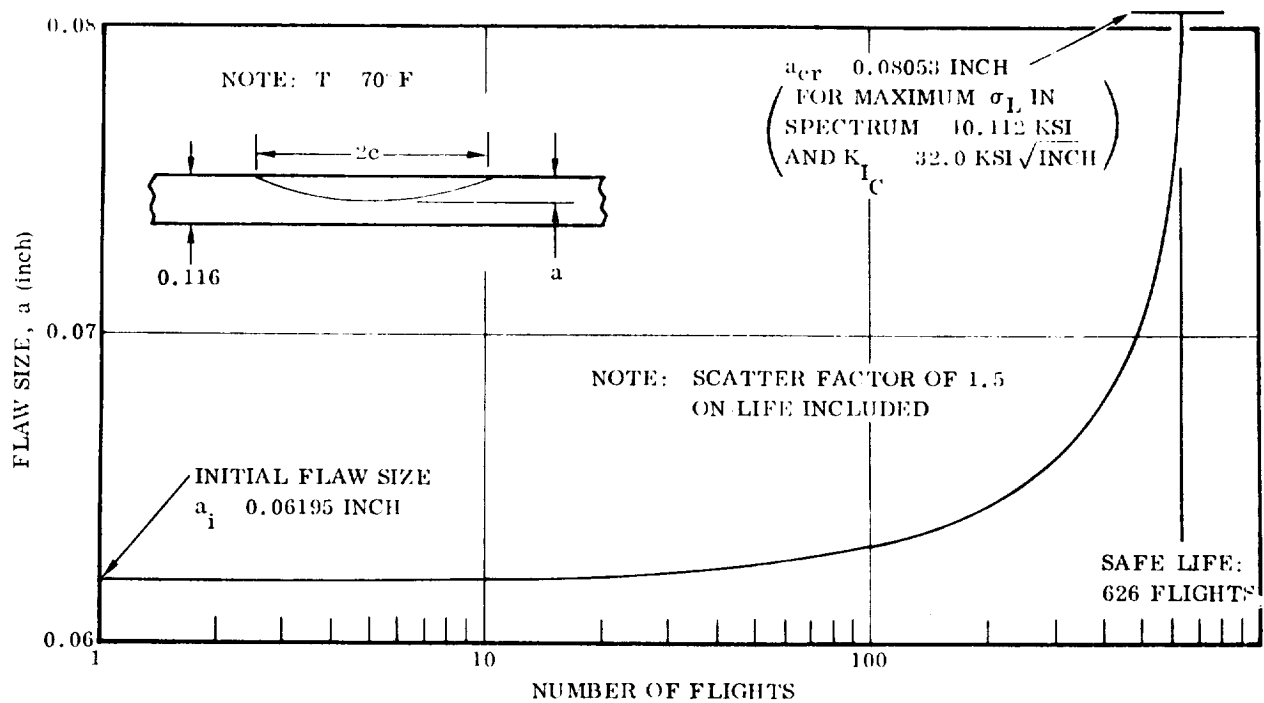


Figure 3-28. Crack Growth in LH<sub>2</sub> Tank for Pressure Load Spectrum  
(Surface Flaw,  $a/2c = 0.1$ )

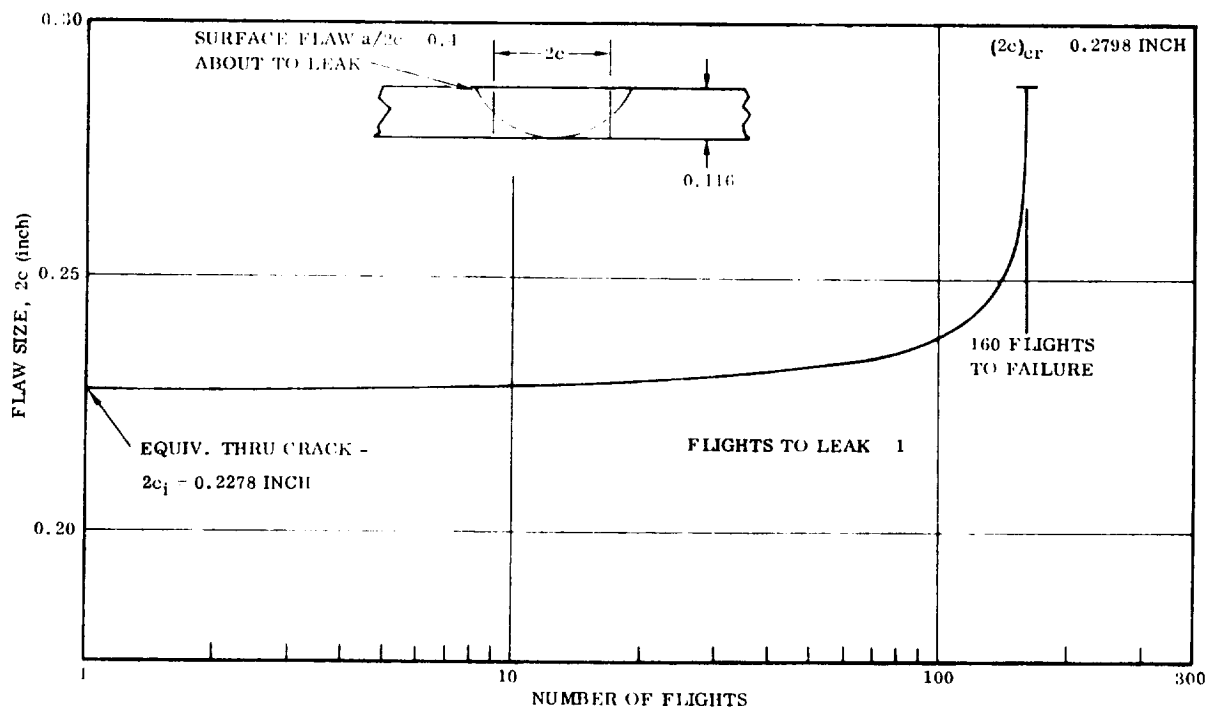


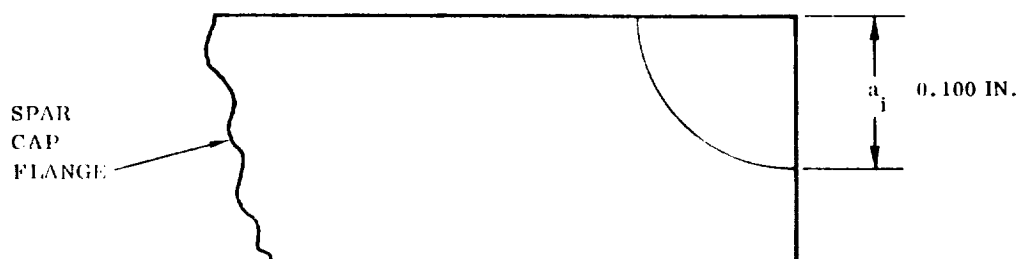
Figure 3-29. Crack Growth in LH<sub>2</sub> Tank for Pressure Load Spectrum  
(Surface Flaw,  $a/2c = 0.4$  and Equivalent Through Crack)

**3.3.4 WING SPAR CAPS SAFE LIFE ANALYSIS.** In the analysis of the wing spar caps, these members were assumed to contain two types of flaws: a corner crack of an initial size of 0.1 inch (see sketch below), and a crack of 0.1 inch initial length emanating from a fastener hole. The initial size of the cracks was chosen based on judgment of the capabilities of nondestructive evaluation.

The wing loading spectrum experienced by the flaws described above is essentially the same spectrum as was used in the wing fatigue analysis and found in Table 3-21. Certain necessary modifications were made, however, to use this spectrum in the crack growth study. These included the addition of some sustained load, which while not necessary for fatigue analysis can be of great significance in crack growth analysis, and the reduction of the spectrum, which is for 100 missions, to a spectrum for only one mission. The results of these modifications and the final wing loading spectrum can be found in Table 3-26. This spectrum is a very severe loading spectrum, much more so than experienced by any of the other components being analyzed in this study.

The crack growth studies were done on the wing assuming the spar caps were maintained at room temperature. Thus room temperature properties were assumed and crack growth rate curves for Ti-6Al-4V annealed titanium base metal at room temperature were used in the flaw propagation computer program.

**3.3.4.1 Corner Crack.** The configuration of the corner crack assumed for the flaw growth analysis was as shown in the sketch.



The maximum stress intensity factor equation for a corner crack is

$$K_I = \frac{\sigma \sqrt{\pi} \sqrt{a} (0.705)}{\sqrt{1 - 0.177 (a/\sigma_Y)^2}}$$

where

$\sigma$  = applied tensile stress

$\sigma_Y$  = tensile yield stress

$a$  = flaw size

Table 3-26. Wing Spar Cap Loading Spectrum

Flight Phase	$\sigma_{\text{Mean}}$ (ksi)	$\sigma_{\text{Alt}}$ (ksi)	Cycles per Flight (Unless Otherwise Noted)
Ascent ↑	0.000	1.368	900
		2.280	90
		3.192	9
		4.104	1
	0.000	5.016	1 cycle every 10 flights
	13.680	3.192	900
		4.560	90
		5.928	9
		7.296	1
	13.680	8.208	1 cycle every 10 flights
	0.000	5.016	900
		8.208	90
		11.400	9
		14.136	1
	0.000	16.872	1 cycle every 10 flights
	36.480	7.296	900
		13.224	90
		19.152	9
		24.624	1
	36.180	30.096	1 cycle every 10 flights
	9.120	9.576	900
		16.872	90
		27.360	9
		41.040	1
	9.120	55.176	1 cycle every 10 flights
	13.680	12.312	900
		18.240	90
		33.744	9
		55.632	1
Ascent Entry ↑	13.680	72.960	1 cycle every 10 flights
	6.840	6.840	900
	12.312	12.312	90
	16.872	16.872	5
	20.976	20.976	2.5
	33.744	33.744	1.5
	42.864	42.864	1
	42.864	42.864	1 minute sustained load per flight
	45.600	45.600	1 cycle every 10 flights
	45.600	45.600	1 minute sustained load every 10 flights
Entry Cruise/ Landing ↓	18.240	19.152	1800
		23.712	180
		29.184	18
		34.656	2
Cruise/ Landing ↓	18.240	40.128	2 cycles every 10 flights

The critical value of the material toughness parameter,  $K_{Ic}$ , used here for the Ti-6Al-4V annealed titanium base metal at room temperature was  $K_{Ic} = 78.0 \text{ ksi } \sqrt{\text{inch}}$ . (Reference 8, Figure 35, Page 89). The tensile yield stress used was  $\sigma_Y = 120.0 \text{ ksi}$ . The maximum operating stress occurring in the spar cap can be found from the spectrum to be  $\sigma = 91.2 \text{ ksi}$ . Substituting all these values into the stress intensity factor equation results in

$$78.0 = \frac{(91.2) \sqrt{\pi} \sqrt{a_{cr}} (0.705)}{\sqrt{1 - 0.177 (91.2/120.0)^2}}$$

This expression can be solved for the critical value of 'a', which turns out to be  $a_{cr} = 0.42057 \text{ inch}$ .

Results of flaw growth calculations:

Under the influence of the applied loading spectrum, it took 31 flights for the initial flaw size of  $a_i = 0.100 \text{ inch}$  to grow to the critical flaw  $a_{cr} = 0.42057 \text{ inch}$ . The reason for the very small number of flights to failure is undoubtedly the very severe loading spectrum experienced by the spar cap. It differs from the other components in this study in that it experiences extreme loads during the entry and cruise/landing flight phases as well as the ascent phase. The flaw growth is shown in Figure 3-30.

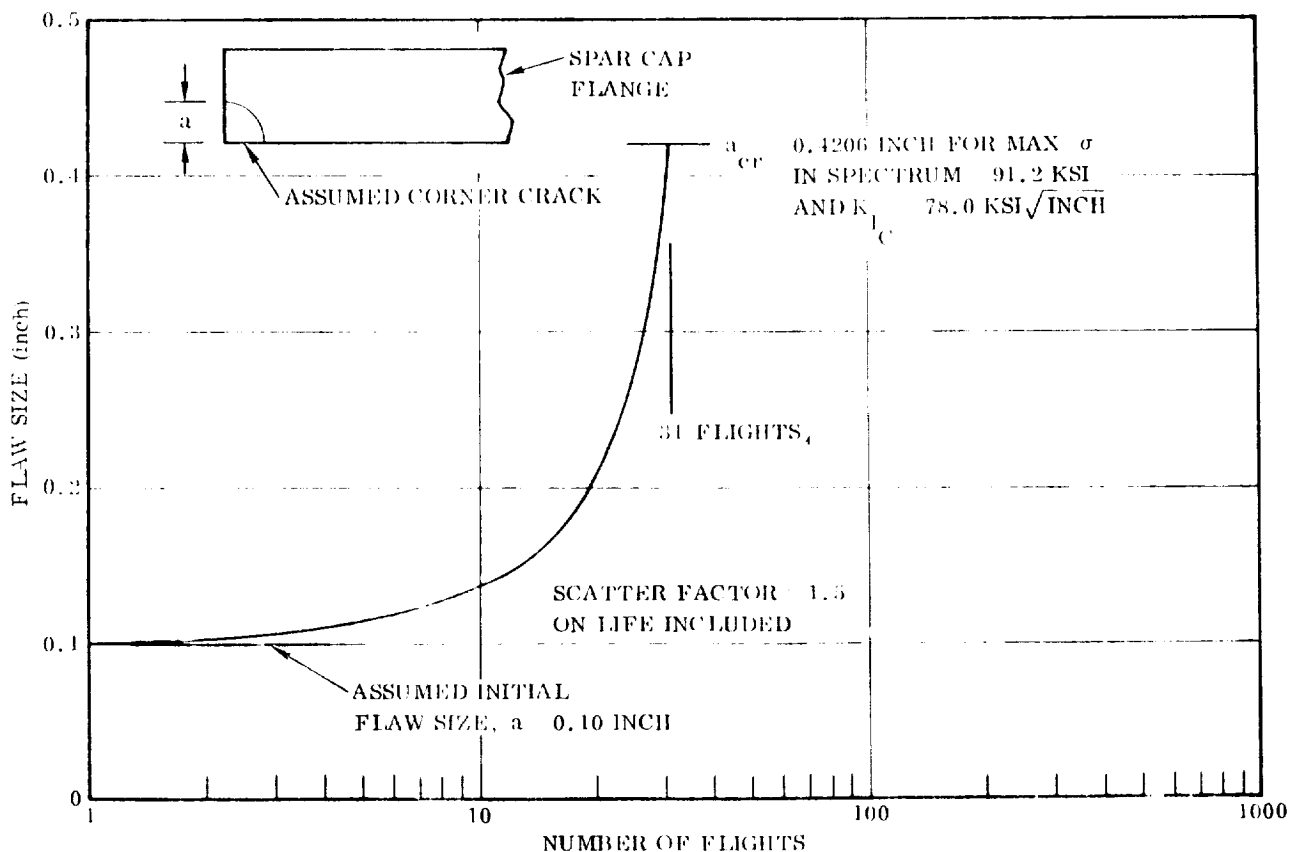


Figure 3-30. Crack Growth in Titanium Wing Spar Caps

3.3.4.2 Crack Emanating from Hole. The flaw configuration investigated in this section is as shown in the sketch. The length of the flaw is specified by 'a', the diameter of the hole is 'D', and the applied tensile stress is ' $\sigma$ '.

The equation for the stress intensity factor at the tip of the crack is

$$K_I = \frac{\sigma \sqrt{\pi a} (GKT)}{\sqrt{1 - 0.177 (\sigma/\sigma_y)^2}}$$

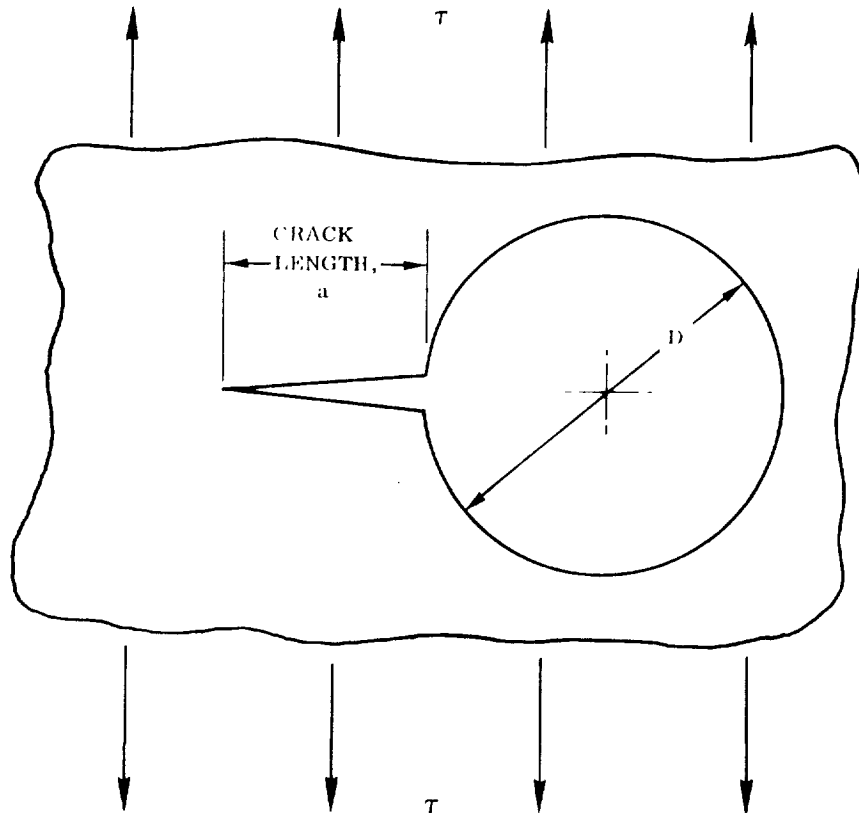
(Reference 3, Equation VII-10 modified to account for the plastic zone correction)

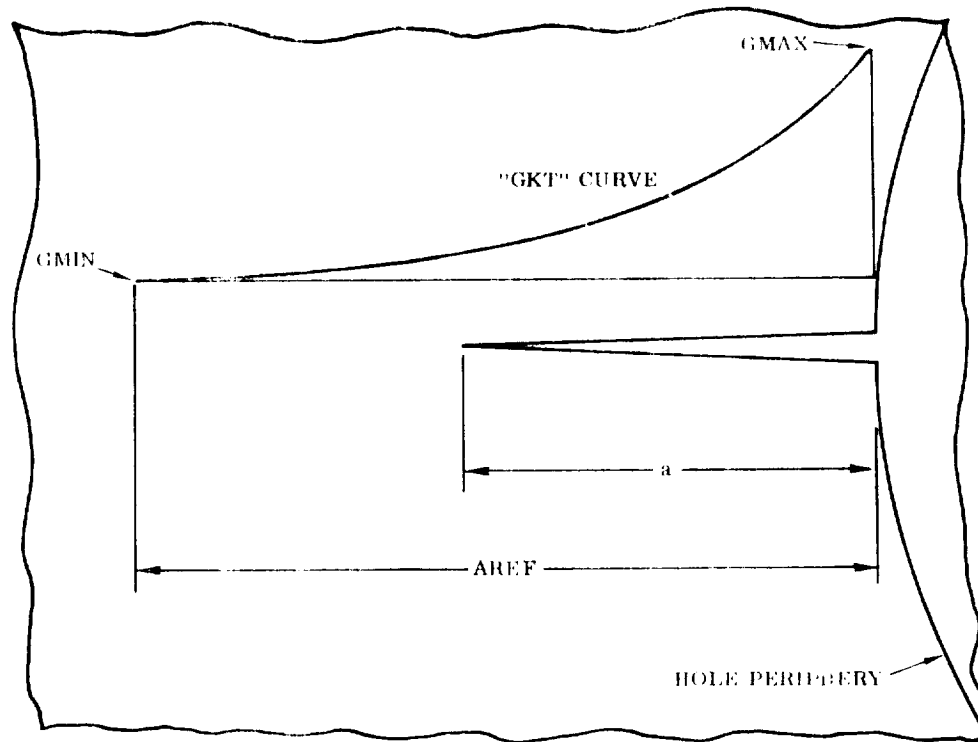
$\sigma$  = applied tensile stress (ksi)

$\sigma_y$  = tensile yield stress (ksi)

a = crack length (inches)

The quantity GKT in the equation is a factor included to account for the stress gradient due to the introduction of the hole into the uniform stress field. It can be thought of as a stress concentration factor. The quantity GKT has a maximum value (GMAX) at the periphery of the hole and decays exponentially to a minimum value (GMIN) at some specified distance (AREF) from the edge of the hole (see sketch on next page).





The curve for GKT is defined by the equation

$$GKT = GMIN + (GMAX - GMIN) e^{\left( \frac{-4.605 a}{AREF} \right)}$$

From the equation, it can be seen that AREF is actually the length at which 99% of the difference between GMAX and GMIN is reached. In other words, if

$$a = AREF, \text{ then } GKT = GMIN + 0.01 (GMAX - GMIN).$$

With GKT defined as shown, the equation for the stress intensity factor becomes

$$K_I = \frac{\sigma \sqrt{\pi a}}{\sqrt{1 - 0.177 \left( \sigma/\sigma_y \right)^2}} \left[ GMIN + (GMAX - GMIN) e^{\left( \frac{-4.605 a}{AREF} \right)} \right]$$

For this portion of the study a value of 3.0 was used for GMAX, 1.0 was used for GMIN, and AREF was taken to be 0.250 inch (one hole diameter). Figure 3-31 is a plot of GKT versus a/AREF for GMAX = 3.0 and GMIN = 1.0. With the specified values for GMAX, GMIN, and AREF, the equation for the stress intensity factor becomes

$$K_I = \frac{\sigma \sqrt{\pi a}}{\sqrt{1 - 0.177 \left( \sigma / \sigma_y \right)^2}} \left[ 1.0 + 2.0 e^{(-18.42a)} \right]$$

This is the final form of the stress intensity factor used in this portion of the study. By substituting values for the maximum operating stress in the spectrum ( $\sigma$ ), the tensile yield stress ( $\sigma_y$ ), and the critical value of  $K_I$  ( $K_{Ic}$  was used here), the critical crack length ( $a_{cr}$ ) can be found from this equation using a trial and error method.

The wing material is taken to be Ti-6Al-4V annealed titanium maintained at room temperature. Therefore, the following material properties are used:

$$K_{Ic} = 78.0 \text{ ksi } \sqrt{\text{inch}} \quad (\text{Reference 8, Figure 35, Page 89})$$

$$\sigma_y = 120.0 \text{ ksi}$$

Again using the wing loading spectrum of Table 3-26, the maximum operating stress is found from the applied loading spectrum to be  $\sigma = 91.2$  ksi. Substituting this stress and the appropriate material properties into the equation for the stress intensity factor for a crack emanating from a hole results in the following expression:

$$78.0 = \frac{91.2 \sqrt{\pi} \sqrt{a_{cr}}}{\sqrt{1 - 0.177 \left( 91.2 / 120.0 \right)^2}} \left[ 1.0 + 2.0 e^{(-18.42a_{cr})} \right]$$

This expression is solved by a trial and error method for the critical value of 'a', which turns out to be  $a_{cr} = 0.18308$  inch.

Under the influence of the applied loading spectrum, it took three flights for the initial flaw ( $a_i = 0.100$  inch) to grow to the critical flaw size ( $a_{cr} = 0.18308$  inch), including a scatter factor of 1.5 on the number of flights to failure.

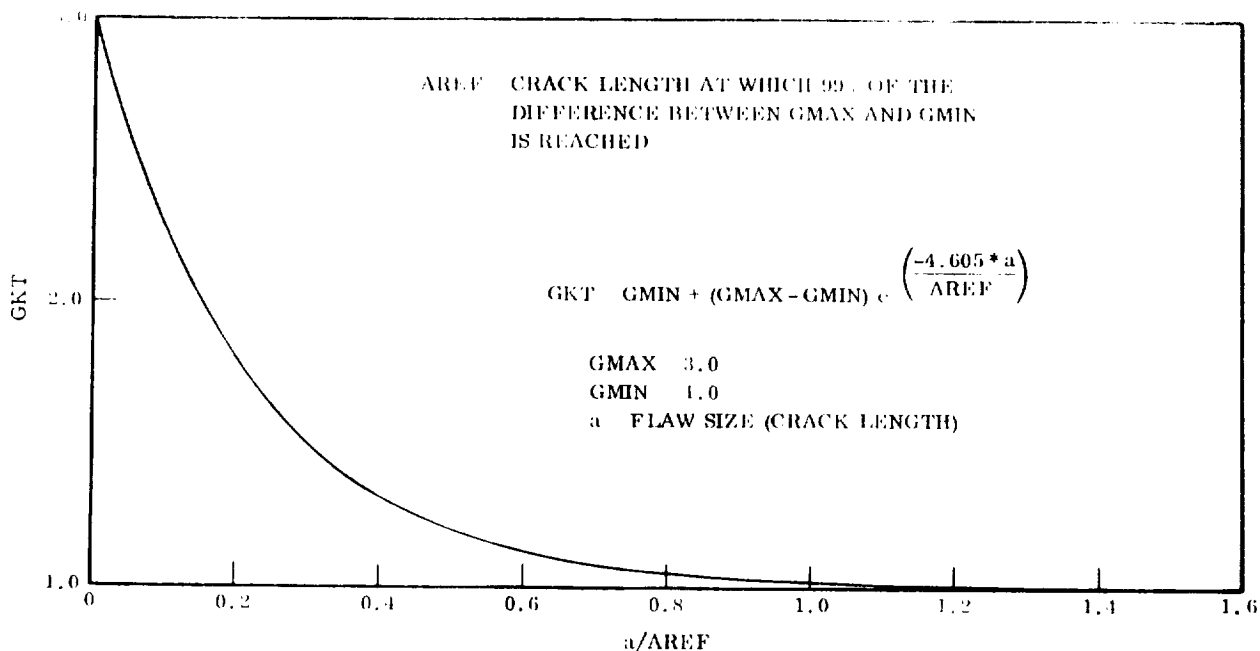


Figure 3-31. Stress Intensity Factor ( $\Delta K_I$ ) Multiple for a Crack Initiating at a Fastener Hole

The small number of flights to failure can be attributed to two things. First is the fact that the loading spectrum experienced by the wing spar cap is an extremely severe spectrum in that it incorporates high magnitude loads during the entry and cruise/landing flight phases as well as the ascent phase. Secondly, the flaw configuration being investigated here is a very critical configuration, especially since a stress gradient multiplication factor is being used on the stress intensity factor to account for the stress concentration around the hole. Consequently, the critical flaw size is not much greater than the initial flaw size, meaning the flaw does not have to grow very much to reach the critical size.

**3.3.4.3 Determination of Acceptable Safe-Life Stress Level for Spar Caps.** In the analysis of the wing for a crack emanating from a hole, the results show that the initial crack ( $a_i = 0.100$  inch) grows to the critical size ( $a_{cr} = 0.18308$  inch) in just three flights. Due to the fact that the number of flights to failure is so small, a study was undertaken to determine the allowable maximum limit stress level that would result in an acceptable safe-life of 100 missions.

The loading spectrum used in the initial analysis of a crack emanating from a hole in the wing spar cap is based on a maximum limit operating stress level of  $\sigma_{MAX} = 91.2$  ksi (see Table 3-26). The procedure used here consists of reducing this maximum limit stress level by some percentage, calculating a new critical flaw size based on



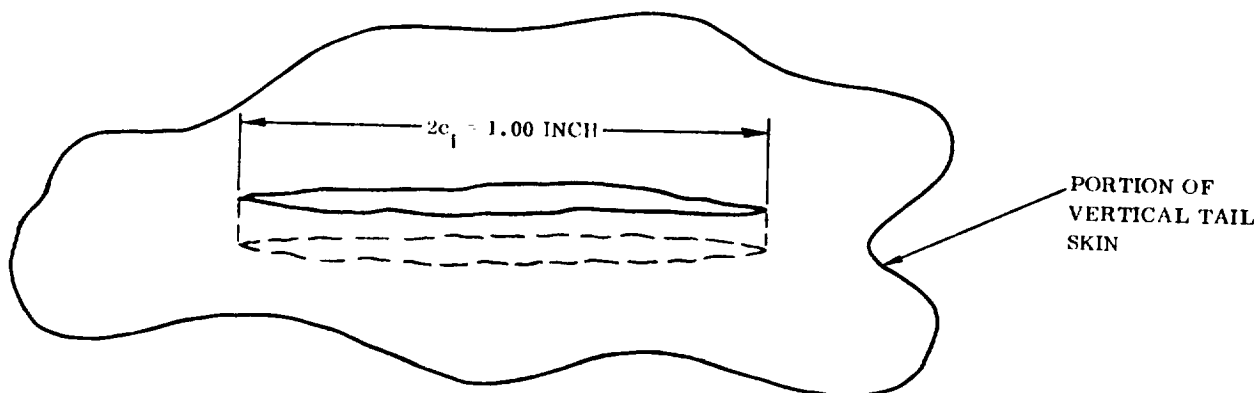
the new maximum stress level, and then propagating an initial flaw size  $a_i = 0.100$  inch to failure using a reduced applied loading spectrum based on the reduced maximum stress level. The critical flaw sizes ( $a_{cr}$ ) were found using the following expression:

$$78.0 = \frac{\sigma \sqrt{\pi} \sqrt{a_{cr}}}{\sqrt{1 - 0.177 \left( \sigma / 120.0 \right)^2}} \left[ 1.0 + 2.0 e^{(-18.42 a_{cr})} \right]$$

By substituting values of the stress level ( $\sigma$ ) into this equation, the critical flaw size ( $a_{cr}$ ) can be found for the stress level by using a trial and error method. Figure 3-32 is a plot of stress level versus critical flaw size for a crack emanating from a hole in the wing spar cap.

After determining the critical flaw size for various maximum stress levels, an initial flaw of size  $a_i = 0.100$  inch was propagated to failure for the various levels and the curve of Figure 3-33 was obtained. From this curve it can be seen that to obtain a safe-life of 100 missions, the maximum allowable operating stress level must be reduced to 50% of the original maximum stress level. In other words, all load levels in the applied loading spectrum must be reduced by 50% so that an initial crack of size  $a_i = 0.100$  inch emanating from a hole will reach criticality in 100 missions, using a scatter factor of 1.5 on the number of missions.

**3.3.5 VERTICAL TAIL SAFE-LIFE ANALYSIS.** The flaw growth analysis of the vertical tail was done assuming that there was an initial through crack in the skin of length  $(2c)_i = 1.00$  inch (see sketch below). This initial size was chosen based on a judgment of the capability of nondestructive evaluation.



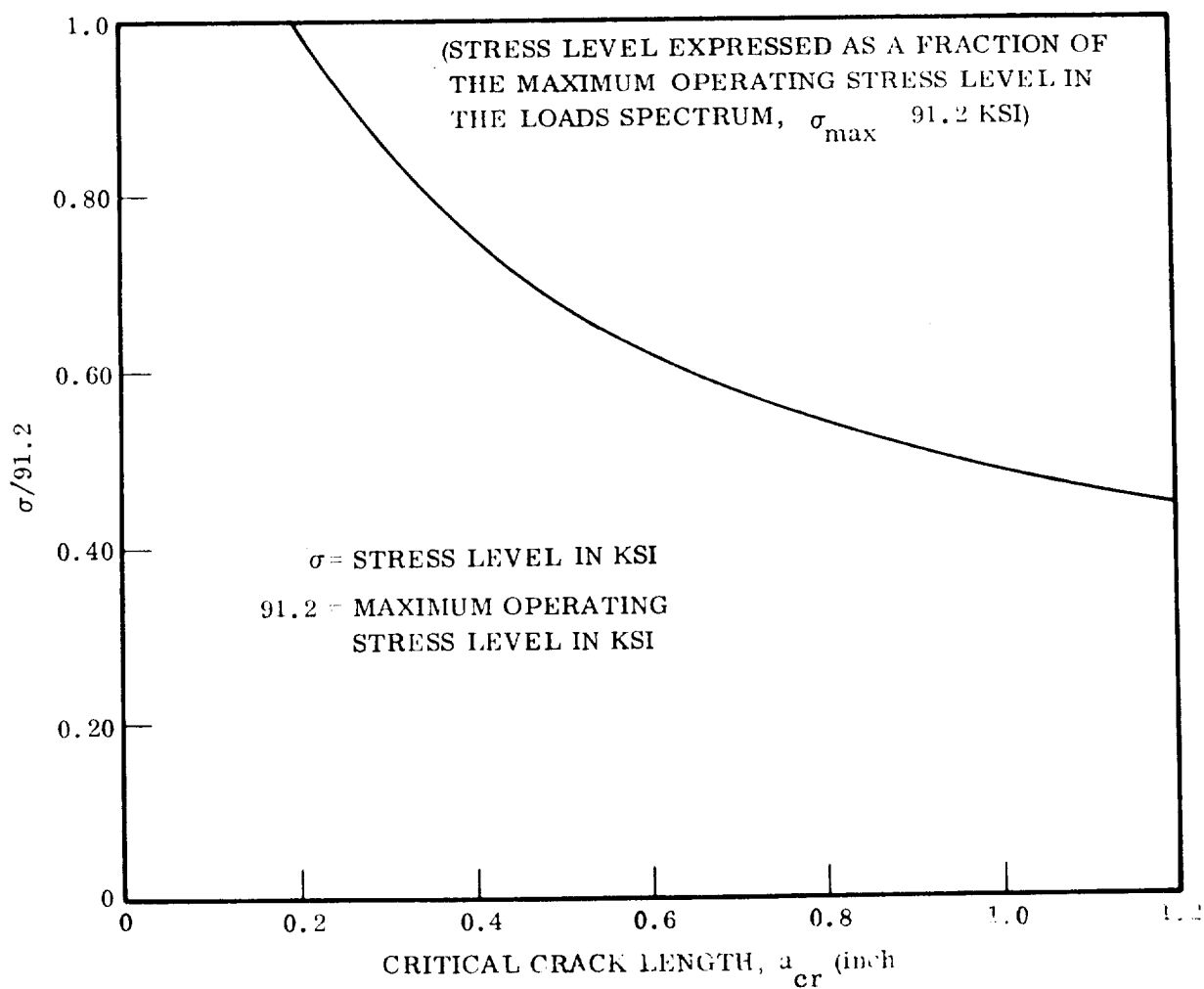
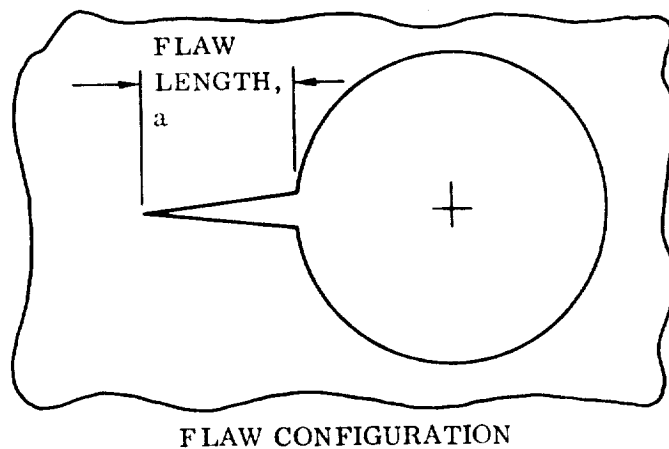


Figure 3-32. Critical Flaw Size Versus Stress Level for the Titanium Wing Spar Caps

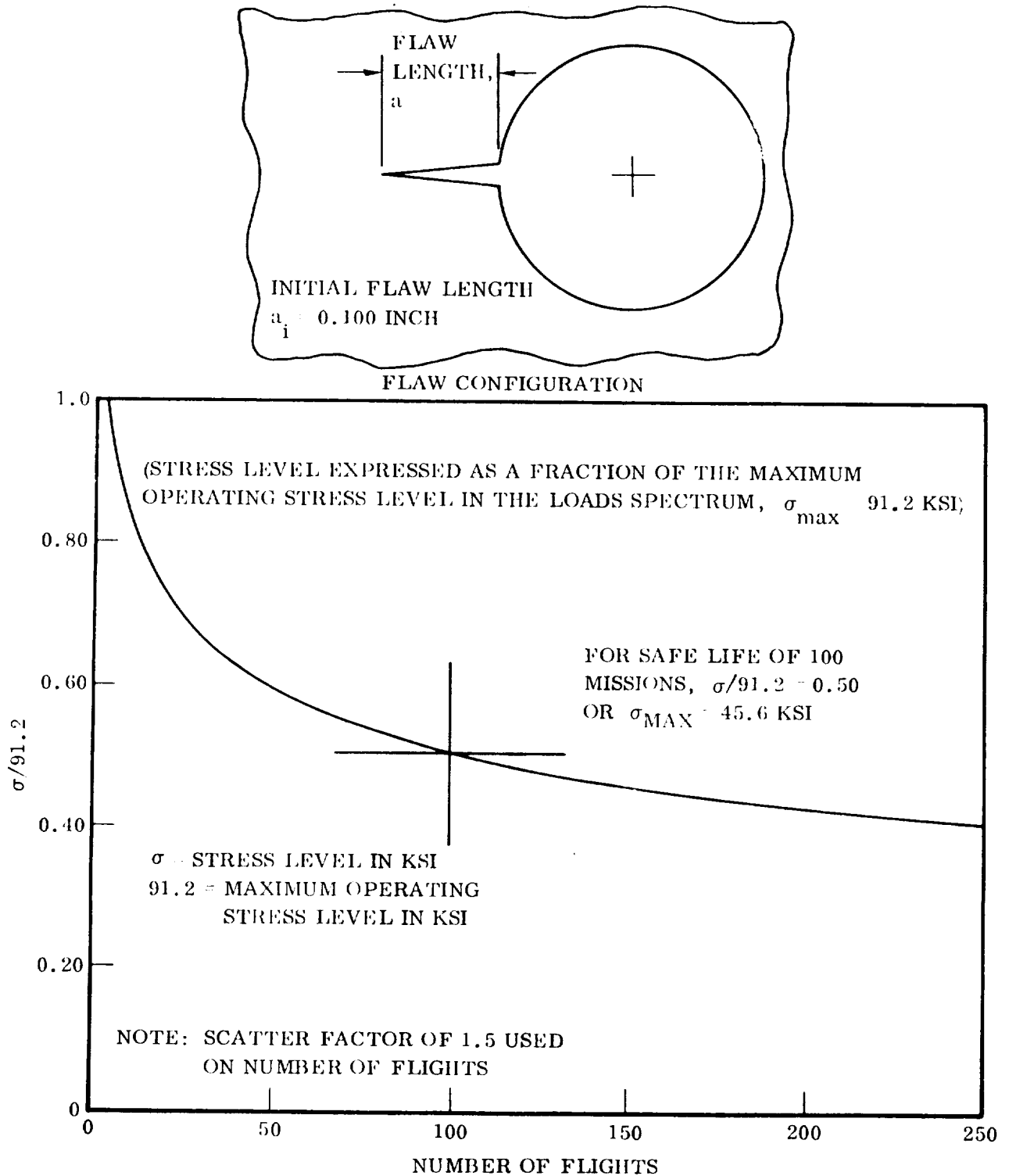


Figure 3-33. Allowable Maximum Operating Stress Level versus the Number of Flights to Failure (Safe-Life) for the Titanium Wing Spar Caps

The vertical tail loading spectrum experienced by the flaw configuration shown in the sketch is essentially the same spectrum that was used in the fatigue life determination shown in Tables 3-22 and 3-23. The only change made was to reduce the spectrum, which is for 100 missions, to a spectrum for only one mission. The results of this modification and the final vertical tail loading spectrum are listed in Table 3-27.

Table 3-27. Vertical Tail Loading Spectrum

Flight Phase	Mean Stress (ksi)	Alternating Stress (ksi)	Cycles per Flight (Unless Otherwise Noted)
Ascent	0.000	1.394	900
		2.584	90
		3.740	9
		4.930	1
		6.120	1 cycle every 10 flights
		3.842	900
		7.480	90
		11.084	9
		14.790	1
		18.530	1 cycle every 10 flights
		6.460	900
		12.614	90
		18.700	9
		24.820	1
		30.940	1 cycle every 10 flights
		4.692	900
		8.908	90
		13.192	9
Ascent	0.000	17.374	1

Table 3-27. Vertical Tail Loading Spectrum (Cont'd)

Flight Phase	Mean Stress (ksi)	Alternating Stress (ksi)	Cycles per Flight (Unless Otherwise Noted)
Ascent	0.000	21.726	1 cycle every 10 flights
		3.094	900
		6.256	90
		9.384	9
		12.444	1
		15.470	1 cycle every 10 flights
		1.972	900
		3.876	90
		5.644	9
		7.344	1
		9.180	1 cycle every 10 flights
		0.884	900
		1.224	90
		1.700	9
		2.210	1
Ascent	0.000	2.686	1 cycle every 10 flights
Cruise/ Landing	0.000	7.140	1800
		9.078	180
		10.948	18
		12.920	2
Cruise/ Landing	0.000	14.824	2 cycles every 10 flights

The crack growth studies were done on the vertical tail assuming the structure was maintained at room temperature. Thus room temperature properties were assumed and crack growth rate curves for Ti-6Al-4V annealed titanium base metal at room temperature were used in the flaw propagation computer program.

The equation for the maximum stress intensity factor for a through crack of length  $2c$  is:

$$K_I = \frac{\sigma \sqrt{\pi} \sqrt{2c}}{\sqrt{2 - (\sigma/\sigma_y)^2}} \quad (\text{Reference 10, Page 28})$$

where

$\sigma$  = applied stress

$\sigma_y$  = tensile yield stress

The critical value of the material toughness parameter,  $K_{Ic}$ , used here for the Ti-6Al-4V annealed titanium base metal at room temperature was  $K_{Ic} = 78.0 \text{ ksi } \sqrt{\text{inch}}$ . (Reference 8, Figure 35, Page 89.) The tensile yield stress was  $\sigma_y = 120.0 \text{ ksi}$ . The maximum operating stress in the vertical tail can be found from the spectrum to be  $\sigma = 30.940 \text{ ksi}$ . Substituting all these values into the stress intensity factor equation results in:

$$78.0 = \frac{30.940 \sqrt{\pi} \sqrt{(2c)_{cr}}}{\sqrt{2 - (30.940/120.0)^2}}$$

This equation can be solved for the critical value of  $2c$ , which turns out to be  $(2c)_{cr} = 3.9115 \text{ inches}$ .

Under the influence of the applied loading spectrum, it took 534 flights for the initial flaw of size  $(2c)_i = 1.00 \text{ inch}$  to grow to the critical flaw size of  $(2c)_{cr} = 3.9115 \text{ inches}$ . Note here that a scatter factor of 1.5 has been used on the number of flights to failure. A plot of flaw size versus flights to failure can be found in Figure 3-34.

**3.3.6 THRUST BEAM CAP SAFE-LIFE ANALYSIS.** For the thrust structure beams, as for the wing spar caps, a safe-life analysis was carried out using two types of initial flaws: a corner crack, and a crack emanating from a fastener hole.

The thrust structure loading spectrum used in the safe-life analysis is the same as that used in the fatigue life determination and shown in Table 3-24.

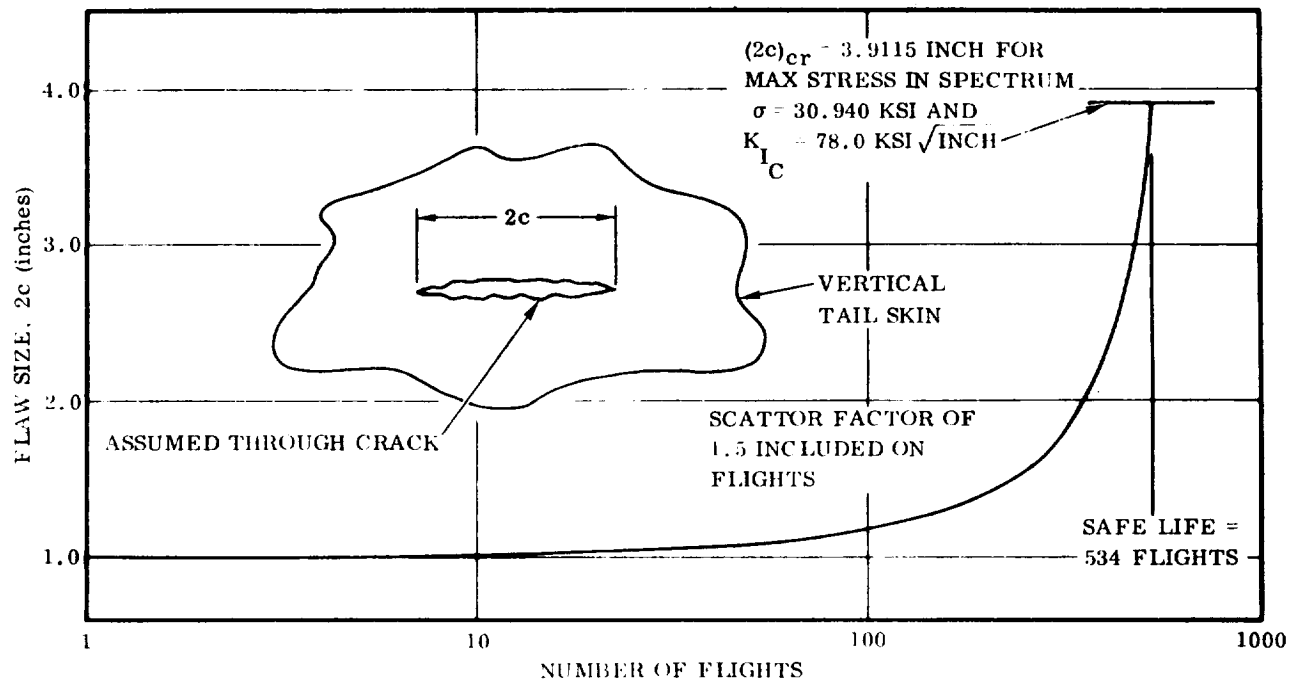
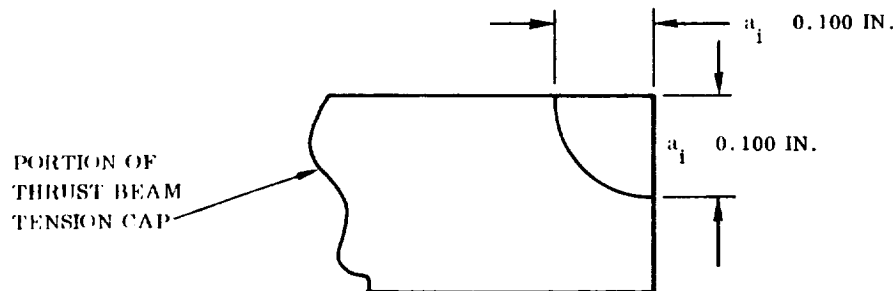


Figure 3-34. Crack Growth in the Vertical Tail Skin

3.3.6.1 Corner Crack. In the analysis of the thrust structure, one of the thrust beam tension caps was assumed to contain a corner crack of an initial size of 0.1 inch (see sketch). This initial size was chosen based on a judgment of the capability of nondestructive evaluation.



The crack growth studies were done on the thrust structure assuming it was maintained at room temperature. Thus room temperature properties were assumed, and crack growth rate curves for Ti-6Al-4V annealed titanium base metal at room temperature were used in the flaw propagation computer program.

The equation for the maximum stress intensity factor for a corner crack is

$$K_I = \frac{\sigma \sqrt{\pi a} (0.705)}{\sqrt{1 - 0.177 (\sigma/\sigma_Y)^2}}$$

(Reference 3, Equation VII-7 modified to account for the plastic zone correction)

$\sigma$  = applied stress

$\sigma_Y$  = yield stress

$a$  = flaw size

The critical value of the material toughness parameter,  $K_{Ic}$ , used here for the Ti-6Al-4V annealed titanium base metal at room temperature was  $K_{Ic} = 78.0 \text{ ksi } \sqrt{\text{inch}}$  (Reference 8, Figure 35, Page 89). The tensile yield stress used was  $\sigma_Y = 120.0 \text{ ksi}$ . The maximum operating stress occurring in the thrust beam cap can be found from the spectrum to be  $= 92.9 \text{ ksi}$ . Substituting all these values into the stress intensity factor equation results in

$$78.0 = \frac{92.9 \sqrt{\pi a_{cr}} (0.705)}{\sqrt{1 - 0.177 (92.9/120.0)^2}}$$

This equation can be solved for the critical value of 'a', which turns out to be  $a_{cr} = 0.4036 \text{ inch}$ .

Under the influence of the applied loading spectrum, it took 1555 flights for the initial flaw of size  $a_i = 0.100 \text{ inch}$  to grow to the critical flaw size of  $a_{cr} = 0.4036 \text{ inch}$ . Figure 3-35 is a plot of flaw size versus flights. A scatter factor of 1.5 was used on the number of flights to failure.

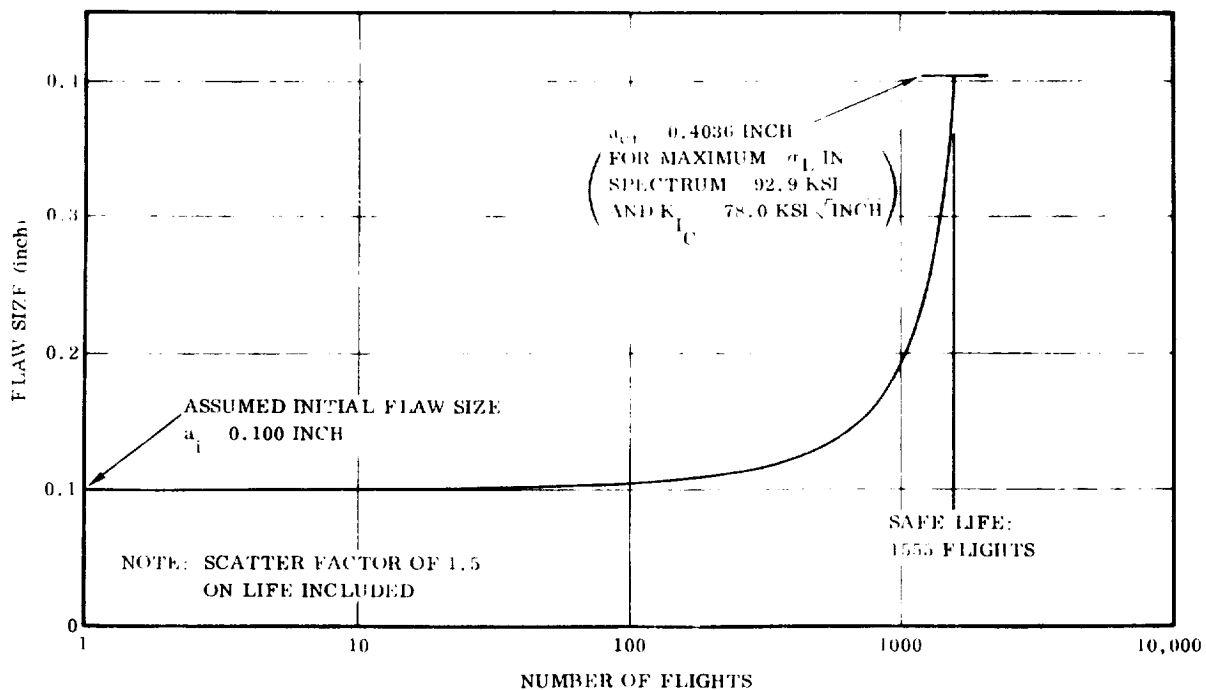


Figure 3-35. Crack Growth in the Titanium Thrust Beam Caps (Flaw Configuration - Corner Crack)



3.3.6.2 Crack Emanating from Hole. The flaw configuration and method of analysis for determining the growth of a crack emanating from a hole is the same as was used in the wing spar cap safe-life analysis and shown on Pages 191 through 192.

The maximum operating stress is found from the applied loading spectrum to be  $\sigma = 92.9$  ksi. Substituting this stress and the appropriate material properties into the equation for the stress intensity factor for a crack emanating from a hole results in the following expression:

$$78.0 = \frac{(92.9) \sqrt{\pi} \sqrt{a_{cr}}}{\sqrt{1 - 0.177 (92.9/120.0)^2}} \left[ 1.0 + 2.0 e^{(-18.42 a_{cr})} \right]$$

This expression is solved by a trial and error method for the critical value of 'a', which turns out to be  $a_{cr} = 0.1694$  inch.

Under the influence of the applied loading spectrum, it took 101 flights for the initial flaw ( $a_i = 0.100$  inch) to grow to the critical flaw size ( $a_{cr} = 0.1694$  inch). Note here that a scatter factor of 1.5 was used on the number of flights to failure. Figure 3-36 is a plot of flaw size versus flights.

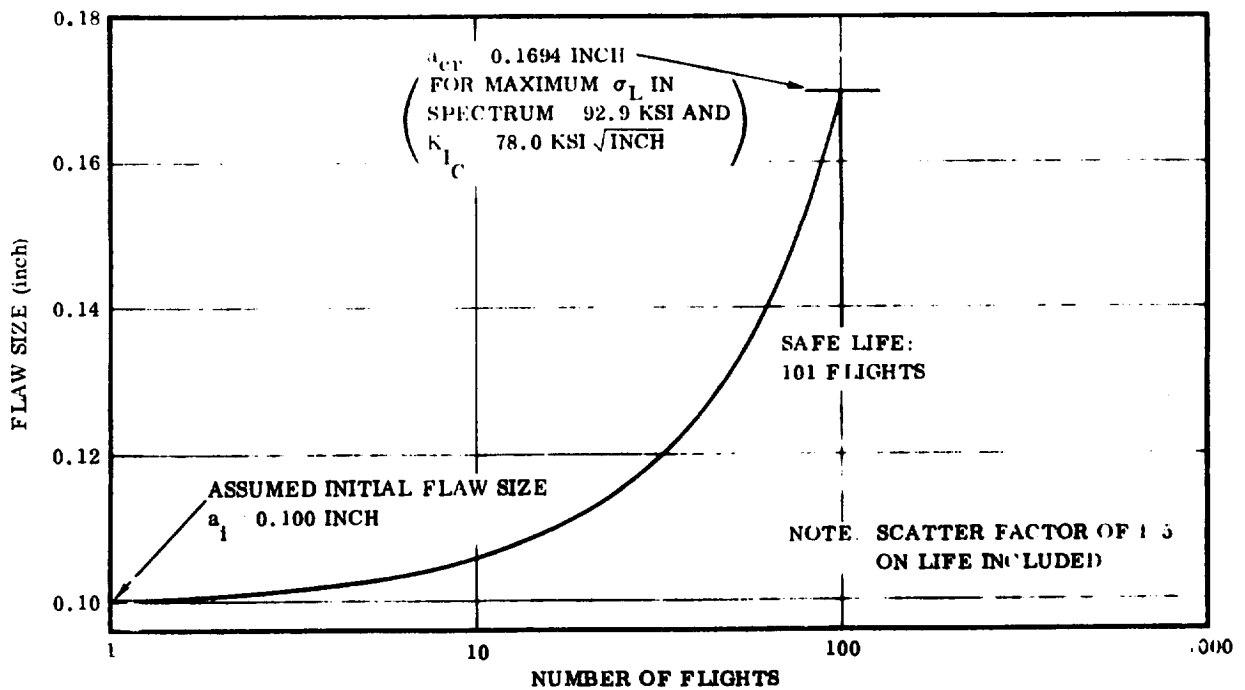



Figure 3-36. Crack Growth in the Titanium Thrust Beam Caps (Flow Configuration — Crack Emanating from a Hole)

**3.3.7 AFT ORBITER SUPPORT FRAME SAFE-LIFE ANALYSIS.** In the analysis of the aft orbiter support frame, one of the frame flanges was assumed to contain a corner crack of an initial size of 0.1 inch, or a crack having a length of 0.1 inch emanating from a hole. This initial size was chosen based on a judgment of the capability of nondestructive evaluation.

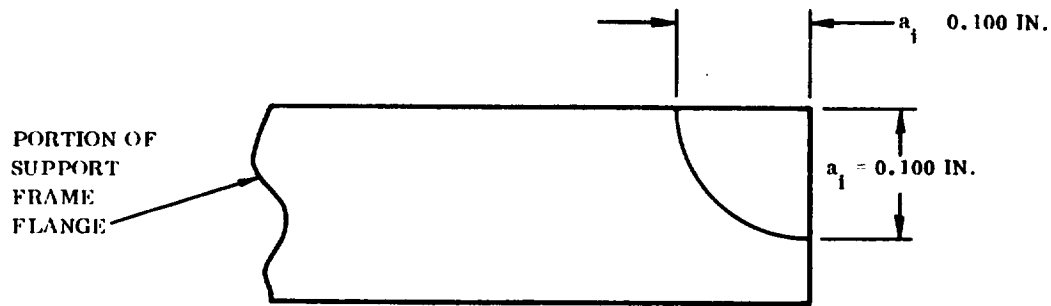
The aft orbiter attachment frame loading spectrum experienced by this flaw configuration is essentially the same spectrum that was used in the safe-life determination for fatigue crack initiation listed in Table 3-25. The only change made was to reduce the spectrum, which is for 100 missions, to a spectrum for only one mission. The results of this modification and the final aft orbiter support frame loading spectrum are listed in Table 3-28.

The crack growth studies were done on the aft orbiter support frame assuming the structure was maintained at room temperature. Thus room temperature properties were assumed and crack growth rate curves for 2219-T87 aluminum base metal at room temperature were used in the flaw propagation computer program.

**Table 3-28. Aft Orbiter Support Frame Loading Spectrum**

Mean Stress (ksi)	Alternating Stress (ksi)	Cvcles per Flight (Unless Otherwise Noted)
12.000	1.000	900
	2.000	90
	2.000	9
	4.000	1
	6.000	1 cycle every 10 flights
	3.000	900
	5.000	90
	9.000	9
	14.000	1
	20.000	1 cycle every 10 flights
12.000		

### 3.3.7.1 Corner Crack



The equation for the maximum stress intensity factor for a corner crack is

$$K_I = \frac{\sigma \sqrt{\pi a} (0.705)}{\sqrt{1 - 0.177 (\sigma/\sigma_y)^2}} \quad \text{(Reference 3, Equation VII-7 modified to account for the plastic zone correction).}$$

$\sigma$  = applied stress

$\sigma_y$  = tensile yield stress

$a$  = flaw size

The critical value of the material toughness parameter,  $K_{Ic}$ , used here for the 2219-T87 aluminum base metal at room temperature was  $K_{Ic} = 32.0 \text{ ksi } \sqrt{\text{inch}}$  (Reference 6, Figure 52, lower curve). The tensile yield stress used was  $\sigma_y = 51.0 \text{ ksi}$ . The maximum operating stress occurring in the support frame can be found from the spectrum to be  $\sigma = 32.000 \text{ ksi}$ .

Substituting all these values into the stress intensity factor equation results in

$$32.0 = \frac{32.000 \sqrt{\pi a_{cr}} (0.705)}{\sqrt{1 - 0.177 (32.000/51.000)^2}}$$

This equation can be solved for the critical value of 'a', which turns out to be  $a_{cr} = 0.5958 \text{ inch}$ .

Under the influence of the applied loading spectrum, the initial flaw of size  $a = 0.100 \text{ inch}$  grew only  $0.00004 \text{ inch}$  in 4000 flights. Consequently, the safe-life of this structural component can be considered to be extremely large.

3.3.7.2 Crack Emanating from Hole. The loading spectrum, material properties and maximum operating stress will be the same as those used in the crack growth analysis of a corner crack, above. Substituting the appropriate values into the equation for the stress intensity factor for a crack emanating from a hole results in the following expression:

$$32.0 = \frac{32.0 \sqrt{\pi} \sqrt{a_{cr}}}{\sqrt{1 - 0.177 (32.0/51.0)^2}} \left[ 1.0 + 2.0 e^{(-18.42 a_{cr})} \right]$$

This expression is solved by a trial and error method for the critical value of  $a_{cr}$  which turns out to be  $a_{cr} = 0.29063$  inch.

Under the influence of the applied loading spectrum, the initial flaw ( $a_i = 0.100$  inch) grew 0.01815 inch to  $a = 0.11815$  inch in 2667 flights, using a scatter factor of 1.0 on the number of flights to failure.

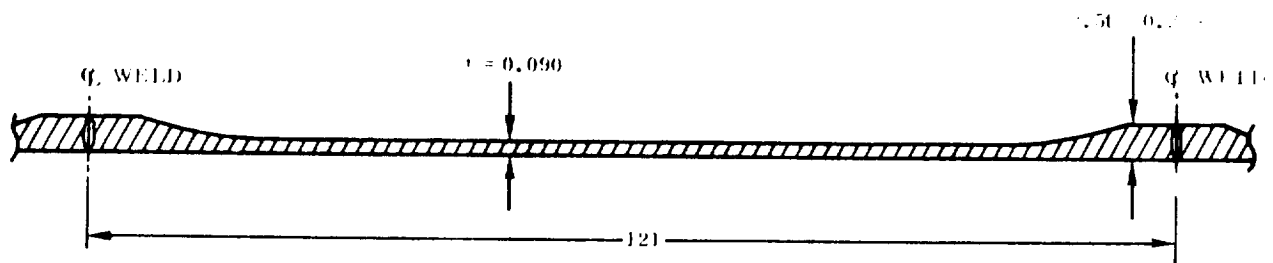
Since the initial flaw of size 0.100 inch grew only 0.01815 inch in 2667 flights, and since the critical flaw size for this structural component has been shown to be  $a_{cr} = 0.29063$  inch, the safe-life of this structural component can be considered to be extremely large.

### 3.4 FAIL-SAFE ANALYSIS

The damage tolerance of each of the selected components is analytically determined below, as a measure of its fail-safe capability. Two criteria are used in judging adequacy of fail-safe design:

- a. In structure composed of a number of discrete elements (e.g., the wing box) a crack can proceed to the point of complete failure of one principal member. The remaining structure must possess a residual strength capability of carrying critical limit design load without failure.
- b. In monolithic structure (e.g., the integrally stiffened vertical tail box) structure arrest can be provided by integral stiffeners, tear straps or other means so that a rapidly propagating crack is arrested at such length as to make detection certain prior to the next flight by normal preflight inspections, but not so long as to degrade residual strength to an unacceptable level.

3.4.1 FAIL-SAFE ANALYSIS - LO<sub>2</sub> TANK SKIN UNDER INTERNAL PRESSURE. A longitudinal section through the tank skin was taken at the upper centerline just aft of the forward dome equator, for analysis of fail-safe capability.



An initial flaw was assumed in the form of a through crack in the center of the panel. Since the weld and frame lands are so widely spaced, the tank skin panel was assumed to be of infinite width. Other assumptions were:

- Material is 2219-T87.
- Temperature is room temperature.
- Gross hoop stress is 44.0 ksi, resulting from maximum relief valve pressure (see Table 3-16).

Determination of Critical Hoop Stress for the Onset of Crack Instability:

$$\sigma_c = \frac{K_c}{\sqrt{\pi a_o + \frac{K_c^2}{2\sigma_{yB}} \left(1 + C \frac{a_o}{R}\right)}} \quad (\text{Equation IX-14 of Reference 3})$$

where

$a_o$  = initial crack half length

$K_c$  = critical stress intensity factor, assumed as  $2 K_{Ic} = 64 \text{ ksi } \sqrt{\text{inch}}$

$C$  = bulge correction, shown as 9.5 for 2024-T3 in Table XVI of Reference 3. This value is used here for 2219-T87

$R$  = radius of curvature = 198 inches

$\sigma_{yB}$  = material yield strength in a 2:1 biaxial stress field, assumed to be  $1.25 F_{ty}$  or 64 ksi

Solution of the equation for a range of values of  $a_o$  gives values of  $\sigma_c$  that are plotted as  $\sigma$  versus  $2a$  in Figure 3-38. They indicate a critical initial crack length of slightly less than one inch at a hoop stress of 44 ksi.

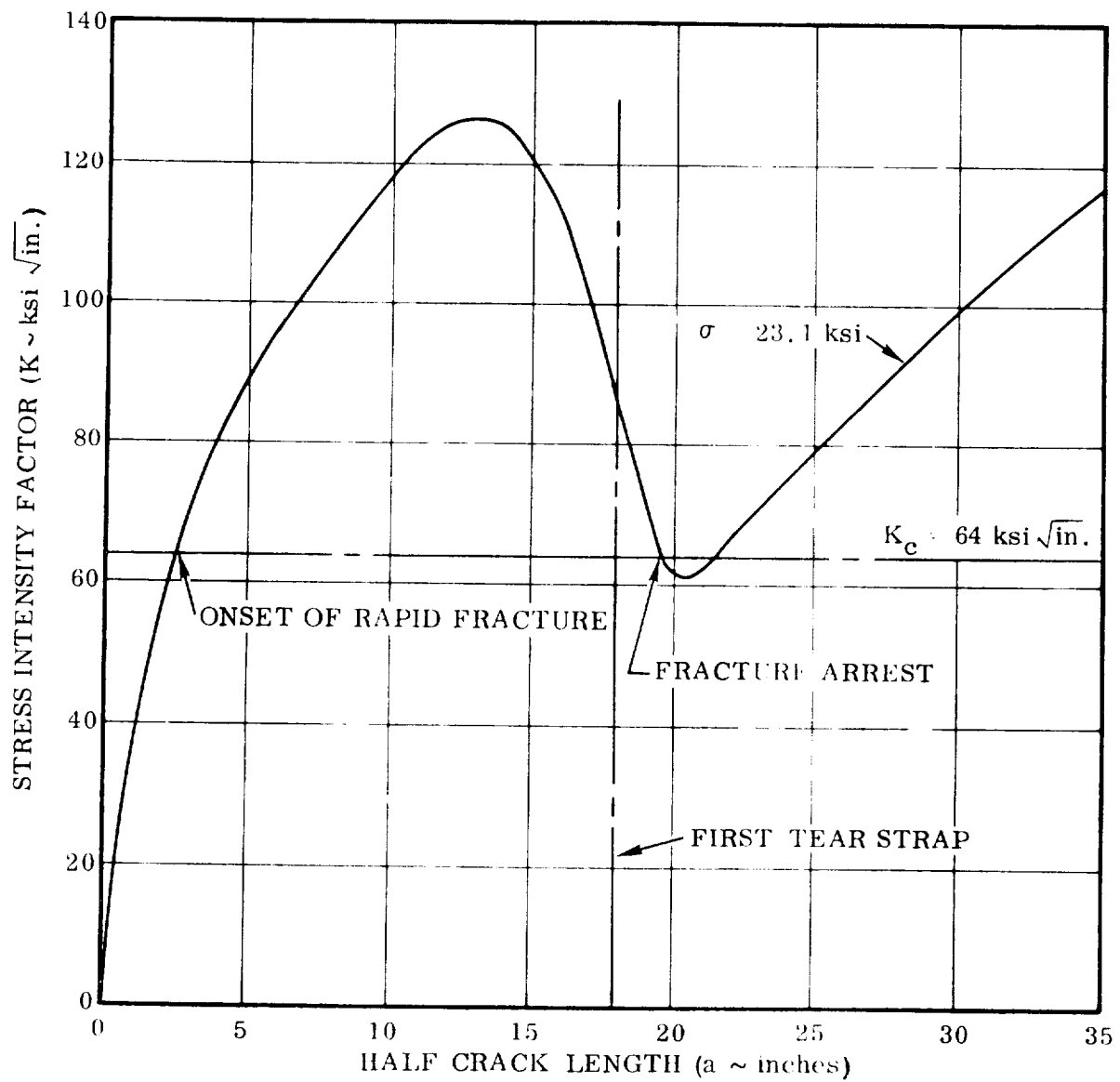


Figure 3-37.  $\text{LO}_2$  Tank Crack Arrest Effectiveness of Graphite/Epoxy Tear Straps, 36-Inch Strap Spacing

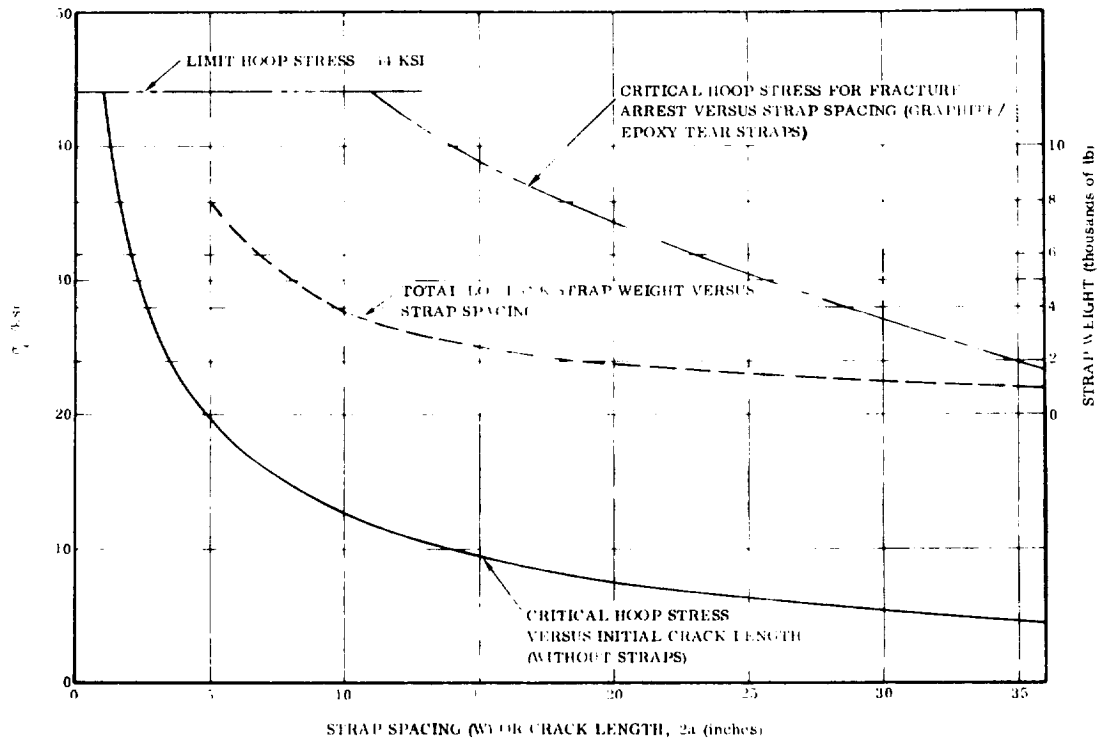


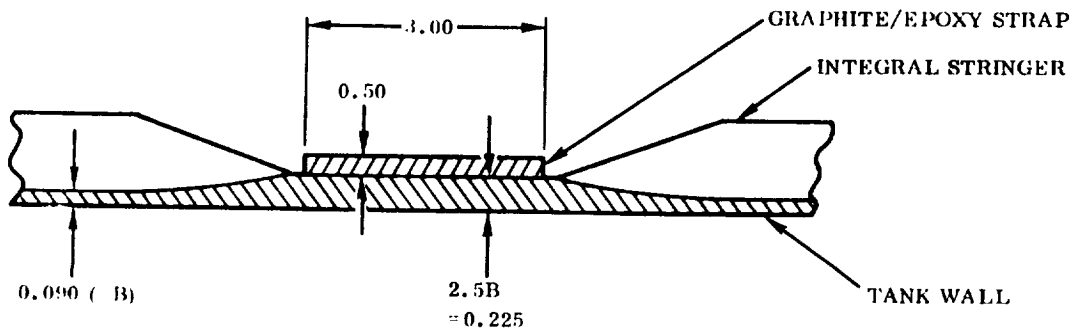
Figure 3-38. LO<sub>2</sub> Tank Crack Arrest Effectiveness of Graphite/Epoxy Tear Straps

In an effort to increase the critical crack length at this gross stress and to evaluate fail-safe tank concepts, crack arresters in the form of graphite/epoxy straps were tried. The straps were assumed to have a 0.50 by 3.00-inch section of HT-S/X904 unidirectional graphite/epoxy with the following properties:

$$F_{tu} = 168 \text{ ksi}$$

$$E = 20 \text{ ksi} \times 10^3$$

#### Section at Strap



Determination of the effectiveness of the Graphite/Epoxy tear straps to arrest unstable cracks is evaluated by the following method for various strap spacings and hoop stress levels. The method is:

- (1) The applied stress intensity for a centrally located crack of variable length between the straps is determined by the method of Reference 11 which accounts for the presence of straps where:

$$K = C \sigma \sqrt{\pi a}$$

C = stress intensity correction factor

A typical plot of applied stress intensity versus crack size is presented in Figure 3-37.

- (2) It is hypothesized that the stress level or strap spacing which causes the applied stress intensity curve to fall below the critical stress intensity factor ( $K_{IC}$ ) of the skin panel (i.e., fracture toughness) will cause dynamic fracture arrest and a fail safe structural arrangement. This condition is illustrated in Figure 3-37. The values of strap spacings and stress levels which satisfy this fracture arrest hypothesis are plotted in Figure 3-38.

Also plotted in Figure 3-38 is the total weight of straps on the  $LO_2$  tank for the strap spacings shown. The curve shows that the weight penalty required to provide fracture arrest at a hoop design stress of 44 ksi is 3450 pounds. Since this is a 19% weight penalty on the  $LO_2$  tank, it is considered impractical to use these crack arrest straps.

#### 3.4.2 FAIL-SAFE ANALYSIS – $LH_2$ TANK SKIN UNDER INTERNAL PRESSURE.

The general constructional features of the  $LH_2$  tank are similar to those of the  $LO_2$  tank described on Page 206. The assumptions for the fail-safe analysis were the same except for the gross hoop stress, which is 40.1 psi per Table 3-17, and the skin thickness, which is 0.116 inch with 0.290 inch land thickness.

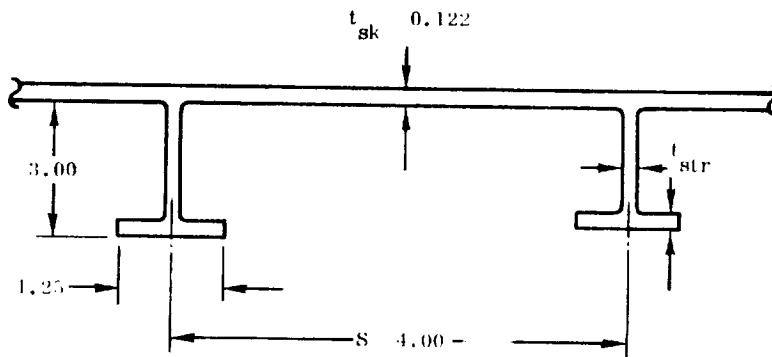
For the tank without tear straps, the critical hoop stress is the same as for the  $LO_2$  tank (see Page 207), for a given initial crack length. If tear straps were added similar to those shown for the  $LO_2$  tank on Page 209, the results would be similar to the  $LO_2$  tank. A check was therefore made on increasing the size of the straps from 1/2 by 3 inches to 1 by 3 inches.



The critical hoop stresses for dynamic fracture arrest for various tear strap spacings were calculated using the same method as for the LO<sub>2</sub> tank and the resulting curve of crack arrest effectiveness of the 1 by 3 inch graphite/epoxy straps as shown in Figure 3-39. A plot of strap weight versus spacing is also shown. It can be seen, by comparing the upper curve of Figure 3-38 for the LO<sub>2</sub> tank with the equivalent curve of Figure 3-39 that the effectiveness of the graphite/epoxy tear straps was not significantly enhanced by a doubling of the cross-sectional area of the straps. It can also be seen from the strap weight curve that the straps are extremely heavy; at the strap spacing required for the limit stress of 40.1 ksi, the weight penalty would be over 20,000 pounds.

### 3.4.3 FAIL-SAFE ANALYSIS — LH<sub>2</sub> TANK SKIN UNDER LONGITUDINAL LOADS.

Taking a transverse section through the integrally stiffened tank skin in the region of the bottom centerline at Station 2600, the following configuration is obtained.



Using the method given in Reference 11:

$$\begin{aligned} \text{Percent stiffening} &= \frac{100}{1 + \frac{A_{sk}}{A_{str}}} \\ &= \frac{100}{1 + \frac{0.488}{0.264}} = 35.1\% \end{aligned}$$

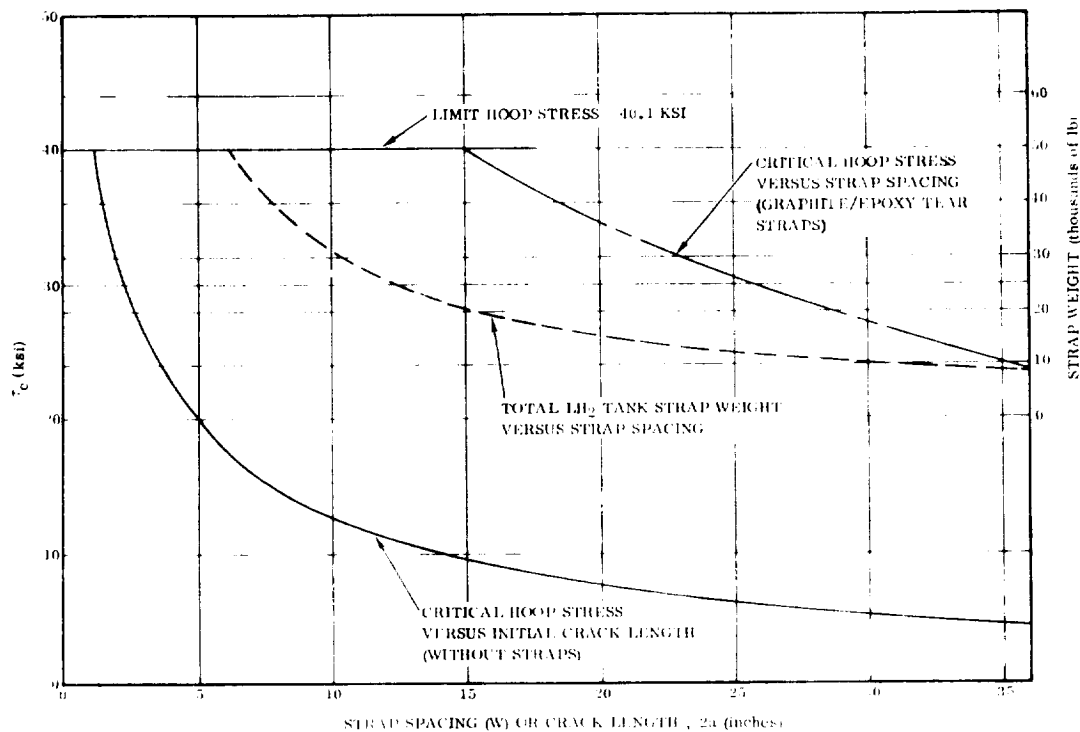


Figure 3-39. LH<sub>2</sub> Tank Crack Arrest Effectiveness of Graphite/Epoxy Tear Straps

Values of the stress intensity factor,  $K$ , are computed by use of the formula

$$K = C \sigma \sqrt{\pi a}$$

where

$C$  = stress intensity correction factor

$\sigma$  = gross stress level

$a$  = crack half length

and  $C$  is from Figure 3-41. The resulting values of  $K$  are plotted versus crack length in Figure 3-40. For this curve it is assumed that the stringer is not completely severed until the crack tip in the sheet has advanced a distance equal to the height of the stringer past the centerline of the stringer. Between the edge of the stringer and the point at which the stringer is assumed to be completely severed,  $K$  is assumed to increase linearly with the crack length,  $a$ , as shown.

Figure 3-40 shows that once rapid fracture has begun for a transverse crack under longitudinal loading the stress intensity doesn't go below the critical value,  $K_c$ , again. Therefore, once rapid fracture begins, it progresses to complete failure and the LH<sub>2</sub> tank therefore has no failsafe capability for transverse cracks under longitudinal loads.

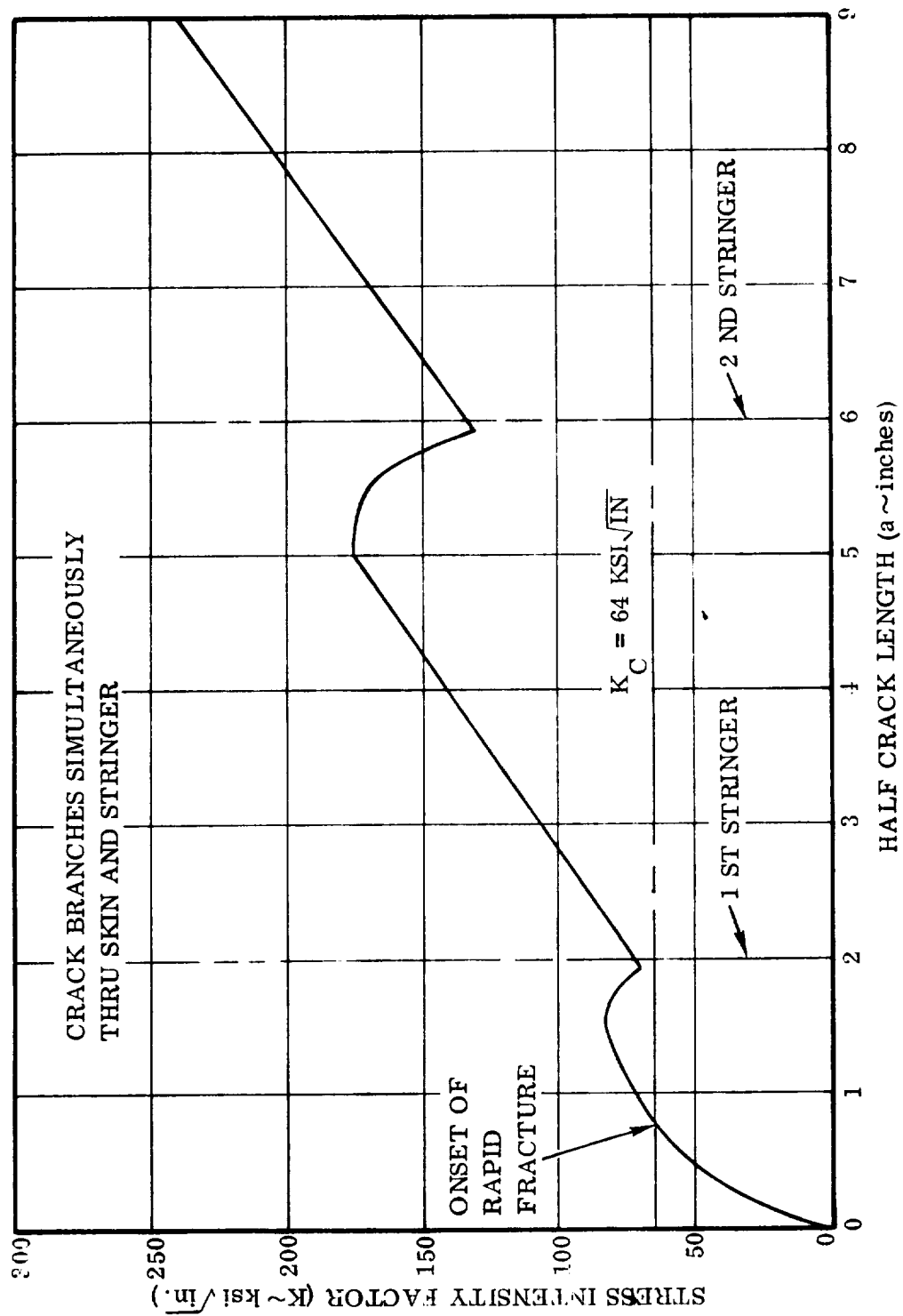


Figure 3-40.  $LH_{\frac{1}{2}}$  Crack Arrestment by Integral Stringers for Longitudinal Loading

**3.4.4 B-9U DELTA WING FAIL-SAFE ANALYSIS.** Fail-safe strength of the B-9U wing was evaluated analytically with the aid of a finite element computer program. The idealized structural model used in the fail-safe analysis is the same as that used in the sizing calculations and shown in Figure 3-15. Major tension or tension/shear members of the model were analytically "failed," one at a time, and limit design loads were applied to the weakened structure. Considerable beef-up was required to make the structure adequate for design limit load. Total added weight was 534 pounds or 2.16% of the total ultimate strength model weight of 24,660 pounds.

The ascent loading condition W-1 (maximum  $\alpha q$  with headwinds) that produces maximum tension in the lower surface was used for the fail-safe analysis.

Structural members "failed," one at a time, were: 1) the spar lower cap between Stations 207 and 267 of Spars 2, 3, 4 and 5; 2) the spar shear diagonal between Stations 207 and 267 of Spar 3; 3) the spar lower cap and web between Stations 267 and 327 of Spars 3 and 4, and 4) the spar lower cap and web of Spar 4 between Stations 447 and 507. In the engine area, where spar shear is carried by webs welded to upper and lower caps, a lower cap/web failure was treated as a single failure with a weld crack assumed to propagate in two directions (i.e., through the tension cap and through the shear web). Note that this type failure appeared only slightly more critical than a simple lower cap failure inboard of the engine area.

Results of the fail-safe analysis are listed in Tables 3-29 and 3-30. Table 3-29 compares wing internal load distribution for ultimate load with the load distribution for limit load with a major tension member failed. The comparison is confined to that part of the wing where the redistribution of limit load due to a single member failure results in loads higher than those experienced by ultimate load on an intact wing. Table 3-30 lists: 1) margins of safety due to fail-safe redistribution of limit load on a structure sized for ultimate load, 2) required increase of bar area (or plate thickness) for zero margins of safety on members under fail-safe limit load redistribution, and 3) weight increases associated with the added material.

Table 3-30 shows a total weight increase of 534 pounds for the requirement that the wing carry limit design load with any reasonable in-service structural failure. Of the 534 pounds, 69% is in spar caps, 21% in spar diagonals, 6% in spar webs, and 4% in skins. All skins requiring beef-up (three per side) were originally 0.016 gage for ultimate requirements. This gage is probably unrealistically thin when handling, sonic fatigue, and thermal stress requirements are considered. Maximum gage increase was 0.009 for a total gage of  $0.016 + 0.009 = 0.025$  inch. therefore, it is doubtful that any skin beef-up would be needed for fail-safe primary loading requirements.

Table 3-29. Internal Loads — Ultimate Versus Fail Safe — B-9U Wing

Member		Member Loads					
					Fail-Safe Failed Elements 90-102 & 89-90- 102-101 (lb)	Failed Elements 92-104 & 91-92- 104-103 (lb)	Failed Elements 58-68 & 57- 58-68-67 (lb)
		Ultimate (lb)	Failed Element 102-112 (lb)	Failed Element 104-114 (lb)			
63-73	Spar 2 Upper Cap	-354,199	-281,238	-273,932	-278,766	-271,280	-276,710
73-87		-497,417	-413,813	-376,286	-416,028	-373,735	-380,104
87-99		-628,314	-524,138	-476,391	-544,319	-478,988	-467,626
99-109		-774,735	-580,767	-594,141	-603,342	-588,782	-562,813
109-119		-769,428	-562,900	-588,978	-579,983	-584,184	-556,712
64-74	Spar 2 Lower Cap	344,726	382,984	279,594	<u>405,867</u>	283,011	266,205
74-88		473,172	557,997	386,942	<u>599,488</u>	390,504	360,845
88-100		580,829	754,527	494,338	<u>766,134</u>	481,679	434,472
100-110		680,139	<u>893,780</u>	564,003	849,089	554,615	501,286
110-120		746,986	<u>856,912</u>	612,343	765,105	601,494	544,571
63-74	Spar 2 Truss Diag's	77,987	104,763	43,457	<u>112,634</u>	44,223	61,353
73-88		98,715	130,333	59,082	<u>152,653</u>	61,161	72,975
87-100		110,340	127,462	63,901	<u>176,297</u>	69,903	78,130
99-110		162,279	62,027	125,919	86,582	111,255	108,811
109-120		50,668	21,085	40,882	22,966	40,799	36,594
43-55	Spar 3 Upper Cap	-528,592	-370,866	-417,546	-381,026	-418,886	-399,785
55-65		-641,513	-465,418	-497,600	-482,734	-496,145	-495,060
65-75		-842,087	-587,695	-674,859	-609,472	-665,296	-643,451
75-89		-1,046,631	-682,779	-865,611	-698,986	-842,755	-764,095
89-101		-1,256,888	-765,161	-1,050,835	-750,035	-1,026,506	-887,269
101-111		-1,590,023	-995,483	-1,275,347	-944,438	-1,279,230	-1,096,750
111-121		-1,537,001	-993,688	-1,210,439	-953,750	-1,215,727	-1,061,835
44-56	Spar 3 Lower Cap	488,278	276,724	450,650	280,787	466,883	417,658
56-66		683,280	318,786	655,159	316,922	675,788	603,218
66-76		731,348	249,463	713,915	233,734	733,795	637,414
76-90		817,553	165,112	812,416	122,890	835,242	677,512

Table 3-29. Internal Loads — Ultimate Versus Fail Safe — B-9U Wing, Contd

Member		Member Loads					
		Ultimate (lb)	Fail-Safe				Failed Elements 58-68 & 57- 58-68-67 (lb)
			Failed Element 102-112 (lb)	Failed Element 104-114 (lb)	Failed Elements 90-102 & 89-90- 102-101 (lb)	Failed Elements 92-104 & 91-92- 104-103 (lb)	
90-102	Spar 3	913,936	63,198	903,960	0	950,683	725,665
102-112	Lower	984,374	0	994,711	39,481	965,102	761,635
112-122	Cap	1,179,282	212,045	1,087,060	323,493	1,004,734	869,468
43-56~	Diag	173,274	90,455	167,025	89,083	167,676	143,874
55-56-66-65	Spar	3,199(1)	1,414(1)	3,267(1)	1,329(1)	3,240(1)	2,866(1)
65-66-76-75		3,471(1)	1,122(1)	3,816(1)	907(1)	3,772(1)	2,108(1)
75-76-90-89		3,540(1)	814(1)	4,003(1)	328(1)	3,953(1)	2,002(1)
89- -101		3,625(1)	996(1)	3,769(1)	0(1)	3,847(1)	2,132(1)
101-112	Truss	338,957	259,118	224,912	227,263	257,611	214,704
111-122	Diag	66,842	73,865	35,034	71,509	38,038	45,605
45-57	Spar 4	-546,210	-383,012	-376,980	-376,685	-386,762	-366,689
57-67		-615,093	-420,090	-446,691	-409,497	-464,523	-386,686
67-77		-750,268	-519,456	-515,431	-502,112	-529,526	-449,000
77-91		-904,096	-642,663	-562,341	-623,832	-557,866	-578,471
91-103	Cap	-1,083,289	-789,176	-593,802	-790,184	-587,508	-723,816
103-113		-1,375,423	-1,003,112	-812,022	-1,030,636	-802,961	-947,346
113-123		-1,365,959	-981,314	-851,983	-1,005,879	-840,493	-939,664
46-58	Spar 4	247,467	225,522	6,333	217,837	-33,114	-16,146
58-68		399,349	365,110	-28,338	353,887	-99,125	0
68-78		687,190	576,154	53,305	569,783	-45,874	200,502
78-92		993,679	808,765	85,586	816,134	-44,716	474,391
92-104	Cap	1,318,270	1,056,206	84,617	1,096,882	0	752,421
104-114		1,457,074	1,177,657	0	1,188,325	164,581	889,401
114-124		1,487,248	1,186,034	159,092	1,161,699	450,694	956,022

Table 3-29. Internal Loads — Ultimate Versus Fail Safe — B-9U Wing, Contd

Member		Member Loads					
		Ultimate (lb)	Fail-Safe				
			Failed Element 102-112 (lb)	Failed Element 104-114 (lb)	Failed Elements 90-102 & 89-90- 102-101 (lb)	Failed Elements 92-104 & 91-92- 104-103 (lb)	Failed Elements 58-68 & 57- 58-68-67 (lb)
45-58 ~ Diag		87,227	80,842	-2,533	75,425	-14,733	4,458
57-58-68-67		2,327(1)	2,061(1)	284(1)	1,980(1)	31(1)	0
67-68-78-77		2,536(1)	2,448(1)	211(1)	2,438(1)	587(1)	1,972(1)
77-78-92-91		2,743(1)	2,752(1)	572(1)	2,938(1)	1,032(1)	2,388(1)
91-92-104-103		3,093(1)	2,906(1)	134(1)	3,634(1)	0	2,562(1)
103-114 } Truss		232,114	162,798	225,701	176,894	198,845	181,784
113-124 } Diag's		69,298	29,374	80,214	30,741	67,574	50,663
69-79		-367,143	-270,251	-157,854	-268,718	-183,944	-238,428
79-93 Spar 5		-467,591	-333,448	-264,572	-336,875	-332,019	289,319
93-105 Upper		-518,177	-383,219	-401,533	-394,563	-413,497	345,348
105-115 Cap		-659,747	-460,291	-412,639	-472,492	-408,899	435,002
115-125		-498,804	-336,421	-244,786	-346,210	-259,481	326,626
70-80		287,356	223,990	326,206	218,433	396,204	334,084
80-94 Spar 5		320,662	269,254	451,116	260,559	558,924	301,793
94-106 Lower		354,609	314,838	644,392	305,804	735,727	288,105
106-116 Cap		417,071	361,265	877,784	364,091	758,517	307,480
116-126		570,641	483,167	904,873	489,670	698,942	415,741
69-80		199,153	130,920	212,179	136,625	251,173	118,345
79-94 Spar 5		204,001	133,985	255,727	138,656	301,802	125,575
93-106 Truss		189,357	126,113	269,086	125,014	212,948	126,414
105-116 Diag's		255,098	185,261	118,626	179,028	120,140	184,415
115-126		-120,755	-93,957	-152,446	-95,340	-120,351	-84,573

Table 3-29. Internal Loads — Ultimate Versus Fail Safe — B-9U Wing, Contd

Member	Member Loads					
	Ultimate (lb)	Fail-Safe				
		Failed Element 102-112 (lb)	Failed Element 104-114 (lb)	Failed Elements 90-102 & 89-90- 102-101 (lb)	Failed Elements 92-104 & 91-92- 104-103 (lb)	Failed Elements 58-68 & 57- 58-68-67 (lb)
<b>Skins</b>						
73-87-89-75	1,659 <sup>(1)</sup>	1,008 <sup>(1)</sup>	1,518 <sup>(1)</sup>	817 <sup>(1)</sup>	1,546 <sup>(1)</sup>	1,159 <sup>(1)</sup>
74-88-90-76	2,029 <sup>(1)</sup>	2,370 <sup>(1)</sup>	2,315 <sup>(1)</sup>	<u>2,416</u> <sup>(1)</sup>	2,171 <sup>(1)</sup>	1,309 <sup>(1)</sup>
87-99-101-89	1,481 <sup>(1)</sup>	978 <sup>(1)</sup>	1,428 <sup>(1)</sup>	679 <sup>(1)</sup>	<u>1,503</u> <sup>(1)</sup>	1,001 <sup>(1)</sup>
88-100-102-90	2,095 <sup>(1)</sup>	<u>2,648</u> <sup>(1)</sup>	2,567 <sup>(1)</sup>	1,782 <sup>(1)</sup>	1,987 <sup>(1)</sup>	1,303 <sup>(1)</sup>
99-109-111-101	1,148 <sup>(1)</sup>	533 <sup>(1)</sup>	981 <sup>(1)</sup>	327 <sup>(1)</sup>	924 <sup>(1)</sup>	734 <sup>(1)</sup>
100-110-112-102	1,017 <sup>(1)</sup>	<u>1,248</u> <sup>(1)</sup>	494 <sup>(1)</sup>	836 <sup>(1)</sup>	1,100 <sup>(1)</sup>	651 <sup>(1)</sup>
75-89-91-77	1,347 <sup>(1)</sup>	1,457 <sup>(1)</sup>	559 <sup>(1)</sup>	<u>1,543</u> <sup>(1)</sup>	392 <sup>(1)</sup>	996 <sup>(1)</sup>
110-120-122-112	24 <sup>(1)</sup>	<u>1,576</u> <sup>(1)</sup>	659 <sup>(1)</sup>	1,371 <sup>(1)</sup>	368 <sup>(1)</sup>	55 <sup>(1)</sup>
89-101-103-91	1,257 <sup>(1)</sup>	<u>1,318</u> <sup>(1)</sup>	456 <sup>(1)</sup>	1,237 <sup>(1)</sup>	651 <sup>(1)</sup>	914 <sup>(1)</sup>
101-111-113-103	1,091 <sup>(1)</sup>	983 <sup>(1)</sup>	516 <sup>(1)</sup>	1,093 <sup>(1)</sup>	460 <sup>(1)</sup>	758 <sup>(1)</sup>
102-112-114-104	1,700 <sup>(1)</sup>	912 <sup>(1)</sup>	2,138 <sup>(1)</sup>	2,165 <sup>(1)</sup>	294 <sup>(1)</sup>	953 <sup>(1)</sup>
65-75-77-67	1,348 <sup>(1)</sup>	1,435 <sup>(1)</sup>	630 <sup>(1)</sup>	<u>1,539</u> <sup>(1)</sup>	460 <sup>(1)</sup>	1,027 <sup>(1)</sup>
112-122-124-114	570 <sup>(1)</sup>	1,094 <sup>(1)</sup>	<u>1,451</u> <sup>(1)</sup>	989 <sup>(1)</sup>	965 <sup>(1)</sup>	239 <sup>(1)</sup>
77-91-93-79	1,260 <sup>(1)</sup>	885 <sup>(1)</sup>	<u>1,720</u> <sup>(1)</sup>	827 <sup>(1)</sup>	1,570 <sup>(1)</sup>	839 <sup>(1)</sup>
78-92-94-80	2,320 <sup>(1)</sup>	1,128 <sup>(1)</sup>	733 <sup>(1)</sup>	1,258 <sup>(1)</sup>	751 <sup>(1)</sup>	2,080 <sup>(1)</sup>
91-103-105-93	1,154 <sup>(1)</sup>	848 <sup>(1)</sup>	992 <sup>(1)</sup>	623 <sup>(1)</sup>	<u>1,438</u> <sup>(1)</sup>	701 <sup>(1)</sup>
92-104-106-94	2,071 <sup>(1)</sup>	1,009 <sup>(1)</sup>	57 <sup>(1)</sup>	1,017 <sup>(1)</sup>	1,690 <sup>(1)</sup>	1,731 <sup>(1)</sup>
103-113-115-105	1,897 <sup>(1)</sup>	1,494 <sup>(1)</sup>	1,726 <sup>(1)</sup>	1,529 <sup>(1)</sup>	1,822 <sup>(1)</sup>	1,217 <sup>(1)</sup>
104-114-116-106	917 <sup>(1)</sup>	824 <sup>(1)</sup>	317 <sup>(1)</sup>	412 <sup>(1)</sup>	<u>3,174</u> <sup>(1)</sup>	977 <sup>(1)</sup>



Table 3-29. Internal Loads — Ultimate Versus Fail Safe — B-9U Wing, Contd

Member		Member Loads					
		Ultimate (lb)	Fail-Safe				
			Failed Element 102-112 (lb)	Failed Element 104-114 (lb)	Failed Elements 90-102 & 89-90- 102-101 (lb)	Failed Elements 92-104 & 91-92- 104-103 (lb)	Failed Elements 58-68 & 57- 58-68-67 (lb)
Skins							
55-65-67-57		1,393 <sup>(1)</sup>	1,390 <sup>(1)</sup>	745 <sup>(1)</sup>	<u>1,489</u> <sup>(1)</sup>	637 <sup>(1)</sup>	1,103 <sup>(1)</sup>
114-124-126-116		755 <sup>(1)</sup>	675 <sup>(1)</sup>	<u>2,027</u> <sup>(1)</sup>	497 <sup>(1)</sup>	1,392 <sup>(1)</sup>	340 <sup>(1)</sup>
43-55-57-45		1,995 <sup>(1)</sup>	1,590 <sup>(1)</sup>	1,432 <sup>(1)</sup>	1,666 <sup>(1)</sup>	1,400 <sup>(1)</sup>	1,485 <sup>(1)</sup>
44-56-58-46		2,775 <sup>(1)</sup>	1,499 <sup>(1)</sup>	2,852 <sup>(1)</sup>	1,531 <sup>(1)</sup>	<u>2,989</u> <sup>(1)</sup>	2,623 <sup>(1)</sup>
67-77-79-69		1,003 <sup>(1)</sup>	690 <sup>(1)</sup>	1,731 <sup>(1)</sup>	714 <sup>(1)</sup>	<u>1,794</u> <sup>(1)</sup>	904 <sup>(1)</sup>
68-78-80-70		2,059 <sup>(1)</sup>	1,001 <sup>(1)</sup>	1,068 <sup>(1)</sup>	1,129 <sup>(1)</sup>	904 <sup>(1)</sup>	<u>2,191</u> <sup>(1)</sup>
57-67-69-59		1,135 <sup>(1)</sup>	758 <sup>(1)</sup>	1,738 <sup>(1)</sup>	815	<u>1,908</u> <sup>(1)</sup>	1,218 <sup>(1)</sup>
58-68-70-60		2,149 <sup>(1)</sup>	1,141 <sup>(1)</sup>	1,433 <sup>(1)</sup>	1,257 <sup>(1)</sup>	1,330 <sup>(1)</sup>	<u>2,156</u> <sup>(1)</sup>
59-69	Spar 5	-263,923	-203,747	-85,067	-199,860	-85,133	-203,680
60-70	Caps	260,917	186,214	258,689	184,229	<u>300,192</u>	296,265
59-70 ~	Diag	181,866	120,609	167,789	125,253	191,049	<u>199,963</u>
47-59	Spar 5	-207,683	-164,768	-67,596	-160,649	-58,932	-131,085
48-60	Caps	223,745	150,512	204,146	151,286	227,955	<u>240,001</u>

Member		Member Loads			
		Ultimate (lb)	Fail-Safe		
			Failed Element 100-110 (lb)	Failed Element 106-116 (lb)	Failed Element 101-112 (lb)
99-110	} Truss	162,279 <sup>(1)</sup>	Not	-	<u>246,200</u> <sup>(1)</sup>
103-114		232,114 <sup>(1)</sup>	Critical	-	<u>259,200</u> <sup>(1)</sup>
78-92-94-80	} Skin	2,320 <sup>(1)</sup>		<u>2,461</u> <sup>(1)</sup>	-
92-104-106-94		2,071 <sup>(1)</sup>		<u>2,463</u> <sup>(1)</sup>	-

Notes:

(1) Designated values are shear flows in pounds per inch.

(2) Underlined values are maximum fail safe load of all cases considered.

**Table 3-30. Margins of Safety for Baseline Structure, and Area Increases  
for Fail-Safe Design, B-9U Delta Wing**

Member	Spar Caps			Spar Diagonals			Spar Webs			Skins		
	M.S.	Added Area (in <sup>2</sup> )	Added Weight (lb)	M.S.	Added Area (in <sup>2</sup> )	Added Weight (lb)	M.S.	Added Thickness (inch)	Added Weight (lb)	M.S.	Added Thickness (inch)	Added Weight (lb)
64-74	-0.15	0.51	5.19									
74-88	-0.21	1.05	10.67									
88-100	-0.24	1.55	15.74									
100-110	-0.24	1.78	18.22									
110-120	-0.13	0.92	6.40									
90-102	-0.04	0.31	3.15									
102-112	-0.01	0.30	3.07									
48-60	-0.07	0.13	1.30									
60-70	-0.13	0.33	3.30									
70-80	-0.17	0.90	9.00									
80-94	-0.43	1.98	19.80									
94-106	-0.52	3.18	31.80									
106-116	-0.53	3.83	38.60									
116-126	-0.35	2.62	18.29									
63-74				-0.31	0.29	3.86						
73-88				-0.35	0.45	6.32						
87-100				-0.37	0.35	8.07						
111-122				-0.07	0.04	0.53						
113-124				-0.14	0.09	1.06						
59-70				-0.04	0.07	0.81						
69-80				-0.17	0.35	4.09						
79-94				-0.29	0.33	8.70						
93-106				-0.26	0.38	7.05						
115-126				-0.17	0.21	2.22						
55-56-66-65							-0.01	0.001	0.68			
65-66-76-75							-0.09	0.004	2.96			
75-76-90-89							-0.11	0.005	3.95			
89-90-102-101							-0.05	0.003	2.50			
77-78-92-91							-0.08	0.003	1.98			
91-92-104-103							-0.16	0.007	4.81			
74-88-90-76										+0.40	0	0
87-99-101-89										+1.26	0	0
88-100-102-90										+0.28	0	0
100-110-112-102										+1.72	0	0
75-89-91-77										+1.20	0	0
110-120-122-112										-0.14	.003	2.98
89-101-103-91										+1.57	0	0
102-112-114-104										+0.56	0	0
65-75-77-67										+1.20	0	0
112-122-124-114										-0.07	.001	0.76
55-65-67-57										+1.28	0	0
44-56-58-46										+0.13	0	0
57-67-69-59										+0.78	0	0
58-68-70-60										+0.57	0	0
67-77-79-69										+0.89	0	0
68-78-80-70										+0.55	0	0
77-91-93-79										+0.97	0	0
91-103-105-93										+1.36	0	0
104-114-116-106										+0.07	0	0
114-124-126-116										-0.37	.008	6.86
78-92-94-80										+0.38	0	0
92-104-106-94										+0.38	0	0
99-110				-0.34	0.70	10.68						
103-114				-0.06	0.13	1.80						
<b>Σ Weight</b>			<b>184.53</b>			<b>55.19</b>			<b>16.88</b>			<b>10.60</b>

Total Added weight for fail-safe = 2 (184.53 + 55.19 + 16.88 + 10.60) = 534 lb/booster.

**3.4.5 B-16B FIVE-SPAR SWEPT WING FAIL-SAFE ANALYSIS.** A five-spar wing with all spar depths being nearly the same is normally considered to be a fail-safe structure (i.e., with one spar failed, approximately four-fifths of the original ultimate strength remains). For the B-16B wing, the calculated distribution of bending moment to the various spars is shown on Page 142 for Wing Station 102.16 and on Page 145 for Wing Station 604.07. Conservatively assuming that the most effective spar at Station 102.16, Spar 2, is completely failed, the percentage of load carried by the remaining spars is  $1.0000 - 0.2375 = 0.7625$ , giving  $0.7625 \times 1.4$  ultimate factor of safety  $\times 100 = 107\%$  of design limit load. Therefore the wing is fail-safe for bending. A similar relation exists for wing shear.

The five-spar B-16B wing is a four-cell torsional structure. With the skin failed on one surface of any one cell, there are three complete cells remaining plus considerable differential bending stiffness and strength because of the wide chord structural box. Since three-fourths of design ultimate strength is greater than design limit, the effectiveness of the five spars in differential bending will provide very adequate torsional fail-safe stiffness and strength.

**3.4.6 B-16B THREE-SPAR SWEPT WING FAIL-SAFE ANALYSIS.** Integrally stiffened skins are the predominant beam bending load carrying members of the three-spar B-16B wing. If a single skin panel between any two spars is fractured on either surface of this wing, the remaining structure is not inherently fail-safe by virtue of number of remaining parts. Accordingly, a crack propagation study was undertaken on the critical lower (tension) surface to determine the critical skin crack sizes and to evaluate the crack stopping properties of the integral skin stiffeners. A crack propagating through skin and stringers is assumed.

The method of analysis employed was that presented by C. C. Poe, Jr., in Reference 11 and extended in Reference 12. In particular, Figure 9(b) of the latter reference is replotted in Figure 3-41, and is the basis of the stress intensity factors calculated and plotted on subsequent pages of this report.

The stress intensity correction factor plot presented in Figure 3-41 of this report and Figure 9(b) of Reference 12 are based on a stiffness ratio  $\mu$  of 0.22 (Reference 12, Page 5).

This ratio for the B-16B three-spar, lower surface skin is 0.42 as shown in Table 3-31; therefore, the data of Figure 2 of Reference 12 can conservatively be applied to the analysis of the wing lower surface.

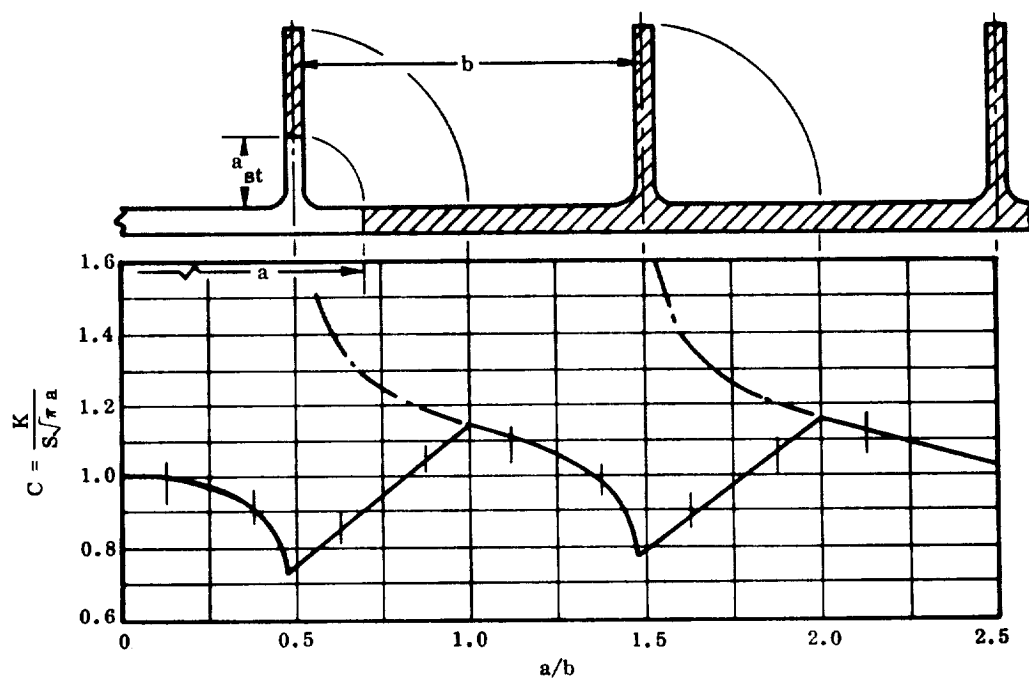


Figure 3-41. Relationship Between Stress Intensity Factor and Crack Length for Panels with Integral Stringers (from Ref. 12)

Table 3-31. Percent Stiffening and Gross Tension Stresses in B-16B Wing Lower Surface

Span Station	Skin Area	Stringer Area	Percent Stiffening(1)	Gross Stress(2)
259	0.1357	0.0975	41.8	50400
379	0.1231	0.0889	41.8	41500
506	0.1050	0.0745	41.5	30200
664	0.0689	0.0505	42.4	13000
776	0.0575	0.0423	42.4	0

(1) Percent stiffening = 
$$\frac{100}{1 + \frac{\text{Skin Area}}{\text{Stringer Area}}}$$

(2) Gross Stress obtained by dividing ultimate stress from Table 3-15 by 1.4 to obtain limit stress.

Applied stress intensities at limit load for two wing stations of the B-16B wing lower surface are calculated as a function of skin crack length and plotted in Figure 3-41, where:

$$K_{\text{applied}} = C (\sigma_{\text{applied}}) \sqrt{\pi a}$$

$C$  = stress intensity correction factor from Figure 3-41.

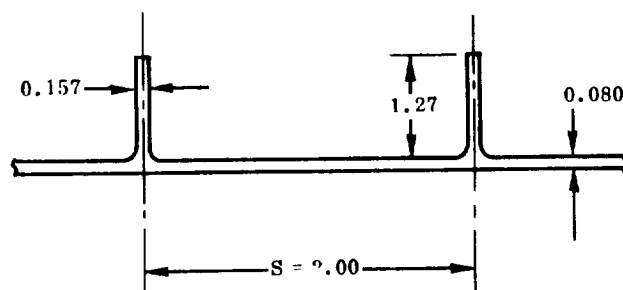
$\sigma_{\text{applied}}$  = applied limit gross area stress (see Table 3-15).

$a$  = half crack length in skin

The allowable stress intensity factor ( $K_{IC}$ ), conservatively taken to be twice  $K_{IC}$  (Reference 3, Figure 13), is also plotted.

Figure 3-41 shows that the B-16B three-spar wing lower cover has critical skin crack lengths varying from 7.2 inches at Station 259 to 8.0 inches at Station 379, and that the stringers have marginal or no crack arrest capability. In addition, the lower tension skin is covered with a permanently attached TPS panel (see Figure 2-17), preventing inspection. From these facts, it is concluded that the B-16B three spar wing is not fail-safe.

**3.4.7 VERTICAL TAIL FAIL-SAFE ANALYSIS.** At Section (A) - (A) (Figure 3-5), the plate-stringer configuration is as shown below.



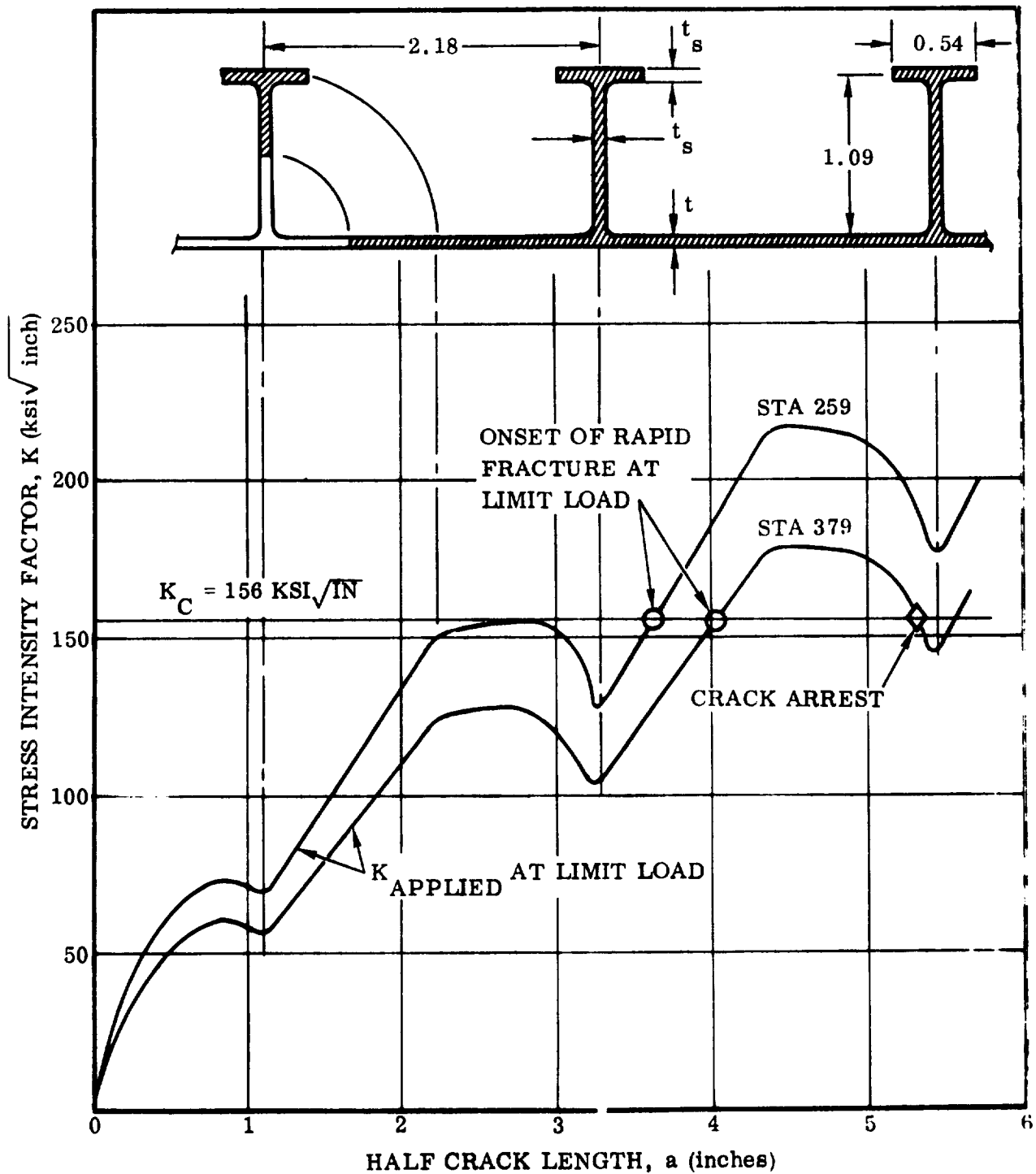


Figure 3-42. B-16B Three-Spar Wing Lower Surface Stress Intensity Factor Versus Crack Length

The material is annealed titanium alloy Ti-6Al-4V, having an ultimate tensile strength of 130 ksi. As in previous examples,  $K_{IC}$  will be taken as 2  $K_{IC}$ , or 156 ksi  $\sqrt{\text{inch}}$ .

Using Poe's method (Reference 12)

$$\text{Percent stiffening} = \frac{100}{1 + \frac{A_{sk}}{A_{str}}} = \frac{100}{1 + \frac{2.00(0.080)}{1.27 (0.157)}} = 55.5$$

$$\text{Stress intensity factor } K = C \sigma \sqrt{\pi a}$$

Values of  $K$  are calculated by the substitution in this expression of values of the stress intensity correction factor  $C$  from Figure 3-41, and the design limit stress level of 34 ksi from Table 3-22. The resulting values of  $K$  are plotted versus crack length in Figure 3-42, which shows that over the range of crack lengths considered (up to eight inches),  $K$  for the integrally stiffened panel does not approach the critical stress intensity level of 156 ksi  $\sqrt{\text{inch}}$ .

One conclusion to be drawn is that the vertical tail box possesses a high degree of fail-safe capability, even though of monolithic construction. The principal reason is that the stiffened covers of the box are designed for compression, which results in low tensile stresses.

**3.4.8 THRUST STRUCTURE FAIL-SAFE ANALYSIS.** Fail-safe strength of the thrust structure was evaluated analytically with the aid of a finite element computer program. The idealized structural model used for the fail-safe analysis is the same as that described in Figures 3-6 through 3-11. Two major tension members of the model were analytically "failed," one at a time, and limit design loads were applied to the weakened structure. Five members required some beef-up because of the redistribution of loads. Total added weight was 76 pounds or 0.34% of the total weight of 22,373 pounds.

Loading conditions considered were: one hour ground sidewinds, maximum alpha g headwinds and 3g maximum thrust.

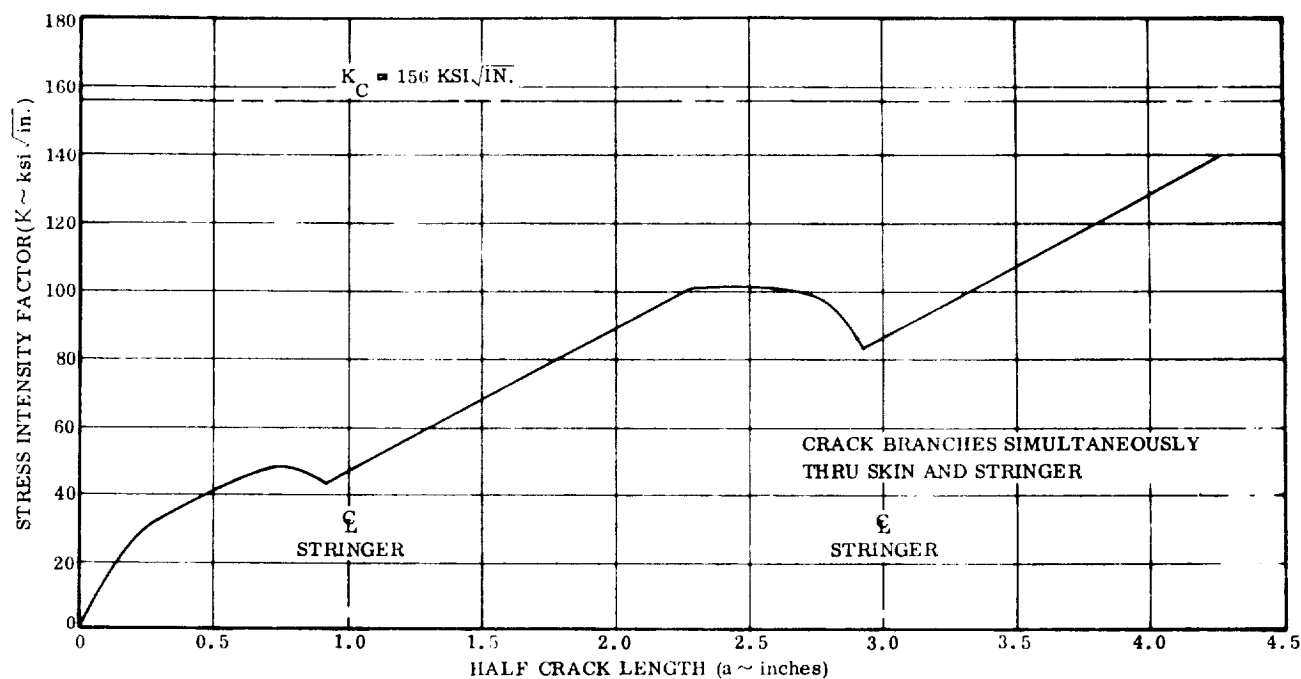


Figure 3-43. Vertical Box Stress Intensity Factor Versus Crack Length

Two major tension members were "failed," one at a time. The members were truss elements from one of the four thrust beams (Figure 3-6) and were selected, first, because they were tension members, and second, because they carried very large loads in the unfailed configuration. Engineering judgment indicated that these were the critical members to be considered in fail-safe analysis.

Results of the fail-safe analysis are listed in Table 3-32. Note that, although the analysis was run for a 360-degree model with a single failed member, the results listed refer to the 45-degree model shown in Figure 3-12. The results are, therefore, maxima for the entire structure. Table 3-32 shows that one element (eight on the complete structure) of the aft thrust bulkhead and four elements of the forward thrust bulkhead have negative margins of safety if fail-safe loading is assumed equal to design limit loading. Four elements are truss members; one is a web stiffener.

Margins of safety vary from a low of -4% on the aft bulkhead to a -37% on the forward bulkhead. It is doubtful that any rational fail-safe criterion could eliminate beef-up of the forward bulkhead with the existing geometric configuration. A slightly different geometry might be less critical for fail-safe loading.



Table 3-32. Thrust Structure Fail-Safe Analysis

Name	Element	P (lb) or q (in./lb)	A (in <sup>2</sup> ) or t (in.)	Stress (psi)			Added for Fail Safe		Margins of Safety		Weight (lb.)			
				Critical	Applied	Allow	Area	Thick- ness	Before Beef-up	After Beef-up	Elem	Sub Total	Added	
Thrust Beams	1	-762000	10.31	Compr.	-73900	99000	0	0	+.34		114.2	Aft Flg	0	
	2	-895000	10.19	Compr.	-87900	99000			+.13		710.9			
	3	-213800	3.44	Compr.	-62100	79000			+.27		240.0			
	4	-175700	2.34	Compr.	-75000	88500			+.18		80.4	1750		
	5	680000	6.10	Tens.	111400	130000			+.17	Same	425.5	Fwd Flg		
	6	458500	3.71	Tens.	123700	130000			+.05	as	596.0			
	7	-104000	3.71	Compr.	-28000	130000			+3.65	Before	49.2	1071		
	8	-259700	4.48	Compr.	-57900	89500			+.54		564.6	Diag &		
	9	669000	6.32	Tens.	105700	130000			+.23		796.5	Web		
	10	-737000	10.23	Compr.	-71300	90600			+.27		1420.3			
	11	(14810)	(.300)	Shear	49400	58700			+.19		585.6	3367		
	12	-578000	14.14	Compr.	-40800	115000			+1.92		742.1	Posts		
	13	-1341000	144.0	Bending	+41900	159000			+2.80					
		-578000	14.14	Compr.	-40800	58700			+.44		1050.3	1792	0	
		-1341000	144.0	Bending	+41900	159000			+2.80					
Thrust Beams Total Weight												7980		
Added Weight for Fail Safe													0	

Table 3-32. Thrust Structure Fail-Safe Analysis (Cont'd)

Name	Element	P (lb) or q(in/lb)	A(in <sup>2</sup> ) or t (in.)	Stress (psi)			Added for Fail Safe		Margins of Safety		Weight (lb.)		
				Critical	Applied	Allow	Area	Thick- ness	Before Beef-up	After Beef-up	Elem	Sub Total	Added
Aft Thrust Blkh'd	14	-24040	.701	Compr.	-34350	40000	0	-	+16	+16	34.6	Braces	3.6
	15	-73100	.995	Compr.	-73500	73500	.038	-	-.04	0.0	98.0	↓	
	16	-47700	.957	Compr.	-49900	73500	0	-	+.47	Same	94.4	227	
	17	-256100	2.54	Compr.	-101000	126000	0	-	+.25	as	177.2	Inner Flg	
Aft Thrust Blkh'd	18	-186100	2.83	Compr.	-65700	126000	0	-	+.92	Before	135.6	↓	430
	19	-213800	2.04	Compr.	-104900	126000	0	-	+.20		117.0	430	
	20	(2880)	(.077)	Shear	37400	58700	-	0	+.57		164.8	Webs	
	21	(9340)	(.211)	Shear	44200	58700	-	0	+.33		259.8	↓	
Aft Thrust Blkh'd	22	(2150)	(.060)	Shear	35900	58700	-	0	+.64		79.3	504	Outer Flg
	23	-324000	2.62	Compr.	-123700	126000	0	-	+.02		184.5	Outer Flg	
	24	-354000	3.28	Compr.	-108000	126000	0	-	+.17		210.0	↓	
	25	-107700	2.62	Compr.	-41100	126000	0	-	+2.06		167.7	562	
Aft Thrust Blkh'd	26	26800	.50	Ten.	53600	130000	0	-	+1.42		11.0	Stiffnrs	76
	27	-144800	2.33	Compr.	62100	100000	0	-	+.61		57.1	↓	
	28	20180	.50	Ten.	40360	100000	0	-	+1.48		8.0	76	
Aft Thrust Bulkhead Total Weight Added Weight for Fail Safe											1799		4

Table 3-32. Thrust Structure Fail-Safe Analysis (Cont'd)

Name	Element	P (lb) or q (in./lb)	A (in. <sup>2</sup> ) or t (in.)	Stress (psi)			Added for Fail Safe		Margins of Safety		Weight (lb.)		
				Critical	Applied	Allow	Area	Thick- ness	Before Beef-up	After Beef-up	Elem	Sub Total	Added
Fwd Thrust Blkh'd	29	109800	0.845	Ten.	130000	130000	.311	-	-.37	0.0	41.6	Braces	15.3
	30	101000	0.777	Ten.	130000	130000	.242	-	-.31	0.0	136.1	↓	42.4
	31	-102600	1.653	Compr.	-62000	62000	.189	-	-.11	0.0	93.9	272	10.8
	32	217500	1.90	Ten.	114400	130000	0	-	+.14	Same	132.5	Inner Flg	0
	33	301000	2.72	Ten.	110800	130000	0	-	+.17	↓	159.5	↓	0
	34	343200	3.14	Ten.	109300	130000	0	-	+.19	↓	172.5	465	0
	35	(3590)	(.063)	Shear	57000	58700	-	0	+.03	↓	62.3	Webs	0
	36	(3260)	(.061)	Shear	53400	58700	-	0	+.10	↓	64.8	↓	0
	37	(698)	(.060)	Shear	11620	58700	-	0	+.05	↓	104.0	231	0
	38	314000	2.72	Ten.	115400	130000	0	-	+.13	↓	191.6	Outer Flg	0
	39	324000	2.64	Ten.	122700	130000	0	-	+.06	↓	169.0	↓	0
	40	141000	2.00	Ten.	70500	130000	0	-	+.84	↓	128.0	489	0
	41	-7090	.50	Compr.	-14180	100000	0	-	+6.05	↓	5.8	Stiff.	0
	42	10990	.50	Ten.	21980	100000	0	-	+3.55	Same	17.1	↓	0
	43	-87700	.88	Compr.	99600	100000	.150	-	-.17	+.01	18.1	41	3.1
Forward Thrust Bulkhead Total Weight											1498		
Added Weight for Fail Safe											72		

Table 3-32. Thrust Structure Fail-Safe Analysis (Cont'd)

Name	Element	P (lb) or q(in/lb)	A(in <sup>2</sup> ) or t (in.)	Stress (psi)			Added for Fail Safe		Margins of Safety		Weight (lb.)		
				Critical	Applied	Allow	Area	Thick- ness	Before Beef-up	After Beef-up	Elem	Sub Total	Added
Backup Frame	44	-38000	.489	Compr.	-77700	115000	0	0	+.50	Same	30.1	Inner Flg	0
	45	16820	.468	Ten.	36000	130000			+2.61	as	26.2		
	46	39500	.450	Ten.	37900	130000			+.48	Before	25.2	81	
	(47)	(398)	.040	Shear	9950	58700			+4.90		65.4	Webs	
	(48)	(882)	.040	Shear	22050	58700			+1.66		59.5		
	(49)	(665)	.040	Shear	16620	58700			+2.53		59.5	185	
	50	-19520	.342	Compr.	-57100	84500			+.48		24.1	Outer Flg	
	51	-14190	.316	Compr.	-44900	80000			+.78		20.2		
	52	25600	.291	Ten.	88000	130000			+.48		18.6	63	
	53	6950	.500	Ten.	13900	100000	0	0	+6.20		48.0	48	0
Backup Frame Total Weight Added Weight for Fail Safe													
												377	0
Hold Down	54	-1289000	15.21	Compr.	-84600	126000	0	0	+.49	+.49	798.2		
	55	-749000	8.84	Compr.	-84800	126000	0	0	+.49	+.49	424.3	1223	0
Holddown Fittings Total Weight Added Weight for Fail Safe												1223	0

Table 3-32. Thrust Structure Fail-Safe Analysis (Cont'd)

Name	Element	Nx (lb/in) or q(in/lb)	A(in <sup>2</sup> ) or t(in.)	Stress (psi)			Added for Fail Safe		Margins of Safety		Weight (lb.)		
				Critical	Applied	Allow	Area	Thick- ness	Before Beef-up	After Beef-up	Elem	Sub Total	Added
↑ Skin Panels ↓	⑤⑥	-13680 (5030)	.302 (.160)	Compr.	-45200	108870	0	0	+.74	Same	1586.2	Aft	
	⑤⑦	-4120 (2050)	.182 (.120)	Compr.	-22700	63270	0	0	+1.39	as Before	956.1	Bay	
	⑤⑧	-3840 (2462)	.142 (.080)	Compr.	-27050	55540	0	0	+.61		820.7		0
	⑤⑨	-9310 (2620)	.222 (.160)	Compr.	-42000	80000	0	0	+.60		1066.4	Ctr. Bay	
	⑥⑩	-8030 (2620)	.222 (.160)	Compr.	-36200	71370	0	0	+.83		1066.6		
	⑥⑪	-7620 (1196)	.202 (.140)	Compr.	-37800	67300	0	0	+.75		1067.6	3201	0
	⑥⑫	-7840 (912)	.202 (.140)	Compr.	-38800	67300	0	0	+.57		970.4	Fwd Bay	
	⑥⑬	-8490 (226)	.202 (.140)	Compr.	-42000	67300	0	0	+.59		970.6		
	⑥⑭	-7950 (788)	.202 (.140)	Compr.	-39400	67300	0	0	+.70		1067.7		0
				Shear	5625	80000		0				3009	0
Skin Panels Total Weight												9573	0
Thrust Structure Total Weight												22450	
Total Added Weight for Fail-Safe													76

### 3.5 FATIGUE AND SAFE-LIFE USING ALTERNATIVE MATERIALS

The effects on fatigue life and crack growth safe-life of the use of alternative materials in certain of the selected components are investigated below.

#### 3.5.1 ANALYSIS OF B-9U DELTA WING BOX USING 2219-T87 ALUMINUM ALLOY.

Aluminum alloy 2219 is a material that could be used in the structural box of the wing. It is assumed that the heating period is so short and the aluminum substructure is of sufficient mass (i.e., heat sink design) that the temperatures essentially remain at 70° F as assumed in the titanium substructure wing design.

For the B-9U wing, the condition producing maximum tension in lower surface is W-1, which is the maximum  $\alpha q$  (headwind) condition in the ascent phase.

This is a room temperature condition, and for Ti-6-4,

$$F_{tu} = 134 \text{ ksi}$$

Using a hole-out factor of 1.05,

$$\text{Maximum } \sigma_{\text{limit}} = \frac{134}{1.05(1.4)} = 91.2 \text{ ksi}$$

This value was used in the titanium wing box damage analysis. If 2219-T87 aluminum alloy is substituted for titanium,

$$F_{tu} = 64 \text{ ksi}$$

and

$$\text{Maximum } \sigma_{\text{limit}} = \frac{64}{1.05(1.4)} = 43.5 \text{ ksi}$$

Table 3-34 presents the fatigue analysis of the aluminum substructure. The aluminum wing substructure has a calculated safe fatigue life of 44 flights versus 175 flights for the titanium wing substructure (see Table 3-21).

Figure 3-44 presents the results of a crack growth analysis of the aluminum wing substructure compared to the titanium wing substructure. It can be seen that the aluminum has a large calculated safe-life versus 31 flights (see Page 190) for the titanium when an initial 0.10 inch corner crack is assumed.

The differences in the calculated fatigue and crack growth safe-life can be attributed to the different material fatigue and crack growth characteristics.

Table 3-33. B-9U Wing Box Fatigue Analysis — 2219 Aluminum Alloy

Mission Phase	T (° F)	$\sigma_{\text{limit}}$ (ksi)	$\frac{\sigma_{\text{mean}}}{\sigma_{\text{limit}}}$	$\frac{\sigma_{\text{alt}}}{\sigma_{\text{limit}}}$	$\sigma_{\text{mean}}$ (ksi)	$\sigma_{\text{alt}}$ (ksi)	$K_t$	N (Cycles)	n (Cycles)	n/N
Ascent	RT	43.5	0	.015	0	.7	3.0	$\infty$	90,000	0
Ascent	RT	43.5	0	.025	0	1.1	3.0	$\infty$	9,000	0
Ascent	RT	43.5	0	.035	0	1.5	3.0	$\infty$	900	0
Ascent	RT	43.5	0	.045	0	2.0	3.0	$\infty$	90	0
Ascent	RT	43.5	0	.055	0	2.4	3.0	$\infty$	9	0
Ascent	RT	43.5	.15	.035	6.5	1.5	3.0	$\infty$	90,000	0
Ascent	RT	43.5	.15	.05	6.5	2.2	3.0	$\infty$	9,000	0
Ascent	RT	43.5	.15	.065	6.5	2.8	3.0	$\infty$	900	0
Ascent	RT	43.5	.15	.08	6.5	3.5	3.0	$\infty$	90	0
Ascent	RT	43.5	.15	.09	6.5	3.9	3.0	$\infty$	9	0
Ascent	RT	43.5	0	.055	0	2.4	3.0	$\infty$	90,000	0
Ascent	RT	43.5	0	.09	0	3.9	3.0	$\infty$	9,000	0
Ascent	RT	43.5	0	.125	0	5.4	3.0	$\infty$	900	0
Ascent	RT	43.5	0	.155	0	6.7	3.0	$\infty$	90	0
Ascent	RT	43.5	0	.185	0	8.0	3.0	$\infty$	9	0
Ascent	RT	43.5	.40	.08	17.4	3.5	3.0	$\infty$	90,000	0
Ascent	RT	43.5	.40	.145	17.4	6.3	3.0	$\infty$	9,000	0
Ascent	RT	43.5	.40	.21	17.4	9.1	3.0	$5.6 \times 10^6$	900	.00016
Ascent	RT	43.5	.40	.27	17.4	11.7	3.0	$6.6 \times 10^4$	90	.00137
Ascent	RT	43.5	.40	.33	17.4	14.4	3.0	$2.8 \times 10^4$	9	.00032
Ascent	RT	43.5	.10	.105	4.4	4.6	3.0	$\infty$	90,000	0
Ascent	RT	43.5	.10	.185	4.4	8.0	3.0	$10^7$	9,000	.00090
Ascent	RT	43.5	.10	.30	4.4	13.1	3.0	$1.1 \times 10^5$	900	.00818
Ascent	RT	43.5	.10	.45	4.4	19.6	3.0	$1.6 \times 10^4$	90	.00562
Ascent	RT	43.5	.10	.605	4.4	26.3	3.0	$4.3 \times 10^3$	9	.00209
Ascent	RT	43.5	.15	.135	6.5	5.9	3.0	$\infty$	90,000	0
Ascent	RT	43.5	.15	.20	6.5	8.7	3.0	$2.4 \times 10^6$	9,000	.00375
Ascent	RT	43.5	.15	.37	6.5	16.1	3.0	$3.4 \times 10^4$	900	.02650
Ascent	RT	43.5	.15	.61	6.5	26.5	3.0	$3.7 \times 10^3$	90	.02433
Ascent	RT	43.5	.15	.80	6.5	34.8	3.0	$9.3 \times 10^2$	9	.00968

Table 3-33. B-9U Wing Box Fatigue Analysis — 2219 Aluminum Alloy, Contd

Mission Phase	T (° F)	$\sigma_{\text{limit}}$ (ksi)	$\frac{\sigma_{\text{mean}}}{\sigma_{\text{limit}}}$	$\frac{\sigma_{\text{alt}}}{\sigma_{\text{limit}}}$	$\sigma_{\text{mean}}$ (ksi)	$\sigma_{\text{alt}}$ (ksi)	$K_t$	N (Cycles)	n (Cycles)	n/N
Entry	350	43.5	.075	.075	3.3	3.3	3.0	$\infty$	90,000	0
Entry	350	43.5	.135	.135	5.9	5.9	3.0	$\infty$	9,000	0
Entry	350	43.5	.185	.185	8.0	8.0	3.0	$3.5 \times 10^6$	500	.00014
Entry	350	43.5	.23	.23	10.0	10.0	3.0	$2.5 \times 10^5$	250	.00100
Entry	350	43.5	.37	.37	16.1	16.1	3.0	$2.0 \times 10^4$	1	.00750
Entry	350	43.5	.47	.47	20.4	20.4	3.0	$6.4 \times 10^3$	100	.01562
Entry	350	43.5	.50	.50	21.8	21.8	3.0	$4.7 \times 10^3$	1	.00021
Cruise/Landg	RT	43.5	.20	.21	8.7	9.1	3.0	$6.3 \times 10^5$	180,000	.28590
Cruise/Landg	RT	43.5	.20	.26	8.7	11.3	3.0	$1.4 \times 10^5$	18,000	.12860
Cruise/Landg	RT	43.5	.20	.32	8.7	13.9	3.0	$5.7 \times 10^4$	1,800	.03159
Cruise/Landg	RT	43.5	.20	.38	8.7	16.5	3.0	$2.6 \times 10^4$	180	.00692
Cruise/Landg	RT	43.5	.20	.44	8.7	19.1	3.0	$1.4 \times 10^4$	18	.00127
Taxi	RT	43.5	-.021	.040	-.9	1.7	3.0	$\infty$	180,000	0
Taxi	RT	43.5	-.021	.060	-.9	2.6	3.0	$\infty$	18,000	0
Taxi	RT	43.5	-.021	.080	-.9	3.5	3.0	$\infty$	1,800	0
Taxi	RT	43.5	-.021	.095	-.9	4.1	3.0	$\infty$	180	0
Taxi	RT	43.5	-.021	.110	-.9	4.8	3.0	$\infty$	18	0
GAG	RT	43.5	-	-	11.1	16.8	3.0	$2.0 \times 10^4$	200	.0100

Summary

Phase	n/N	Safe Life = $\frac{100}{.5717(4)} = 44$ Missions
Ascent	.0829	
Entry	.0245	
Cruise/Landg	.4543	
Taxi	0	
GAG	.0100	
$\Sigma(n/N)$	.5717	



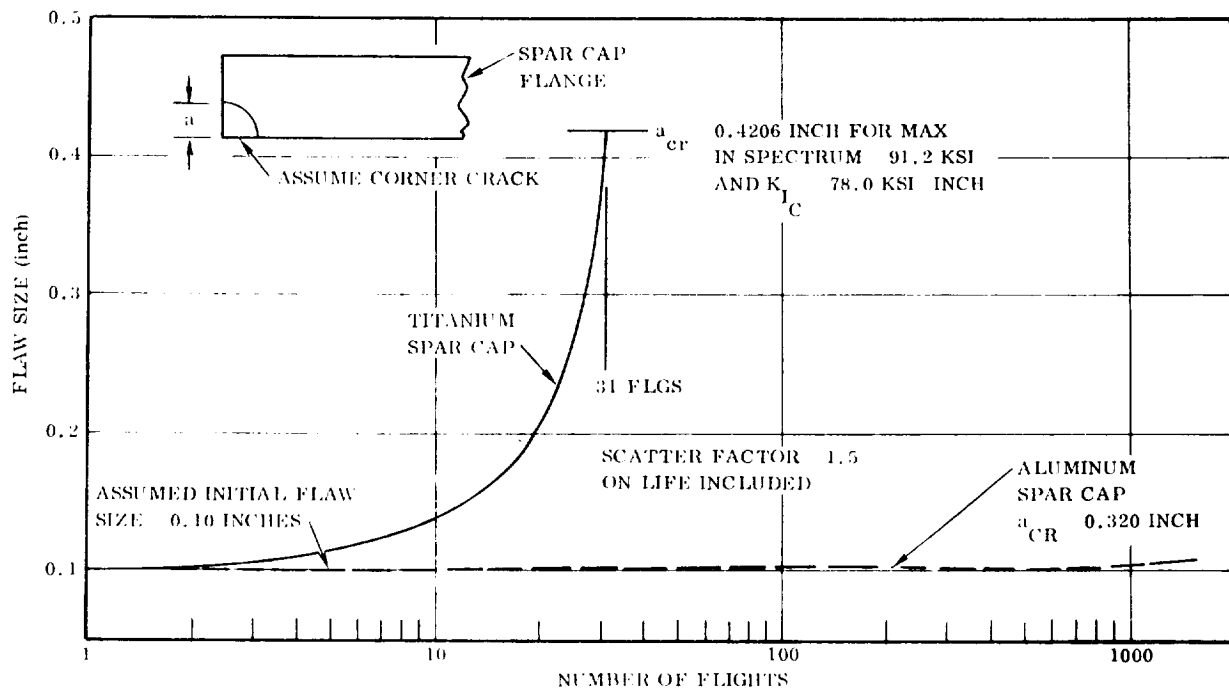


Figure 3-44. Comparison of Crack Growth in Aluminum and Titanium Wing Span Caps

### 3.5.2 ANALYSIS OF THRUST STRUCTURE USING 2219-T87 ALUMINUM ALLOY.

Aluminum alloy 2219 is a material that could be used in the thrust structure because the base heat shield prevents heating of the thrust structure during the ascent flight phase when the main rocket engines are operating.

For the titanium thrust structure, a maximum limit stress ( $\sigma_{\text{limit}} = F_{tu}/\text{ultimate factor of safety} = 130/1.4 = 92.9 \text{ ksi}$ ) was used. If 2219-T87 aluminum is substituted for titanium:

$$F_{tu} = 64.0 \text{ ksi}$$

$$\sigma_{\text{limit}} = 64.0/1.4 = 45.7 \text{ ksi}$$

Table 3-34 presents a fatigue analysis of an aluminum thrust structure for comparison with that of the titanium thrust structure presented in Table 3-24. The aluminum thrust structure has a calculated safe fatigue life of 824 flights versus 887 flights for the titanium thrust structure.

Table 3-34. Thrust Beam Cap Damage Analysis, 2219 Aluminum Alloy

Design $\sigma_{\text{limit}}$ (ksi)	Temp. (°F)	$K_t$	$T_m$ (2) (%)	$T_a$ (2) (%)	$\sigma_m$ (ksi)	$\sigma_a$ (ksi)	$n_e$ (Cycles)	$n$ (Cycles)	$\sigma_a$ (ksi)	N (Cycles)	$n/N$
45.7	RT	3.0	100	0.05	45.7	0.02	$10^5$	90,000	0.095	$\infty$	0
45.7	RT	3.0	100	0.37	45.7	0.17	$10^4$	9,000	.330	$\infty$	0
45.7	RT	3.0	100	1.08	45.7	0.49	$10^3$	900	.660	$\infty$	0
45.7	RT	3.0	100	1.79	45.7	0.83	$10^2$	90	.985	$\infty$	0
45.7	RT	3.0	100	2.50	45.7	1.14	10	9	1.300	$\infty$	0
45.7	RT	3.0	100	3.20	45.7	1.46	1				
45.7	RT	3.0	51	51.00	23.3	23.30	$10^2$	100	23.30	$3.3 \times 10^3$	0.0303

$(n/N) = 0.0303$  for thrust beam cap

$$\text{Safe Fatigue Life} = \frac{100}{4(0.0303)} = 824 \text{ Missions}$$

## NOTES:

1. Material is 2219-T87
2. Thrust in percent of design thrust (see Section 2.7.5).

Figure 3-45 presents the result of a crack growth analysis of the aluminum thrust structure compared to the titanium thrust structure. It can be seen that the aluminum thrust structure has a calculated crack growth safe-life greater than 3,000 flight versus 1,555 flights for the titanium thrust structure for an assumed initial flaw of a 0.10 inch corner crack.

The difference in the calculated fatigue and crack growth safe-life can be attributed to the different material fatigue and crack growth characteristics. Figure 3-46 compares the crack growth rates of the two materials. The  $\Delta K_{\max}$  with the initial flaw size at the maximum stress levels in the aluminum and titanium thrust structures are shown. It can be seen that the average flaw growth rate between the initial  $\Delta K_{\max}$  and  $K_{IC}$  is generally higher for titanium which leads to the more rapid crack growth shown in Figures 3-44 and 3-45.

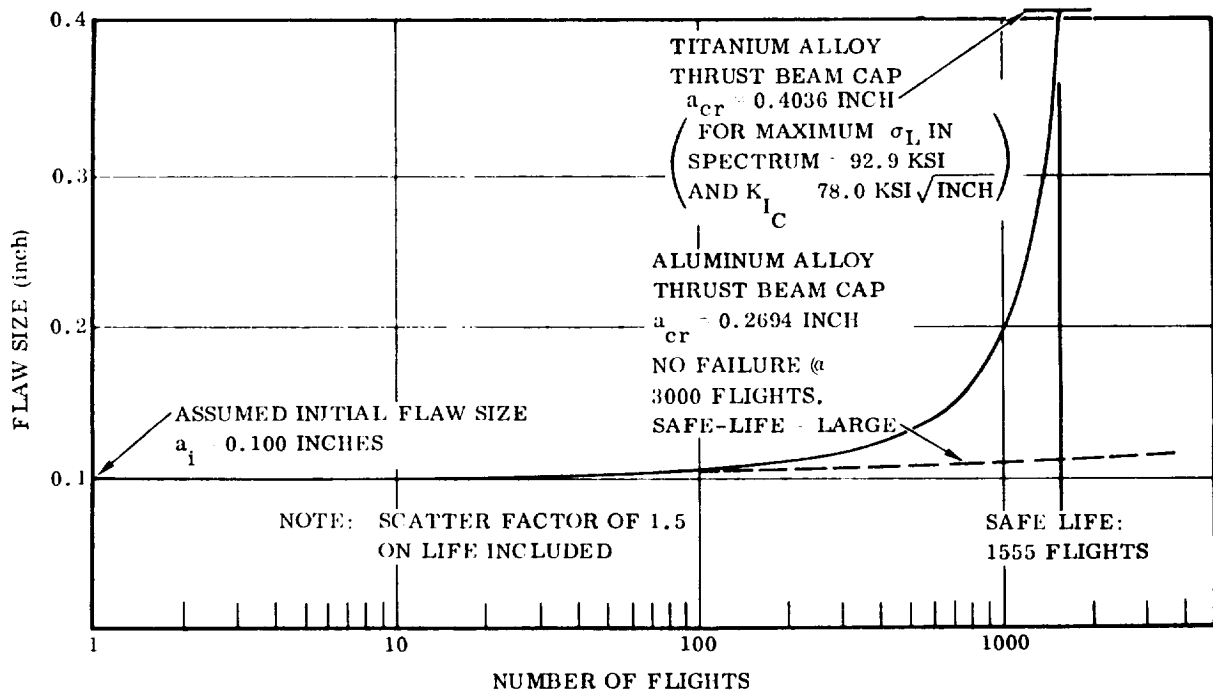


Figure 3-45. Comparison of Crack Growth in Titanium and Aluminum Thrust Beam Caps (Flaw Configuration - Corner Crack)

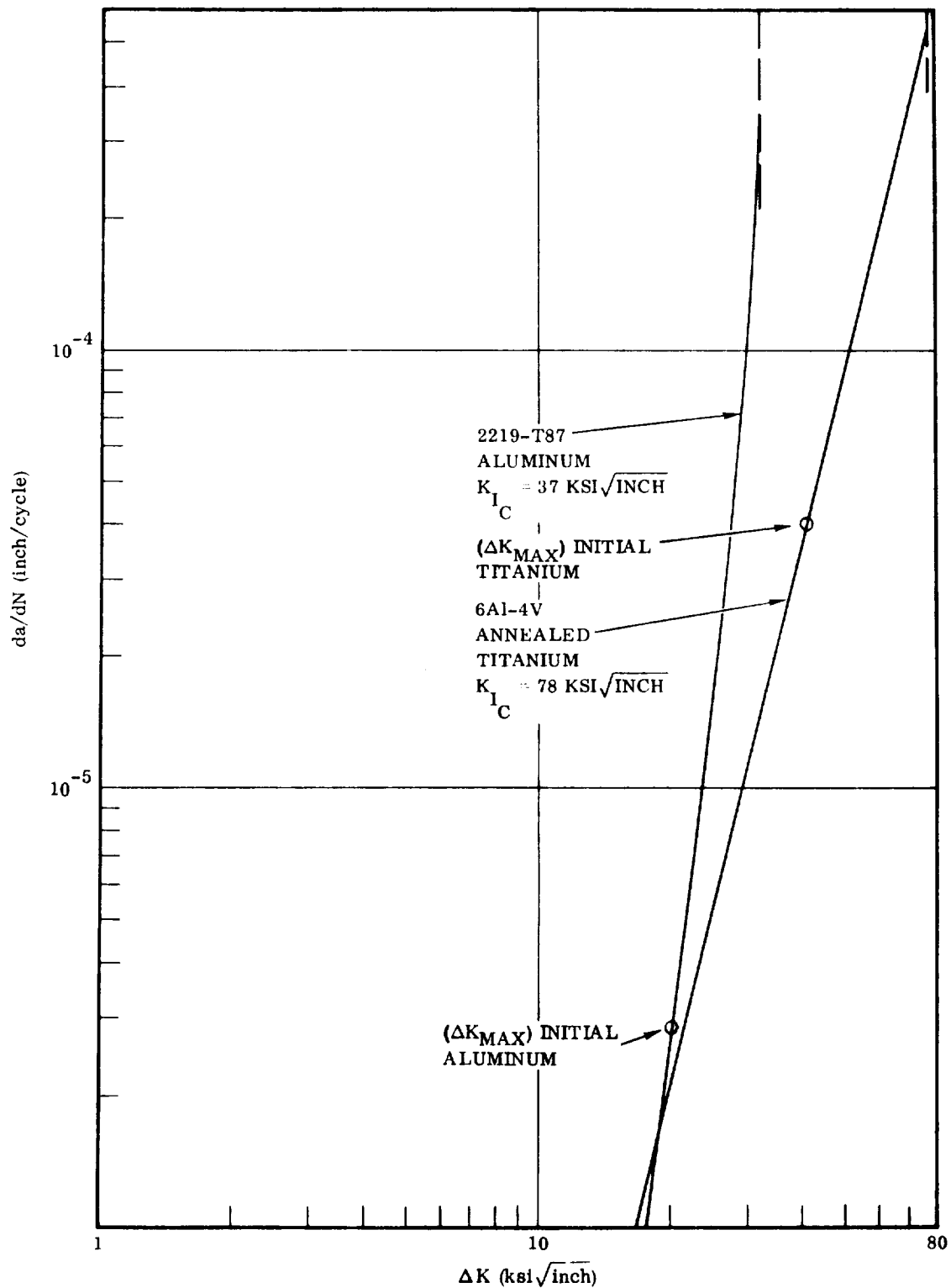


Figure 3-46. Comparison of Cyclic Crack Growth Rate in Titanium and Aluminum Material at Room Temperature

## SECTION 4

### DEVELOPMENT OF SAFE-LIFE BOOSTER

The results of the fatigue, safe-life, and fail-safe analyses in Section 3 are summarized in Section 6, which shows that (1) all studied baseline booster components have adequate fatigue life from the standpoint of crack initiation of flawless material, and (2) all components but the wing box possess safe-life capability of 100 missions or more when initial flaws of the assumed type and size are present (reference Section 3.3). The wing box is shown to lack this capability in all three configurations (B-9U delta and the three-spar and five-spar B-16B swept wings) when the initial flaw is taken to be a critically located crack of 0.10-inch length originating at a 0.25 inch diameter fastener hole. This initial flaw size is considered to be the largest that is likely to escape detection in manufacturing inspection, given the present state-of-the-art capabilities of the available NDE processes.

The measures that can be taken to provide the required safe-life generally involve one or more of the following:

- a. Reducing the working stress level to a point where cyclic and sustained load propagation of a flaw will not cause it to reach critical size in the required service life.
- b. Reducing the inspection interval to less than the number of flights in which the flaw will reach critical size. This method requires a maximum allowable flaw size sufficiently large to be detectable by methods of inspection to be used in in-service NDE, and also requires that all critical structural areas be accessible for such inspection.
- c. Changing the material in critical areas to one having superior flaw growth characteristics.

In the following paragraphs the recommended means of enhancing the safe-life capability of the wing box and other critical safe-life components are described. Tables 4-1 and 4-2 summarize details of these changes while their impact on weight and performance is discussed in Section 6.1.

Where no changes are given, the baseline configuration and development plans are considered adequate.

Table 4-1. Development of Safe-Life Booster Design - B-9U Configuration

Component	Structural Design Concept	Change From Baseline Booster				$\Delta$ Wt <sup>(2)</sup> (lb)	$\Delta$ Cost (\$M)
		Description	Material	Test Plan	Maintenance Plan		
LO <sub>2</sub> Tank	Thin-wall pressure vessel with integral longitudinal stiffeners of 2219-T87 aluminum alloy	None <sup>(1)</sup>	None	None	None	—	—
LH <sub>2</sub> Tank	Same as LO <sub>2</sub> tank	None <sup>(1)</sup>	None	None	None	—	—
Wing Box	Delta planform multi-spar box beam with chord-wise corrugated skin, Ti-6-4 annealed	Increase lower surface spar cap areas by 30%	None	Add development test program to verify safe-life of wing elements	Perform in-service inspection for cracks in lower spar caps every 25 flights	+1030	(3)
Vertical Tail	Three-spar box (largely Ti-6-4) Truss-type beam	None <sup>(1)</sup>	None	None	None	—	(3)
Thrust Structure	Assembly (Ti-6-4)	None <sup>(1)</sup>	None	Same as wing box	None	—	(3)
Aft Orbiter Support Frame	Ti-6-4 I-section ring	None <sup>(1)</sup>	None	None	None	—	(3)
Totals						+1030	+3.225 <sup>(3)</sup>

(1) Baseline design provides adequate safe life, based on crack initiation and on flaw growth

(2) Weight increases include a non-optimum factor of 1.25

(3) Total cost contains amounts not broken down to specific components

Table 4-2. Development of Safe-Life Booster Design - B-16B Configuration

Component	Structural Design Concept	Change From Baseline Booster				$\Delta Wt^{(3)}$ (lb)	$\Delta Cost$ (\$M)
		Description	Material	Test Plan(2)	Maintenance Plan		
LO <sub>2</sub> Tank	Thin-wall pressure vessel with integral longitudinal stiffeners of 2219-T87 aluminum alloy	None <sup>(1)</sup>	None	None	None	-	-
	Same as LO <sub>2</sub> tank	None <sup>(1)</sup>	None	None	None	-	-
Wing Box	Three-spar swept wing box with chord-wise corrugated skin, Ti-6-4 annealed	Increase lower surface by 30% in wing root region	None	Add development test program to verify safe-life of wing elements	Perform in-service inspection for cracks in lower spar caps every 25 flights	1151	(4)
Vertical Tail	Three-spar box (largely Ti-6-4)	None <sup>(1)</sup>	None	None	None	-	(4)
Thrust Structure	Truss-type beam assembly, Ti-6-4	None <sup>(1)</sup>	None	Same as wing box	None	-	(4)
Aft Orbiter Support Frame	Ti-6-4 I-section ring	None <sup>(1)</sup>	None	None	None	-	(4)
Totals						+1151	+3.512

(1) Baseline design provides adequate safe life, based on crack initiation and on flaw growth

(2) Based on a "bare bones" baseline test plan

(3) Weight increases include a non-optimum factor of 1.25

(4) Total cost contains amounts not broken down to specific components

#### 4.1 DESCRIPTION OF STRUCTURAL AND OPERATIONAL CHANGES

Since the material and stress levels are assumed to be identical in both the B-9U delta wing and the B-16B swept wing boosters, the same changes are considered applicable to both.

The achievement of the required safe-life (i.e., 100 flights) solely by reducing the operating stress in the lower wing surface necessitates a 50-percent reduction in stress, as indicated by Figure 3-33. This effectively doubles the weight of the wing lower surface bending material, and results in a weight increase of approximately 3400 pounds in the B-9U wing and 2300 pounds in the three-spar B-16B wing. To reduce this weight increase to a more acceptable level, it is recommended that the stress level be reduced by 30 percent rather than 50 percent, which imposes a limitation of 25 flights between inspections of the wing lower spar caps (see Figure 3-33). The resulting weight increase is 1030 pounds to the B-9U wing and 1151 pounds to the B-16B wing.

#### 4.2 EFFECTS OF SAFE-LIFE APPROACH ON DEVELOPMENT PLANS

Previous paragraphs describe the changes required to achieve full safe-life capability in the B-9U and B-16B boosters as (1) reduction in wing lower surface working stresses of 30 percent by a similar increase in lower surface bending material, and (2) inspection of the wing lower surface for cracks every 25 flights. Also, additional structural development and qualification tests are required to verify the predictions of safe-life and demonstrate the adequacy of the inspection plan. The effect of these changes on structural test plans, quality control, and maintenance plans and costs is discussed below.

##### 4.2.1 STRUCTURAL TEST PLANS

4.2.1.1 Additional Element Tests. Cycling tests for 240 wing and 60 thrust structure element specimens will be conducted in a fixture incorporating four loading frames. Each frame will be capable of loading three specimens simultaneously in tandem arrangement. Each frame will contain a servo-controlled hydraulic cylinder and a two-bridge load cell for load feedback and monitoring. Loads will be programmed to the desired spectrum by a General Automation SPC-12 digital computer, using the basic command signal from an oscillator generating a sine wave function. This programmer can intersperse up to 20 different load levels for up to 8 control channels, while varying frequency with load level for optimum cycling speed. Loads will be monitored on a cathode ray tube bar graph display. Periodic inspections will be conducted to observe flaw growth.

Specimens will be designed to represent 20 wing locations and 5 thrust structure locations. Two initial flaw sizes will be selected for each of two types of flaws, and



three specimens will be tested for each data point. Wing specimens will be run to failure or 200 simulated flights (assuming 2000 load cycles per flight), whichever comes first. Thrust structure specimens will be run to failure or 400 simulated flights (assuming one load cycle per flight with a 3-minute-dwell at load), whichever comes first. Load spectrums will be applied to approximate a flight-by-flight loading profile for the respective structural areas. All testing will be at room temperature.

**4.2.1.2 Additional Tests On Three-Spar Wing Box.** Safe-life tests will utilize the baseline test setup and equipment, for application of 100 simulated flights, assuming 240 load cycles per flight. Aerodynamic heating will be simulated by programming surface temperatures to a flight profile. Initial flaws will be introduced by cuts with a jeweler's saw, and precracking induced by cycling (without heating) for approximately 500 load cycles. Loads will be programmed by a digital computer-programmer and electro-hydraulic servo system; temperatures will be programmed by an analog computer-programmer with drum type function generator. Heating will be accomplished using quartz infra-red tubular lamps with radiant reflectors mounted over the box surfaces, powered by ignitron voltage controllers. NDE will be accomplished at intervals of 25 flights to monitor flaw growth and verify the NDE methods.

**4.2.1.3 Additional Tests On Fatigue Wing.** Safe-life testing on the fatigue qualification wing test article will be conducted at the Convair Aerospace Fort Worth operation. Tests will utilize the baseline setup, and the same general plan as described above for the wing box specimen will apply.

**4.2.1.4 Additional Tests On Fatigue Thrust Structure.** The fatigue qualification thrust structure, which is a part of a full-body structure in the baseline plan, will be tested at NASA-MSFC. Tests will utilize baseline equipment, and the same general plan as described above will apply, except that 300 simulated flights of one 3-minute cycle each will be assumed, with no temperature profile. Inspections will be conducted at 75-flight intervals.

**4.2.1.5 Test Costs.** Safe-life test costs are given in Table 4-3.

**4.2.2 QUALITY CONTROL AND MAINTENANCE PLANS.** The development of a safe-life design for the structure of the selected components requires a maintenance approach that provides for determination of changes in structural integrity. This requirement places emphasis on time consuming inspection and NDE methods to trace known defects and identify the intensity of new defects (crack size and location).

In the development of the baseline values in Section 2.9, all routine and phased maintenance requirements were established without detailed structural data. Also reflected in Table 2-12 was a constant factor of 56 percent applied to the scheduled maintenance to establish the unscheduled maintenance values. The safe-life concept

Table 4-3. Costs for Safe-Life Tests

A. ELEMENTS TESTS - SPECTRUM FATIGUE (CONTRACTOR)

20 Wing Configurations × 12 Specimens	=	240
5 Thrust Structures × 12 Specimens	=	60
Total		300

Tasks	Engrg M-H	Shop M-H	Matl \$
Specimen Design			
25 Configurations @ 20 hr	500		
Specimen Material			
Assume 8 × 2 × 20 in. bar/specimen			
Titanium @ 0.16 lb/in <sup>3</sup> = 5 lb/specimen			
(5 lb/specimen) (300 specimens) (\$12/lb)			18,000
Specimen Fabrication 300 @ 20 hr		6000	
Attach Fixture Design			
25 Configurations @ 8 hr	200		
Load Setup Design 1 man 4 weeks	160		
Assume 4 Load Frames, Hydraulic Servo			
With Sine Wave Oscillator Type Programmer			
Fixture Material			
5000 lb steel @ 0.15			750
Bolts/nuts, weld rod			200
Load Setup Material			
Assume erector beams on hand			
Assume hydraulic cylinders on hand			
Servo valves 4 @ 600			2,400
Load cells 4 @ 500			2,000
Hydraulic fittings, tube			250
Load Setup Fabrication			
Shop 4 men 3 weeks		480	
Eng 2 men 3 weeks	240		
Drill Specimens 300 @ 4 hr		1200	
Flaw Preparation 300 @ 1 hr	300		
Setup 300 Specimens @ 1 hr	300		

Table 4-3. Costs for Safe-Life Tests, Contd

Tasks	Engrg M-H	Shop M-H	Matl \$
Test-Wing. Assume 3.3 cps (240 spec) (200 flts/spec) (2000 cyc/flt) $\left(\frac{\text{hr}}{3.3 \times 60 \times 60 \text{ cyc}}\right) = 9600 \text{ hr}$ Assume 3 specimens in tandem, 4 setups, 9 specimens in test simultaneously average Full time attendance: $\frac{9600 \text{ hr}}{9} =$	1070	100	
Test - Thrust Structure (60 spec) (400 flts/spec) $\left(\frac{3 \text{ min}}{\text{hr}}\right) \left(\frac{\text{hr}}{60 \text{ min}}\right) = 1200 \text{ hr}$ $\frac{1200}{9} =$	133	20	
Inspections 300 specimens @ 1 hr	300		
Equipment Down Time 25% run $\frac{1070 + 133}{4}$	300	100	
Test Report 1 man 4 weeks; photos 30 @ 15	160		450
Tear Down		120	
Design, Stress Support Scheduling $1070 + 133 + 300 + 300 = 1803 \text{ hr}$ $\frac{1803}{167} = 11 \text{ mo. } 2 \text{ men @ } 2 \text{ mo}$	668		
Project office, supervision 10%	433		
Totals	4764	8020	\$24,050
B. 3-SPAR WING BOX (CONTRACTOR) 4 cpm =			
240 cph			
Flaw Preparation, Setup 1 wk			
3 eng	120		
2 shop		80	
Pre-crack (500 cyc) $\left(\frac{\text{hr}}{240 \text{ cyc}}\right) = 2 \text{ hr}$	6	4	

Table 4-3. Costs for Safe-Life Tests, Contd

Tasks	Engrg M-H	Shop M-H	Matl \$
Test (100 flts) $\left(\frac{240 \text{ cyc}}{\text{flt}}\right) \left(\frac{\text{hr}}{240 \text{ cyc}}\right) = 100 \text{ hr}$			
Heat Up and Cool Down 1 hr/flt = 100 hr			
Equipment Down Time 50% Run = 50			
Total 250	750	500	
Materials: Quartz Lamps 25 in. 50 @ 12			600
CO <sub>2</sub> 0.1 ton/flt x 100 = 10 tons @ 100			1,000
Inspections 4 @ 8 hr = 32 hr	96	64	
Test Report 4 photos @ 15	40		60
Design/Stress			
$\frac{300 \text{ hr}}{167} = 2 \text{ mo } 3 \text{ men } 1/2 \text{ time for } 2 \text{ mo}$	500		
Project office, Supervision 10%	150		
Totals	1662	648	\$ 1,660
C. FATIGUE WING (CONTRACTOR) 4 cpm = 240 cph			
Flaw Preparation 1 wk			
4 eng 1 shift	160		
4 shop 1 shift		160	
Pre-Crack 500 cyc 2 hr	8	8	
Test (Same as Wing Box) = 250 hr	1000	1000	
Materials: Quartz Lamps 300 @ 12			3,600
CO <sub>2</sub> 0.5 ton/flt x 100 = 50 tons at 100			5,000
Inspections 4 @ 24 hr = 100 hr	400	400	
Reliability Control Support; X-ray/Ultrasonic	100		200
Test Report: Photos 20 @ 15	120		300
Design/Stress Support			
$\frac{650}{167} = 4 \text{ mo } 6 \text{ men } 1/2 \text{ time}$	1000		
Project Office, Supervision 10%	280		
Totals	3068	1568	\$ 9,100

Table 4-3. Costs for Safe-Life Tests, Contd

Tasks	Engrg M-H	Shop M-H	Matl \$	
D. FATIGUE THRUST STRUCTURE (NASA MSFC)				
Flaw Preparation 1 wk				
6 eng	240			
10 shop		400		
Pre-Crack 2 hr	12	20		
Run Time (300 flts) (3 min/flt) $\left(\frac{\text{hr}}{60 \text{ min}}\right)$				
15 hr + 25 downtime = 40 hr	240	400		
Materials: Oil, Fittings, Bolts, etc.			1,000	
Inspections 4 @ 24 hr = 100 hr	600	1000		
Reliability Control X-Ray, etc.	100		200	
Test Report: 20 photos @ 15	120		300	
Design /Stress 6 men 1 mo	1000			
Project Office, Supervision 10%	230			
General Dynamics Totals	2542	1820	\$ 1,500	
NASA Support				
6 eng   1 mo	1000			
10 shop		1700		
E. Summary				
Assume following rates for both General Dynamics and NASA:				
Engineering: \$20/hr				
Shop: \$15/hr				
	<u>Engineering</u>	<u>Shop</u>	<u>Materials</u>	<u>Total</u>
Element Tests	\$ 95,280	\$120,300	\$24,050	\$239,630
3-Spar Wing Box	33,240	9,720	1,600	44,620
Fatigue Wing	61,360	23,520	9,100	93,980
Thrust Structure (GD)	50,840	27,300	1,500	79,640
GD Total	240,720	180,840	36,310	457,870
Thrust Structure (NASA)	20,000	25,500	0	45,500
NASA Total	20,000	25,500	0	45,500

provides for structure that is not designed for easy repairability, and inspection results that indicate out-of tolerance defects will lead to replacement rather than repair. With this concept the ratio of scheduled maintenance (inspection) to unscheduled maintenance (repair) will be higher. For the safe-life concept a value of 25 percent of scheduled maintenance is a more viable apportionment than the 50 percent used for the baseline concept.

For the establishment of maintenance values for the safe-life design, the structural data developed by this study and the application of the 25 percent constant to determine unscheduled maintenance was used. The results of this evaluation is shown in Table 4-4.

Table 4-4. Maintenance Manhours/Turnaround Safe-Life Concept

	Scheduled		Unscheduled	Total
	Routine	Phased		
LO <sub>2</sub> Tank	3	7-1/2	2-1/2	13
LH <sub>2</sub> Tank	3	7-1/2	2-1/2	13
Wing Box	3	10	3-1/2	16-1/2
Vertical Tail	1	6	2	9
Thrust Structure	2	6	2	10
Aft Orbiter	1	4	1-1/2	6-1/2
				68

4.2.3 **COSTS.** Consistent with the objectives of the economic analysis task, program cost differences between the baseline design and a design based on safe-life criteria were calculated. These cost differences were expressed as total booster program cost increments (deltas) from the baseline B-9U delta-wing configuration. This baseline configuration for costing was as documented in the Space Shuttle Phase B Final Report (Reference 15). Delta costs were calculated for two cases: a safe-life design of the B-9U delta wing booster, and a safe-life design of the B-16B swept-wing booster. The methodology employed in the analysis involved the calculation of cost differences in three distinct categories: direct costs, cascaded costs, and growth costs.

The direct cost differences are those program costs that are attributable to the specific subsystem hardware element being analyzed, such as the thrust structure, wing, etc. Weight and complexity changes from the baseline design result in differences to the respective subsystem's engineering design and development (EDD),

ground test hardware, flight test hardware, flight vehicle production, test article conversion, and operational spares costs. Tooling cost differences, which normally contribute to the direct cost differences, were felt to be negligible for this analysis because of the relatively small weight changes encountered and the absence of any significant shape or surface area differences in the components. The basic methodology used in determining these changes in EDD and hardware costs was to locate the detailed estimate of the corresponding B-9U element (wing, thrust structure, etc.) on a logarithmic plot of cost versus weight and pass a parametric scaling line through the point. The slope utilized for unit manufacturing cost scaling was 0.667, which was consistent with that used in the parametric cost model. Similar plots of component EDD costs were made with 0.187 slopes. No complexity factor changes were made in these plots.

The cascaded cost differences are those program costs that are not attributable to any specific subsystem or hardware component, but are a function of the complete booster program task. Elements included in the cascaded costs were vehicle installation, assembly, and checkout (IA&C/O); subsystem development testing (major ground test program); system engineering and integration; and booster program management. In our analysis the IA&C/O cost differences were assumed to be negligible because the major effort in this program cost element is related to tasks involving vehicle subsystems rather than the major structural elements of concern in this study. The subsystem development testing cost differences were generated as detailed estimates of unique safe-life and fail-safe testing requirements and included estimates of specific material, engineering labor, and shop labor requirements. For details of this analysis, see Sections 4.2.3 and 5.2.3. System engineering and integration costs were calculated as a percentage of the booster engineering design and development effort in the baseline cost model. This same percentage (15.5 percent) was applied to the summation of direct EDD delta costs calculated for each subsystem component (wing, thrust structure, aft orbiter attach frame) to obtain the cascaded SE&I delta costs. Booster program management is similar to SE&I in that a percentage of booster EDD costs was taken. This percentage (3.5 percent) was similarly applied to the summation of direct EDD delta costs.

The vehicle growth cost differences are those program costs that occur because of the spiraling effect of increased weight in a subsystem or group of subsystems. An example of this spiraling phenomena occurs when some incremental weight introduced into the wing causes greater load to be exerted in the thrust section, thus requiring a beefed-up structure, which in turn requires more attitude control system capability and more propellant tankage, etc., etc. The vehicle growth costs account for this phenomenon and they are applied in the form of a program cost penalty per pound of direct weight increase. For this study effort vehicle growth cost penalties applicable to the nonrecurring, recurring production, and recurring operations program phases were utilized. The values for these growth cost penalties were developed from a series of cost model runs on a set of vehicle configurations that had been resized

with varying amounts of contingency weight. The plotted results of these cost model runs gave us the isolated program delta costs corresponding to the weight spiraling effect of a one pound increase in structure weight. The resulting actual values that were used to generate the vehicle growth cost differences reported in this study were:

	Structure Wt Increase (\$/lb)
a. Nonrecurring program (development phase) cost =	725
b. Recurring production (procurement phase*) cost =	49
c. Recurring operations program cost =	101

These cost penalties were applied to the total structural weight increase due to the safe-life design concept. In addition to the hardware-associated operations costs (spares and repair parts), vehicle turnaround labor requirements were analyzed independently by Convair Aerospace operations personnel. Based on the results of this analysis, no cost penalties were applied to the safe-life design concept. The details of this analysis appear in Reference 16.

The following list of ground rules and assumptions apply to the cost developed in this analysis:

- a. All cost deltas represent increases from the baseline B-9U configuration program costs of Reference 15.
- b. The following weight penalties were used for costing:

	B-9U Safe-Life (lb)	B-16B Safe-Life (lb)
Wing	+1030	+1151
Thrust Structure	+0	+0
Orbiter Support Frame	+0	+0

---

\*Represents only about 1.5 equivalent vehicles due to conversion of flight test articles to operational inventory.



- c. The following equations were used to evaluate theoretical first unit (TFU) and engineering design and development (EDD) delta costs due to safe-life weight increases:

	<u>TFU</u>	<u>EDD</u>
Wing	0.02036 (wt) <sup>0.667</sup>	5.06851 (wt) <sup>0.187</sup>
Thrust Structure	0.02687 (wt) <sup>0.667</sup>	4.52167 (wt) <sup>0.187</sup>
Orbiter Support Frame (LH <sub>2</sub> Tank)	0.00916 (wt) <sup>0.667</sup>	2.79049 (wt) <sup>0.187</sup>

- d. The following hardware quantities (equivalent units) were assumed for calculating direct cost differences due to TFU changes:

	<u>Test Hardware</u>	<u>Production Articles</u>	<u>Test Article Conversion</u>	<u>Spares</u>
Wing	3.5	2	0	0.2
Thrust Structure	6.21	1	0.3	0.01
Orbiter Support Frame (LH <sub>2</sub> Tank)	6.01	1	0.3	0.005

- e. An inventory of four operational booster vehicles is assumed to perform 444 operational flight missions over 10 years. The first manned orbital flight is assumed to be in the development program.
- f. No main rocket engine costs are included.
- g. No prime contractor's fee is included.
- h. All costs assume constant 1970 dollars.

Table 4-5 shows the booster program cost penalties that were determined for the safe-life design concepts of a delta wing (B-9U) booster and a swept wing (B-16B) booster. Also shown are the delta costs attributable to direct, cascading, and vehicle growth cost effects. In the case of the direct weight cost deltas, individual penalties traceable to the wing, thrust structure, and orbiter aft support structure are shown.

Table 4-5. Booster Program Cost Penalties, Safe-Life Design

Vehicle Configuration	Direct Weight Cost Δ (\$M)	Cascading Program Cost Δ (\$M)	Weight Spiraling Cost Δ (\$M)	Total Cost Δ (\$M)
B-9U Booster	+1.799	+0.525 <sup>(1)</sup>	+0.901	+3.225
Wing	+1.799	—	—	
Thrust Structure	0	—	—	
Orbiter Support Structure	0	—	—	
B-16B Booster	+1.979	+0.527 <sup>(1)</sup>	+1.006	+3.512
Wing	+1.979	—	—	
Thrust Structure	0	—	—	
Orbiter Support Structure	0	—	—	

(1) Unique safe-life development program testing effort represents \$0.505M of this item. (Reference Section 4.3.1.)

## SECTION 5

### DEVELOPMENT OF FAIL-SAFE BOOSTER

In Section 3.4, the fail-safe capabilities of the selected booster components were investigated, with a summary of the results of this analysis shown in Tables 5-1 and 5-2 (and in Section 6). The analysis indicates that only the  $\text{LO}_2$  and  $\text{LH}_2$  tanks do not lend themselves to a fail-safe design philosophy. One component, the vertical tail, is inherently highly fail-safe in its baseline configuration by virtue of the extremely large crack length that may be sustained before the stress intensity factor reaches its critical value (reference Section 3.4.7). The five-spar B-16B swept wing is shown to be fail-safe (Section 3.4.5) because of the multiplicity of bending, shear, and torsional elements. The remaining components (the B-9U delta wing, thrust structure, and aft orbiter support frame) require various types and amounts of reinforcement to achieve fail-safe capability. These changes are described in subsequent paragraphs. As a matter of interest, the fail-safe characteristics of the three-spar B-16B swept wing were investigated in Section 3.4.6. This configuration was, not unexpectedly, found deficient in the crack arrest capability of the integrally stiffened skin. No remedial measures were determined, since the three-spar configuration was included in the study primarily as a safe-life design, the five-spar arrangement being the fail-safe configuration.

#### 5.1 DESCRIPTION OF STRUCTURAL CHANGES

The degree to which the baseline B-9U delta wing approaches a fail-safe design was determined in Section 3.4.4, which also shows the increase in section size required in certain members to achieve full fail-safe capability. Section 3.4.8 similarly shows the required increases in members of the thrust structure.

The baseline aft orbiter support frame does not possess fail-safe capability, because of its monolithic construction. An alternative fail-safe design concept was developed, and is presented in Figure 5-1(b). The alternative design consists of multi-element caps and dual shear webs, and retains the welded attachment to the tank wall for sealing against hydrogen leakage. With the failure of a single web or cap element, the remaining elements are sized to carry limit design load. An advanced composite (unidirectional graphite/epoxy) reinforcement is used at the inner flange of the frame. When tension stresses design the flange elements, a 0.75 rivet factor is used to account for the fasteners used to assemble the elements. Revised frame flange and web sizes are presented in Table 5-3, which shows the weight increase for the fail-safe frame design to be 720 pounds.

Table 5-1. Development of Fail-Safe Booster Design - B-9U Configuration

Component	Structural Design Concept	Change From Baseline Booster			$\Delta Wt.$ <sup>(3)</sup> (lb)	$\Delta Cost$ (\$M)
		Description	Material	Test Plan <sup>(2)</sup>	Maintenance Plan	
LO <sub>2</sub> Tank	Thin-wall pressure vessel with integral longitudinal stiffeners of 2219-T87 aluminum alloy	None-provision of fail-safe capability impractical	None	None	None	-
LH <sub>2</sub> Tank	Same as LO <sub>2</sub> Tank	Same as LO <sub>2</sub> Tank	None	None	None	-
Wing Box	Delta planform multi-spar box beam with chordwise corrugated skin, T1-6-4 annealed	Section increases required in certain spar caps, diagonals, webs and skins	None	Add fail-safe qualification test program	TBD	+668 (4)
Vertical Tail	Three-spar box (largely T1-6-4)	None (1)	None	None	None	-
Thrust Structure	Truss-type beam assembly, T1-6-4	Size increases required in five members	None	Same as wing box	TBD	+95 (4)
Aft Orbiter Support Frame	I-section ring, T1-6-	Change in design concept to box type section with composite reinforcement	Graphite epoxy composite reinforcement added	Same as wing box	TBD	+720 (4)
		Totals			+1483	+6.160 <sup>(4)</sup>

(1) Baseline configuration is inherently fail-safe.

(3) Weight increases include a non-optimum factor of 1.25.

(2) Based on a "bare bones" baseline test plan.

(4) Total cost contains amounts not broken down to specific components.

Table 5-2. Development of Fail-Safe Booster Design - B-16B Configuration

Component	Structural Design Concept	Change From Baseline Booster				$\Delta$ Wt. <sup>(2)</sup> (lb)	$\Delta$ Cost (\$M)
		Description	Material	Test Plan	Maintenance Plan		
LO <sub>2</sub> Tank	Thin-wall pressure vessel with integral longitudinal stiffeners of 2219-T87 aluminum alloy	None-provision of fail-safe capability impractical	None	None	None	-	-
LH <sub>2</sub> Tank	Same as LO <sub>2</sub> tank	Same as LO <sub>2</sub> tank	None	None	None	-	-
Wing Box	Five-spar swept wing box with chord-wise corrugated skin Ti-6-4 annealed	None(1)	None	Add fail-safe qualification test program	TBD	-	(3)
Vertical Tail	Three-spar box (largely Ti-6-4)	None(1)	None	None	None	-	-
Thrust Structure	Truss-type beam assembly, Ti-6-4	Size increases required in five members	None	Same as wing box	TBD	+95	(3)
Aft Orbiter Support Frame	I-section ring, Ti-6-4	Change in design concept to box type section with composite reinforcement	Graphite epoxy composite reinforcement added	Same as wing box	TBD	+720	(3)
Totals						+815	+4.373

(1) Baseline configuration is inherently fail-safe.

(2) Weight increases include a non-optimum factor of 1.25.

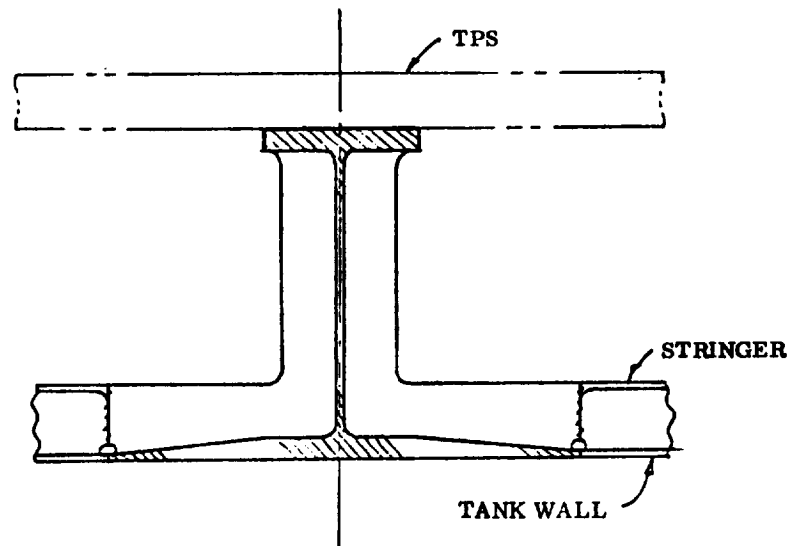
(3) Total cost contains amounts not broken down to specific components.

Table 5-3. Aft Orbiter Support Frame Modifications for Fail-Safe Capability

Bar <sup>1</sup>	Length (in.)	Critical Limit Axial Loads		Flange Members						Web Panels				
				Required Section Area (sq in)			Original Section Area <sup>1</sup> (sq in)	$\Delta A$ (sq in)	$\Delta W^7$ (lb)	Area <sup>1</sup> (in <sup>2</sup> )	Original $t^1$ (in.)	$t^8$ required (in.)	$\Delta t^9$ (in.)	$\Delta W^{10}$ (lb)
		Tension (kips)	Compression (kips)	Basic Member <sup>3</sup>	Aluminum Reinforcement <sup>4</sup>	Composite Reinforcement <sup>5</sup>								
1	40	216	-268	5.8	5.8	-	11.6	4.1	16.7	1	0.29	0.21	0.13	9.6
2	40	-	-167	3.3	-	0.99	3.8	-0.8	-3.3	2	0.34	0.24	0.14	20.6
3	50	157	-269	5.4	5.4	-	10.8	3.3	16.8	3	0.11	0.08	0.05	12.4
4	53	62	-129	2.6	-	0.77	3.0	-0.6	-3.2	4	0.42	0.30	0.18	37.6
5	52	-	-186	3.7	3.7	-	7.4	2.2	11.7	5	0.50	0.36	0.22	33.0
6	62	53	-	1.4	-	0.32	1.6	0.1	-0.6	6	0.33	0.24	0.15	32.2
7	117	-	-303	6.1	6.1	-	12.2	3.7	44.2	7	0.13	0.09	0.05	8.3
8	64	62	-115	2.3	-	0.68	2.7	-0.5	-3.3	8	0.04	0.04	0.04	10.1
9	98	-	-79	1.6	1.6	-	3.2	1.0	10.0	9	0.04	0.04	0.04	11.6
10	91	18	-132	2.6	-	0.79	3.4	-0.3	-2.8	10	0.04	0.04	0.04	16.1
11	102	24	-4	0.64	0.64	-	1.3	0.8	8.3					
12	91	-	-62	1.2	-	0.37	1.4	-0.3	-2.8					
13	55	1	-	0.30	0.30	-	0.60	0.10	0.56					
14	47	9	-5	0.50	-	0.15	0.58	0.08	0.4					
15	69	0	-4	0.30	0.30	-	0.60	0.10	0.70					
16	57	16	0	0.50	-	0.15	0.58	0.08	0.5					
17	67	-	-5	0.30	0.30	-	0.60	0.10	0.68					
18	53	10	-	0.50	-	0.15	0.58	0.08	0.4					
19	80	-	-4	0.30	0.30	-	0.60	0.10	0.82					
20	62	4	-	0.50	-	0.15	0.58	0.08	0.5					
										$\Sigma = 191.5$				
										$\Sigma = 96.3$				

- Note: 1. Information from Section 3.1.5.  
2. Limit loads are equal to ultimate loads from Table 3-6, divided by 1.4.  
3. Required basic member section area:  
Outer flange (odd numbered bars)  
 $A = \text{greater of: critical limit tension load/37.5, critical limit compression load/50 or minimum area of } 0.30 \text{ in}^2$   
Inner flange (even numbered bars)  
 $A = \text{greater of: critical limit load (tension or compression)/50 or minimum area of } 0.50 \text{ in}^2$   
4. For outer (odd numbered) members, required area of graphite/epoxy composite reinforcement is greater of: critical limit tension load/37.5, critical limit compression load/50, or minimum area of  $0.30 \text{ in}^2$ .  
5. For inner (even numbered) members, required area of aluminum reinforcement is greater of: critical limit tension load/37.5, critical limit compression load/50, or minimum area of  $0.15 \text{ in}^2$ .  
6. Aluminum equivalent of composite is section to give same weight, and  $A_{\text{comp}} (\rho_{\text{comp}}/\rho_{\text{alum}}) = A_{\text{comp}} (0.066/0.102) = 0.549 A_{\text{comp}}$   
7.  $\Delta W = L(\Delta A)(\rho_{\text{alum}})$   
8. For each of 2 webs,  $t_{\text{required}}$  is greater of:  $t_{\text{orig}}/1.4$  or minimum gage of 0.04.  
9.  $\Delta t = 2t_{\text{required}} - t_{\text{orig}}$   
10.  $\Delta W = A(\Delta t)(\rho_{\text{alum}})$

(a) Baseline Design Concept (Monolithic/Safe-Life)



(b) Alternate Fail-Safe Design Concept

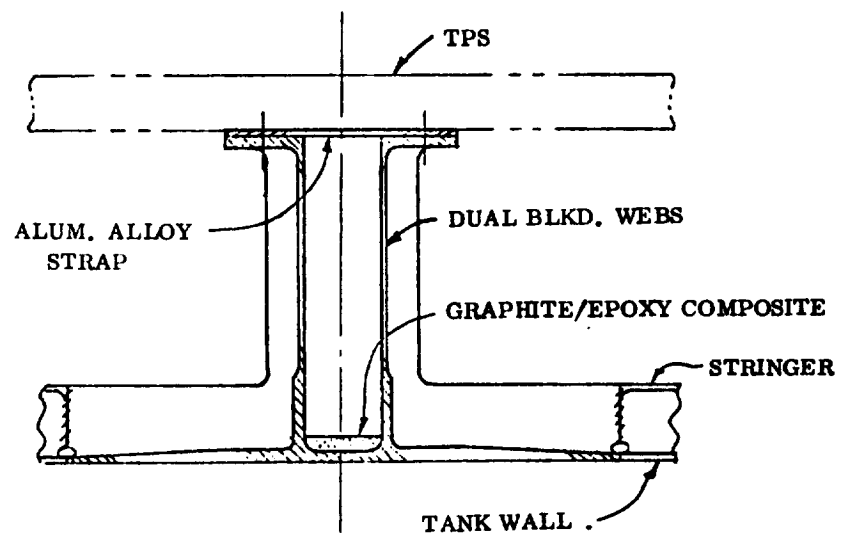


Figure 5-1. Aft Orbiter Support Frame Design Concepts

## 5.2 EFFECTS OF FAIL-SAFE APPROACH ON DEVELOPMENT PLANS

In the foregoing paragraphs, the structural changes necessary to accomplish a fail-safe design in each of the studied components are described. The resulting modifications to the baseline structural test plans, quality control and maintenance plans, and the overall effects on booster program costs due to application of the fail-safe philosophy are outlined below.

### 5.2.1 STRUCTURAL TEST PLANS

5.2.2.1 Additional Wing Tests. The fatigue qualification wing test article will be used after fatigue tests are completed. Tests will be conducted by the contractor. Static limit load tests at room temperature will be performed 30 times, each with a different pre-damaged location. Approximately 20 locations will be in spar caps, 5 in spar truss diagonals, and 5 in spar webs. Ten of these will be partial cuts with sharpening by applying approximately 500 load cycles. The previously damaged areas will be repaired, using a non-production type of repair, prior to proceeding with each predamage and test. Data will be recorded at five load increments from 40 strain gages in each test. It is assumed that 20 of these will be newly-installed gages. Baseline loading and data acquisition equipment will be used.

5.2.1.2 Additional Thrust Structure Tests. The fatigue qualification thrust structure will be used after fatigue tests are completed. This structure will be installed on the full body structure tested at NASA-MSFC. Static limit load tests at room temperature will be performed ten times, each with a different pre-damaged location. Approximately six locations will be in cap elements and four in diagonal elements. Three of these will be partial cuts with sharpening by applying 500 load cycles. Previously damaged areas will be repaired prior to proceeding with each pre-damage and test. Data will be recorded at five load increments from 20 strain gages on each test. It is assumed ten of these are newly-installed gages. Baseline loading and data acquisition equipment will be used.

5.2.1.3 Test Costs. Fail-safe test costs are given in Table 5-4.

5.2.2 QUALITY CONTROL AND MAINTENANCE PLANS. A fail-safe design requires a maintenance approach that inspects for gross defects, and the inspection interval must be much smaller than for the safe-life design, because of the potential accelerated growth of defects in the structure adjacent to the gross failures.

Table 5-5 reflects the above differences for all structural components evaluated except propellant tanks, which of necessity are considered safe-life structures.



Table 5-4. Costs for Fail-Safe Tests

	Engrg M-H	Shop M-H	Matl \$
<b>A. Wing Fatigue Article (Contractor)</b>			
Damage Preparation			
30 Locations @ 8 hr = 240			
4 engineering	960		
4 shop		960	
Repair Design 29 @ 40 hr	1,160		
Repairs 29 @ 6 Shifts			
Average = 1390 hr	5,560	5,560	
Material: (300 lb) (29) (0.15/lb) steel			1,300
bolts (29) (50)			1,500
Pre-Cracking			
(10) (500 cyc) ( $\frac{\text{hr}}{100 \text{ cyc}}$ ) = 50 hr	200	200	
Install 20 Strain Gages/Test			
(30 tests) (20 gages) (10 hr/gage)	6,000		
Material (30) (20) (\$10/gage)			6,000
Test - Limit Load - 1 Condition			
(30 tests) (8 hr/test) = 240 hr	960	960	
Data Processing 4 hr/test @ 4 men	480		
Computer (\$350) (30)			10,500
Test Report 1 man, 2 mo; 30 photos @ 15	336		450
Design/Stress			
Schedule 240 + 1390 + 50 + 240 = 1,920			
$\frac{1920}{167} = 1 \text{ yr or } 6 \text{ mo @ } 2 \text{ shifts}$			
6 men, 6 months	6,000		
Project Office, Supervision 10%	2,165		
Totals	23,821	7,680	19,750

Table 5-4. Costs for Fail-Safe Tests, Contd

	Engrg M-H	Shop M-H	Matl \$
<b>B. Thrust Structure Fatigue Article (NASA MSFC)</b>			
Damage Preparation			
10 Locations @ 8 hr = 80			
6 engineering	480		
10 shop		800	
Repair Design 9 @ 40	360		
Repairs 9 Locations @ 10 Shifts			
Average = 720 hr	4,320	7,200	
Material: (300 lb) (9) (0.15/lb) steel			400
Bolts (9) (50)			450
Pre-Cracking			
(3) (500 cyc) ( $\frac{\text{hr}}{100 \text{ cyc}}$ ) = 15 hr	90	150	
Install 10 Strain Gages/Test			
(10 tests) (10 gages) (10 M-H)	1,000		
Material: (10) (10) (\$10)			1,000
Test (10 tests) (8 hr) = 80 hr	480	800	
Data Processing 4 hr/test @ 4 men	160		
Test Report 1 man, 5 weeks, 10 photos @ 15	200		150
Design/Stress			
Schedule 80 + 720 + 15 + 80 = 895 hr			
$\frac{895}{147} = 5.4 \text{ mo or } 2.7 \text{ mo @ 2 shifts}$			
6 men, 3 mo.	3,000		
Project Office, Supervision 10%	1,000		
G.D. Totals	11,090	8,950	2,000
NASA: 6 engineering   3 mo	3,000	5,000	
10 shop			
Computer (MSFC) (\$350) (10)			3,500

Table 5-4. Costs for Fail-Safe Tests, Contd

C. Summary

Assume following rates for both General Dynamics and NASA:

Engineering: \$20/hr

Shop: 15/hr

	<u>Engineering</u>	<u>Shop</u>	<u>Materials</u>	<u>Total</u>
Wing	\$ 476,420	\$ 115,200	\$ 19,750	\$ 611,370
Thrust Structure (SD)	<u>221,800</u>	<u>134,250</u>	<u>2,000</u>	<u>358,050</u>
Contractor Total	698,220	249,450	21,750	969,420
NASA Total	60,000	75,000	3,500	138,500

Table 5-5. Maintenance Manhours/Turnaround,  
Fail-Safe Design

	<u>Scheduled</u>		<u>Unscheduled</u>	<u>Total</u>
	<u>Routine</u>	<u>Phased</u>		
LO <sub>2</sub> Tank	3	7 1/2	2 1/2	13
LH <sub>2</sub> Tank	3	7 1/2	2 1/2	13
Wing Box	2	4 1/2	3 1/2	10
Vertical Tail	1/2	4 1/2	3	8
Thrust Structure	2	1	2	5
Aft Orbiter Support Frame	1/2	1	1	<u>2</u>
				51

5.2.3 COSTS. The approach taken in the determination of the program cost differences between the baseline design and a design based on fail-safe criteria was similar to that followed for the safe-life design and described in Section 4.2.3, except for the direct cost delta for the aft orbiter attach frame, which required boron/epoxy composite reinforcement. As this item's  $\Delta$ cost is calculated within the LH<sub>2</sub> tank cost, the effects of complexity differences were diluted in proportion to this item's

fraction of the total tank weight. A complexity factor of 12 (as compared to aluminum sheet stringer construction) was assumed for the composite portion of the frame. This resulted in an equivalent complexity increase on the whole  $LH_2$  tank of about 10 percent in TFU cost. Using these cost versus weight plots and an appropriate complexity factor, TFU manufacturing and EDD costs for the higher-weight safe-life and fail-safe components were determined. The  $\Delta$ TFU cost was then multiplied by appropriate hardware quantities for the test, test article conversion, production and spares programs. When combined with the  $\Delta$  EDD costs the total direct cost delta for the respective subsystem element was obtained. The computation of these deltas is shown below.

$$TFU^* = 0.009066 (88193)^{0.667} = \$18.031M$$

$$TFU_{FS B9U} = 0.009157 (88193 + 720)^{0.667} = \$18.310M$$

$$\Delta TFU = 0.279$$

$$EDD_{B9U} = \$23.468M$$

$$EDD_{FSB9U} = 2.79049 (88193 + 720)^{0.187} = 23.504$$

$$\Delta EDD = +0.036$$

$$\begin{aligned} \Delta \text{Test Hardware} &= (\text{No. Ground Test Units} + \text{No. Flight Test Units} \\ &\quad + \text{Equivalent Flight Test Spares}) \Delta TFU \\ &= (4 + 2 + 0.01) (+0.279) = 1.677 \end{aligned}$$

$$\Delta \text{Tooling} = \text{No Change}$$

$$\text{Direct Nonrecurring Cost } \Delta = 1.713$$

$$\begin{aligned} \Delta \text{Production} &= (\text{No. Production Units}) (\Delta TFU) \\ &= (1.0) (+0.279) = +0.279 \end{aligned}$$

$$\begin{aligned} \text{Test Article Conversion} &= (\text{Equiv. Units for TAC}) (\Delta TFU) \\ &= (0.3) (+0.279) = +0.83 \end{aligned}$$

$$\text{Direct Recurring Production Cost } \Delta = +0.362$$

$$\begin{aligned} \Delta \text{Recurring Operations Hardware} &= (\text{Equivalent Operations Spares Units}) (\Delta TFU) \\ &= 0.005 (+0.279) = +0.001 \end{aligned}$$

$$\text{Direct Recurring Operations Cost } \Delta = +0.001$$

$$\text{Total Direct Cost Delta, B-9U Fail-Safe Orbiter Support Frame} = \$ + 2.076M$$

---

\*Theoretical First (Production) Unit Cost

Table 5-6 shows the booster program cost penalties that were determined for the fail-safe design concepts of a delta wing (B-9U) booster and a swept wing (B-16B) booster. Also shown in the table are the delta costs attributable to direct, cascading, and vehicle growth cost effects. In the case of the direct weight cost deltas, individual penalties traceable to the wing, thrust structure, and orbiter aft support structure are shown.

Table 5-6. Booster Program Cost Penalties,  
Fail-Safe Design

Vehicle Configuration	Direct Weight Cost Δ (\$M)	Cascading Program Cost Δ (\$M)	Weight Spiraling Cost Δ (\$M)	Total Cost Δ (\$M)
B-9U Booster	+ 3.729	+ 1.131 <sup>(1)</sup>	+ 1.300	+ 6.160
Wing	+ 1.188	-	-	
Thrust Structure	+ 0.465	-	-	
Orbiter Support Structure	+ 2.076	-	-	
B-16B Booster	+ 2.541	+ 1.119 <sup>(1)</sup>	+ 0.713	+ 4.373
Wing	0	-	-	
Thrust Structure	+ 0.465	-	-	
Orbiter Support Structure	+ 2.076	-	-	

(1) Unique fail-safe development program testing effort represents \$1.108M of this item.

Significant uncertainty exists in the cost results shown both in safe-life and fail-safe designs. Any extrapolation of these results to other subsystems would, of course, be at least as uncertain as for the specific subsystems analyzed. The weights utilized in developing the cost penalties are a significant source of uncertainty because the booster design concept is still relatively immature and the indicated weight differences between the design concept represent only about  $\frac{1030}{626933} = 0.16\%$  for the B-9U safe-life design.

Another reason for uncertainty is that these cost differences between safe-life and fail-safe are extremely small (\$1 to \$3 million) when compared to the total program cost of almost \$4 billion. Compounding this uncertainty is the fact that schedule effects were not analyzed. The peak year funding requirements as opposed to total program cost or operations cost per flight has been of primary importance to NASA in recent months.



## SECTION 6

### CONCLUSIONS AND RECOMMENDATIONS

This section summarizes the analytical results obtained for the baseline booster vehicles and presents the conclusions to be drawn therefrom. Finally, recommended space shuttle booster design approaches and changes to the preliminary structural design criteria (Reference 2) are presented. These recommendations are based primarily on the study results.

#### 6.1 SUMMARY OF STUDY RESULTS

**6.1.1 CAPABILITY OF BASELINE BOOSTERS.** Table 6-1 presents in a highly visible form the results of the fatigue, safe-life, and fail-safe analyses conducted on the baseline booster structural components, and represents the capability of these components when designed for static strength and the factor of safety criteria of Section 2.5.

As can be seen, all structural components investigated show adequate fatigue life for the assumed stress concentration factor (i.e.,  $K_T = 3.0$ ) and the scatter factor of four on life. The majority of the components exhibit fatigue lives many times greater than the required design service life of 100 missions. The component with the lowest fatigue life is the delta wing lower spar caps which have a fatigue life of 175 missions.

The results of the safe-life analysis of structural components containing initial flaws are similar to the fatigue analysis, with many components having a safe-life to failure in excess of the 100 mission design service life with initial flaw sizes within reasonable non-destructive inspection detection limits. The wing box structures show very short safe-lives to failure (i.e., 3 flights for the B-9U delta wing and 12 flights for the B-16A swept wing) for the initial flaw types and sizes assumed. These short safe-lives are caused by the severity of the wing load spectrum, the poor flaw growth properties of titanium (Reference Section 3.3), and the high limit stress level used in sizing the wing spar cap members. As discussed in Section 4, a lowering of the wing spar cap limit stress level is required (i.e., causing a B-9U wing weight increase of 1030 pounds) to show a wing safe-life equal to a selected 25 flight safe-inspection interval.

The results of the fail-safe analysis show that the propellant tanks and orbiter support bulkhead have no fail-safe capability (i.e., a residual strength representing a very low percentage of limit design load) when obvious partial failures (i.e., gross flaws

Table 6-1. Summary of Analytical Results for Baseline Booster Vehicles

Component Description <sup>1</sup>				Safe-Life <sup>3</sup>				Fail-Safe				
Component	Material	Type of Load	Fatigue Life <sup>2</sup> σ <sub>limit</sub> (missions)	Type of Flaw	Flaw Aspect Ratio (a/2c)	Initial Flaw Size a <sub>i</sub> (inches)	Critical Flaw Size a <sub>c</sub> (2C <sub>cr</sub> ) (inches)	Life to Leak (missions)	Safe-Life to Failure (missions)	Assumed Partial Failure	Fail-Safe Capability (% of limit load)	Remarks
A. LO <sub>2</sub> Tank Wall (upper dome equator)	2219-T87	Pressure	44.0	a. Surface	0.10	0.0546	0.0709	294	294	—	—	No fail-safe capability with obvious partial failures
				b. Surface	0.41	0.09 = t	—	1	—	—		
				c. Through	—	(0.1767)	(0.3066)	—	867	—	—	
B. LH <sub>2</sub> Tank Wall (upper dome equator)	2219-T87	Pressure	40.1	a. Surface	0.10	0.0620	0.0805	626	626	—	—	
				b. Surface	0.40	0.116 = t	—	1	—	—		
				c. Through	—	(0.2278)	(0.2798)	—	160	—	—	
				Flight Conditions Not Critical				1.6 in. circumferential thru-crack				
C. Thrust Structure	Ti-6Al-4V	Thrust	92.9	a. Corner	—	0.10	0.4036	—	1555	a. Thrust beam diagonal	96	Only small area of thrust structure critical with assumed partial failures.
				b. Through crack from 1/4 in. hole	—	0.10	0.1694	—	101	b. Thrust beam cap	63	
D. Vertical Tail Box Cover	Ti-6Al-4V	Flight	34.0	Through crack	—	1.00	3.912	—	534	Chordwise crack through skin and stringers.	100	Cover sized by compression results in high fail-safe capability.
E. Orbiter Support Bulkhead	2219-T87	Flight	35.0	a. Corner	—	0.10	0.586	—	large	—	—	No fail-safe capability with obvious partial failures.
				b. Through crack from 1/4 in. hole	—	0.10	0.2906	—	large	—	—	
F. B-9U Delta Wing Box	Ti-6Al-4V	Flight	91.2	a. Corner	—	0.10	0.4206	—	31	a. Lower spar cap failed	47	Critical elements are adjacent to failed members
				b. Through crack from 1/4 in. hole	—	0.10	0.1831	—	3	b. Spar diagonal failed	66	
G. B-16B Swept Wing Box (Five Spar)	Ti-6Al-4V	Flight	73.0	Through crack from 1/4 in. hole	—	0.10	0.340	—	12	Lower spar cap failed	107	—

Notes: 1. When not defined, the component is common to both the B-9U delta wing and B-16B swept wing configurations.

2. Scatter factor of 4 on life included;  $K_T = 3.0$ .

3. Scatter factor of 1.5 on life included.

4. Minimum fail-safe capability for all assumed partial failures of the type specified.



detectable by normal visual inspection) are assumed. Attempts to provide fracture arrest capability at crack stoppers on the propellant tanks (similar to commercial transport practices) showed prohibitive weight increases. The fail-safe analysis also showed the wing, thrust, and vertical tail structures to have a high degree of fail-safe capability, although not sufficient to provide for limit load residual strength in the case of the B-9U delta wing and the thrust structure. This high fail-safe capability is due to the inherent features of the structural arrangement (i.e., multiplicity of members and redundancy) in the case of the wing and thrust structure, and due to low tensile stresses resulting from compression critical design in the case of the vertical tail. For the thrust structure and the B-9U delta wing, it was found that the critical elements were generally in the area of the assumed partial failure, and that the weight increases required to obtain limit load fail-safe capability were small (e.g., 95 pounds for the thrust structure and 670 pounds for the B-9U delta wing) when compared to the total component weight (Reference Table 2-3).

**6.1.2 ADEQUACY OF BASELINE DEVELOPMENT PLANS.** The structural test and maintenance plans presented in Sections 2.8 and 2.9 for the baseline booster vehicles have been examined to determine if they are adequate for their intended purpose (i.e., that of qualifying the structural system and maintaining it free of defects) in the light of the analysis that has been accomplished.

The structural test plans presented in Section 2.8 provide a "bare-bones" structural test plan adequate to demonstrate that the booster structure is free of design deficiencies which could lead to fatigue or static failures; however, additional tests are required to demonstrate residual life or residual strength in the wing and thrust structures when safe-life or fail-safe design approaches are adopted. These additional tests and associated costs are described in detail in Sections 4 and 5 for the safe-life and fail-safe boosters respectively.

The detail maintenance plan presented in Section 2.9 for the baseline boosters appears to be generally adequate with the following exceptions. The phased non-destructive evaluation (NDE) tasks on the safe-life LO<sub>2</sub> and LH<sub>2</sub> propellant tanks and safe-life orbiter support bulkheads can be reduced to a minimum because of the large safe-lives calculated and proof test approach used. Similarly the phased NDE tasks on the fail-safe delta wing, swept wing, thrust structure, and orbiter support frame can be reduced to a minimum because the fail-safe approach requires only a visual search for gross defects and failures. The minimum NDE tasks mentioned above should retain a phased NDE of points of severe stress concentration such as lugs and load carrying doors. The phased NDE inspection interval of the safe-life delta wing, swept wing, and thrust structure can be modified to be equal to or less than the selected safe inspection intervals presented in Section 2.9. In the case of the safe-life

wings where the selected safe inspection interval was 25 flights (requiring reduced stresses from the baseline booster wings), the optimum approach would probably be a phased NDE inspection every 5 flights of 20 percent portions of the wing spar caps, such that after 25 flights all the spar caps would have been inspected. This procedure would provide a more uniform spread of maintenance tasks with minimum impact on turn-around time and efficient manpower utilization. The interiors of the fail-safe delta and swept wings require a visual inspection for gross defects every flight because of the high stress in the members adjacent to a failed member and the potential rapid growth of defects if present in these adjacent members. It is anticipated that visual inspections aided by spotlights from spaced access points would be adequate.

**6.1.3 IMPACT OF SAFE-LIFE/FAIL-SAFE DESIGN APPROACHES.** Table 6-2 summarizes the weight impact of alternately emphasizing safe-life and fail-safe design approaches to the maximum practical extent on the B-9U delta wing and B-16B swept wing boosters. It can be seen that the weight impact is small (less than 1 percent when compared to the total weight of the components investigated).

When considering the impact of safe-life on fail-safe approaches on performance, the reduced performance is expressed in terms of pounds of payload delivered to orbit. Phase B studies show that for every 1000 pounds of booster weight added, the payload in orbit is reduced by 165 pounds. The total baseline booster payload is 40,000 pounds. Table 6-3 presents the performance penalties when the increases in the booster structural weight are conservatively extended to the entire booster structure (excluding TPS) on the percentage basis identified in Table 6-2. These losses are less than one percent of the total payload weight.

Table 6-4 presents the impact of safe-life or fail-safe design approaches on total space shuttle booster program costs. The cost increases are due primarily to the component weight increases, and to some extent to increased component complexity (e.g., fail-safe orbiter support bulkhead).

The delta costs due to the revised structural test plans discussed in Sections 4.2.1 and 5.2.1 were found to be highly significant (Reference Tables 4-2 and 5-3), while the delta costs due to the revised maintenance plans discussed in Sections 4.2.2 and 5.2.2 were of lesser significance, compared to the delta costs due to the structural weight increase.

**6.1.4 EFFECTS OF ALTERNATE MATERIALS.** Section 3.5 presents an analysis of the effect of substituting 2219-T87 aluminum for titanium-6Al-4V (annealed) in the wing spar caps and thrust beam caps of the baseline B-9U delta wing booster. These members are tension critical and susceptible to fatigue and brittle fracture failures. The results of fatigue and safe-life analysis of these components and materials are summarized in Table 6-5.

Table 6-2. Weight Impact of Safe-life/Fail-safe Design Approaches  
(Pounds of Structure Added)

Design Booster Configuration	Safe-Life		Fail-Safe	
	Component	ΔWt.	Component	ΔWt.
B-9U Delta Wing [ Total wt. of components investigated = 169,734 lb Total struct. wt. excluding TPS = 251,023 lb ]	LO <sub>2</sub> Tank	0	LO <sub>2</sub> Tank	0
	LH <sub>2</sub> Tank	0	LH <sub>2</sub> Tank	0
	Wing Box	1030	Wing Box	668
	Vertical Tail	0	Vertical Tail	--
	Thrust Structure	0	Thrust Structure	95
	Orb. Supt. Frame	0	Orb. Supt. Frame	720
		Σ = 1030 lb % increase = 0.61		Σ = 1483 lb % increase = 0.88
B-16B Swept Wing [ Total wt. of components investigated = 166,892 lb Total struct. wt excluding TPS = 248,181 lb ]	LO <sub>2</sub> Tank	0	LO <sub>2</sub> Tank	0
	LH <sub>2</sub> Tank	0	LH <sub>2</sub> Tank	0
	Wing Box	1151	Wing Box	0
	Vertical Tail	--	Vertical Tail	0
	Thrust Structure	--	Thrust Structure	95
	Orb. Supt. Frame	--	Orb. Supt. Frame	720
		Σ = 1151 lb % increase = 0.68		Σ = 815 lb % increase = 0.49

**Table 6-3. Performance Impact of Safe-Life/Fail-Safe Design Approaches (Pounds of Payload Lost)**

<b>Booster Configuration \ Design Concept</b>	<b>Safe-Life</b>	<b>Fail-Safe</b>
B-9U Delta Wing	$0.165(0.61 \times 251,023)/100$ = 253 lb	$0.165(0.88 \times 251,023)/100$ = 364 lb
B-16B Swept Wing	$0.165(0.68 \times 248,181)/100$ = 278 lb	$0.165(0.49 \times 248,181)/100$ = 200 lb

**Table 6-4. Cost Impact of Safe-Life/Fail-Safe Design Approaches ( $\Delta$  \$ on Total Program)**

<b>Booster Configuration \ Design Approach</b>	<b>Safe-Life (\$M)</b>	<b>Fail-safe (\$M)</b>
B-9U Delta Wing	+ 3.225	+ 6.160
B-16B Swept Wing	+3.512	+ 4.373

As can be seen, the aluminum shows lower fatigue life; however, most significantly, a large increase in safe-life occurs when initial flaws are assumed. This increased safe-life when 2219-T87 aluminum is substituted is attributed to the fact that aluminum and titanium have similar flaw growth curves (i.e.,  $da/dn$  versus  $\Delta K$ ) as shown in Figure 3-45, and the fact that the  $\Delta K$ 's in aluminum are approximately 50 percent of the  $\Delta K$ 's in titanium, due to lower working stresses based on strength design. However, if the design stresses for the titanium were reduced to give the same structural weight with aluminum the titanium safe-life design would more closely approach the life of the aluminum design.

## 6.2 CONCLUSIONS

It is concluded from the fatigue and safe-life analyses that:

- a. Except for the wing (reference Table 3-34) conventional fatigue is not a critical design condition for the booster structure because of its short service life.

Table 6-5. Summary of Fatigue Life and Safe-Life of Titanium and Aluminum Components

Component	Material	$\sigma_{LIMIT}$ (ksi)	Fatigue (1)		Safe-Life <sup>(1)</sup> Missions
			Life (missions)	Assumed Flaw	
Thrust Beam Caps	Ti-6Al-4V	92.9	887	0.10 in. corner	824
	2219-T87	45.7	824	crack	large
B-9U Delta Wing Spar Caps	Ti-6Al-4V	91.2	111	0.10 in. corner	31
	2219-T87	43.5	44	crack	large

(1) Includes S.F. = 4 for fatigue and S.F. = 1.5 for safe-life

- b. The wing service load spectrum is severe because of many near-design limit loads applied during ascent and entry, and conversely, the vertical tail and orbiter support load spectrum is mild.
- c. The fatigue analysis and fatigue test tasks on the booster structure can be reduced to a minimum; however, the full scale fatigue qualification tests should be retained because their primary objective is to drive out design deficiencies not apparent from the fatigue and strength analysis.
- d. The stress analysis can afford the luxury of assuming the booster structure to contain initial flaws, and show adequate safe-life without serious weight penalties. Adequate safe-life is a safe-life that exceeds the lesser of the selected inspection interval or the design service life.
- e. The weight impact of safe-life or fail-safe design approaches is approximately 0.5 to 1.0 percent, and probably less than the weight increase due to other design considerations such as machining tolerances.
- f. The choice of safe-life or fail-safe design criteria and approach does not exert a strong influence on the space shuttle booster weight, performance, or cost.
- g. The choice of safe-life or fail-safe design approach is not significantly sensitive to booster configuration, provided design ingenuity is used to minimize the weight penalty of selected fail-safe approaches.
- h. The analytical results regarding the fatigue life, safe-life, and fail-safe capability of the booster components, and the weight penalties associated with the selected safe-life and fail-safe requirements are highly dependent on the factor of safety criteria and life scatter factors selected.

### 6.3 RECOMMENDED SPACE SHUTTLE BOOSTER STRUCTURAL DESIGN APPROACH

The optimum choice of criteria and approaches for the space shuttle booster structural system is a mixture of safe-life and fail-safe approaches that:

- a. Are dependent on the vehicle and component size and shape.
- b. Take advantage of the inherent features of the structural arrangement (e.g., multiplicity of members such as in thrust structures and low aspect ratio wing boxes, and lack of severe stress concentration points because of sculptured or welded construction).
- c. Are influenced by mild service load spectra when compared to other design conditions (i.e., compression or stiffness requirements, etc.).

The recommended booster structural design approach is a program that includes the following elements:

- a. Development of service load spectra concurrent with the design loads.
- b. A program of fatigue, safe-life, and fail-safe analysis concurrent with the component design.
- c. A program of component safe-life/fail-safe design trade studies which considers the design criteria, desired safe-life or fail-safe characteristics, design stress levels based on (a) above, variation of material flaw growth and fracture characteristics, inspection plans, access provisions, NDT capability, manufacturing constraints, weight, and cost, as well as the usual static strength, stiffness, and functional requirements.
- d. Development of quality control, nondestructive testing (NDT), and maintenance plans concurrent with the booster design.
- e. Development of a comprehensive fracture control plan to integrate and coordinate the above tasks, and to monitor the booster structural integrity during its service life.

### 6.4 RECOMMENDED CHANGES TO DESIGN CRITERIA

This section contains recommended revisions to Reference 2, NASA SP-8057, Structural Design Criteria Applicable to a Space Shuttle. This document, discussed in Section 1.1, was developed by NASA and other governmental agency and industry representatives. These revisions are based on the experience gained in performing

the analyses of Section 3, and also incorporate conclusions arrived at in other portions of the study. All paragraph and page numbers referred to herein are those of Reference 2. The underlined paragraphs have the same meaning as the bold-faced ones in Reference 2.

## 1.6 DEFINITIONS

Add the following definition:

"FATIGUE LIFE. The life of an unflawed structural component to the initiation of visible fatigue cracks."

Change the definition of safe-life to:

"SAFE LIFE. The life for initial defects in a component to grow to critical size for catastrophic failure."

Reason: To give precise definitions to terms which will be used subsequently.

## 2. RELATED DOCUMENTS

On page 2-2, OTHER NASA PUBLICATIONS, add:

"Preliminary Criteria for the Fracture Control of Space Shuttle Structures, June 1971."

Reason: To add a recent reference pertinent to sound structural design and construction.

On page 2-3, OTHER PUBLICATIONS, add:

"DMIC Memorandum 252, Broek, David: Concepts in Fail-Safe Design of Aircraft Structures. Defense Metals Information Center, March 1971."

Reason: To add a reference showing good practice.

### 4.7.3.1 FATIGUE

Change title to "FATIGUE AND SAFE-LIFE," and rewrite the section as follows:

"The fatigue-life and safe-life characteristics of structural materials shall be determined by experiment for appropriate cyclic loading and temperature conditions."

"Both crack initiation and crack-propagation characteristics should be evaluated with geometric parameters (i.e., gages and stress concentrations) which simulate the design conditions. It should be assumed that the fabricated structure contains flaws of the maximum size that cannot be detected by ordinary inspection processes or by proof test. For the selected material, the number of stress cycles required to initiate fatigue flaws and the number of stress cycles required to grow the maximum possible initial flaw to a size sufficient to initiate fracture shall exceed the specified fatigue life and safe-life respectively which are based on multiples or increments of the specified service life. If it is suspected or known that the environment in which the structure operates will accelerate the flaw initiation and growth, then this environment should be accounted for by the analysis or test. If the analysis shows that a specific vehicle or component with a specific material has more than adequate fatigue life and safe-life with proper allowances for extension of the vehicle life, then some of the requirements of this section can be waived."

Reason: The criteria of this section lump discussion of fatigue (i.e., crack initiation) and safe-life (i.e., crack propagation) under the common title of fatigue, which is not consistent with the definitions of section 1.6. In addition, the life of structures which contain flaws cannot be expected to exceed the specified fatigue life or service life of the vehicle. Also, it is not necessary to perform extensive fatigue and crack-propagation tests if it can be shown by analysis with preliminary data that the structure possesses more than adequate fatigue life and safe-life.

#### 4.7.3.2 BRITTLE FRACTURE

Based on the comments noted for 4.7.3.1 above, it is recommended that the following be added to Section 4.7.3.2:

"If analysis shows that a specific vehicle or component with a specific material is not prone to brittle fracture or has adequate safe-life with proper allowances for extension of the vehicle life, then some of the requirements of this section can be waived."

Reason: Same as for 4.7.3.1.

#### 4.8 SERVICE LIFE

Add the following:

"All structures vital to the integrity of the vehicle or the safety of the personnel shall be designed for adequate fatigue life. The fatigue life



shall be determined by analysis and fatigue test to be at least four times the specified service life.

"In addition, safe-life or fail-safe design concepts, analysis, and tests shall be employed to determine the residual strength and residual life of structures containing flaws or defects due to manufacturing or service conditions, and to establish fracture control approaches and plans for all structural components of the vehicle.

"The choice of safe-life or fail-safe design approaches should exploit the inherent safe-life or fail-safe features of the vehicle configuration and structural arrangement, and should be selected based on minimum impact to the vehicle weight, performance, and costs. The basic objective of the design approach and fracture control plan shall be to ensure that unacceptable structural failures due to crack-initiated fractures will not occur during the service life of the vehicle."

Reason: The confusion that exists regarding the precise definitions of fatigue life and safe-life is apparent in this section. Section 4.8.1 (i.e., safe-life) dictates that safe-life design concepts shall be applied to all structures vital to the integrity of the vehicle or the safety of personnel. This is not necessary since fail-safe design concepts with fatigue lives of at least four times the specified service life are equally as acceptable as safe-life design concepts.

#### 4.8.1 SAFE-LIFE

Delete the first paragraph of 4.8.1 and substitute the following:

"Safe-life design concepts shall be applied to all structure where a safe-life approach has been selected as the optimum structural approach based on weight, performance, and cost, or a fail-safe design approach is not practical. The safe-life shall be determined by analysis and test to be at least TBD times the specified service life or the selected inspection interval."

Reason: Same as for Section 4.8.

#### 4.8.2 FAIL-SAFE

Delete the first two paragraphs of Section 4.8.2 and replace with the following:

"Where practical, fail-safe design concepts shall be applied; however, the concepts shall be compared to safe-life design concepts for impact on total

program cost and performance. The impact of additional or more severe stress raiser on the fatigue life of the structure shall also be investigated.

'Where inherent fail-safe features such as stringers, splices, or redundant structural arrangements exist in the selected design, these features shall be enhanced and exploited to the extent required to comply with the fail-safe requirements.

'Fail-safe designs can be provided by multi-element or redundant structural arrangements, and by fracture arrest by non-integral or integral crack stoppers and stiffening elements. For all multi-element or redundant fail-safe structures, the fail of a single principal structural element shall not degrade the strength or stiffness of the structure below that necessary to carry a specified percentage of limit load. For fail-safe structures relying on fracture arrest capability, the propagating crack shall be arrested by the crack stopper at the specified percentage of limit load and shall account for the dynamic effect of suddenly failing elements.'

Reason: Same as for Section 4.8.

#### 4.8.3 MATERIAL PROPERTIES

Delete the first sentence in the second paragraph of Section 4.8.3 and replace with the following:

'Analysis of flaw growth shall account for material properties, loading conditions and associated stress levels, environmental conditions, the scatter of flaw growth data, the effect of cyclic load rate, and the size and source of flaws throughout the structure.'

Reason: Flaw growth scatter must be accounted for in the prediction of safe-life.

#### 4.8.7.1 METALLIC PRESSURE VESSELS

Delete the first paragraph of Section 4.8.7.1 and replace with the following:

'Flaw growth shall not exceed the growth required to increase the maximum undetectable initial flaw to a size where the stress intensity under limit-stress levels exceeds the critical stress intensity values for the design geometry. The effect of load excursions which result in stress intensities above the threshold ( $K_{TH}$ ) shall account for both cyclic and sustained load flaw growth in the predictions. Where the design geometry is thinner than

that required to produce plane strain conditions, the fracture toughness determined by specific tests which duplicate the design conditions may be used to establish the critical stress intensity values."

Reason: The applied stress intensity under maximum service load conditions may exceed the threshold stress intensity values, provided that sustained load flaw growth is accounted for in the flaw growth safe-life prediction. To restrict the applied stress intensity values to values lower than the threshold stress intensity values would result in prohibitive weight increases for space shuttle pressure vessels.

## 7.2 ANALYSES

Add the following sentence after the second sentence of Item 3 of Section 7.2:

"The stress analysis shall include fatigue, safe-life, and fail-safe analyses to establish the tolerance of the structure to the initiation and propagation of crack-like defects during the testing and service life of the vehicle."

Reason: Stress analysis is the primary method to verify structural adequacy. The stress analysis should encompass fatigue, safe-life, and fail-safe analyses as well as conventional static strength and deformation analyses.

### 7.4.1 PHYSICAL PROPERTIES

Delete MIL-A-8860 (ASG) and MIL-STD-143A, and replace with MIL-A-008860 (USAF) and MIL-STD-143B.

Reason: To add current references and correct typographical error.

### 7.4.3 FAILURE MECHANISMS

Delete entire section on "Brittle Fracture" and rewrite as follows:

"Brittle Fracture. The brittle-fracture properties of thick-wall and heavy-forged sections will be required for the vehicle structural design. The tentative standard testing procedures developed by ASTM Committee E-24 should be applied.

"In conjunction with evaluation of brittle fracture, fracture toughness should be determined by experiment. For materials selected for structural components designed using a safe-life approach, flaw-growth characteristics and threshold stress intensity should be experimentally determined.

"When experimentally determining the fracture toughness of materials, the test specimens should be sufficiently wide to prevent in-plane bending and should be of the same material and thickness as the component, and processed in the same manner. A sufficient number of specimens having flaws of various sizes and simulating the parent metal, weldments, and heat-affected zones of welded components, should be tested to allow meaningful statistical values of fracture toughness to be established."

"When experimentally determining the flaw growth characteristics of materials, the test specimens shall be designed to eliminate detrimental effects such as in-plane bending and backface corrections. Sufficient tests should be conducted in the simulated service environments and at the service load frequencies to allow meaningful statistical values of flaw-growth characteristics to be established. In addition, flaw growth tests of test specimens simulating the actual structural thicknesses, expected service loading and environment, and anticipated flaw geometries shall be conducted on critical structural components such as pressure vessels to experimentally verify the calculated flaw growth predictions.

"When experimentally determining the threshold stress-intensity characteristics and sustained stress flow growth rates of materials selected for components subjected to sustained loads, the specimens should be tested in environments simulating the actual service environments as nearly as practicable. A sufficient number of specimens should be tested to allow meaningful statistical values of the material's threshold stress intensities to be established.

"For recommended practices for pressure vessels, refer to NASA SP-8040."

Reason: The section entitled "Brittle Fracture" is written specifically for metallic pressure vessels. The entire section should be rewritten making it applicable to all structural components selected for fracture control.

#### 7.6.1.2 ULTIMATE CONDITIONS

Delete MIL-A-8867 (ASG) and replace with MIL-A-008867 (USAF).

Reason: To update the reference.

#### 7.6.1.3 COMBINED LOADS AND INTERNAL PRESSURE

Change and reason same as for 7.6.1.2.

#### 7.6.1.4 COMBINED LOADS AND THERMAL EFFECTS

Change and reason same as for 7.6.1.2.

#### 7.6.2.3 BUCKLING AND CRIPPLING

Change and reason same as for 7.6.1.2.

#### 7.6.7 LIFE TESTS

Add section 7.6.7.1 as follows:

##### "7.6.7.1 Fatigue Life

Fatigue tests shall be conducted for all structural components and assemblies that are vital to the integrity of the vehicle and the safety of personnel, unless fatigue analysis and meaningful element tests show that fatigue is not a critical failure mode and approval is obtained from the contracting agency. The fatigue test lives with appropriate reduction factors for inherent scatter in fatigue test results may be used to establish the fatigue life of components."

Reason: The confusion that exists regarding the precise definitions of fatigue-life and safe-life is also apparent in this section.

##### 7.6.7.1 SAFE-LIFE

Renumber this section to 7.6.7.2, and rewrite as follows:

"Safe-life tests shall be conducted for structural components and assemblies that have little or no tolerance for damage during operation in accordance with the criteria of Section 4.8 and designed using safe-life approaches. For safe-life designs concepts that depend on nondestructive inspection (NDI) and flaw growth predictions for structural life assurance, safe-life tests of the structure with artificial flaws shall be conducted to verify the safe crack growth predictions and to demonstrate that NDI techniques are adequate. The induced initial artificial flaws shall simulate flaws created by manufacturing or service conditions and shall not exceed the maximum permissible flaw sizes established as NDI standards for design of the component."

"The safe-life tests with appropriate reduction factors for scatter may be used to establish the safe-life and safe inspection intervals of components.

"For safe-life design concepts utilizing the proof test as the final inspection, the amount and type of preproof nondestructive inspection (NDI) required should be determined considering the impact of a proof-test failure on vehicle and program costs and schedules.

"For safe-life design concepts which depend on NDI for structural life assurance, it should be demonstrated that the techniques are adequate to ensure detection of significant defects."

Reason: Separate and specific fatigue, safe-life and fail-safe tests are required depending on the service load conditions and design approaches.

#### 7.6.7.2 FAIL-SAFE

Renumber this section to 7.6.7.3 and rewrite the first paragraph as follows:

"Fail-safe tests shall be conducted on structures depending on fail-safe design approaches for damage containment and fracture control. Fail-safe tests shall be conducted in accordance with the criteria of Sections 4.8.2 through 4.8.7 to demonstrate structural tolerance to damage, fracture arrest capability, and the residual load-carrying ability at the specified percentage of limit loads.

"Fail-safe tests may be conducted either on structure containing cracks in a single component developed during fatigue testing or on structure which has been purposely cut to simulate accidental severance of members.

"During these tests, the load applied to the structure should not be greater than the specified fail-safe load."

Reason: Same as for Section 7.6.7.1.

#### 7.6.7.3 MATERIAL PROPERTIES

Renumber this section to 7.6.7.4.

#### 7.6.7.4 CYCLIC LOADS

Change and reason same as for 7.6.1.2.

Renumber this section to 7.6.7.5.

#### 7.6.7.5 SUSTAINED LOADS

Renumber this section to 7.6.7.6.

#### 7.6.8 INTERFACE-COMPATIBILITY TESTS

Change and reason same as for 7.6.1.2.

SECTION 7  
REFERENCES

1. Fracture Control of Metallic Pressure Vessels, NASA SP-8040, National Aeronautics and Space Administration, May 1970.
2. Structural Design Criteria Applicable to a Space Shuttle, NASA SP-8057, National Aeronautics and Space Administration, January 1971.
3. Wilhem, D.P., Fracture Mechanics Guideline for Aircraft Structural Applications, Air Force Flight Dynamics Laboratory Report AFFDL-TR-69-111, February 1970.
4. Space Shuttle Booster Test Requirements Study for Structural Test, Convair Aerospace Report 76-548-4-012, 16 December 1970.
5. Emero, D.H. and Spunt, L., Optimization of Multirib and Multiweb Wing Box Structures Under Shear and Moment Loads, Sixth AIAA Structures and Materials Conference, Palm Springs, California, 5-7 April 1965.
6. Tiffany, C.F., Lorenz, P.M. and Hall, L.R., Investigation of Plane-Strain Flaw Growth in Thick Walled Tanks, NASA CR-54837, February 1966.
7. Tiffany, C.F., Lorenz, P.M. and Shah, R.C., Extended Loading of Cryogenic Tanks, NASA CR-72252, December 1966.
8. Hall, L.R., Plane Strain Cyclic Flaw Growth in 2014-T62 Aluminum and 6Al-4V (ELI) Titanium, NASA CR-72396, November 1968.
9. Tiffany, C.F. and Masters, J.N., Investigation of the Flaw Growth Characteristics of 6Al-4V Titanium Used in Apollo Spacecraft Pressure Vessels, NASA CR-65586, March 1967.
10. Little, C.D. and Wheeler, O.E., Fracture Mechanics Technology Relevant to Space Shuttle, General Dynamics Convair Aerospace Division, Fort Worth operation Report FZM-5633, 3 December 1970.
11. Poe, C.C. Jr., The Effect of Riveted and Uniformly Spaced Stringers on the Stress Intensity Factor of a Cracked Sheet, M.S. Thesis, Virginia Polytechnic Institute, 1969.

12. Poe, C.C. Jr., Fatigue Crack Propagation in Stiffened Panels, ASTM Symposium on Crack Propagation, Toronto, 21-26 June 1970.
13. Detail Mass Properties Report (Final), Volume II, Booster, Book 1, Mass Properties Data, North American Rockwell, Space Division Report MSC-03317, 25 June 1971.
14. Metallic Materials and Elements for Aerospace Vehicle Structures, Department of Defense, Washington, D.C., MIL-HDBK-5A, 8 February 1966.
15. Program Cost and Schedule Estimates Plan for Phase C/D, North American Rockwell Report No. SD 71-107, 25 June 1971.
16. Maintenance Analysis for Fail-Safe/Safe-Life Study, General Dynamics Convair Aerospace Division Report No. SS-76-116-2-061, 16 December 1971.